BMI/ONWI-631

Laboratory Investigation of Crushed Salt Consolidation and Fracture Healing

Technical Report

January 1987

IT Corporation

prepared for

Office of Nuclear Waste Isolation
Battelle Memorial Institute
505 King Avenue
Columbus, OH 43201-2693

ONWI
Office of Nuclear Waste Isolation

BATTELLE Project Management Division

DISCLAIMER

BIBLIOGRAPHIC DATA

IT Corporation, 1987. *Laboratory Investigation of Crushed Salt Consolidation and Fracture Healing,* BMI/ONWI-631, prepared for Office of Nuclear Waste Isolation, Battelle Memorial Institute, Columbus, OH.

NOTICE

Printed in the United States of America
Available from
National Technical Information Service
U.S. Department of Commerce
5285 Port Royal Road
Springfield, VA 22161

NTIS price codes
Printed copy: A10
Microfiche copy: A01

BMI/ONWI-631
Distribution Category UC-70

BMI/ONWI--631

DE87 005487

Laboratory Investigation of Crushed Salt Consolidation and Fracture Healing

Technical Report

January 1987

IT Corporation

prepared for

Office of Nuclear Waste Isolation
Battelle Memorial Institute
505 King Avenue
Columbus, OH 43201-2693

The content of this report was effective as of August 1984. The report was prepared by IT Corporation, Albuquerque, NM, for Battelle Project Management Division, Office of Nuclear Waste Isolation, under Contract No. DE-AC02-83CH10140 with the U.S. Department of Energy.

ABSTRACT

A laboratory test program was conducted to investigate the consolidation behavior of crushed salt and fracture healing in natural and artificial salt. Crushed salt is proposed for use as backfill in a nuclear waste repository in salt. Artificial block salt is proposed for use in sealing such a repository.

Four consolidation tests were conducted in a hydrostatic pressure vessel at a maximum pressure of 2,500 psi (17.2 MPa) and at room temperature. Three 1-month tests were conducted on salt obtained from the Waste Isolation Pilot Plant and one 2-month test was conducted on salt from Avery Island. Permeability was obtained using argon and either a steady-state or transient method. Initial porosities ranged from 0.26 to 0.36 and initial permeabilities from 2,000 to 50,000 md. Final porosities and permeabilities ranged from 0.05 to 0.19 and from $<10^{-5}$ md to 110 md, respectively. The lowest final porosity (0.05) and permeability ($<10^{-5}$ md) were obtained in a 1-month test in which 2.3% moisture was added to the salt at the beginning of the test. The consolidation rate was much more rapid than in any of the dry salt tests.

The fracture healing program included 20 permeability tests conducted on fractured and unfractured samples. The tests were conducted in a Hoek cell at hydrostatic pressures up to 3,000 psi (20.6 MPa) with durations up to 8 days. For the natural rock salt tested, permeability was strongly dependent on confining pressure and time. The effect of confining pressure was much weaker in the artificial salt. In most cases the combined effects of time and pressure were to reduce the permeability of fractured samples to the same order of magnitude (or less) as the permeability measured prior to fracturing.

FOREWORD

The National Waste Terminal Storage (NWTS) program was established in 1976 by the U.S. Department of Energy's (DOE) predecessor, the Energy Research and Development Administration. In September 1983, this program became the Civilian Radioactive Waste Management (CRWM) Program. Its purpose is to develop technology and provide facilities for safe, environmentally acceptable, permanent disposal of high-level waste (HLW). HLW includes wastes from both commercial and defense sources, such as spent (used) fuel from nuclear power reactors, accumulations of wastes from production of nuclear weapons, and solidified wastes from fuel reprocessing.

The information in this report pertains to the Rock Mechanics studies of the Salt Repository Project of the Office of Geologic Repositories in the CRWM Program.

TABLE OF CONTENTS

TABLE OF CONTENTS
(Continued)

LIST OF TABLES

LIST OF FIGURES

1.0 INTRODUCTION

Current schematic designs for shaft and tunnel seals and backfills for a repository in salt rely (in part) on two aspects of salt behavior which are expected to provide favorable conditions for waste isolation:

- Consolidation of crushed salt backfill over time due to creep closure of the underground openings, resulting in a backfill barrier with very low permeability
- Healing of fractures (created by excavation) around the underground openings with time, restoring the salt to the low permeability of the intact salt state.

If effective within reasonable time periods (tens to hundreds of years), these processes will result in encapsulation of the wastes in an essentially impermeable, homogeneous salt monolith, thus reducing the long-term requirements for other parts of the seal system, and enhancing the general confidence regarding the isolation capabilities of the site as a whole.

A previous report (IT Corporation, 1984) reviewed the current status of knowledge regarding crushed salt consolidation and fracture healing processes. It included a review of the properties of crushed salt as determined from laboratory testing and presented analyses of the rates at which crushed salt consolidation and fracture healing might occur in a repository. The report concluded that some properties required for analysis are poorly known and that additional laboratory testing was required to add confidence to the results of the analyses.

This report presents results from a 6-month laboratory test program conducted by IT Corporation (IT). Properties investigated include

- Consolidation of crushed natural salt under hydrostatic loading
  - Permeability as a function of porosity
  - Bulk modulus as a function of porosity
  - Creep properties as a function of time, porosity, and stress
- Fracture healing in natural and artificial block salt
  - Permeability as a function of stress and time
  - Tensile strength as a function of stress and time
- Block salt characterization
  - Porosity
  - Permeability as a function of porosity
  - Bulk modulus as a function of porosity.

Tests have been conducted on natural bedded salt from the Waste Isolation Pilot Plant (WIPP) site in New Mexico, on natural dome salt from Avery Island, Louisiana, and on artificial block salt manufactured by International Salt Company and Morton Salt Company. All tests were conducted at room temperature (approximately 21°C). Test parameters are summarized in Table 1-1.

Table 1-1. Test Matrices

Crushed Salt Consolidation

Test No.	Salt Type	Maximum Particle Size (mm)[a]	Moisture Condition	Maximum[b] Stress (psi)[c]	Duration (days)
1	WIPP	10	dry	2,500	28
2	WIPP	0.9	dry	2,500	35
3	WIPP	20	2.3%	2,500	32
4	Avery Is.	10	dry	2,500	62

Fracture Healing[d]

Test No.	Salt Type	Fracture Type	Moisture Condition	Maximum[b] Stress (psi)	Duration (days)
1	block	unfractured		3,000	1
2	block	unfractured		3,000	1
3	block	unfractured		3,000	1
4	block	saw	dry	3,000	3
5	block	saw	moist	3,000	2
6	block	split	moist	2,500	3
7	WIPP	unfractured		3,000	2
8	WIPP	split	dry	2,500	2
9	WIPP	unfractured		2,500	1
10	WIPP	split	moist	2,500	3
11	WIPP	unfractured		2,500	1
12	WIPP	saw	moist	2,500	2
13	Avery Is.	unfractured		2,500	7
14	Avery Is.	split	dry	2,500	7
15	Avery Is.	unfractured		2,500	8
16	Avery Is.	split	moist	2,500	8
17	block	unfractured		2,500	7
18	block	saw	dry	2,500	10
19	block	unfractured		2,500	3
20	block	saw	moist	2,500	8

(a) 1 mm = 0.039 in.
(b) Maximum effective hydrostatic stress.
(c) 1 psi = 6.9 kPa.
(d) Including permeability and deformability tests on unfractured artificial block salt.

The current test program is limited in scope and does not address all of the parameters that are believed to influence crushed salt consolidation and fracture healing behavior. It is anticipated that a more complete program will be conducted in the future to evaluate parameters such as salt type, gradation (or fracture characteristics), moisture content, stress conditions, and temperature.

2.0 BLOCK SALT CHARACTERIZATION

Manufactured salt bricks might be used in repository sealing systems as panel seals or tunnel bulkheads (Kelsall et al., 1984). A short test program has been conducted to characterize the porosity, permeability, and constitutive properties of commercially manufactured salt bricks.

2.1 SAMPLE DESCRIPTIONS

The salt bricks tested are salt "licks" produced for livestock. All of the fracture healing tests on artificial salt have been performed on bricks produced by International Salt Company. Additional porosity measurements have been made on bricks produced by Morton Salt Company.

The International Salt Company bricks are manufactured at Cleveland, Ohio, from salt produced from conventional mining. The mean particle size is about 0.3 mm (0.012 in) with a range from 0.06 to 3.0 mm (0.0024 to 0.12 in) (Figure 2-1). The insolubles content of a 50-g (1.76-oz) sample dissolved in distilled water by IT was 1.98%. Each block weighs 50 lb (22.7 kg) and has approximate dimensions 8 in square by 11 in high (20.3 by 28 cm). The blocks are formed in a press at room temperature at a pressure of 1,500 psi (10.3 MPa) applied for a few seconds. As described below, the porosity varies from about 8% to about 16%. The fabric of the salt is described in Appendix A.

The Morton Salt Company blocks are manufactured at Manistee, Michigan, from salt produced by evaporation. A complete particle size distribution is not available; the manufacturer indicates that 85% of the particles fall in the 0.2 to 0.6-mm (0.08 to 0.024-in) range. The insolubles content of a 50-g (1.76-oz) sample dissolved in distilled water by IT was 0.03%. Each block weighs 50 lb (22.7 kg) and has dimensions similar to those of the International blocks. As discussed below, the porosity (in a single block tested) varies from about 4% to about 14%.

2.2 POROSITY AND PERMEABILITY

The porosity distributions within two International blocks and one Morton block are shown in Table 2-1. In all cases, the porosity is higher at the top of the block than at the base. At the top of the blocks the porosity tends to be lower in the center than at the edges, whereas the porosity tends to be fairly constant across the block in the middle and at the base. The two International blocks (presumably from the same batch) have similar porosities at equivalent points. The average porosities of the International blocks are higher than the average of the Morton block.

Argon-gas permeabilities were obtained from three unfractured samples of International block salt using the steady-state test method described in Section 4.1.1. The results are shown in Table 2-2 and the apparatus in Figure 4-1.

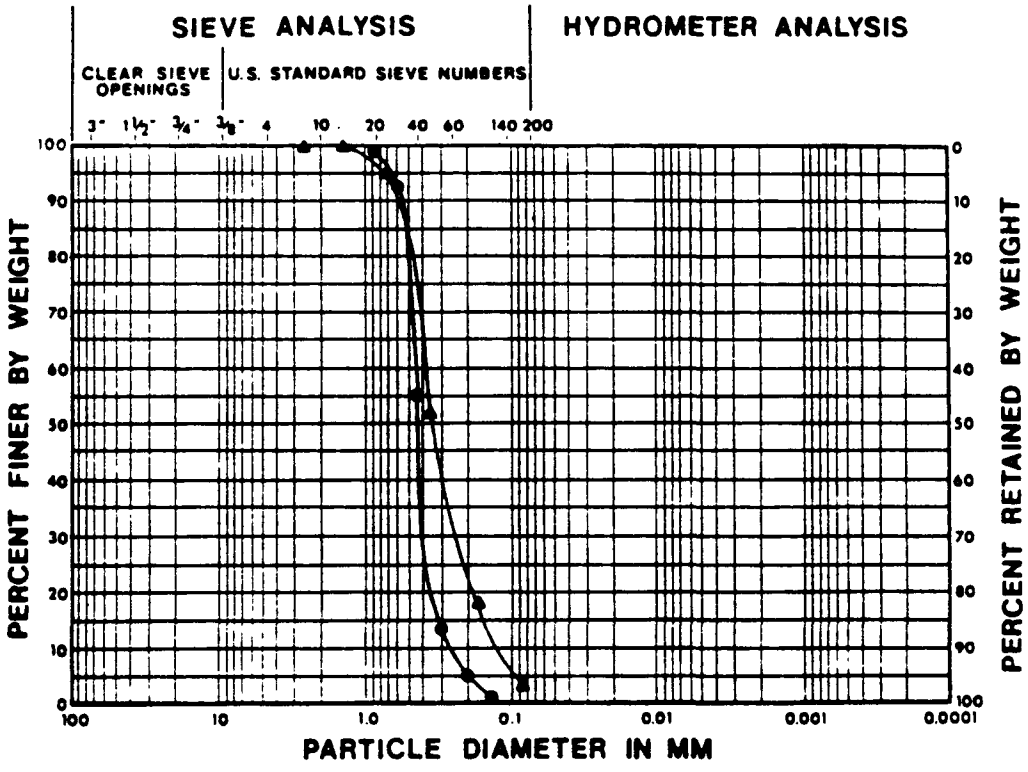

▲ International Salt Co. - Artificial block salt
$CU = \frac{d60}{d10} = 2.9$*

● Morton Salt Co. - Artificial block salt
CU = 1.5

*Note: CU is Coefficient of Uniformity.

$$CU = \frac{d60}{d10} \left(\text{i.e., } \frac{\text{particle diameter that 60\% of the sample is finer than}}{\text{particle diameter that 10\% of the sample is finer than}} \right).$$

Particle Size Distribution for Artificial Block Salt

Figure 2-1

Table 2-1. Porosity Distributions in Block Salt Samples

Morton Block 1

1	2	3	4	5	6	7	8	9	Mean
0.111	0.099	0.103	0.116	0.126	0.139	0.135	-	0.067	0.11
0.094	0.082	0.086	0.094	0.103	0.088	0.112	-	0.084	0.09
0.075	0.070	0.073	0.075	0.076	0.051	0.081	0.086	0.072	0.07
0.046	0.065	0.060	0.065	0.042	0.048	0.040	0.062	0.059	0.05
							whole block		0.08

International Block 1

1	2	3	4	5	6	7	8	9	Mean
0.149	0.142	0.141	0.139	0.162	0.130	0.154	0.134	-	0.14
0.131	0.131	-	0.129	0.134	0.114	0.123	0.122	0.141	0.13
0.114	0.115	0.110	0.116	0.113	0.100	0.092	0.104	-	0.11
0.102	0.110	0.108	0.098	0.096	0.091	0.077	0.100	-	0.10
							whole block		0.12

International Block 2

1	2	3	4	5	6	7	8	9	Mean
0.154	0.147	0.156	0.151	0.156	0.136	0.141	-	0.129	0.15
0.113	0.125	0.127	0.140	0.148	0.121	0.122	0.129	0.127	0.13
0.106	0.109	0.111	0.117	0.116	0.113	0.107	0.111	0.111	0.11
0.089	0.093	0.091	0.108	0.110	0.100	0.095	0.097	-	0.10
							whole block		0.12

Note: Cores 1 thru 8 are from perimeter of block, 9 from center. Odd-numbered cores are from corners, even from middle edges. Porosities are listed from top-of-block to bottom.

Table 2-2. Summary of Permeability Tests on Artificial Block Salt

Sample No.	Initial Porosity	Permeability @ 50 psi confining Pressure (md)	Permeability @ 3,000 psi confining Pressure (md)
COHND	0.151	43	37
COIND	0.124	14	13
COLND	0.096	4	3
I1	0.138	66	24(a)
I2	0.135	54	26(b)

(a) After 165 hours at 2,500 psi (17.2 MPa).
(b) After 72 hours at 2,500 psi (17.2 MPa).

The effect of confining pressure on permeability is much weaker than that exhibited by natural salt (Section 4.3). This suggests that the block material is relatively homogeneous and unfractured, whereas the natural salt contains many microfractures which heal under applied stress.

2.3 CONSTITUTIVE PROPERTIES

Axial strain was monitored in five tests, three with durations of 5 to 6 hours, one with a duration of 3 days, and one with a duration of 7 days. Figure 2-2 shows axial strain as a function of time for the two longer-duration tests. The two samples show essentially the same behavior as expected from their similar porosities. Both exhibit very small creep rates in the latter stages of the tests.

Bulk modulus values obtained from the five tests are given in Table 2-3 as a function of pressure. For each test, the moduli are fairly constant above a pressure of 1,000 psi (6.9 MPa). The average modulus tends to increase with decreasing porosity, but the correlation is weak.

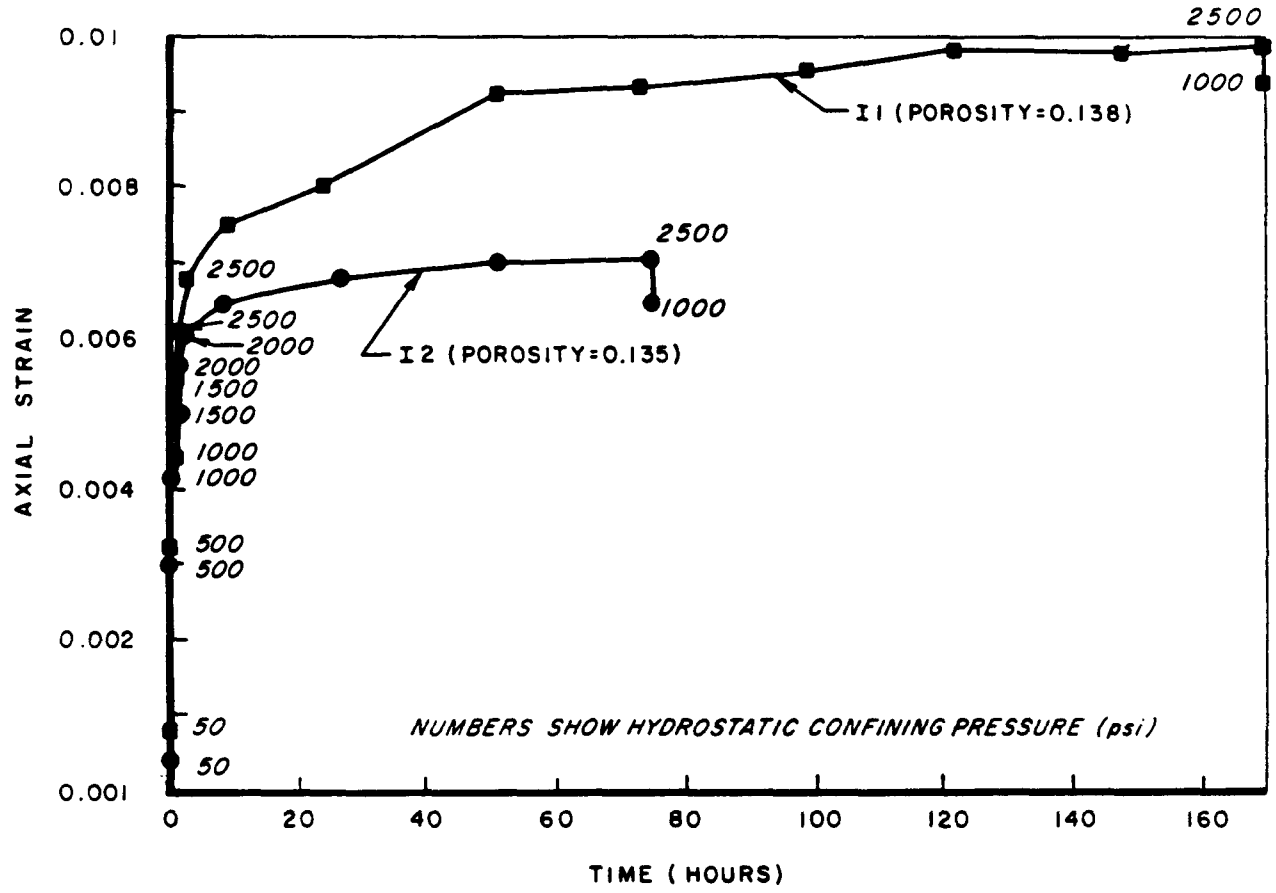

Axial Strain Versus
Time, Block Salt

Figure 2-2

Table 2-3. Bulk Modulus of Block Salt
(Page 1 of 2)

Sample No.	Initial Porosity	Pressure Increment (psi)	Bulk Modulus (psi)
COIND	0.12	50-500	2.0×10^5
		500-1,000	1.4×10^6
		1,000-1,500	1.6×10^6
		1,500-2,000	2.6×10^6
		2,000-2,500	1.6×10^6
COHND	0.147	50-500	3.0×10^5
		500-1,000	5.7×10^5
		1,000-1,500	4.8×10^5
		1,500-2,000	5.6×10^5
		2,000-2,500	6.3×10^5
COLND	0.09	50-500	7.8×10^5
		500-1,000	9.4×10^5
		1,000-1,500	7.1×10^5
		1,500-2,000	5.8×10^5
		2,000-2,500	7.1×10^5
I1	0.138	50-500	6.2×10^4
		500-1,000	1.4×10^5
		1,000-1,500	1.6×10^5
		1,500-2,000	2.5×10^5
		2,000-2,500	2.4×10^5

Table 2-3. Bulk Modulus of Block Salt
(Page 2 of 2)

Sample No.	Initial Porosity	Pressure Increment (psi)	Bulk Modulus (psi)
I2	0.135	50-500	5.8×10^4
		500-1,000	1.4×10^5
		1,000-1,500	2.0×10^5
		1,500-2,000	2.7×10^5
		2,000-2,500	3.6×10^5

3.0 CRUSHED SALT CONSOLIDATION TESTING

The objective of the crushed salt consolidation testing is to obtain stress-strain and permeability-porosity relations for crushed salt consolidated under hydrostatic loading at room temperature (approximately 21°C). Four tests have been conducted as follows:

- One-month duration test on dry WIPP salt, maximum particle size 10 mm (0.39 in) (sample M10)
- One-month duration test on dry WIPP salt, maximum particle size 0.9 mm (0.035 in) (sample M1)
- One-month duration test on moist (2.3% moisture content) WIPP salt, maximum particle size 20 mm (0.78 in) (sample AR)
- Two-month duration test on dry Avery Island salt, maximum particle size 10 mm (0.39 in) (sample AM10).

All samples were loaded hydrostatically at increments of 500 psi (3.45 MPa) to a maximum effective confining stress of 2,500 psi (17.25 MPa). In the first three tests the maximum load was held constant for about 2 weeks; in the fourth test the maximum load was held constant for about 7 weeks.

3.1 TEST APPARATUS AND PROCEDURES

Crushed salt consolidation tests are conducted in a high-pressure (maximum 3,300 psi [22.75 MPa]) vessel using a sample that is sealed from the confining fluid by latex and neoprene membranes. Permeability tests may be conducted with either a steady-state method (Figure 3-1) or transient method (Figure 3-2). Porous stones and platens are installed at the ends of the sample and connected to gas lines for permeability testing. Other key test equipment includes a gas/hydraulic oil intensifier for maintaining a constant hydrostatic pressure on the test specimen, a permeability test control panel, and an argon gas supply. Test data are monitored using various types of electronic sensors attached to a 16-channel analog-to-digital (A/D) converter and time module linked to a microcomputer. Software packages have been designed for data acquisition, retrieval, and reduction. Specific equipment features and test methods are described below.

3.1.1 Pressure Vessel

The test chamber consists of a conventional pressure vessel typically used for high pressure/temperature thermodynamic reaction studies. The vessel has been modified to allow anchoring a base pedestal to support the sample and to provide outlets for gas inflow and outflow, displacement transducers, and bleed venting. The sample is constructed using conventional soil mechanics techniques used to prepare granular soil media for shear strength testing. The sample is constructed within a latex membrane-lined mold having the nominal dimensions 2.8 in in diameter by 4.5 in high (7.1 by 11.4 cm). The sample is compacted within the mold using a compactive effort equivalent to

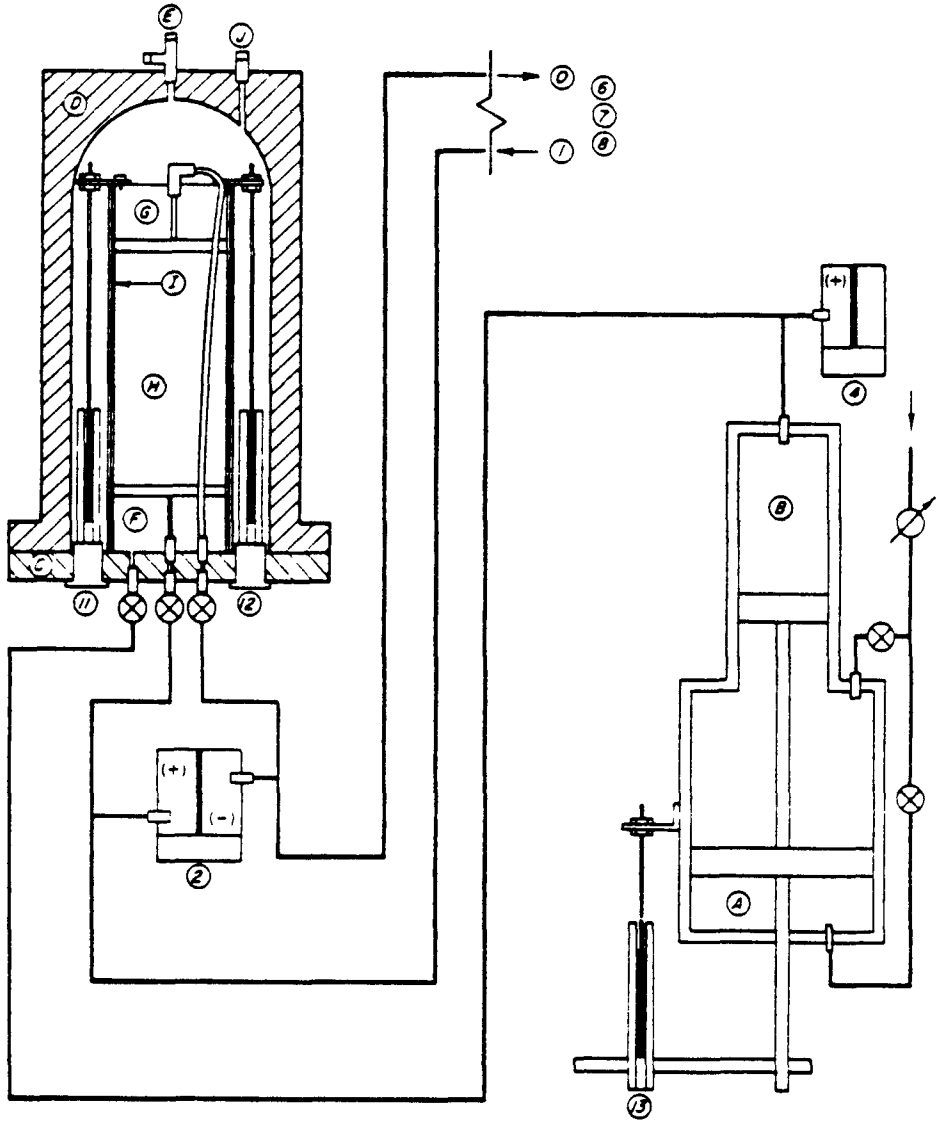

Legend

Consolidation Test Assembly - Steady-State Tests

Identification[a]	Description
0	Flowmeter for volumetric flowrate (0.01 to 5.0 l/min [0.003 to 0.13 gpm]), mounted in pressure control panel
1	Pressure transducer for total upstream gas pressure (0 to 800 psi [0 to 5.5 MPa]), mounted in pressure control panel at downstream outlet of 2,250-cm³ (0.6-gal) reservoir
2	Differential-pressure transducer (6 to 20 psi [41 to 138 kPa]) for gas pressure drop across sample
4	Pressure transducer for intensifier/pressure vessel oil pressure, 0 to 3,200 psi (0 to 22 MPa)
6	Temperature sensor adjacent to pressure transducer No. 1
7	Temperature sensor at sample inlet
8	Temperature sensor at sample outlet, all temperature sensor monitor temperature of argon permeant
11,12	Linear variable displacement transducers (LVDTs) (±1-in [2.56-cm] travel) mounted to base of pressure vessel and top platen to monitor sample length change
13	LVDT (±1-in [2.56-cm] travel) mounted to air/oil intensifier to monitor piston displacement in intensifier
A	Gas pressure side of air/oil intensifier
B	Pressure from A is multiplied and transferred to oil side of air/oil intensifier and to pressure vessel
C	Base of pressure vessel with gas inlet to bottom platen (F), gas outlet from top platen (G), oil inlet from intensifier (B), mounting sockets for LVDTs (11, 12)
D,E	Top chamber of pressure vessel with inlet-outlet (E also used for hoisting), temperature sensor inlet (J, not in use)
F	Bottom platen with gas port to sample
G	Top platen with gas port from sample and gas line to base outlet
H	Prepared sample (one-fifth standard Proctor) with porous stones
I	Multiple latex and neoprene rubber membranes secured to platens with hose clamps

(a) I.D. numbers refer to sensor connections to A/D converter.

Crushed Salt Consolidation Test Assembly for Steady-State Permeability Test

Figure 3-1

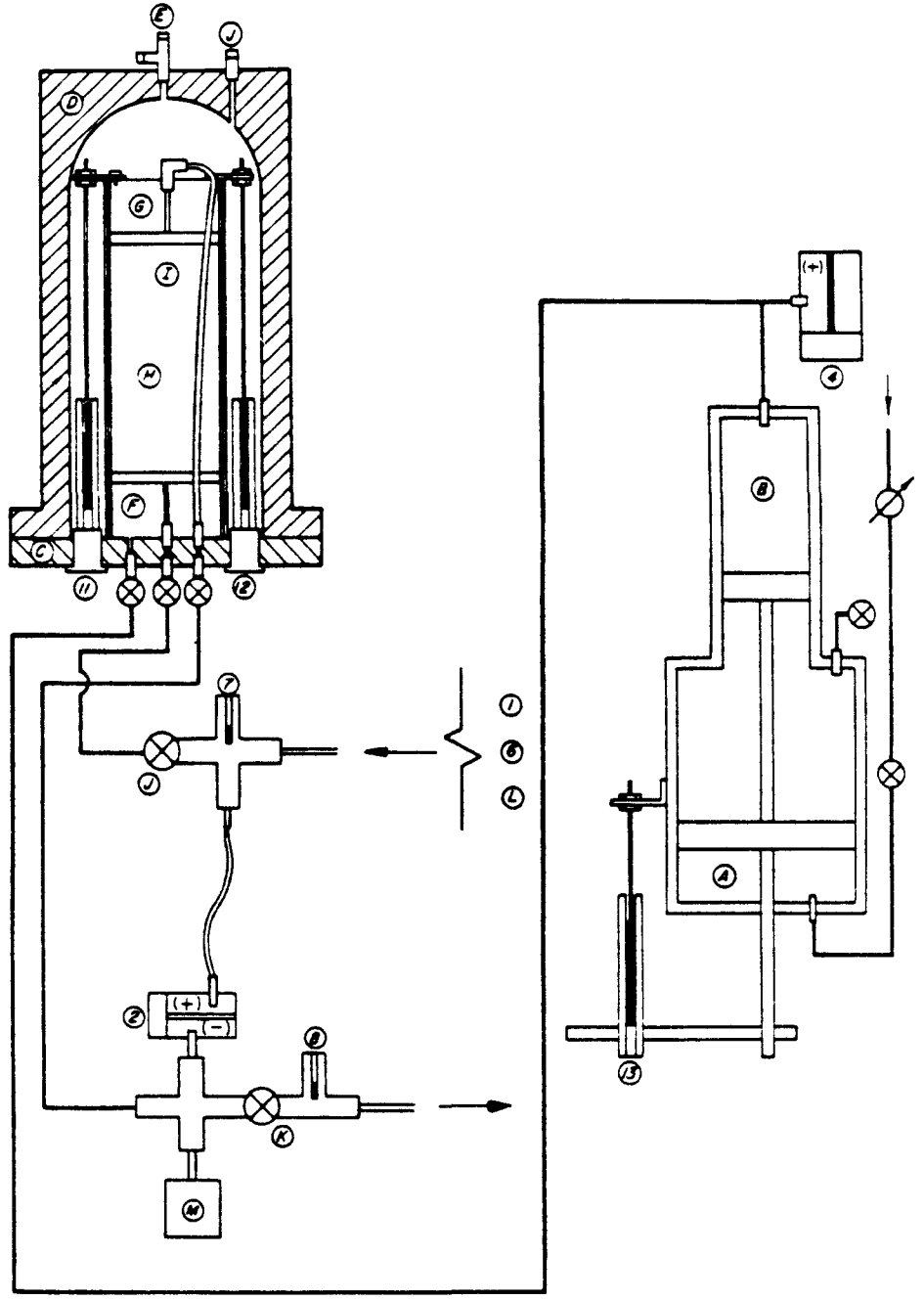

Legend

Consolidation Test Assembly - Transient Tests

Identification[a]	Description
1 or 3	Pressure transducer for total upstream gas pressure (0 to 800 psi [0 to 5.5 MPa]), mounted in panel at downstream outlet of 2,250-cm^3 (0.6-gal) reservoir
1 or 2	Differential-pressure transducer for gas pressure drop across sample
3	Pressure transducer for intensifier/pressure vessel oil pressure, 0 to 3,200 psi (0 to 22 MPa)
6	Temperature sensor adjacent to pressure transducer No. 1
7	Temperature sensor at sample inlet
8	Temperature sensor at sample outlet, all temperature sensors monitor temperature of argon permeant
11,12	LVDTs (±1-in [2.56-cm] travel) mounted to air/oil intensifier to monitor piston displacement in intensifier
13	LVDT (±1-in [2.56-cm] travel) mounted to air/oil intensifier to monitor piston displacement in intensifier
A	Gas pressure side of air/oil intensifier
B	Pressure from A is multiplied and transferred to oil side of air/oil intensifier and to pressure vessel
C	Base of pressure vessel with gas inlet to bottom platen (F), gas outlet from top platen (G), oil inlet from intensifier (B), mounting sockets for LVDTs (11, 12)
D,E	Top chamber of pressure vessel with inlet-outlet (E, also used for hoisting), temperature sensor inlet (J, not in use)
F	Bottom platen with gas port to sample
G	Top platen with gas port from sample and gas line to base outlet
H	Prepared sample (one-fifth standard Proctor) with porous stones
I	Multiple latex and neoprene rubber membranes secured to platens with hose clamps
J	Plug valve at sample inlet
K	Plug valve at sample outlet
L	Ball valve at upstream inlet of 2,250-cm^3 reservoir
M	10-cm^3 (0.3-fl oz) reservoir

(a) I.D. numbers refer to sensor connections to A/D converter.

Crushed Salt Test Assembly for Transient Permeability Tests

Figure 3-2

one-fifth of standard Proctor (11 blows/layer instead of 56 blows/layer, ASTM D698). Additional latex and neoprene membranes (one each) are placed around the sample after the mold has been removed for added sample integrity to resist the high confining pressures developed during testing. The membranes are sealed to the platens with steel bands. Prior to filling the reservoir with oil, the flow-through line between the top platen and vessel base is attached and a pair of linear variable displacement transformers (LVDTs) are inserted and anchored to the top platen for monitoring axial sample deformations.

3.1.2 Confining Pressure System

Hydrostatic confining pressures are maintained in the pressure vessel using a gas/oil intensifier having a 5 to 1 ratio of oil pressure to gas pressure. Gas pressure to the intensifier is controlled using a precision regulator. During periods of long-term constant pressure application, gas pressures are periodically monitored and manually adjusted as needed to minimize excessive gas loss through the precision gas regulators. The position of the piston inside the intensifier is electronically monitored so that the volume of oil entering or leaving the vessel can be measured. This feature permits determination of sample volume changes, provided that measurements are corrected for system compliance (i.e., corrected for change in volume of system components due to changes in hydrostatic pressure).

3.1.3 Permeability Test System

The key elements of the permeability test system are an interchangeable set of precision gas regulators (0 to 7 psi, 0 to 200 psi, and 0 to 500 psi [0 to 48 kPa, 0 to 1.4 MPa, and 0 to 3.45 MPa]) for controlling gas flowrates through the sample, an electronic differential-pressure transducer for measuring sample and system head losses during gas flow, and an electronic flowrate sensor. The possible wide range of permeabilities which must be measured (i.e., <0.1 md to 1,000 md) necessitates the use of different test methods and equipment depending on the sample type and condition.

For constant-head (steady-state) tests, a 0- to 20-psi (0- to 138-kPa) electronic differential-pressure transducer and a 0.01- to 5.0-l/min (0.003- to 0.13-gpm) flowmeter are used (Figure 3-1). With this test method, corrections are applied to measured differential pressures to account for system head losses associated with the system plumbing and the porous stones located at each end of the sample. The effects of system head losses are minimized by placing the differential-pressure transducer as close as possible to the sample.

For samples having permeabilities <0.1 md, transient pressure-decay tests are used. These tests require sealed, high-pressure reservoir systems upstream and downsteam from the sample, 0-20 to 0-500 psi (0-4.8 kPa to 0-3.45 MPa) electronic differential-pressure transducers, and 0-800 to 0-3,200 psi (0-5.5 to 0-22 MPa) electronic pressure transducers for measuring the total system pressure in the reservoirs (Figure 3-2). Corrections for system head loss are not applied due to the very low flowrates that are generated during transient testing.

3.1.4 Instrumentation

The relatively rapid response of crushed salt samples to changes in pressure gradients requires a monitoring system that is able to adjust to changing test conditions. Consequently, several electronic sensors are used to provide the needed response rate. The array of electronic test sensors consists of the following:

- Flowmeter (0.01 to 5.0 l/min [0.003 to 1.3 gpm])
- Differential-pressure transducer (0-20 to 0-500 psi [0-4.8 to 0-3,450 kPa], constant-head tests only)
- Pressure system transducer (0-800 to 0-3,200 psi [0-55 to 0-22 MPa], transient tests only)
- Confining-pressure transducer (0 to 3,200 psi [0 to 22 MPa])
- Three temperature sensors (0 to 30°C)
- Two axial deformation LVDTs (0 to 1 in [0 to 2.5 cm])
- Intensifier piston-displacement LVDT (0 to 2 in [0 to 5.0 cm]).

All sensors are calibrated and traceable to the National Bureau of Standards (NBS). For purposes of data reduction, regression analyses (correlation coefficients $\geq$0.9998) have been performed to numerically relate sensor outputs to the measured parameters.

All of the sensors are monitored using a 16-channel, 12-bit precision analog/digital data-acquisition module and a clock module linked to a 64-K Apple II* microcomputer. Test-specific software packages have been developed to allow data acquisition at prescribed time intervals in addition to data retrieval and data reduction. All software has been verified to assure the correctness of computed test results.

3.1.5 Test Procedure

Constant-head permeability tests are conducted by permeating argon gas up through the test specimen using a range of pressure gradients. Typically, four pressure gradients are used in addition to a series of readings at zero gradient which act as a baseline or null reference for the differential-pressure transducer and flowmeter readings. Pressure gradients are selected to maximize the output of the flowmeter, which is nonlinear at low flowrates. Usually three readings of test sensors are taken at each gradient within a 30-sec interval. Accordingly, less than 10 min is required to conduct and reduce the test data for each test.

---

* Apple II is a trademark of the Apple Computer Company.

Transient (falling-head) permeability tests are used for materials with a permeability lower than about 1 md. Transient tests are conducted by elevating the pressure in the permeability test system to a nominal pressure of approximately 500 psi (3.45 MPa). This high back-pressure is needed to assure that the argon gas will behave as an incompressible fluid for the pressure gradients imposed during transient testing. The pressure in the upstream reservoir and a set of baseline readings is taken prior to the start of the test. The test is initiated by opening the downstream reservoir valve and periodically measuring changes in the differential pressure across the sample as the sealed pressures between the upstream and downstream reservoir systems equilibrate. Differential pressures were selected to try to minimize both the change in effective stresses across the ends of the sample and the time required to complete the test. Differential pressures varied from 20 to 500 psi (4.8 to 3,450 kPa), depending on the permeability of the sample. Detailed test procedures are given in Appendix B.

3.2 SAMPLE DESCRIPTIONS

Crushed salt consolidation tests have been conducted on two types of salt, bedded salt from the Permian Salado Formation obtained from the WIPP site in New Mexico, and dome salt from the Avery Island dome in Louisiana.

3.2.1 WIPP Salt

Crushed salt for the first three consolidation tests was obtained from underground excavations at the WIPP site excavated using a roadheader-type continuous mining machine. The salt tested in the study was sampled from immediately behind the machine in the south exploratory drift. Occasional large pieces of salt which have fallen from the tunnel walls without being crushed by the machine were excluded from the sample.

As sampled at the site, the crushed material had a maximum particle size of about 40 mm (1.6 in) (Figure 3-3). Test 1 was conducted on this material with the 10+ mm fraction removed. Figure 3-3 shows that these materials were moderately-to-well graded (poorly sorted) with coefficients of uniformity in the range 5.6 to 15.2. (It is noted in Figure 3-3 that the Test 1 curve crosses the as-sampled curve at a percent-finer value of 80%. This is presumed to arise because the Test 1 subsample was not exactly representative of the as-sampled material.) Test 2 was conducted on a finer subsample which had a maximum particle size of about 0.9 mm (0.04 in). This subsample was less well graded than the Test 1 and 3 materials, with a coefficient of uniformity of 3.2.

The WIPP salt has been characterized in detail from samples obtained from boreholes drilled from the surface (Powers et al., 1978) and by geologic mapping of the underground shafts and tunnels (DOE, 1983). The WIPP underground facility is excavated at a depth of about 2,150 ft (655 m) in the Lower Salado Unit of the Permian Salado Formation. Seven lithologic units are laterally continuous throughout the facility, including the south exploratory drift. All of the units are composed primarily of halite with the contents of water-insoluble minerals ranging from 0.02 to 5.9% by weight. One sample

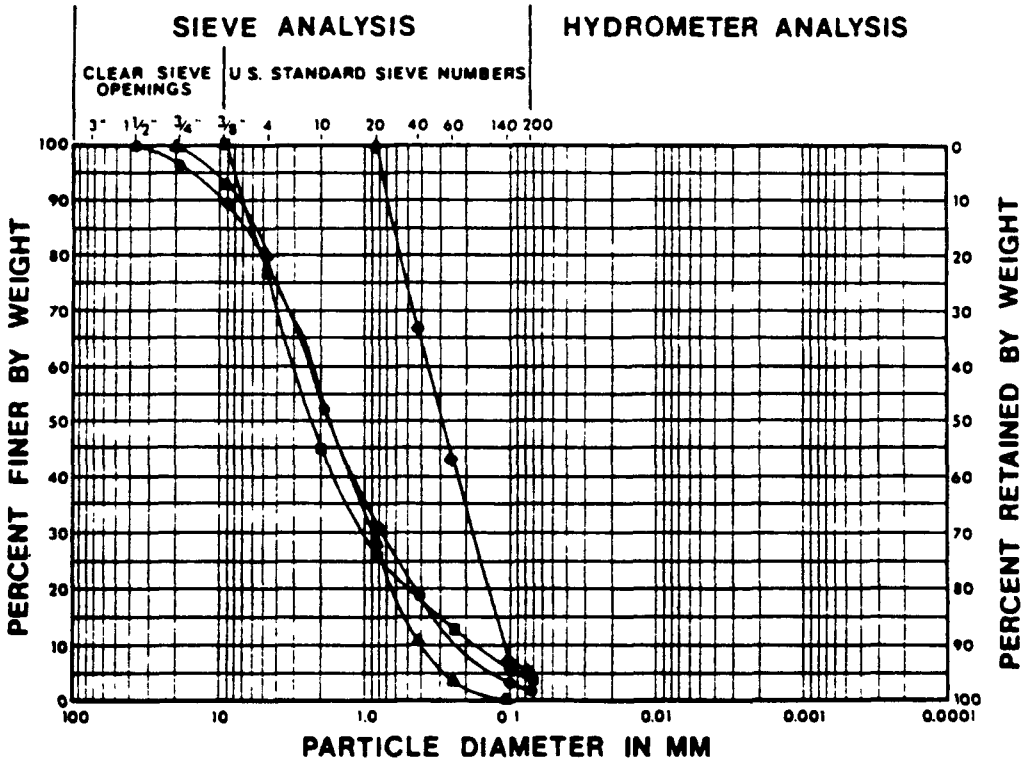

		CU *
●	AS-SAMPLED WIPP CRUSHED SALT	11.0
▲	WIPP CRUSHED SALT (AR)-TEST NO. 3	5.6
■	COARSE WIPP CRUSHED SALT (MIO)-TEST NO. 1	15.2
	COARSE AVERY ISLAND CRUSHED SALT (AI)-TEST NO. 4	14.3
◆	FINE WIPP CRUSHED SALT (MI)-TEST NO. 2	3.2

* $CU = \frac{d60}{d10}$

Particle Size Distributions for Crushed Salt

Figure 3-3

tested by IT had an insolubles content (determined by dissolving in distilled water) of 1.03%. Accessory minerals include polyhalite, clay, hematite, pyrite, anhydrite, calcite, dolomite, and quartz. Fluid inclusions occur in the halite. The DOE (1983) examined data from various sources and estimated the maximum water content to be 1.8% with a mean of 0.59%.

The crystal size of the intact WIPP salt is mostly in the range of 5 to 15 mm (0.2 to 0.6 in) with a complete range from 1 to 50 mm (0.04 to 2.0 in). The fabric of the intact salt has been described by Powers et al. (1978) and Carter and Hansen (1983). The fabric of the WIPP salt used in the fracture healing tests in this study is described in Section 4.2.1 and Appendix A.

The creep behavior of intact WIPP salt is well characterized (Herrmann et al., 1980; Herrmann and Lauson, 1981; Mellegard and Senseny, 1981). As discussed by Nelson and Kelsall (1984), there is a scatter of two orders of magnitude in the measured steady-state creep rates which has not been correlated with petrological characteristics. Creep tests on crushed WIPP salt are reported by Holcomb and Hannum (1982).

3.2.2 Avery Island Salt

Samples of intact Avery Island salt were obtained from RE/SPEC Inc. and crushed by IT into various fractions. The test sample was then prepared by mixing the fractions to match the gradation of the WIPP M10 sample (used in Test 1) as closely as possible. The particle size distribution of the material tested is shown in Figure 3-3.

Generally, the intact Avery Island salt consists of halite with <1% anhydrite and traces of clay (Jacoby, 1977). The material received by IT appeared to be very clean with no visible impurities. The crystal size ranges from 1 mm to 15 mm (0.04 to 0.6 in) with an average of 7.5 mm (0.3 in). The fabric of the intact salt has been described by Carter and Hansen (1983). The fabric of the Avery Island salt used in the fracture healing tests in this study is described in Section 4.2.2.

The creep behavior of the intact Avery Island salt is well characterized (Mellegard and Senseny, 1981). The average steady-state creep rate is slightly faster than that of the average for WIPP salt, although both salts exhibit significant (1 to 2 orders of magnitude) overlapping scatter in measured rates. Creep tests on crushed Avery Island salt are reported by Ratigan and Wagner (1978).

3.3 COMPACTION CHARACTERISTICS

Compaction characteristics of crushed WIPP salt have been reported previously (IT Corporation, 1984). Three samples were tested, including a "coarse" sample with a gradation similar to that of Sample AR used in Test 3 (Figure 3-3), and a finer sample with a gradation similar to that of Sample M1 used in Test 2. The minimum density of the coarser sample, determined by pouring the salt into a container without compaction, was 1.30 g/cm^3 (81.0 lb/ft^3), corresponding to a porosity of 0.403. With the finer sample (<6 mm), the minimum density was 1.21 g/cm^3 (75.7 lb/ft^3), corresponding to a porosity

of 0.442. Porosities were calculated assuming a grain density of 2.16 g/cm^3 (135 lb/ft^3).

The samples were compacted using various methods including standard Proctor (ASTM D698), one-fifth standard Proctor, and vibration (ASTM D2049). All tests were conducted dry, without adding water to the salt. A moderate compactive effort (one-fifth standard Proctor) was found to achieve a relatively large increase in density, whereas further compaction had a proportionately diminishing effect. (This is typical for granular materials.) The porosity of the coarse subsample was 0.28 after compaction by the one-fifth standard Proctor method and 0.248 after the standard Proctor compaction.

3.4 TEST RESULTS

3.4.1 Porosity and Permeability

The porosities of samples were obtained before and after consolidation testing by measuring sample volumes, weights, and mineral-grain specific gravities. As shown by Table 3-1, the initial porosities in the four tests ranged from 0.36 to 0.26. Because all samples were precompacted with an effort equivalent to one-fifth of standard Proctor, the differences in initial porosity are believed to be related to differences in particle size, gradation, and moisture content. After consolidation for 1 month in the first three tests, the final porosities ranged from 0.19 to 0.05. As discussed further in this section, the significantly greater degree of consolidation achieved in Test 3 is believed to result from the presence of a small amount of moisture in that sample. After consolidation for 2 months in Test 4, the final porosity was 0.14.

Porosities at intermediate points during a test (i.e., points at which permeability tests were conducted) were calculated by two methods. First, the change in sample volume was calculated according to the volume of hydraulic fluid progressively injected into the pressure vessel, making appropriate corrections for oil and vessel compliance. By this method, the calculated porosity at the end of the test was found to differ (by a few percent absolute porosity) from the porosity obtained by direct measurement after the sample was removed from the cell. Accordingly, we decided to obtain a "corrected porosity," using the measured axial strain as an index of sample volume change rather than the measured volume of oil injected into the pressure vessel. This decision was justified because the measurement of axial strains, using LVDTs, was considered to be more accurate than measurement of oil volume, which had to account for system compliance.

Theoretically, under hydrostatic loading, the volumetric strain should equal three times the axial strain. For the first three tests, the ratio of total volumetric strain (obtained from the difference between the initial and final porosities) to total axial strain varied from 1.8 to 2.2. The reasons for this departure from theoretical behavior are not fully understood, but may be related to the resistance to deformation offered by the membranes.

Table 3-1. Summary of Permeabilty Tests on Crushed Salt

Test No.	Salt Type	Maximum Particle Size (mm)	CU[a]	Moisture Content	Initial[b] Porosity	Initial Permeability (md)	Duration (days)	Final[c] Porosity	Permeability (md)
1	WIPP (M10)	10	15.2	dry	0.26	4,000	28	0.16	110
2	WIPP (M1)	0.9	3.2	dry	0.36	2,170	35	0.19	90
3	WIPP (AR)	20	5.6	2.3%	0.31	50,400	32	0.05	10^{-5}
4	Avery Is. (AM10)	10	14.3	dry	0.26	3,530	62	0.14	48

(a) Coefficient of uniformity = D_{60}/D_{10}.

(b) From direct measurement of sample volume and weight before test.

(c) From direct measurement of sample volume and weight after test.

The corrected porosity at time (t) in the test was calculated as follows:

$$\text{corrected porosity} = \text{initial porosity} - \left[\frac{\text{axial strain at } t^*}{\text{total axial strain}} \times (\text{initial porosity} - \text{final porosity})\right]$$

The data tables in Appendix D include both the porosities calculated from the oil volume change ("compliance porosity") and the corrected porosities calculated from the axial strain as described above. In the remainder of this report, all reported porosities corresponding to permeability tests during consolidation are the corrected values.

Permeability was measured at intervals throughout each consolidation test without removing the samples from the pressure vessel. Permeabilities above about 1 md were measured using a steady-state (constant head) method with argon gas as the permeant (Section 3.1). The possible error of these measurements (Appendix C) is estimated to be ±3 md or 10%, whichever is the greater, suggesting that the method is not completely satisfactory for permeabilities below about 10 md. Permeabilities below about 1 md were measured using a transient (pressure decay) method again with argon gas. The possible error of these measurements related directly to instrument readings is estimated to be $\pm 10^{-6}$ md or 1%, whichever is the greater. As noted in Appendix C, however, a significantly greater error may occur in the interpretation of the results. This process requires establishing a linear portion of a semilog pressure decay versus time plot. In many cases the plots did not include an obviously linear portion and there is some subjectivity in curve fitting. From the relatively large degree of scatter exhibited in the test results obtained by the transient method compared with those obtained by the constant head method, the error in the interpretation of the transient tests is estimated to be about ±50%. Although this appears at first to be a large error, its practical significance is diminished by consideration that the total range over which permeability is measured for the crushed salt is 11 orders of magnitude.

The nonlinearity of the pressure decay curves may be related to the relatively high porosities of the samples tested. Generally, the transient-test method, as developed by Brace et al. (1968), is used for rocks such as granite that have low porosity as well as low permeability. Accordingly, Brace et al. developed a simplified method of analyzing test results which ignores the influence of compressive storage in the sample. Brace et al.'s method of interpretation has been used in this study. Hsieh et al. (1981), Neuzil et al. (1981), and Trimmer (1981) discuss errors which may be involved in using Brace et al.'s solution for cases where the specimens have significant porosity or where certain experimental parameters (e.g., the relative size of the upstream and downstream reservoirs) do not match the assumptions of the solution. As described in Appendix C, Brace et al.'s

---

* Time (t) is the time when the strain is measured, usually at each pressure increment.

solution will systematically underestimate permeability by up to 40% for samples with porosities up to 15%.

Correction of the test results would require a numerical analysis of each test. As noted above, an error of up to 40% does not have major practical significance in relation to the wide range of permeabilities measured. In a future test program, it would be appropriate to use numerical modeling (of the type described by Neuzil et al., 1981) to assist in test planning (e.g., to select pressure transducers with appropriate ranges) and to develop type curves which can be used in data analysis.

Permeability as a function of porosity is shown in Figure 3-4 for the consolidated crushed salt and for the International Salt Company block salt. Table 3-1 is a summary of the test data which are reported more fully in Appendix D.

At porosities above about 0.2, permeability is determined by gradation as well as by porosity. At the same porosity, the coarser sample AR (<20 mm) (<0.8 in) in Test 3 has a permeability about two orders of magnitude greater than that of the finer sample M1 (<0.9 mm) (<0.04 in) in Test 2. At porosities above 0.2 the trend between permeability and porosity is similar for the three WIPP samples, for the Avery Island sample, and for the block salt, and is similar to the trend reported previously by IT Corporation (1984).

At porosities below about 0.2, the permeability of sample AR (Test 3) decreases rapidly with decreasing porosity and the trend of permeability versus porosity appears to diverge from the trend obtained in the other tests. At porosities less than 0.10 the permeabilities are less than 1 md, and are thus lower than the permeabilities obtained in this program from natural WIPP salt (with the exception of one test - see Section 4.3.1). This may occur because the natural samples are fractured due to disturbance, whereas the consolidated sample, which has never been subjected to stress relief, is unfractured.

The relatively rapid consolidation and low final permeability of sample AR (Test 3) is believed to have occurred as a result of the addition of moisture to this sample at the beginning of the test. As shown by petrographic examination (Appendix A), the dominant consolidation mechanisms in samples M10 and M1 (Tests 1 and 2) appear to have been compaction and adhesion between grains due to plastic flow. In sample AR (Test 3) there is much greater evidence of pressure solution and reprecipitation. It is remarkable that the marked effect on consolidation behavior was achieved with a moisture content of only 2.3% in a sample which had a initial porosity of 31%.

When sample AR was removed from the pressure vessel, the porous stones firmly adhered to the sample. (This was not observed in the other tests.) Moreover, later petrographic examination of the sample revealed that some salt had been precipitated in the porous stones. Accordingly, the porous stones were sawed off and the sample was reinserted in the pressure vessel. A permeability test was then conducted at a confining pressure of 2,500 psi (17.2 MPa). The permeability obtained was not significantly greater than that

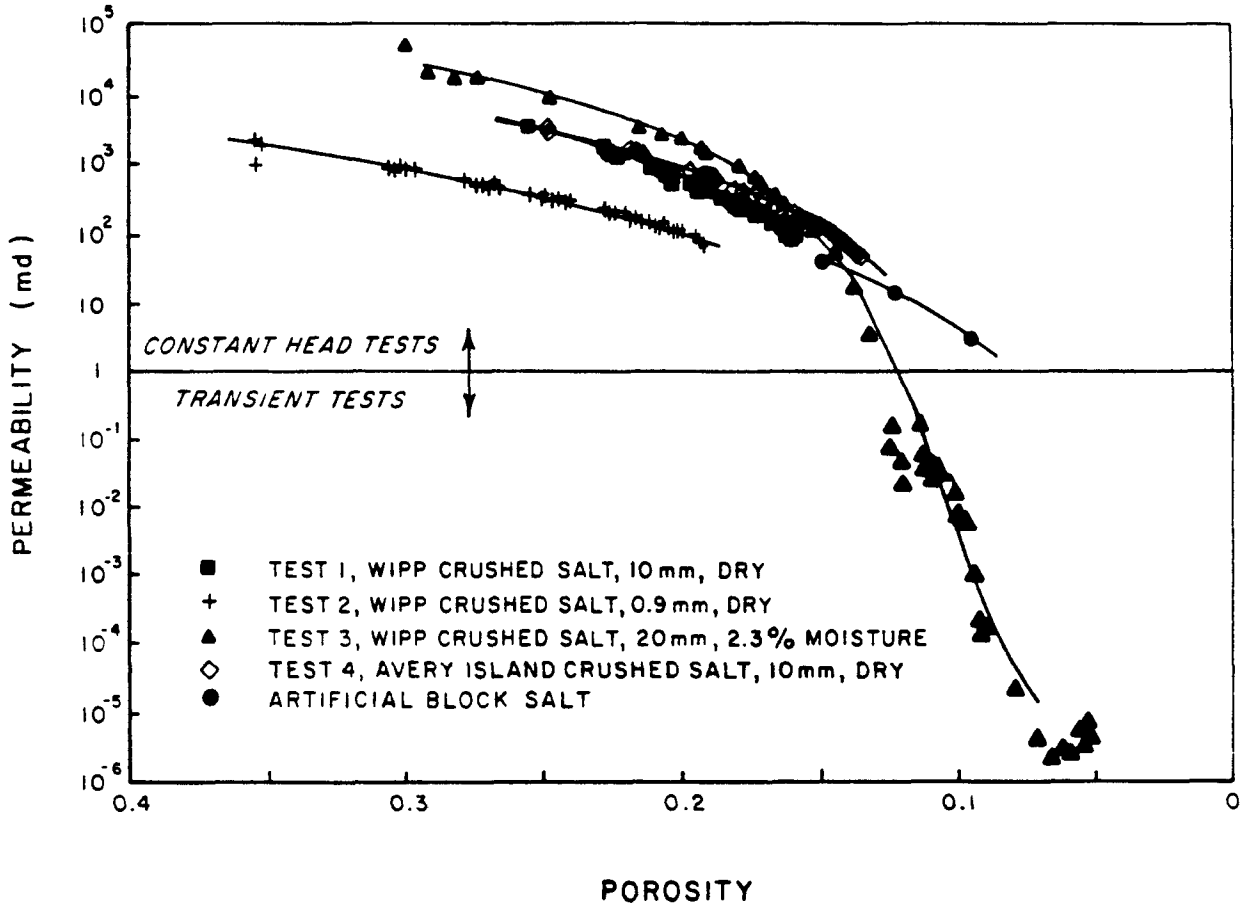

Permeability Versus Porosity for Consolidated Crushed Salt and Artificial Block Salt

Figure 3-4

obtained at the end of the initial test, indicating that clogging of the porous stones had not had a significant effect on the measured permeabilities.

3.4.2 Bulk Modulus

Bulk modulus was calculated for each quasi-static pressure increment (e.g., 0 to 50, 50 to 500 psi) from the pressure difference divided by the volumetric strain over the increment.

$$K = \frac{\Delta P}{\varepsilon_v}$$

where

K = bulk modulus
ΔP = pressure difference
ε_v = volumetric strain

The volumetric strain was calculated by the following method, analogous to that used to calculate "corrected porosity," described in Section 3.4.1.

$$\text{volumetric strain} = \frac{\text{volume change over pressure increment}}{\text{volume at beginning of pressure increment}}$$

where

$$\text{volume change at time t} = \frac{\text{axial strain at t}}{\text{total axial strain}} \times \text{total volume change}$$

The total volume change for the test was obtained from the difference between the initial and final measured volumes.

The data obtained are shown in Table 3-2 and Figure 3-5. For all samples, a relatively rapid increase in bulk modulus occurs below a porosity of about 0.25. Of the samples tested, the finer grained sample, M1 (Test 2), was found to be stiffer at equivalent porosities. This may occur because this sample was less graded (tending towards a more uniform grain size) than the other samples tested. Generally, the overall trend of the data from all tests agrees well with data obtained by previous workers as reported by IT Corporation (1984).

Table 3-2. Bulk Modulus of Consolidated Crushed Salt

Test No.	Sample No.	Pressure Increment (psi)[a]	Porosity range	Average Porosity	Bulk Modulus[b] (psi)
1	M10	0-50	0.262-0.255	0.259	6,200
		53-501	0.255-0.228	0.242	14,000
		504-994	0.223-0.211	0.217	33,400
		1,000-1,501	0.203-0.196	0.200	55,900
		1,498-2,003	0.189-0.185	0.187	94,000
		2,007-2,494	0.175-0.173	0.174	187,700
2	M1	0-49	0.36- 0.355	0.358	8,500
		53-496	0.353-0.310	0.332	8,200
		498-1,009	0.297-0.279	0.288	20,800
		1,011-1,506	0.267-0.255	0.261	29,900
		1,504-1,993	0.241-0.229	0.235	27,100
		2,003-2,505	0.218-0.215	0.217	120,800
		2,492-1,987	0.193-0.193	0.193	-6,276,500[c]
		1,999-994	0.193-0.194	0.193	1,561,900
3	AR	0-36	0.307-0.3	0.304	4,900
		53-499	0.274-0.247	0.261	15,100
		507-999	0.166-0.163	0.165	123,500
		1,039-1,522	0.109-0.109	0.109	545,900
		1,528-2,114	0.096-0.092	0.094	--[d]
		1,989-2,499	0.079-0.070	0.074	--[d]
		2,496-1,986	0.046-0.045	0.046	-583,300[c]
		1,977-999	0.046-0.045	0.046	-811,300[c]
4	AM10	0-55	0.256-0.252	0.254	12,600
		54-504	0.252-0.221	0.237	12.400
		501-1,001	0.217-0.200	0.209	23,700
		998-1,493	0.190-0.182	0.186	50,700
		1,494-1,990	0.171-0.167	0.169	97,200
		2,012-2,502	0.153-0.152	0.153	213,500

(a) 1 psi = 6.9 kPa.
(b) Pressure change divided by change in volumetric strain where volumetric strain is referenced to the volume at the beginning of the pressure increment.
(c) Negative values may occur because creep during pressure drop is greater than the elastic rebound.
(d) Axial strain not measured immediately after pressure application.

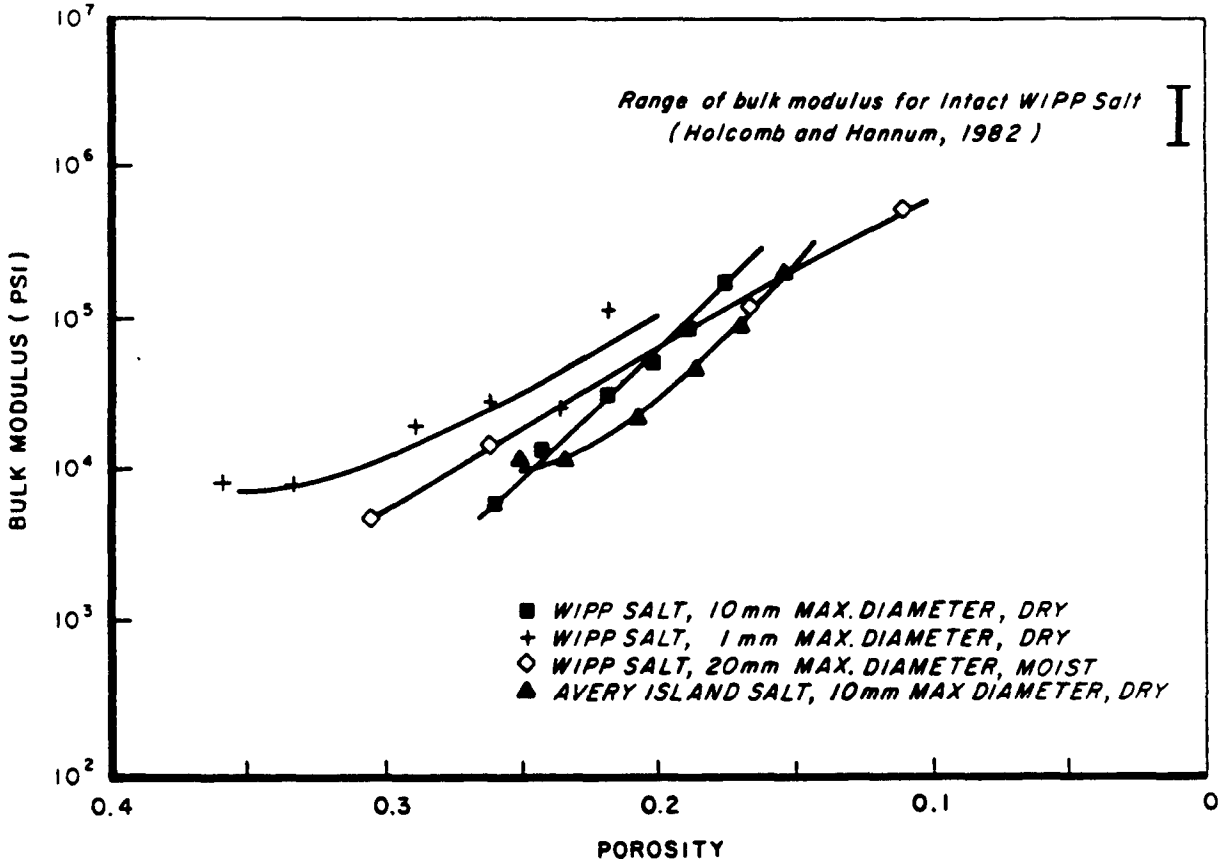

Bulk Modulus Versus Porosity for Consolidated Crushed Salt

Figure 3-5

4.0 FRACTURE HEALING TESTS

The objective of the fracture healing testing is to evaluate the degree to which fractures in salt heal when subjected to increasing confining stress. Healing is measured as change in permeability and increase in tensile strength. Permeability tests have been conducted on three types of salt and two types of fractures, as shown in Table 4-1. Tensile strength tests have been conducted on the same types of salt for sawcut fractures.

4.1 TEST APPARATUS AND PROCEDURES

4.1.1 Permeability Tests

Permeability testing of unfractured and fractured block salt and natural salt cores is conducted in a Hoek triaxial cell (Hoek and Franklin, 1968) (Figures 4-1 and 4-2). The sample is sealed from the lateral confining fluid by a urethane membrane along the circumference of the sample and an axial force is applied to the ends of the sample using a load frame to maintain a hydrostatic stress state. Other key test equipment includes a hydraulic pressure generator for maintaining the lateral stress on the sample and a gas supply and measuring system for permeating argon gas through the sample. Test data are monitored using various types of electronic sensors attached to a 16-channel A/D data acquisition module linked to a microcomputer which is equipped with a time module. Software packages have been designed for data acquisition, retrieval, and reduction. Specific equipment features and test methods are described in the following discussion.

4.1.1.1 Hoek Cell and Sample Preparation

The test chamber consists of a conventional Hoek triaxial cell with end platens that have been modified to allow gas flow through the test specimen. The cell and urethane membranes are designed to accommodate HQ-size (2.4-in [6.1-cm] nominal diameter) core samples. Unfractured samples are prepared by drilling oversize block samples with a diamond core barrel to a nominal diameter of 2.4 in (6.1 cm), and then cutting the sample to length with a bandsaw equipment with a carbide-tipped blade. The sample ends are polished using a grinding wheel or sandpaper. All sample preparation is conducted without cutting fluids to eliminate possible interactions between the salt sample and fluid that might affect the permeability test results. Considerable difficulty has been encountered in preparing the ends of coarse-grained crystalline salt samples due to chipping. The impact of these difficulties is minimized by controlling the rate of sample advance through the saw blade, banding the sample near the cut with pairs of metal straps to reduce chipping, and by preparing several samples and selecting those which are the least disturbed after end preparation has been completed.

Longitudinal fractures (tension or sawcut) are introduced after a sample has been tested in an unfractured state. In this way, baseline permeability data are available for each sample so that the impact of fracturing and healing processes can be assessed. The longitudinal tension fractures are

Table 4-1. Test Matrix for Fracture Healing Tests

Test No.	Sample No.	File Name	Salt Type	Fracture Type	Moisture Condition	Maximum Hydrostatic Stress (psi)[a]	Duration (days)
1	IT1-1	COHND	block	unfractured		3,000	1
2	IM1-1	COIND	block	unfractured		3,000	1
3	IB1-1	COLND	block	unfractured		3,000	1
4	(b)	COISD	block	saw	dry	3,000	3
5	(b)	COISM	block	saw	moist	3,000	2
6	IM1-1	COIFM[c]	block	split	moist	2,500	3
7	CR5	CRAND	WIPP	unfractured		3,000	2
8	CR5	CRAFD	WIPP	split	dry	2,500	2
9	CR6	CRAND2	WIPP	unfractured		2,500	1
10	CR6	CRAFM	WIPP	split	moist	2,500	3
11	CR7	CRAND3	WIPP	unfractured		2,500	1
12	CR7	CRASM	WIPP	saw	moist	2,500	2
13	AI1	AI1	Avery Is.	unfractured		2,500	7
14	AI1FD	AI1FD	Avery Is.	split	dry	2,500	7
15	AI3	AI3	Avery Is.	unfractured		2,500	8
16	AI3FM	AI3FM	Avery Is.	split	moist	2,500	8
17	I1	I1	block	unfractured		2,500	7
18	I1FD1	*1FD	block	saw	dry	2,500	10
19	I2	I2	block	unfractured		2,500	3
20	I2FM	I2FM	block	saw	moist	2,500	8

(a) 1 psi = 6.9 kPa.
(b) No sample number assigned.
(c) Same sample as COIND (Test 2).

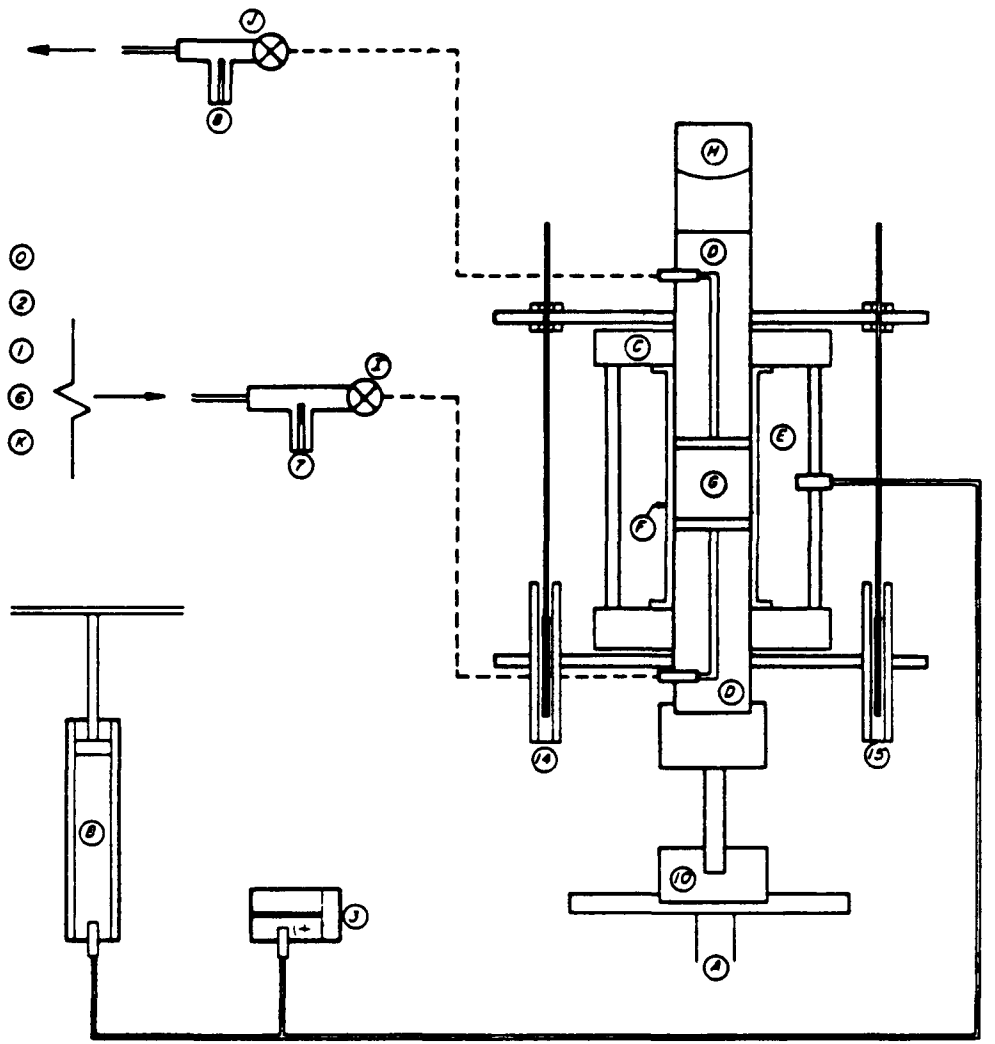

Legend

Hoek Cell Test Assembly for Steady State Test

Identification[a]	Description
0	Flowmeter for volumetric flowrate, mounted in pressure control panel
1	Pressure transducer for total upstream gas pressure (0-800 psi [0-55 MPa]), mounted in pressure control panel at downstream outlet of 2,250 cm^3 (0.6 gal) reservoir
2	Differential-pressure transducer (0 to 20 or 0 to 80 psi [0 to 138 or 0 to 552 kPa])
4	Pressure transducer for Hoek cell oil pressure (0 to 3,200 psi [0 to 22 MPa])
6	Temperature sensor adjacent to pressure transducer No. 1
7	Temperature sensor at sample inlet
8	Temperature sensor at sample outlet, all temperature sensor monitor temperature of argon permeant
10	Load cell (40-kip [177,920-N] capacity) for axial load on sample
14,15	(LVDTs) (±1/2-in [1.3-cm] travel) mounted on platens to monitor sample length change
A	Axial load applied by manually operating 10-ton (9-metric ton) load frame
B	Manually operated oil pressure generator for application of Hoek cell oil pressure, vernier readings provide means of determining sample volume change
C	Hoek cell
D	Platens (2) with gas ports to sample
E	Hoek cell oil pressurized by B
F	Hoek cell membrane
G	Prepared salt sample and porous stones
H	Swivel platen attached to load frame
I	Plug valve at sample inlet
J	Plug valve at sample outlet

(a) I.D. numbers refer to sensor connections to A/D converter.

Test Assembly for Steady-State Fracture Healing Tests

Figure 4-1

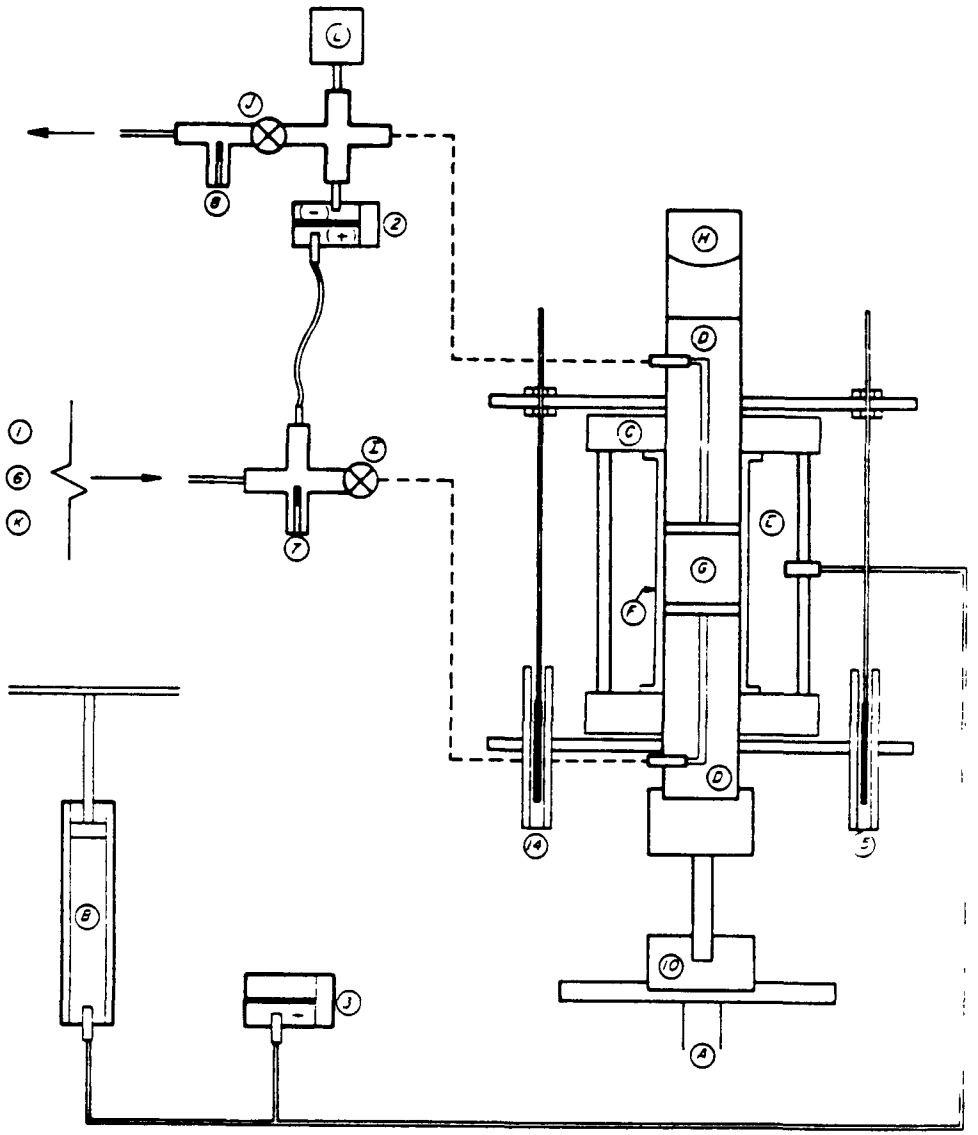

Legend

Hoek Cell Test Assembly for Transient Tests

Identification(a)	Description
1	Pressure transducer for total upstream gas pressure (0 to 800 psi [0 to 5.5 MPa]), mounted in panel at downstream outlet of 2,250-cm^3 (0.6 gal) reservoir
2	Differential-pressure transducer (variable range) for gas pressure drop across sample
3	Pressure transducer for Hoek cell oil pressure (0 to 3,200 psi ([0 to 5.5 MPa])
7	Temperature sensor at sample inlet
8	Temperature sensor at sample outlet, all temperature sensors monitor temperature of argon permeant
10	Load cell (40-kip [177,920-N] capacity) for axial load on sample
14,15	(LVDTs) (±1/2-in [1.3-cm travel]) mounted on platens to monitor sample length change
A	Axial load applied by manually operating 10-ton (9-metric ton) load frame
B	Manually operated oil pressure generator for application of Hoek cell oil pressure; vernier readings provide means of determining sample volume change
C	Hoek cell
D	Platens 2) with gas ports to sample
E	Hoek cell oil pressurized by B
F	Hoek cell membrane
G	Prepared salt sample and porous stones
H	Swivel platen attached to load frame
I	Plug valve at sample inlet
[illegible]	Plug valve at sample outlet

(a) I.D. numbers refer to sensor connections to A/D converter.

Test Assembly for Transient Fracture Healing Tests

Figure 4-2

created by pushing a brick chisel into the sample using a screw-type loading mechanism. Nominal length-to-diameter ratios of 0.5 to 0.6 are required to maintain a vertical fracture through the sample. Sawcut samples are prepared using a bandsaw (artificial salt) or a metal wire hand saw (natural salt). Fractures are moistened (in some tests) by spraying the surface with a fine mist of tap water.

After the sample is assembled in the triaxial cell, two LVDTs are secured to the load platens using bracket supports. The LVDTs are used to monitor axial deformation of the sample.

4.1.1.2 Confining Pressure System

Confining pressure is maintained in the Hoek cell using a screw-type pressure generator. Because the position of the piston in the pressure generator remains fixed unless it is manually adjusted, the pressure in the sealed system fluctuates somewhat due to changes in sample volume and changes in the ambient temperature, but the fluctuations are typically less than $\pm$25 psi (173 kPa). The confining pressure is monitored by an electronic pressure transducer and the oil volume entering or leaving the vessel can be measured by a vernier attached to the pressure generator. The latter feature permits changes in the sample diameter to be monitored by correcting the displaced oil volumes for system compliance.

4.1.1.3 Permeability Test System

The key elements of the permeability test system are an interchangeable set of precision gas regulators (0 to 7, 0 to 200, and 0 to 500 psi [0 to 48 kPa, 0 to 1.4 MPa, and 0 to 3.45 MPa]) for controlling gas flowrates through the sample, an electronic differential-pressure transducer for measuring sample and system head losses during gas flow, and an electronic flowrate sensor. The possible wide range of permeabilities which must be measured (i.e., <0.1 md to 1,000 md) necessitates the use of different test methods and equipment depending on the sample type and condition.

For constant-head (steady-state) tests, a 0 to 20-psi (0 to 138-kPa) electronic differential-pressure transducer and a 0.01 to 5.0-l/min. (0.003 to 1.3-gpm) flowmeter are used (Figure 4-1). With this test method, corrections are applied to measured differential pressures to account for system head losses associated with the system plumbing and the porous stones located at each end of the sample. The effects of system head losses are minimized by placing the differential-pressure transducer as close as possible to the sample.

For samples having permeabilities <0.1 md, transient pressure-decay tests are used. These tests require sealed, high-pressure reservoir systems upstream and downstream from the sample, 0-20 to 0-500 psi (0-138 kPa to 0-3.45 MPa) electronic differential-pressure transducers, and 0-800 to 0-3,200 psi (0-5.5 to 0-22 MPa) electronic pressure transducers for measuring the total system pressure in the reservoirs (Figure 4-2). Corrections for system head loss are not applied due to the very low flowrates that are generated during transient testing.

4.1.1.4 Instrumentation

The relatively rapid response of the salt samples to changes in pressure gradients requires a monitoring system that is able to adjust to changing test conditions. Consequently, several electronic sensors are used to provide the needed response rate. The array of electronic test sensors consists of the following:

- Flowmeter (0.01 to 5.0 l/min [0.003 to 1.3 gpm]) constant-head tests only
- Differential-pressure transducer (0 to 20, 0 to 80, 0 to 500 psi [0 to 138 kPa, 0 to 552 kPa, 0 to 3.45 MPa])
- Pressure transducer (0 to 800, 0 to 3,200 psi [0 to 5.5, 0 to 22 MPa]), transient tests only
- Confining-pressure transducer (0 to 3,200 psi [0 to 22 MPa])
- Three temperature sensors (0 to 30°C)
- Two axial deformation LVDTs ($\pm$ 1/2 in [$\pm$ 1.3 cm])
- Load cell (0 to 40,000 lb [0 to 18,182 kg]).

All sensors are calibrated and traceable to NBS. For purposes of data reduction, regression analyses (correlation coefficients >0.9998) have been performed to numerically relate sensor output to the measured parameter.

All of the sensors are monitored using a 16-channel, 12-bit precision analog/digital data acquisition module linked to a 64-K Apple II microcomputer which is equipped with a time module. Test-specific software packages have been developed to allow data reduction. All software has been verified to assure the correctness of computed test results.

4.1.1.5 Test Procedures

Constant-head permeability tests are conducted by permeating argon gas up through the test specimen using a range of pressure gradients. Typically, four pressure gradients are used in addition to a series of readings at zero gradient, which act as a baseline or null reference for the differential-pressure transducer and flowmeter readings. Pressure gradients are selected to maximize the output of the flowmeter, which is nonlinear at low flowrates. Usually three readings of test sensors are taken at each gradient within a 30-sec interval. Accordingly, less than 10 min is required to conduct and reduce the test data for each test.

Transient tests are conducted by elevating the pressure in the permeability test system to a nominal pressure of approximately 500 psi (3.45 MPa). This high back-pressure is needed in order that the argon gas should behave as an incompressible fluid for the pressure gradients imposed during transient testing. The pressure in the upstream reservoir is then increased relative to the start of the test. The test is initiated by opening the downstream

reservoir valve and periodically measuring changes in the differential pressure across the sample as the sealed pressures between the upstream and downstream reservoir systems equilibrate. A range of differential pressures and test time intervals was used depending on the permeability of the sample. Differential pressures were selected to try to minimize both the difference in effective stress between the ends of the sample and the time required to conduct the test. Differential pressures ranged from 20 to 500 psi (138 kPa to 3.45 MPa). Test durations ranged from less than 10 min to several hours. Detailed test procedures are given in Appendix B.

4.1.2 Tensile Strength Tests

Tensile strength tests were conduced on 2.4-in- (6.1-cm-) diameter samples consolidated in a soils consolidometer (Figure 4-3) under normal loads up to 500 psi (3.45 MPa) for periods up to 8 days. The test procedure is simple and, by comparison of the results against the tensile strength of unfractured samples, provides a valuable index of fracture healing.

The samples placed in the 2.5-in- (6.4-cm-) diameter consolidometer were 2.4-in- (6.1-cm-) diameter cores, 1.25 to 1.75 in (3.2 to 4.4 cm) in height. End preparation consisted of saw cutting, then polishing both ends. Samples were then sawed in half and each end flipped so that polished surfaces mated for the healing test. Irregularities were ground off the sawcut surfaces. Because of the relatively large sample diameter relative to the height, it was not possible to prepare test specimens with tensile fractures. For tests on moistened fractures, each surface was blotted with a damp towel prior to placement in the consolidation unit. Samples were consolidated for 7 to 8 days at nominal pressures of 5, 50, 100, and 500 psi (34.5, 345, 690, and 3,450 kPa). Consolidation pressures were corrected for the diametrical difference of the consolidometers and the samples tested. Bulging of some samples was noted at higher consolidation pressures.

The healed samples were secured to 4-in- (10.2-cm-) square wooden end platens with 3M Brand Scotchweld Structural Adhesive* and allowed to set for 24 hr. Tacks were used to center the samples on the platens while the adhesive hardened. The tensile load was applied to the sample through eye bolts attached to each end platen. Two methods were used to apply tensile loads to the sample: a direct-load method for tensile strengths up to approximately 7 psi (48 kPa), and a lever-arm method for tensile strengths greater than 7 psi. Direct loading was performed by suspending the sample and end-platen assembly between a frame and pail. The pail was then gradually filled with sand until failure occurred. The lever arm test was conducted in a similar manner, except that loading was supplied through a lever-arm apparatus which offered a mechanical advantage of five over the direct load method.

---

* Registered trademark of Minnesota Mining and Manufacturing Company (3M).

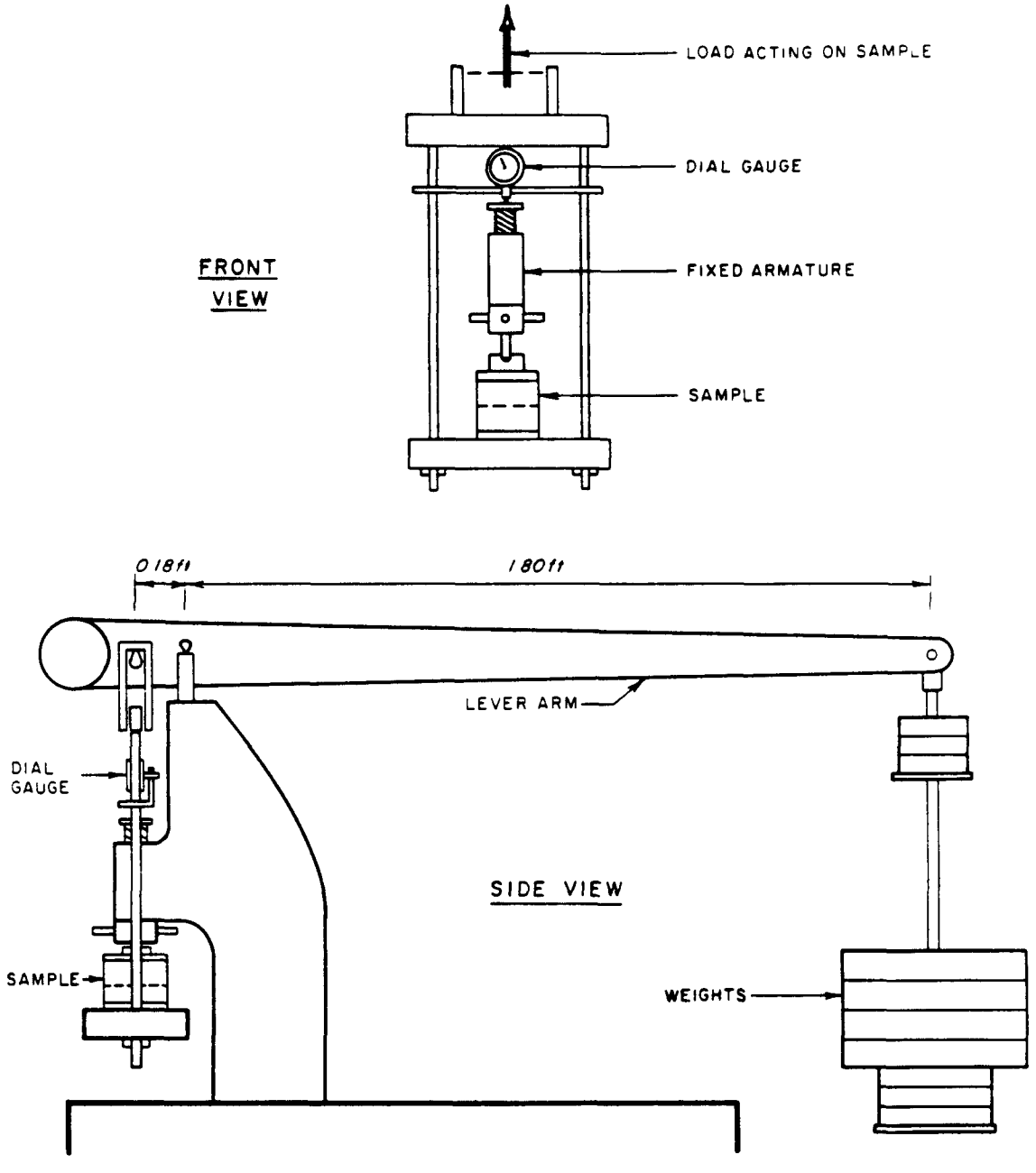

NOTE: SCHEMATIC SHOWS EQUIPMENT FOR CONSOLIDATING SAMPLES PRIOR TO STRENGTH TESTS

Test Assembly for
Tensile Strength
Fracture Healing Tests

Figure 4-3

4.2 SAMPLE DESCRIPTIONS

Fracture healing tests have been conducted on three types of salt: bedded salt from WIPP, dome salt from Avery Island, and artificial block salt manufactured by International Salt Company.

4.2.1 WIPP Salt

The general characteristics of the WIPP salt have been described in Section 3.2.1. The samples used in the fracture healing tests were obtained from a depth interval of 0.9 to 1.4 ft (27.4 to 42.6 cm) in the floor of Test Room No. 4. The salt is a clear-to-light-red halite with a trace of polyhalite. The crystal size ranges from 5 to 40 mm (0.2 to 1.6 in) with most crystals in the test specimens in the range 5 to 15 mm (0.2 to 0.6 in). There is no visible fabric and the impurity content is about 1%.

The permeability of intact WIPP salt has been measured as a function of confining pressure by Sutherland and Cave (1980) and DOE (1983). These tests demonstrated that the permeability of even "intact" samples is strongly dependent on confining pressure. Permeabilities measured under low confining pressure may be as high as 1,000 md, whereas at higher confining pressures (>2,000 psi [13.8 MPa]) measured permeabilities are generally <1 μd and as low as 0.01 μd. Sutherland and Cave concluded that the permeability of undisturbed unfractured salt in situ is less than 5×10^{-2} μd. Strength and elastic properties are summarized by Hansen et al. (1982). The mean indirect tensile strengths obtained from two data sets (two levels in an exploratory borehole) were 1.26 MPa (183 psi) and 1.63 MPa (236 psi).

Fractures were created by cutting with a bandsaw and by splitting. Fractures created with the bandsaw are smooth with no discernible roughness. Fractures created by splitting follow crystal boundaries and cleavage faces and have a typical roughness amplitude in the range 5 to 10 mm (0.2 to 0.4 in).

4.2.2 Avery Island Salt

The Avery Island salt has been described in Section 3.2.2. The samples tested by IT were a white-to-gray, visually very pure rock salt with a range of crystal sizes from 1 mm to 15 mm (0.04 to 0.6 in). Banding of white and gray salt was visible in the large (0.3 by 0.3 by 0.4-m [1 by 1 by 1.3-ft]) block received by IT, but not in the test specimens that were prepared by drilling approximately perpendicular to the banding. By comparison with the WIPP salt, the Avery Island salt (as tested) was finer and purer.

Strength and elastic properties of intact Avery Island salt are given by Hansen and Mellegard (1980). The mean indirect (Brazilian) tensile strength was 1.17 MPa (170 psi) with a range from 0.83 to 1.79 MPa (120 to 260 psi).

Fractures were created with a bandsaw and by splitting, and have roughness profiles similar to those described above for WIPP salt.

4.2.3 Block Salt

The International Salt Company artificial block salt has been described in Section 2.1. As with the natural salt, fractures were created with a bandsaw and by splitting. The sawcut fractures were very smooth, whereas the split fractures had a roughness amplitude of 2 to 3 mm (0.08 to 0.12 in).

4.3 PERMEABILITY TESTS

Permeability tests were conducted using either the transient or the steady-state technique described in Section 4.1.1, whichever was more appropriate for the permeability range measured. Generally, the steady-state method was used for permeabilities greater than about 1 md. The estimated maximum possible error for the method is ± 3 md or 10%, whichever is greater (Appendix C). This suggests that the method is not completely reliable for permeabilities less than about 10 md. With the transient method, the estimated possible error related directly to instrument readings is $\pm 10^{-6}$ md or 1%. As noted in Appendix C, however, a significantly greater error may occur in the interpretation of the results. This process requires establishing a linear portion of a semilog pressure decay versus time plot. In many cases the plots did not include an obviously linear portion and there is some subjectivity in curve fitting. It is estimated that this could result in an error of $\pm 50\%$. This error does not have major practical significance given that changes in permeability of up to several orders of magnitude are recorded in the tests.

4.3.1 WIPP Salt

Permeability tests were conducted at hydrostatic pressures up to 3,000 psi (20.6 MPa) at room temperature (approximately 21°C). Tests were conducted at 50 or 500 psi (345 kPa or 3.45 MPa) mean effective confining pressure and at 500 psi increments to a maximum of 2,500 or 3,000 psi (17.2 or 20.6 MPa). For some samples the maximum confining pressures were maintained for a period of up to 46 hr and the permeability test was repeated. Test results are shown in Figures 4-4 and 4-5 as permeability plotted versus confining pressure.

All of the samples, unfractured as well as fractured, showed a strong dependence of permeability on confining stress, suggesting a significant degree of sample disturbance. In this regard, it is noteworthy that the CR5 sample used in Test 7 (Figure 4-5), which had been preloaded prior to fracture healing testing, showed a significantly lower permeability than the other unfractured samples at corresponding confining pressures.

The sawcut fracture (Test 12) had a higher permeability than the equivalent tensile fracture (Test 10). This may have occurred because of better "mating" or because the tensile fracture is more tortuous. In terms of permeability (comparing Tests 8 and 10) there does not appear to be a significant difference in healing behavior between moist and dry fractures, although petrographic examination (Appendix A) suggests a greater degree of healing in the moist sample. Permeability continued to reduce as the confining pressure was maintained at a constant level, suggesting that healing was occurring.

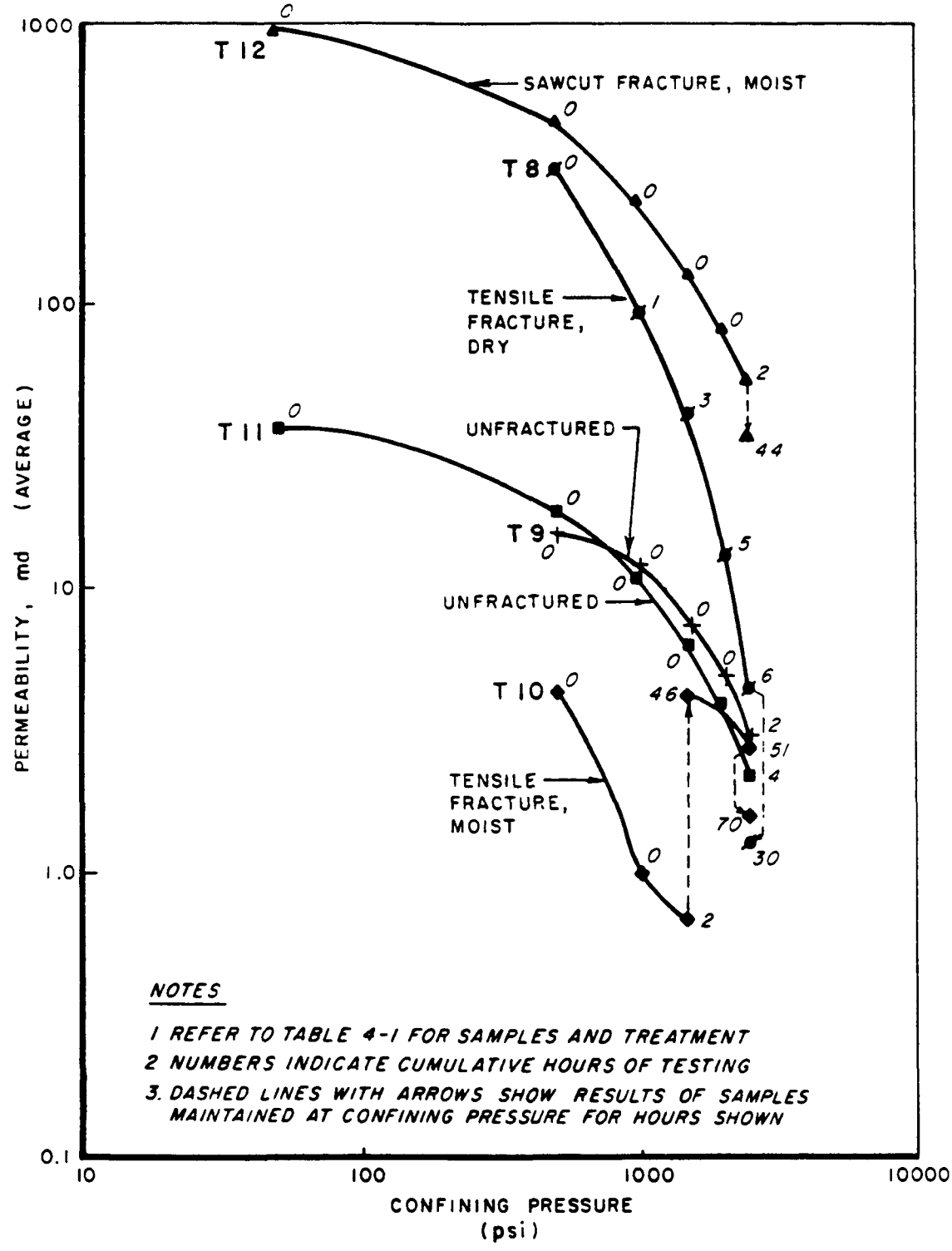

Fracture Healing Results
for Natural WIPP Salt

Figure 4-4

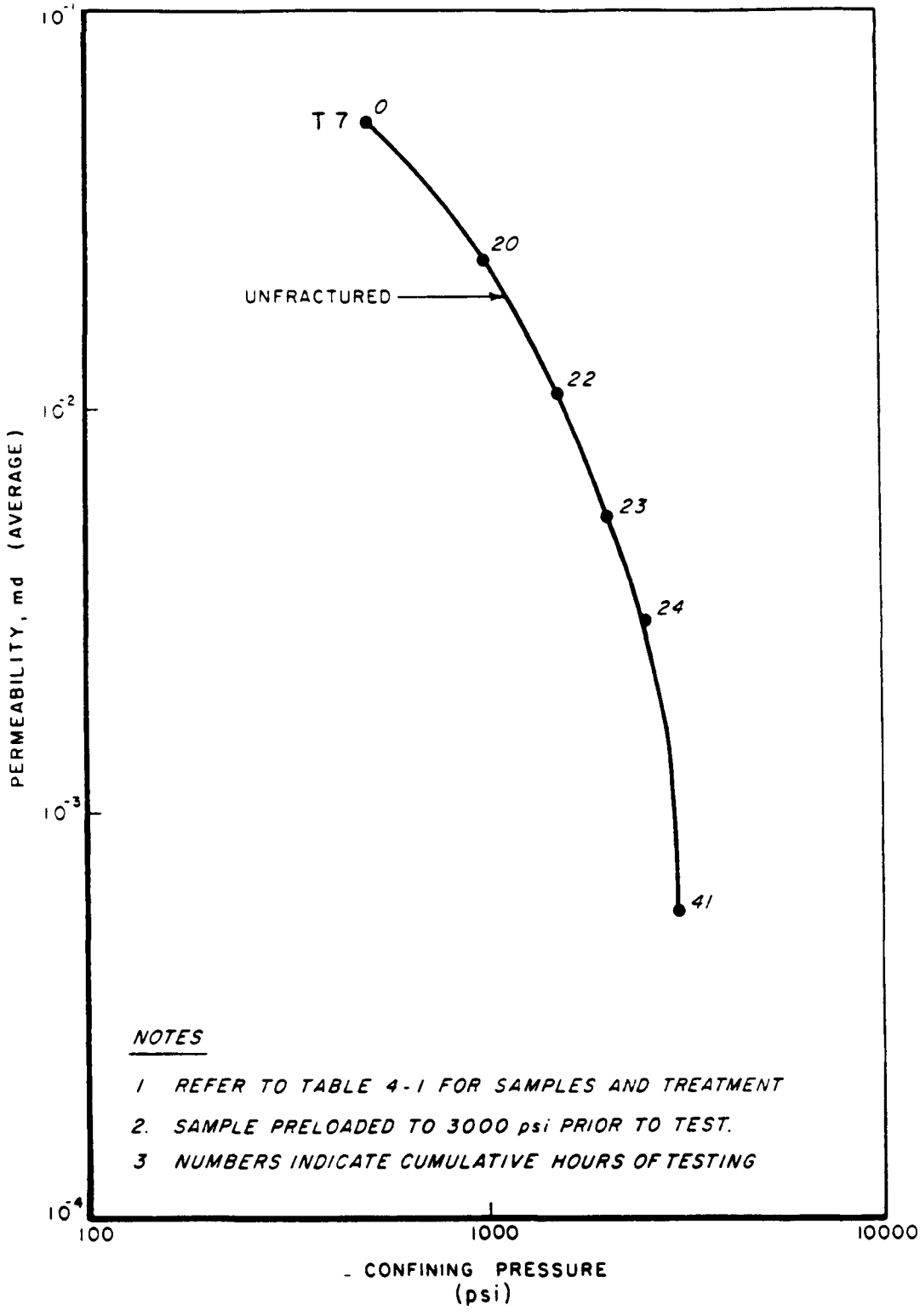

Fracture Healing Results for Natural WIPP Salt (Test 7)

Figure 4-5

One unexpected result occurred in Test 10 (natural salt with moist fracture, Figure 4-4), which showed an initial permeability well below that obtained for the unfractured sample and a rapid decline in permeability with increased confining pressure. With increased time of application of confining pressure, however, permeability returned to the initial level. At present the cause of this phenomenon is not known but may be related to fracture healing in the sample induced by the water introduced in the fracture, or it may indicate an equipment problem. No equipment malfunctions were indicated by subsequent checks.

4.3.2 Avery Island Salt

Tests were conducted on two intact samples of Avery Island salt and repeated on the same samples after a sawcut fracture had been made. One fracture was tested dry and the other moist, after blotting with a moist towel. All samples were loaded quasistatically at 500-psi (3.45-MPa) increments to a maximum hydrostatic load of 2,500 psi (20.6 MPa), which was maintained for approximately 7 days. All tests were conducted at room temperature (approximately 21°C).

Figure 4-6 shows permeability versus confining pressure for one of the samples (AI1). Essentially the same behavior was exhibited before and after fracturing. (The other sample [AI2] also showed essentially the same behavior [Appendix D].) As the confining pressure was increased from 50 to 2,500 psi, permeability decreased by about two orders of magnitude. Permeability continued to decrease as the confining pressure was maintained and then increased slightly as the pressure was reduced. Figure 4-7 shows the effect of time more clearly for both samples. In these tests, there was no major difference in degree or rate of healing between the moist and dry fractures.

4.3.3 Block Salt

In the Phase 1 tests (maximum duration 2 days), two of the fractured samples (both with sawcut fractures, Tests 4 and 5) showed a reduction in permeability of approximately an order of magnitude with increased confining pressure (Figure 4-8). In contrast, the sample with the tension fracture (Test 6) showed little reduction in permeability. In this case the results from the fractured sample were essentially the same as those obtained from the same sample prior to fracturing (Test 2). This effect was possibly seen because of the good mating between the two fracture surfaces. Tests 4 and 5 showed no significant difference which could be related to the moisture condition of the fracture.

In Phase 2 tests, two samples of International block salt were tested before and after fracturing. Both fractures were saw cut; one was tested dry and the other moist. All samples were loaded quasistatically at 500-psi (3.45-MPa) increments to a maximum hydrostatic load of 2,500 psi (20.6 MPa), which was maintained for approximately 7 days. All tests were conducted at room temperature (approximately 21°C).

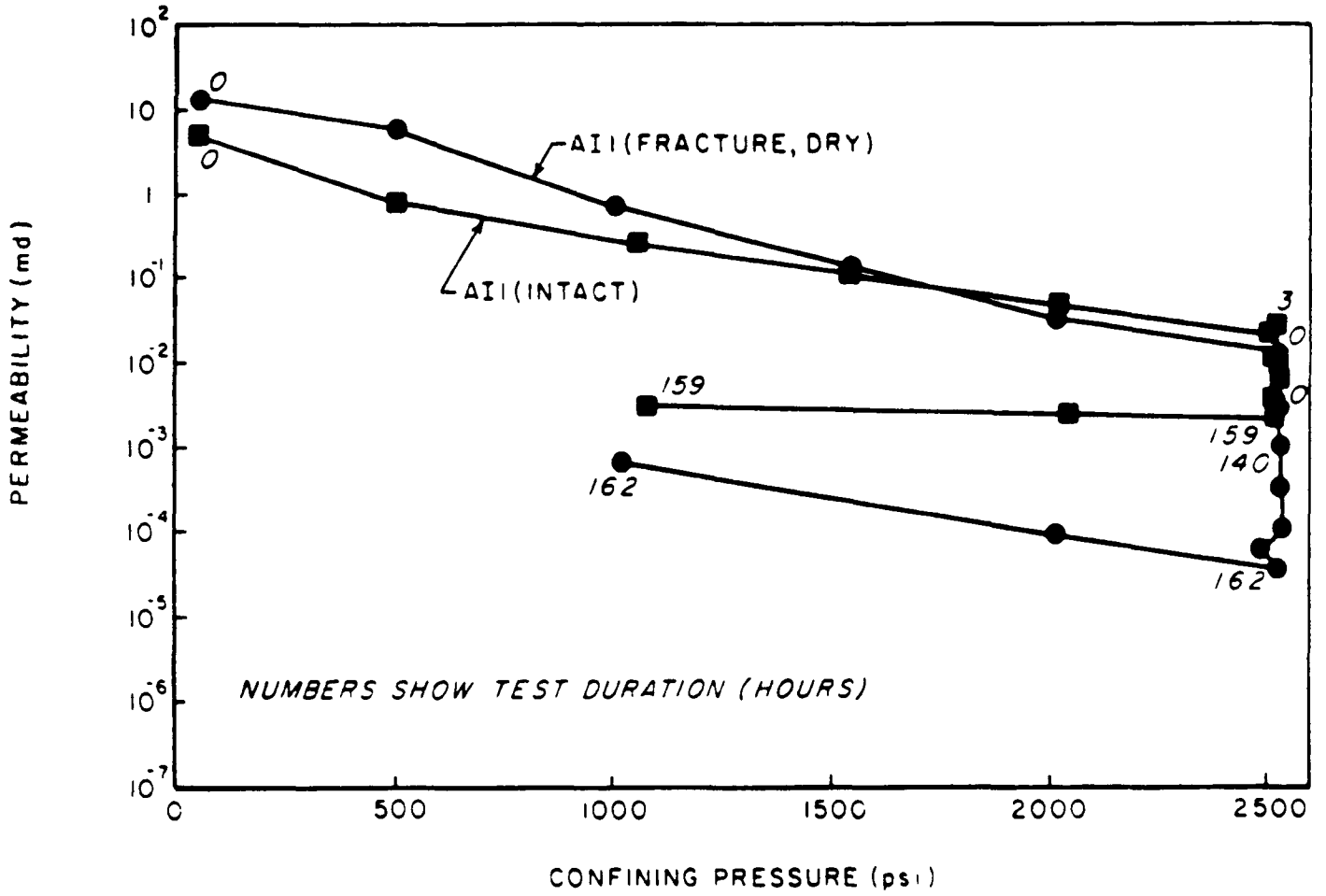

Permeability Versus Confining Pressure, Avery Island Salt

Figure 4-6

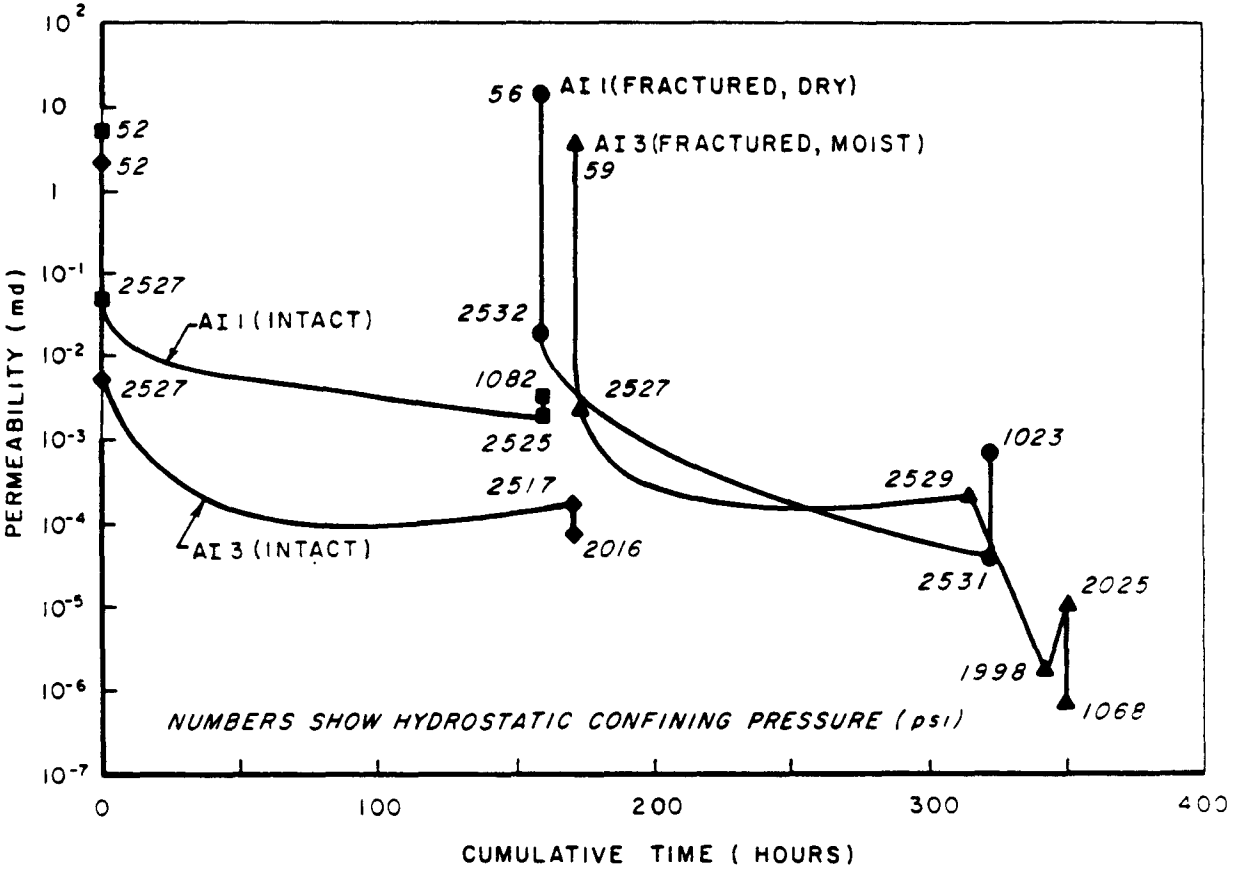

Permeability Versus Time, Avery Island Salt

Figure 4-7

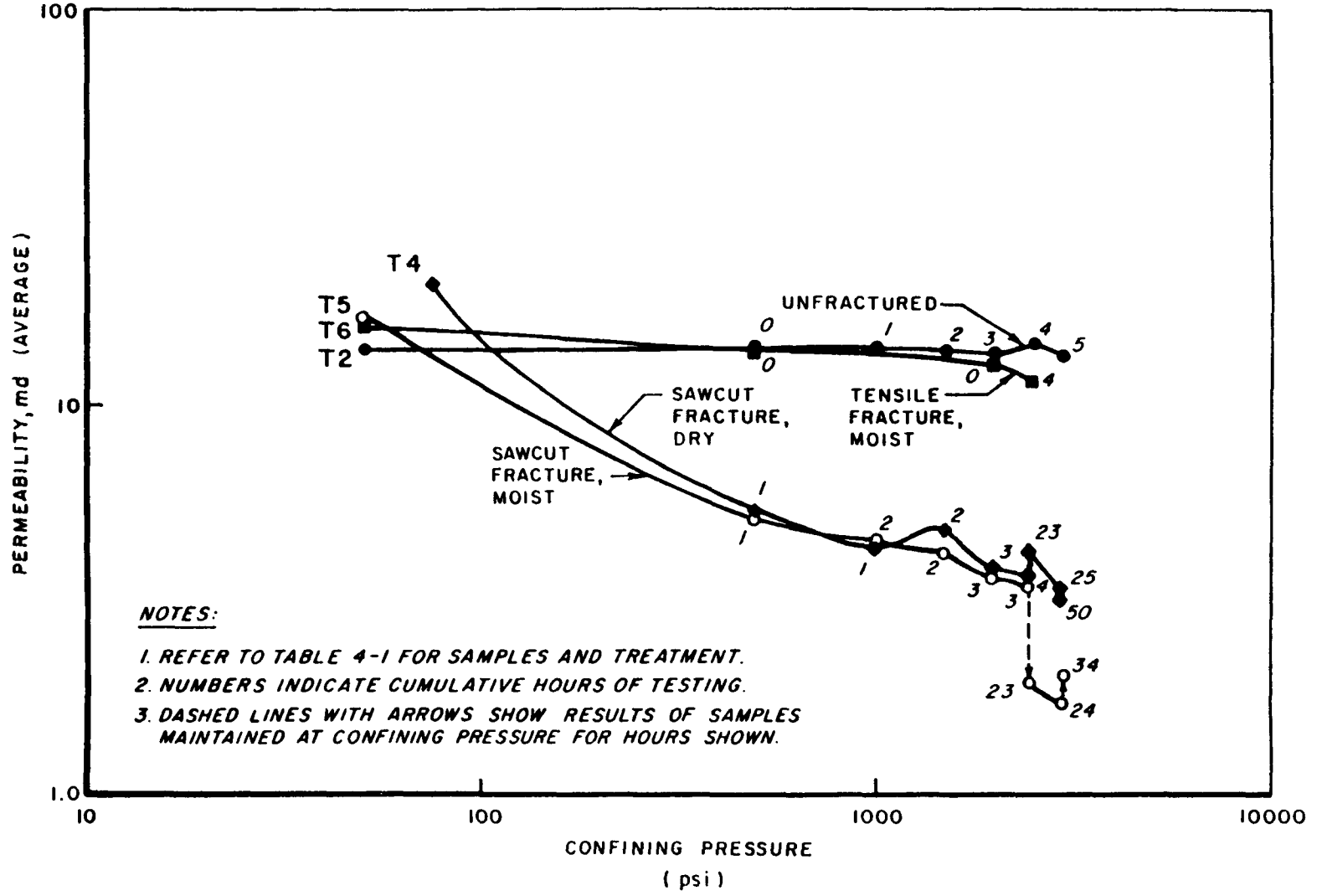

Fracture Healing Results for the Block Salt (Phase 1 Tests)

Figure 4-8

Figure 4-9 shows permeability versus confining pressure for one of the samples (I2) before and after fracturing. (The other sample showed essentially the same behavior.) Before fracturing, the permeability reduced slightly between 50 psi and 500 psi confining pressure, but was essentally constant at pressures above 500 psi. This behavior would be expected for a material in which the porosity is due to spherical pores and which contains few microfractures. After fracturing, the permeability at 2,500 psi was the same as that at the same pressure prior to fracturing. Figure 4-10 shows permeability as a function of time for both samples before and after fracturing, confirming that permeability was essentially constant after an initial reduction during loading.

4.4 TENSILE STRENGTH TESTS

Tensile strengths were measured for fractured samples which had been loaded in a soils consolidometer, using the methods described in Section 4.1.2. Each sample was loaded for 7 or 8 days at normal loads acting across the fracture varying from 4 to 544 psi (27.6 kPa to 3.75 MPa). Because of difficulties encountered in splitting the relatively thin samples, only saw-cut fractures were tested. Both natural salt (Avery Island) and block salt (International) were tested.

The results obtained are summarized in Table 4-2. For the block salt, a significantly greater degree of healing is observed for the fractures which were moistened prior to consolidation. After 7 or 8 days consolidation at approximately 500 psi (3.45 MPa), the average tensile strength of 3 moistened fractures was about 60 psi (413.7 kPa). This is about 40% of the tensile strength of a single intact specimen of block salt. In contrast, the tensile strength of a dry fracture after 7 days consolidation at 544 psi was only 2.1 psi (14.5 kPa). The Avery Island salt also exhibited a much lower degree of healing after 7 days consolidation, regardless of moisture condition.

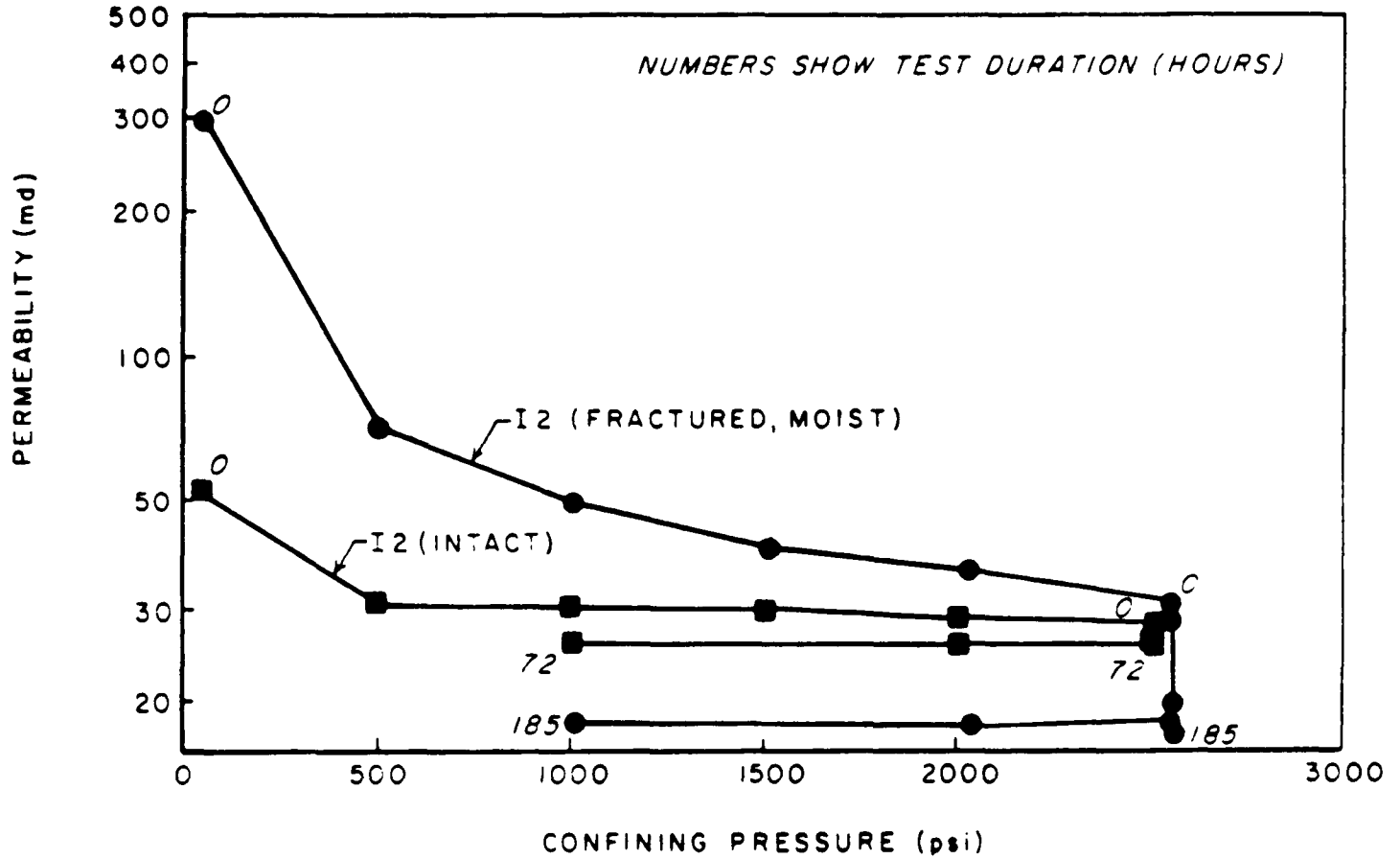

Permeability Versus Confining Pressure, Block Salt

Figure 4-9

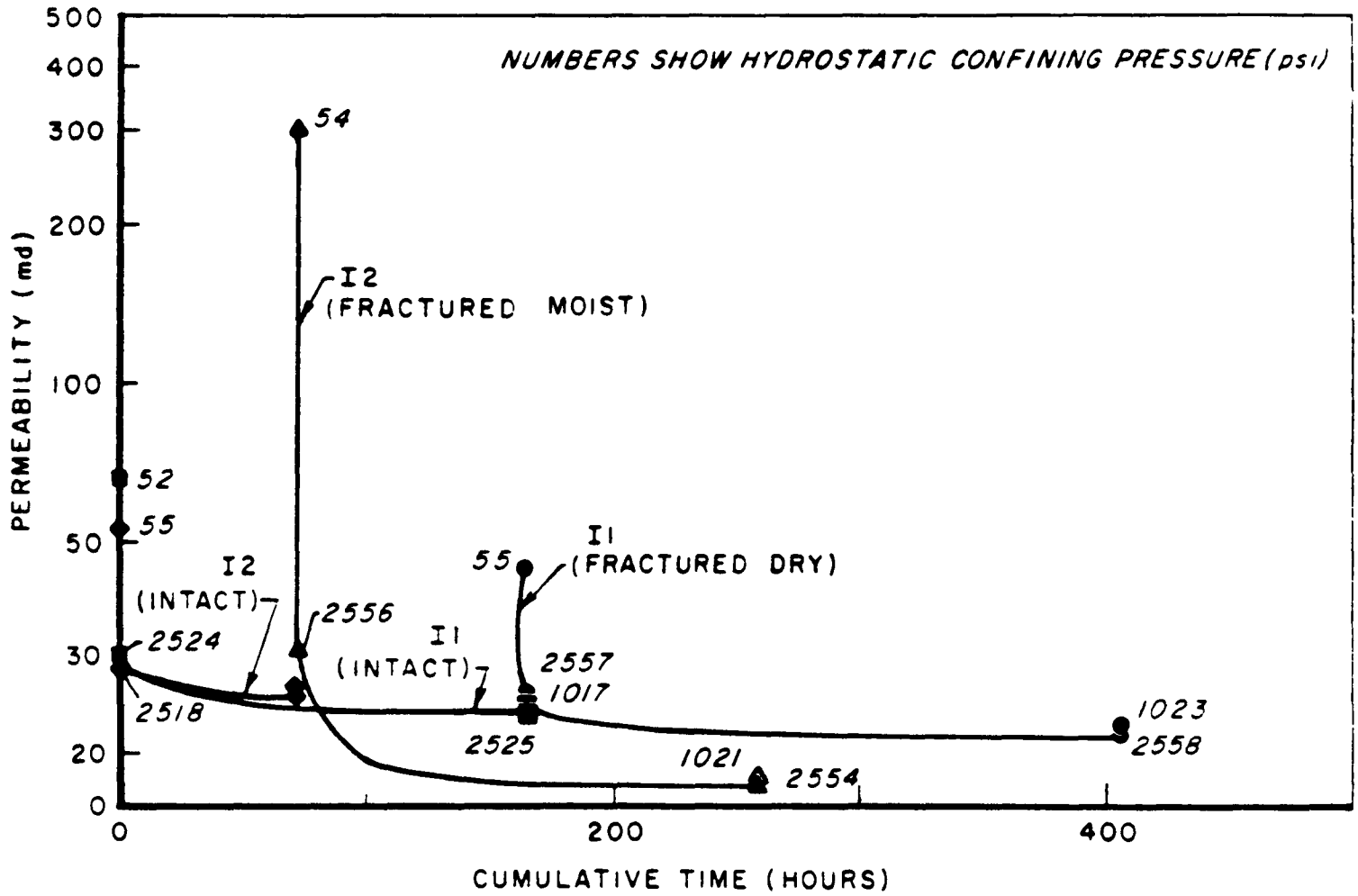

Permeability Versus Time, Block Salt

Figure 4-10

Table 4-2. Tensile Strength Tests Results

Type of Salt	Fracture Type	Moisture condition	Consolidation Pressure (psi)[a]	Consolidation Time (days)	Tensile Strength (psi)
block	saw	moist	4	8	3
			8	8	5
			15	8	6
			30	8	10
			60	8	19
			120	7	(b)
			178	7	56
			223	7	18
			293	7	18
			458	7	56
block	intact	--	--	--	141
block	saw	dry	6	7	(c)
			60	7	1.9
			60	7	0.8
			121	7	1.5
			544	7	2.1
block	saw	moist	6	7	0.9
			60	7	9.4
			60	7	8.7
			121	7	10.8
			544	7	50.9
block	saw	moist	6	7	1.2
			60	7	2.6
			60	7	2.5
			121	7	(b)
			544	7	67.8
Avery Is.	saw	dry	6	7	(c)
			60	7	(c)
			60	7	(c)
			121	7	(c)
			544	7	1.2
Avery Is.	saw	moist	6	7	6.6
			60	7	12.9
			60	7	(b)
			121	7	(b)
			544	7	5.3

(a) 1 psi = 6.9 kPa.
(b) Failed during preparation for strength testing.
(c) Unhealed.

5.0 REFERENCES

American Society for Testing and Materials. Moisture-Density Relations of Soils and Soil Aggregate Mixtures Using 5.5-lb (2.49-kg) Rammer and 12-in. (305-mm) Drop, ASTM D698, Philadelphia, PA.

American Society for Testing and Materials. Relative Density of Cohesionless Soils, ASTM D2049, Philadelphia, PA.

ASTM, see American Society for Testing and Materials.

Brace, W. F., J. B. Walsh, and W. T. Frangos, 1968. "Permeability of Granite Under High Pressure," Journal of Geophysical Research, Vol. 73, pp. 2225-2236.

Carter, N. L., and F. D. Hansen, 1983. "Creep of Rocksalt," Tectonophysics, Vol. 92, pp. 275-333.

DOE, see U.S. Department of Energy.

Hansen, F. D., and K. D. Mellegard, 1980. Quasi-Static Strength and Deformational Characteristics of Domal Salt from Avery Island, Louisiana, ONWI-116, prepared by RE/SPEC Inc. for Office of Nuclear Waste Isolation, Battelle Memorial Institute, Columbus, OH.

Hansen, F. D., K. D. Mellegard, and P. E. Senseny, 1982. "Elasticity and Strength of Ten Natural Rock Salts," Proceedings of the First Conference on the Mechanical Behavior of Salt, Pennsylvania State University, State College, PA.

Herrmann, W., and H. S. Lauson, 1981. Analysis of Creep Data for Various Natural Rock Salts, SAND81-2567, Sandia National Laboratories, Albuquerque, NM.

Herrmann, W., W. R. Wawersik, and H. S. Lauson, 1980. Analysis of Steady-State Creep of Southeastern New Mexico Bedded Salt, SAND80-0558, Sandia National Laboratories, Albuquerque, NM.

Hoek, E., and J. A. Franklin, 1968. "A Simple Triaxial Cell for Field and Laboratory Testing of Rock," Transactions of the Institute for Mining and Metallurgy, London, Section A, Vol. 77, pp. 22-26.

Holcomb, D. J., and D. W. Hannum, 1982. Consolidation of Crushed Salt Backfill Under Conditions Appropriate to the WIPP Facility, SAND82-0630, Sandia National Laboratories, Albuquerque, NM.

Hsieh, P. A., J. V. Tracy, C. E. Neuzil, J. B. Bredehoeft, and S. E. Silliman, 1981. "A Transient Laboratory Method for Determining the Hydraulic Properties of 'Tight' Rocks; I - Theory," International Journal of Rock Mechanics, Mining Sciences and Geomechanics Abstracts, Vol. 18, pp. 245-252.

IT Corporation, 1984. Assessment of Crushed Salt Consolidation and Fracture Healing Processes in a Nuclear Waste Repository in Salt, BMI/ONWI-546, prepared for Office of Nuclear Waste Isolation, Battelle Memorial Institute, Columbus, OH.

Jacoby, C. H., 1977. Geology - Hydrology of Avery Island Salt Dome, Y/OWI/SUB-77/16523/1, Office of Waste Isolation, Union Carbide Corporation, Oak Ridge, TN.

Kelsall, P. C., J. B. Case, W. E. Coons, J. G. Franzone, and D. Meyer, 1984. Schematic Designs for Penetration Seals for a Repository in the Permian Basin, BMI/ONWI-564, prepared by IT Corporation for Office of Nuclear Waste Isolation, Battelle Memorial Institute, Columbus, OH.

Mellegard, K. D., and P. E. Senseny, 1981. Exponential-Time Creep Law for Avery Island Salt, ONWI-329, prepared by RE/SPEC Inc. for Office of Nuclear Waste Isolation, Battelle Memorial Institute, Columbus, OH.

Nelson, J. W., and P. C. Kelsall, 1984. "Prediction of Long-Term Creep Closure in Salt," 25th Symposium on Rock Mechanics, Society of Mining Engineers, New York, NY, pp. 1115-1125.

Neuzil, C. E., C. Cooley, S. E. Silliman, J. D. Bredehoeft, and P. A. Hsieh, 1981. "A Transient Laboratory Method for Determining the Hydraulic Properties of 'Tight' Rocks; II - Application," International Journal of Rock Mechanics, Mining Sciences and Geomechanics Abstracts, Vol. 18, pp. 253-258.

Powers, D. W., S. J. Lambert, S. E. Shaffer, L. R. Hill, and W. D. Weart, eds., 1978. Geological Characterization Report, Waste Isolation Pilot Plant Site, Southeastern New Mexico, SAND78-1596, Sandia National Laboratories, Albuquerque, NM.

Ratigan, J. L., and R. A. Wagner, 1978. "Thermomechanical Analysis of Crushed-Salt Backfilled Disposal Rooms in a Conceptual Radioactive Waste Repository in Dome Salt," in Conceptual Design Report, National Waste Terminal Storage Repository for Storing Reprocessing Wastes in Dome Salt Formation, Special Study No. 2, Vol. XVIII, Stearns-Roger Engineering Company, Denver, CO.

Sutherland, H. J., and S. P. Cave, 1980. "Argon Gas Permeability of New Mexico Rock Salt Under Hydrostatic Compression," International Journal of Rock Mechanics, Mining Sciences and Geomechanics Abstracts, Vol. 17, pp. 281-288.

Trimmer, D. A., 1981. "Design Criteria for Laboratory Measurements of Low Permeability Rocks," Geophysical Research Letters, Vol. 8, No. 9, pp. 973-975.

U.S. Department of Energy, 1983. Results of Site Validation Experiments, Waste Isolation Pilot Plant, Vols. I and II, TME 3177, U.S. Department of Energy, Albuquerque, NM.

APPENDIX A
PETROGRAPHIC DESCRIPTIONS OF CONSOLIDATED SAMPLES

The following report was prepared by Dr. N. L. Carter
of Texas A & M University.

IT ROCKSALT CONSOLIDATION EXPERIMENTS

Summary of Results From Optical Examination

N. L. Carter

Seven specimens of rocksalt, in various states, dominantly of Salado salt from the WIPP site consolidated both in the presence and absence of added water at 2500 psi for different durations were received for purposes of identification of consolidation mechanisms by means of optical techniques. The as-received specimens were first examined carefully using a hand lens and binocular microscope and because of the friable nature of some of them, they were impregnated in EPOTEC, a blue-stained epoxy, in vacuum for 15 minutes and allowed to set for one day prior to sectioning; EPOTEC has a room-temperature viscosity about 100 times that of water. Two samples were subsequently impregnated for 1 hour at 1000 psi to determine if further penetration occurred. The blue-stain in the impregnating medium was a substantial aid in identifying nature, path, and depth of penetration into the variously consolidated samples.

The specimens received were of two basic types: A, sized consolidated rocksalt rubble with or without water added; and B, intact WIPP coarsely-crystalline samples and a fine-grained artificial preconsolidated specimen all consolidated following introduction of a through-going tension fracture. Dry samples M10 and M1 of group A were friable and showed somewhat similar impregnation effects, dominantly within the fine-grained matrix, and the poor consolidation of these specimens must arise predominantly by adhesion and mechanical interlocking in the matrix and at matrix-crystal interfaces. Much better cohesion was obtained by moistened sample AR-5, evidently primarily through consolidation of the matrix by pressure solution-precipitation effects. Because of the consequent reduction in porosity and permeability, only thin impregnation rims were observed during the normal 15-minute vacuum impregnation, although pale blue stain was observed throughout the matrix following impregnation for 1 hour at 1000 psi.

While endpieces are partially clogged by salt flow into pores, apparently a sufficient number remain open to permit reasonably accurate specimen permeability measurements. The very low permeability measured in this specimen is thus ascribed to reduction of porosity and interconnected channels of flow by means of pressure solution during consolidation.

Type B specimens were separated along the pre-induced tension fracture for binocular examination prior to impregnation. IMI-1, the fine-grained (<1mm) artificial rocksalt fracture, showed a glazed surface resulting from solution and rounding of grains at the moistened surface of the fracture. WIPP specimen CR-5 showed a very irregular fracture surface induced along grain boundaries and cleavage planes. The cleavage planes are mirror-like, grain edges are sharp, and hence it is difficult to determine the physical nature of consolidation of this pre-fractured specimen, although mechanical interlocking and other adhesion effects must play an important role. The fracture surface of CR-6 is similar in nature and irregularity to CR-5, but the relatively dull luster of cleavage planes attest to solution effects along the moistened fracture surface. Crystal edges are relatively more rounded, also indicative of solution, and this process must have played some role in the consolidation.

It is thus concluded that the presence of water, rather than duration of consolidation or other factors, plays an important role at room temperature by facilitating pressure solution. This process is evidently most effective in fine-grained matrix material, presumably because of the high surface area and energy. Mechanical interlocking is also important, as may be other processes leading to cohesion and adhesion. Etching techniques and scanning electron microscopy (SEM) are required to clarify the nature and relative contributions of the various consolidation processes.

Optical Examination-Descriptions

Consolidated Crushed Salt

M10 Large cylinder; grainsize ≤1cm - friable. Dry, 2500 psi, 25°C; 16.5%, 110md.

Impregnation heavy around edge to 12-25mm into center - then 25mm diameter clear area - section cut perpendicular to consolidation axis for maximum area. Bright-field examination reveals poorly sorted aggregate with long-axes of smaller chips of NaCl (≅ 5mm) preferentially aligned normal to specimen axis. Larger crystals generally are rather equant and set in a finer-grained matrix, the size of which ranges downward to powder. This matrix tends to separate the larger, optically obvious fragments and is most commonly permeated by blue-stained epoxy (indicating substantial porosity), the stain rarely penetrating larger grains except occasionally along fractures. There are few sharp intergranular contacts where stress concentrations may arise, but in such instances indentation occurs, giving rise to photoelastic effects which indicate stress relaxation by plastic flow on the primary system (110) [110]. It must be concluded, however, that the poor consolidation of this specimen is due mainly to adhesion effects, including mechanical interlocking, of the very fine-grained matrix which, somewhat paradoxically, shows a high porosity as revealed by the blue-stained epoxy. Unstained matrix has a brownish, impure, opaque appearance. (3 photomicrographs taken)

M1 Large cylinder, grainsize ≤ 1mm - friable. Dry, 2500 psi, 25°C, 19.3%, 90md.

Impregnation heavy, about 4mm from outside - then uniform medium blue throughout section cut as M10. Much more uniform grainsize of this specimen is evident in the 1mm-sized angular grains. These appear to be uniformly-spaced, and these elongate fragments are aligned with long axis perpendicular to specimen axis. Fine-grained matrix separates these larger fragments and there appears to be a bimodal grainsize distribution - large crystals, and very fine-grained matrix. Because of the uniformity in specimens of the larger crystals, separated by matrix,

there are few intergranular contacts and no evidence for plastic flow or interlocking on this scale. Thus, once again, adhesion takes place, though poor as indicated by friability in the matrix of high, uniform porosity by chemical and mechanical interlocking. (2 photomicrographs)

Small Discs

AR-5 Central disc - moistened (2.3% water initially). Grainsize <20mm, 2.3% H_2O, 2500 psi, 25°C, 4.9%, $<10^{-5}$md.

Impregnation thin (approximately 6mm) sporadic blue rim around cut - no further penetration - thus differs appreciably from M10, presumably consolidated under the same conditions without the added moisture. This specimen has the same overall poorly-sorted appearance as M10, again with elongate cleavage - bounded grains preferentially oriented normal to the specimen axis. However, the large fragments show some evidence of rounding of sharp edges and the matrix has a much cleaner appearance. While the brownish-impurity appearance is still maintained, it is much less evident than in M10, there being areas of cleaner, apparently continuous and relatively impurity-free matrix. It is suggested that the very fine angular fragments of halite in M10 have become continuous in AR-5 through dissolution and precipitation processes aided by both surface energy and pressure solution in the presence of water. Such processes would, of course, reduce both porosity and permeability in accord with the IT results and epoxy staining procedure. No photoelastic effects at all in this specimen - the larger fragments are separated by clear matrix with no obvious penetration. (3 photomicrographs)

AR-5 Disc connected with porous endpiece (same specimen as above)

One endpiece fell off following slabbing, but initially disc was not impregnated because of apparent coherency. It is apparent from both reflected light observations of endpiece initially in contact with specimen and in thin section that the rocksalt is flowing into and clogging pores in the endpiece - stress concentrations at the interface enhance this process. Therefore, permeability measurements, both in the

presence and absence of water, should reflect this clogging effect and hence true permeabilities would be expected to be somewhat greater than those measured by this technique. However, the flow of EPOTEC appears to be similar at the free end of the disc and at the interface, suggesting that a sufficient volume of pores in the endpieces remain open to permit permeability determinations nearly representative of the sample which, in this end-cut, is identical in nature and texture to the central disc. Accordingly, the approximately sever orders of magnitude decrease in permeability of AR-5 is tentatively ascribed primarily to solution, precipitation, and mechanical softening within the rocksalt sample itself. It is worth noting that impregnation at 1000 psi for 1 hour, following initial impregnation, led to coloring the entire rocksalt disc, again by migration along grain boundaries primarily, but some matrix was involved as well, contrary to results from impregnation procedures and those to be discussed below for CR-6. (1 photomicrograph)

Healed Fractures

Two specimens of WIPP salt, CR-5 and CR-6, both coarse-grained (ca. 1cm avg. diameter) and one specimen of fine-grained artificial salt (IMI-1) were fractured in tension and then reconsolidated at 2500 psi, two moistened and 1 dry, for durations of from 24-65 hours. The notch used for fracturing of the 1-1/2 inch by 2 inches thick discs was evident and all three specimens were deliberately separated parallel to the plane of the initial tension fracture by hand, moderate force being required, in order to examine the fracture surfaces. For the fine-grained specimen, the fracture surface is reasonably regular and uniform and has the appearance of a slight glaze or coating, probably due to solution of the moistened surface during consolidation. Coarse-grained specimens CR-5 and CR-6 broke along cleavage fractures and grain boundaries, producing very irregular surfaces. Cleavage surfaces of CR-5 (consolidated dry) are mirror-like, whereas those of CR-6 (consolidated moistened) have a satin-like sheen and have obviously been affected by solution of the moistening fluid. All three specimens were impregnated normally and two sections were cut from each; one normal to and containing the tension

fracture, and one in a plane parallel to the disc axis and slightly inclined to the fracture plane.

IMI-1 Artificial salt, fractured, moistened and consolidated for 51 hours. Impregnation produced virtually no (very thin) blue skin parallel to cylinder axis, uniform 4mm line or front from top of specimen (deduced from lettering) and uniform 7mm front measured from bottom.

A. Section subparallel to fracture plane
Specimen somewhat similar to M1 in that it is composed largely of angular, elongate (parallel to cleavage planes) salt fragments, though with apparently less matrix and lower porosity. There is also much less tendency for elongated fragments to align normal to consolidation axis in this pre-consolidated specimen, as expected. Blue-stained epoxy also reflects this difference in that it has impregnated M1 throughout (although a darker blue front extends 3mm from top and 5mm from bottom of specimen), whereas the epoxy forms a sharp, though thicker (7mm), dark blue front in this specimen. The matrix is impure and generally uniformly separates larger fragments so that grain contacts are few. Where present, no photoelastic effects, obvious indentation, or plastic flow are evident. (2 photomicrographs)

B. Section cut perpendicular specimen axis
No gross noticeable difference between this specimen and A, described above, in general. A careful study of the fracture surface revealed that most halite grains are rounder rather than the usual angular shapes, thus indicating substantial pressure solution. No photoelastic effects are observed, indicating that plastic flow did not play an important role in the consolidation - solution and precipitation dominating under these conditions. Impregnation of EPOTEC is also restricted along most of this surface, though sporadic in some parts, also indicating reduction of porosity and permeability along the surface.

CR5-CRAFD WIPP salt, 2500 psi, dry, 24 hours consolidation.

A. Section subparallel tension fracture

EPOTEC has penetrated only along cracks and grain boundaries. This specimen has all aspects of ordinary-as-cored WIPP salt, being impure, coarse-grained, replete with brine inclusions, no evidence of plastic flow, etc. Consolidation at 25°C has had no effect on these well-known textural characteristics.

B. Section perpendicular to fracture

Thin EPOTEC impregnation as before for this sample. No obvious rounding, microcracking or plastic flow adjacent to the fracture surface, or any other hint of basis for consolidation. However, the latter must be due to mechanical interlocking of some sort along with other unspecified adhesion effects (1 photomicrograph), perhaps partially of a chemical nature.

CR6-CRAFM WIPP salt, 2500 psi, moistened, 65 hrs. consolidation

A. Section sub-parallel to fracture

Like CR-5, specimen CR-6 shows all typical textural and structural characteristics of typical WIPP salt. The EPOTEC impregnated very little surficially but did migrate along grain boundaries and cracks - dominantly of the cleavage type. Further, impregnation for 1 hour at 1000 psi resulted in no obvious change and nothing diagnostic of consolidation was noted.

B. Section perpendicular to fracture

EPOTEC staining as usual for this sample along fracture surface. While there is definite evidence of rounding of some corners (photomicrograph), there are also some sharp edges and re-entrants. It is clear from this section and surface observations cited above that solution helped to provide reconsolidation. A SEM photo of the surface would have been helpful to determine the extent to which such was the case; mechanical interlocking probably played some role.

APPENDIX B
TEST PROCEDURES

This appendix provides detailed test procedures used in the fracture healing and crushed salt consolidation tests. The apparatus for both types of tests was described in the main text of the report (Sections 3.1 and 4.1).

B.1 PROCEDURES FOR FRACTURE HEALING TESTING OF SALT CORE SPECIMENS

B.1.1 Salt Acquisition

Natural rock salt and compacted artificial salt were used for fracture healing testing. The natural salt was obtained from the Waste Isolation Pilot Plant (WIPP) near Carlsbad, New Mexico and from the Avery Island salt dome in Louisiana. In the case of the WIPP salt, six and four-inch diameter by approximately one-foot long samples were shipped to the laboratory. Each core was individually wrapped in padded plastic to minimize the potential for breakage. The Avery Island salt was received from RE/SPEC, Inc. in the form of a single 12 inch x 12 inch x 16 inch block.

The compacted salt was obtained directly from International Salt Company in Cleveland, Ohio. The salt was shipped in the form of 50-pound blocks (nominal weight) having the approximate dimensions of eight inches square by 11 inches high. The blocks were bound to a wooden pallet and covered with thick plastic for moisture protection.

B.1.2 General Test Equipment and Set-Up

Prepared samples are placed in a conventional Hoek triaxial cell for permeability testing (Figure B-1). The ends of the sample are sandwiched between porous stones and load platens containing gas flow ports, and the entire set-up is placed in a ten-ton capacity load frame. The hydraulic confining pressure to the Hoek cell oil is maintained by a manually operated screw type pressure generator and monitored by a 0 to 3200-psi pressure transducer. The pressure generator is equipped with a Vernier to allow the position of the piston in the device to be monitored. In this manner, the volume of oil entering or leaving the pressure generator with time could be monitored. A 0 to 40,000 pound load cell beneath the lower platen monitors the axial force applied to the sample by manual operation of the load frame. Two ± 0.5-inch linear voltage displacement transformers (LVDT's) are secured to the platens using bracket supports and monitor axial deformation of the sample.

The constant head gas permeability test system consists of a pressure control panel and associated plumbing connected to the platens at each end of the sample. A 0 to 20-psi differential pressure transducer monitors the difference in gas permeant pressure between the upstream (bottom of sample) and downstream ends of the sample. In the general test procedure, the differential pressure transducer is located as close as possible to the ends of the sample to minimize the correction for system head loss. (Some of the initial constant head tests of artificial salt samples were conducted with the differential pressure transducer located in the pressure control panel.) Three 0 to 30°C temperature sensors monitor the temperature of the gas permeant at the pressure control panel, sample inlet, and sample outlet positions. One of a pair of gas regulators (0 to 7 psi and 0 to 500 psi) mounted in the pressure control panel is selected to control the pressure of the gas permeant supplied to the upstream end of the sample. A 0.01 to 5.0 liter/min. electronic flowmeter mounted in the pressure control panel monitors the gas permeant flow rate at the downstream end of the sample during constant head permeability tests.

Transient falling head permeability tests utilize sealed, high pressure reservoir systems upstream and downstream from the sample and a 0 to 800 psi pressure transducer which monitors the total upstream pressure of the gas permeant. The upstream reservoir volume is three orders of magnitude greater than the downstream reservoir volume and is located in the pressure control panel with the upstream pressure transducer. The differential pressure transducer and the downstream reservoir are located immediately adjacent to the Hoek cell.

All of the sensors are monitored using a 16-channel, 12-bit precision analog/digital data-acquisition module linked to a 64-K Apple II microcomputer which is equipped with a time module. Software packages for data acquisition and data reduction have been developed and verified, and are described subsequently.

B.1.3 General Permeability Test Procedures

1. Constant Head Test

The constant head permeability test is performed on samples of sufficiently high permeability such that flow rates of argon gas permeant through the sample can be measured with the flowmeter using a maximum 20-psi differential pressure. The sample is first subjected to the desired hydrostatic confining stress by adjustments to the pressure generator and load frame. In the present test series, the minimum confining pressure applied was 50 psi and was followed by tests at 500 psi. Subsequent tests were performed at 500-psi increments up to a maximum of 2500 or 3000 psi. (The 3000-psi increment was omitted from the later tests so that the duration of confining pressure application at higher pressures could be extended to examine the effects of longer term confinement.) Tests were also conducted as the confining pressure was decreased from the maximum pressure to 2000 psi and then 1000 psi.

After adjusting the confining pressure, the gas permeant is admitted to the sample to determine whether the limiting constraint for the test is flow rate measurement or differential pressure measurement. Assuming that constant flow rates can be measured, incremental flow rates are then selected and the required number and timing of sensor readings entered on the data acquisition system. Three sensor readings are typically taken at each of several flow rates (for each confining pressure), where the first three readings establish the zero reference for the flowmeter and differential pressure transducer. The time interval between sensor readings is selected (typically 15 to 30 seconds) so that the flow can be adjusted to a constant rate prior to the start of each set of three sensor readings. Upon completion of the test a data file is recorded and identified by a unique filename denoting the type of sample tested, confining pressure and time of pressure application. Vernier readings for each test are taken from the pressure generator and recorded on a log sheet for each sample tested.

2. Transient Falling Head Test

The transient test procedure is used when no measurable flow can be detected through the sample for a differential pressure application of 20 psi. The confining pressure is first adjusted as in the constant head test. The gas pressure in the permeability test system is then elevated to a nominal pressure of approximately 500 psi. Secondary adjustments are then made to the lateral and axial stresses to compensate for the effects induced by application of the back pressure. This high back pressure is needed to assure that the argon gas would behave as an incompressible fluid for the pressure gradients imposed during transient testing. The pressure in the upstream reservoir is then increased relative to the downstream reservoir by approximately 20 psi and a set of baseline readings is taken prior to the start of the test. The test is initiated by opening the downstream reservoir valve and periodically measuring changes in the differential pressure across the sample as the sealed pressures between the upstream and downstream reservoir systems equilibrate. The use of a 20-psi differential pressure assures that the effective stresses on the ends of the sample are nearly the same and that testing can be completed within 15 to 20 minutes.

B.1.4 Detailed Test Procedures

1. Sample Preparation

A. Sample Coring

1. WIPP Crystalline Salt

Obtain HQ-size cores from six and four-inch diameter cores by the following steps:

Step 1 Apply a protective coating to the outer surface of the bulk core using waterproof tape or wax.

Step 2 Place the bulk core in a suitable container and fill the annulus with Randustrial F-181 Bolt Anchor Sulfaset and allow to set for one hour. If necessary, glue the container to a plywood base for added stability. Six-inch diameter cores need not

be secured in the capping compound if the core rig contains a clamping apparatus.

Step 3 Drill a single HQ-size core from each bulk core using compressed air as a drilling fluid. Allow the drill to advance under its own weight if the core rig is not secured to the floor.

2. Avery Island Crystalline Salt and Compacted Salt Blocks
Drill HQ-size cores from each block sample using compressed air as a drilling fluid. The bulk samples possess sufficient dead weight to allow multiple cores to be drilled from each sample without clamping or casting.

B. End Sawcutting
Cut all sample types to the desired length using a band saw equipped with a mitre box and carbide-tipped blade. Hold each side of the sample on either side of the blade to minimize breaking of the sample prior to completion of the sawcut. Samples to be used for fracture healing testing should be cut to a length of approximately 1-1/2 inches to permit a nearly vertical and longitudinal fracture to be obtained.

C. End Polishing
Compacted salt sample ends can be polished by sandpaper or a surfacing grinding machine. Avery Island and WIPP crystalline salt samples should be polished using sandpaper to minimize chipping of crystals from the sample edges.

D. Sawcut Fractures
Prepare sawcut fractures of compacted and crystalline salt samples by the following steps:

Step 1 Cut the sample longitudinally using a band saw equipped with a mitre box and carbide-tipped blade.

Step 2 Polish each surface with sandpaper to provide intimate contact between the mating surfaces.

E. Tensile Fractures

Induce tensile fractures of compacted and crystalline salt samples by the following steps:

Step 1 Place the sample in an upright position on the table of the surface grinding machine under the shaft housing.

Step 2 Place a sharpened, four-inch wide brick chisel blade on the top diameter of the sample holding the chisel in a vertical position.

Step 3 Lower the upper assembly of the surface grinding machine with the screw advance until the shaft housing contacts the brick chisel.

Step 4 Tilt the brick chisel so that the vertical side of the bevel makes an angle of about 85° with the horizontal.

Step 5 Slowly advance the upper assembly downward into the sample with the screw advance until the sample fractures.

Care should be exercised in completing Steps 1-5 as tensile fractures are induced in samples which have been previously subjected to permeability testing in an unfractured condition.

2. Sample Set-Up

Set-up samples in the Hoek cell by the following steps:

Step 1 Photograph the sample.

Step 2 Measure and record the sample weight to the nearest 0.01 gram.

Step 3 Obtain the average sample length by measuring the sample length at three positions around the sample (120° spacing) to the nearest 0.001 inch using calipers.

Step 4 Measure and record the sample diameter to the nearest 0.001 inch using a Pi Tape.

3. Test Equipment Set-Up

Set up the prepared, intact or fractured sample in the Hoek cell permeability apparatus by the following steps:

Step 1 Fill the pressure generator with oil by opening the valves to the Hoek cell and oil reservoir and turning the generator to a vernier reading of 0-0-0.

Step 2 Close the valve to the oil reservoir.

Step 3 Insert the porous stones and sample in the Hoek cell.

Step 4 Place the lower LVDT bracket on the bottom platen and slide the bracket down the platen to rest on the plug valve assembly which is attached to the bottom platen.

Step 5 Place the Hoek cell on the bottom platen and slide the cell down the platen to rest on the LVDT bracket.

Step 6 Place the upper LVDT bracket on the top platen and the insert platen into the top of the Hoek cell.

Step 7 Align the cell and platen assembly in the load frame and apply an axial load equivalent to an axial stress of approximately 50 psi.

Step 8 Lift the Hoek cell to the midpoint between the upper and lower platens and adjust the pressure generator to apply a lateral confining stress of approximately 500 psi.

Step 9 Adjust pressure generator to 50 psi confining pressure and record the initial vernier reading.

Step 10 If necessary, adjust the load frame to apply a 50 psi axial stress to the test specimen.

Step 11 Secure the LVDT brackets to platens so that brackets do not contact Hoek cell.

Step 12 Secure each LVDT for axial deformation measurement in the brackets and zero the voltage output from each sensor with the signal conditioning system.

4. Test Procedures

A. Sample Confinement

1. Confining Pressure and Permeability Test Schedule

Apply effective hydrostatic confining pressures and perform permeability tests on Hoek cell samples according to the following schedule:

Effective Confining Pressure (psi)	Total Time of Application (hrs)	Permeability Test Schedule (hr)
50	0.5	0.5
500	0.5	0.5
1000	0.5	0.5
1500	0.5	0.5
2000	0.5	0.5
2500	0.5+N[1]@24 hr.	0.5+N @ 24 hr.
2000	0.5	0.5
1000	0.5	0.5

2. Confining Pressure Application

Apply hydrostatic confining pressures to the specimen by the following steps:

Step 1 Adjust the load frame to the required axial load.

Step 2 Adjust the pressure generator to the required confining pressure.

Step 3 Record the date, time and pressure generator vernier reading.

B. Permeability Test Procedure

1. Sensor Channels, Types and Voltage Ranges

Set-up the data acquisition system to monitor the following sensors and voltage ranges:

---

(1) N = Variable

a. Hoek Cell Constant

Sensor Channel No.	Sensor Type	Voltage Range (v)
0[1]	Flowmeter	-1.0 to 1.0
2	Differential Pressure	-5.0 to 5.0
3	Lateral Confining Pressure	0.0 to 5.0
6	Temperature	-0.5 to 0.5
7	Temperature	-0.5 to 0.5
8	Temperature	-0.5 to 0.5
10	Load Cell	0.0 to 1.0
14	Axial Deformation	-5.0 to 5.0
15	Axial Deformation	-5.0 to 5.0

b. Hoek Cell Transient

Sensor Channel No.	Sensor Type	Voltage Range (v)
1	Upstream Back Pressure	0.0 to 5.0
2	Differential Pressure	0.0 to 5.0
3	Lateral Confining Pressure	0.0 to 5.0
6	Temperature	-0.5 to 0.5
7	Temperature	-0.5 to 0.5
8	Temperature	-0.5 to 0.5
10	Load Cell	0.0 to 1.0
14	Axial Deformation	-5.0 to 5.0
15	Axial Deformation	-5.0 to 5.0

B.1.5 Data Reduction and Presentation

1. Constant Head Test

The computer program 'Hoek Cell Constant' was developed to reduce the data collected during the constant head permeability testing of core samples in the Hoek cell assembly. Program inputs consist of the initial sample length, diameter, weight, specific gravity, and

[1] Number refers to sensor identification for data acquisition system.

the incremental volume change of the system oil at the time of the test. The first set of sensor readings used for permeability calculations are also specified as an intermediate input. The program output includes initial sample properties, properties at the time of test, confining pressure and pressure gradient, flow and permeability values for each set of sensor readings after the baseline readings.

Calibration equation constants were developed for all of the electronic sensors by performing various regression analyses on the calibration data. Calibration equations were also developed to define pressure versus displaced oil volume relations for the permeability test system. These relations allow the program to compute the volume change of the sample corrected for the volume change of the system and the head loss through the sample corrected for the head loss of the system. A detailed explanation of the program and computations is presented in the 'Hoek Cell Constant Program Verification' project file, along with a typical program output.

Further data reduction is performed manually so that the test data can be presented in a tabular form. A table is prepared for each sample tested which lists the tests in order of ascending confining pressure. The data presented for each test consist of sample porosity, confining pressure, time of pressure application, bulk modulus, and average standard deviation and coefficient of variation for permeability.

2. Transient Falling Head Test

The computer program 'Hoek Cell Transient' is used to reduce the data collected during transient falling head testing of salt core samples in the Hoek cell. The program operates in the same manner as 'Hoek Cell Constant' with the main difference being the method of permeability calculation due to the different test procedure. The voltage corrections applied to the cell pressure transducer and load

cell to compensate for the back pressure are included as program inputs. In addition, the first and last points of the linear portion of the pressure decay vs. time curve must also be input.

These points are selected by viewing a plot of the decay curve for the test displayed by the 'Plotter' program prior to running the 'Hoek Cell Transient' program. The program then uses this linear portion to perform a slope computation which is used in the calculation of permeability. A detailed explanation of the program and typical program output is presented in the 'Hoek Cell Transient Program Verification' project file. The data presentation for the results of the transient falling head tests is identical to that described for the constant head tests.

B.2 PROCEDURE FOR CONSOLIDATION TESTING OF CRUSHED SALT

B.2.1 Salt Acquisition

Bulk samples of crushed salt (two nominal 100-pound bags) from the WIPP Facility were obtained by IT personnel. The bulk samples represent the result of mining operations using a roadheader. The maximum particle size of the as-received samples was approximately 3/4-inch diameter. The Avery Island salt was received as a solid block from RE/SPEC, and crushed into various size fractions by IT.

B.2.2 General Sample Set-Up and Test Equipment Description

Prepared samples are placed in a pressure vessel for testing (Figure B-2). The test specimens are constructed in a number of steps. The first step consists of placing a 0.012-inch thick latex membrane over the bottom platen on the pressure vessel base and porous stone. A 2.8-inch nominal inside diameter split sample mold was then fitted around the platen and secured with hose clamps and the membrane stretched over the top. A sample about 4.5 inches in height was then constructed by compacting five layers of material with ten blows per layer using a specially designed rammer. The rammer applied one-fifth the compactive effort of a Standard Proctor test (2475 ft-lbs/ft.^{3}) to a 2.5-inch diameter face for the 4.5 by 2.8-inch sample.

The top platen and porous stone are then placed on top of the compacted sample and the membrane pulled over the top platen. A plastic cap is placed over the top platen gas line fitting and a vacuum is applied to the bottom platen gas line prior to removal of the split mold. The sample dimensions are then measured using a Pi Tape and calipers and the weight determined by weighing the unused portion of the original material. The length measurement is made by measuring from the top platen to the pressure vessel base and computing the sample length from a reference measurement made on a 4.5-inch 'dummy' sample set-up. The sample diameter is computed by subtracting twice the membrane thickness from the average of the Pi Tape measurements. Additional membranes are then placed around the vacuum stabilized sample prior to securing the membranes with hose clamps and connecting the gas line from the top platen to the pressure base. A minimum of four additional membranes (two 0.024-inch thick latex and two 0.024-inch thick neoprene) are used to minimize the potential for membrane failure under the high cell pressures.

Two ± 0.5 inch-travel LVDT's are installed on opposite sides of the sample through the base of the pressure vessel. The core rods are then attached to the top platen and the electronic output of the sensors is 'zeroed'. The body of the pressure vessel is then clamped to the base and filled with hydraulic oil by pressurizing an oil-filled reservoir and forcing oil from the reservoir through the base of the pressure vessel. This operation continues until oil is emitted from an exhaust line connected to the top of the vessel. When the vessel is filled, the vacuum is released from the sample and the initial length corrected for the displacement observed on the LVDT outputs. The LVDT's are then re-zeroed, the vessel sealed and the connections made to the oil and gas supplies.

The oil pressure in the vessel is supplied by an air/oil intensifier and the oil pressure monitored by a 0 to 3200-psi pressure transducer. The gas is supplied to the intensifier from a high pressure nitrogen tank equipped with a high pressure regulator. More precise control is main-

tained by a 0 to 500-psi regulator. For confining pressures greater than 2000 psi the high pressure regulator is connected directly to the intensifier. A 0 to 50-psi regulator is used to fill the intensifier with oil prior to each test. A ± 1.0-inch travel LVDT connected to the intensifier piston is used to monitor the piston travel so that the volume of oil displaced from the intensifier can be measured.

The permeability test system for consolidation testing is identical to the system set-up for the fracture healing testing. The 0 to 20-psi differential pressure transducer is located at the base of the pressure vessel so that system head losses were minimized.

B.2.3 Permeability Test Procedures

1. Constant Head Test

   The confining pressure sequence used for constant head tests in the pressure vessel was the same as the sequence used for the Hoek cell. The time of pressure application was extended for each cell pressure interval, however, so that a single test series lasted about 30 days. The 2500 psi cell pressure was maintained for a period of approximately two weeks. The constant head permeability tests in the pressure vessel were conducted in the same manner as the Hoek cell tests. Data filenames were assigned based on the grain size of the sample, confining pressure and time of pressure application.

2. Transient Falling Head Test

   The pressure vessel transient test procedure was identical to that used for the Hoek cell, except that pressure transducers were exchanged so that a maximum 800 psi differential pressure could be applied to the sample. Sensor readings were extended for several hours so that the decay of the differential pressure could be maximized. A continuous back pressure of 500 psi was maintained in the sample during the transient testing phase of the test series. The maximum total cell pressure was increased to 3000 psi in order to achieve an effective pressure of 2500 psi on the sample.

B.2.4 Detailed Test Procedures

1. Sample Preparation

A. Grain Size Determination

1. WIPP Crushed Salt

Prepare a sample with the desired maximum particle size by the following steps:

Step 1 Prepare a sample of several pounds by repeated quartering of the as-received bulk sample.

Step 2 Limit the maximum particle size by sieving the sample through the desired sieve and retain the material passing.

Step 3 Prepare a sample of ± 2000 grams using the sample splitter.

2. Avery Island Crushed Salt

Prepare samples to match the WIPP grain size distribution by the following steps:

Step 1 Calculate the weight of material required to be retained on each sieve size for a total sample weight of 2000 grams.

Step 2 Calculate the cumulative weight retained for each sieve.

Step 3 Prepare a 2000 gram sample using the calculated batch weights.

2. Sample Set-up

Construct a specimen for permeability testing in the pressure vessel by the following steps:

Step 1 Split the 2000 gram sample prepared in Section I.B using a sample splitter.

Step 2 Perform a sieve analysis on half of the sample from Step 1.

Step 3 Place a porous stone on the bottom platen of the pressure vessel.

Step 4 Place a 0.025 inch thick by 2.8 inch diameter latex membrane over the bottom platen and porous stone.

Step 5 Place the nylon ring spacer on the base of the pressure vessel around the bottom platen.

Step 6 Assemble the split mitre box around the bottom platen and membrane and secure with a hose clamp.

Step 7 Stretch the membrane over the top of the split mitre box.

Step 8 Determine the initial weight of the sample to be used for the permeability test specimen to the nearest 0.01 gram.

Step 9 Construct a sample to the top of the mitre box by compacting a sample in 5 layers, 10 blows per layer with the specially designed rammer.

Step 10 Determine the weight of the permeability test specimen by weighing the remainder of the sample to the nearest 0.01 gram and subtracting the weight from the initial weight obtained in Step 8.

Step 11 Place the porous stone and top platen on top of the prepared sample and align the metal LVDT support holes and flow-through tube fitting with the connections on the pressure vessel base.

Step 12 Stretch the membrane over the top platen and place a plastic cap vacuum seal over the top platen tube fitting.

Step 13 Connect the vacuum pump to the bottom platen valve on the pressure vessel base and turn on the vacuum pump with the valve in the open position.

Step 14 Remove the split mitre box and the nylon ring spacer.

Step 15 Make three length measurements at a 120° circumferential spacing to the nearest 0.001 inch from the top platen to the base of the pressure vessel using a caliper.

Step 16 Determine the average sample length by referencing the average measurements in Step 15 to the 4.500-inch high dummy steel specimen.

Step 17 Make three diameter measurements to the nearest 0.001 inch at the top, middle and bottom of the sample using a Pi Tape.

Step 18 Subtract twice the membrane thickness from the average of the Pi Tape measurements to determine the average sample diameter.

Step 19 Using the 2.8" sample stretcher, place three additional 0.025" thick latex membranes around the vacuum stabilized sample.

Step 20 Place two 0.025 inch thick neoprene membranes around the sample using the membrane stretcher.

Step 21 Secure the membranes to the platens using hose clamps.

Step 22 Connect the flexible tubing for the top platen to the base of the pressure vessel and close the valve.

Step 23 Carefully remove the plastic cap vacuum seal from the top platen tube fitting and quickly attach the flexible tubing.

Step 24 Tighten the tube fittings on the top platen and pressure vessel base.

Step 25 Close the bottom platen valve and turn off the vacuum pump. Check that the sample remains rigid due to the internal vacuum.

3. Test Equipment Set-up

Assemble the pressure vessel with the constructed crushed salt specimen by the following steps:

Step 1 Install the LVDT's for axial deformation measurement through the base of the pressure vessel.

Step 2 Attach the LVDT cores and rods to the top platen fittings.

Step 3 Zero the voltage output from the LVDT's using the signal conditioning system.

Step 4 Place the five-inch diameter O-ring on the base of the pressure vessel and lower the top chamber onto the base using the pulley system.

Step 5 Bolt the base and body of the pressure vessel together following the manufacturer's specifications.

Step 6 Attach plastic tubing from the valve at the bottom of the oil reservoir to the oil inlet valve on the pressure vessel base and open both valves.

Step 7 Attach plastic tubing from the regulated air supply to the air inlet fitting at the top of the oil reservoir.

Step 8 Attach plastic tubing from the fitting on the top of the pressure vessel to an overflow container.

Step 9 Turn on the air supply and force oil from the reservoir to the pressure vessel until it emits from the overflow line.

Step 10 Reduce the air pressure and slowly continue filling the pressure vessel until air bubbles are absent from the overflow line.

Step 11 Close the valve at the oil inlet to the pressure vessel base.

Step 12 Turn off the air supply and bleed off the excess pressure from the oil reservoir.

Step 13 Disconnect the air supply line to the oil reservoir and open the valve at the bottom outlet.

Step 14 Disconnect the oil lines to the pressure vessel inlet and overflow fittings.

Step 15 Connect the high pressure nitrogen gas supply to the air/oil intensifier and fill the intensifier with oil if necessary.

Step 16 Close the valve to the oil reservoir on the intensifier.

Step 17 Open the valve from the intensifier oil supply to the pressure vessel and bleed out the air.

Step 18 Open the valve at the pressure vessel oil inlet to bleed out the air.

Step 19 Connect the intensifier oil supply to the pressure vessel oil inlet and open both valves.

Step 20 When oil emits from the top of the pressure vessel, seal the vessel with a 1/4 inch plug.

Step 21 Close the valve to the intensifier oil reservoir.

4. Test Procedures

A. Sample Confinement

1. Confining Pressure and Permeability Test Schedule

Apply hydrostatic confining pressures and perform permeability tests on pressure vessel samples according to the following schedule:

Effective Confining Pressure (psi)	Total Time of Application (days)	Permeability Test Schedule
50	1	1 @ 0 hr. 4 @ 2 hr. 1 @ 24 hr.
500	2	SAA[1] + 2 @ 4 hr. 1 @ 24 hr.
1000	2	SAA
1500	2	SAA
2000	5	SAA + 3 @ 24 hr.
2500	5 + N[2]	SAA + N @ 24 hr.

2. Confining Pressure Application

Apply each increment of hydrostatic confining pressure after the 50 psi increment to the pressure vessel specimen by the following steps:

---

(1) SAA = Same as Above

(2) N = Variable

Step 1 Set-up the data acquisition system for 20 sensor readings at ten second intervals using the pressure vessel constant sensors as outlined in Section 4.B.1.a.

Step 2 Begin taking sensor reading and start Argon gas flow through the permeability test system following the third sensor reading.

Step 3 Increase the gas pressure to the intensifier so that the vessel pressure is increased ± 50 psi between sensor readings (every ten seconds).

Step 4 Fine tune the gas regulator to achieve the required vessel pressure.

Step 5 Save the data file at the end of the test.

3. Unload-Reload Schedule

Upon completion of the permeability test series, apply hydrostatic confining pressures on pressure vessel samples according to the following schedule:

Initial Confining Pressure (psi)	Final Confining Pressure (psi)
2500	50
50	2000
2000	50
50	1500
1500	50
50	1000
1000	50
50	500
500	50

4. Unload-Reload Confining Pressure Application

Apply each increment of hydrostatic confining pressure for the unload-reload sequence by the following steps:

Step 1 Set-up the data acquisition system for 20 readings at 20 second intervals using sensor channels 4, 11, 12 and 13 as outlined in Section 4.B.1.a.

Step 2 Begin taking sensor readings and start the cell pressure adjustments after the first reading.

Step 3 Adjust the gas pressure to the intensifier so that the vessel pressure is increased/decreased incrementally to the desired final confining pressure on the tenth reading.

Step 4 Save the data file at the end of the test.

Step 5 Repeat Steps 1 through 4 until each unload or reload pressure increment is completed.

B. Permeability Test Procedure

1. Sensor Channels, Types and Voltage Ranges

Set up the data acquisition system to monitor the following sensors and voltage ranges:

a. Pressure Vessel Constant

Sensor Channel No.	Sensor Type	Voltage Range (v)
0	Flowmeter	-1.0 to 1.0
2	Differential Pressure	-5.0 to 5.0
4	Hydrostatic Cell Pressure	0.0 to 5.0
6	Temperature	-0.5 to 0.5
7	Temperature	-0.5 to 0.5
8	Temperature	-0.5 to 0.5
11	Axial Deformation	-5.0 to 5.0
12	Axial Deformation	-5.0 to 5.0
13	Intensifier Displacement	-5.0 to 5.0

b. Pressure Vessel Transient

Sensor Channel No.	Sensor Type	Voltage Range (v)
1	Upstream Back Pressure	0.0 to 5.0
2	Differential Pressure	0.0 to 5.0
4	Hydrostatic Cell Pressure	0.0 to 5.0
6	Temperature	-0.5 to 0.5
7	Temperature	-0.5 to 0.5
8	Temperature	-0.5 to 0.5
11	Axial Displacement	-5.0 to 5.0
12	Axial Displacement	-5.0 to 5.0
13	Intensifier Displacement	-5.0 to 5.0

2. Constant Head Test

Conduct constant head permeability tests by the following steps:

Step 1 Connect the gas lines to the test chamber to provide upward flow through the sample.

Step 2 Install the differential pressure transducer so that the positive side of the sensor is connected to the upstream side of the sample.

Step 3 Open the valve to the flowmeter and start Argon gas flow through the sample.

Step 4 Determine whether the limiting constraint on the test is due to the maximum capacity of the flowmeter or the differential pressure transducer.

Step 5 If the differential pressure transducer controls, select a flow rate to maximize the pressure transducer voltage output (i.e., 5 volts) and three other flow rates which are approximately 1/2, 1/4 and 1/8 of the maximum, but not less than 0.05 Standard Liters Per Minute (SLPM).

Step 6 If the flowmeter controls, select flow rates of 1, 2, 3, 4 and 5 SLPM.

Step 7 Determine the total number of sensor readings required for three 'zero' readings and three at each selected flow rate.

Step 8 Set-up the data acquisition system for the number of sensor readings determined above using a sufficient time interval after each third reading to allow for adjustment of the next flow rate.

Step 9 Adjust the confining pressure to the required value.

Step 10 Adjust the regulator to the lowest flow rate to be used for testing and turn off the Argon gas supply.

Step 11 Bleed off the upstream pressure and begin the sensor readings after the differential pressure transducer output goes to zero.

Step 12 Start Argon gas flow through the sample after the third reading and adjust the flow rate for each subsequent set of three sensor readings.

Step 13 Upon completion of the test, turn off the gas supply and flowmeter.

Step 14 Save the data file.

3. Transient Test

a. 'Low' Pressure Method

Conduct 'low' pressure transient permeability tests by the following steps:

Step 1 Connect the gas lines to the test chamber to provide upward flow through the sample.

Step 2 Install the differential pressure transducer so that the positive side of the sensor is connected to the upstream side of the sample.

Step 3 Close the valve to the flowmeter so that both the upstream and downstream systems of the permeability panel board are connected to the Argon gas supply.

Step 4 Open both platen valves to the sample.

Step 5 Admit Argon gas to the sample while monitoring the upstream back pressure transducer.

Step 6 Adjust the back pressure to 500 psi minus the capacity of the differential pressure transducer.

Step 7 Back pressure saturate the sample for a minimum of 10 to 15 minutes.

Step 8 Make confining pressure adjustments to the Hoek cell system according to the instructions on the test form.

Step 9 Set-up a minimum of 10 sensor readings on the data acquisition system using an appropriate reading interval. Reading intervals have varied from 6 seconds for permeability (K) values of 10^{-1} millidarcy (md) to 3600 seconds for K values of 10^{-6}md.

Step 10 Close both platen valves to the sample.

Step 11 Adjust the argon gas pressure to increase the upstream pressure by the capacity of the differential pressure transducer.

Step 12 Maintain this pressure for a minimum of 5 to 10 minutes until the differential pressure transducer output remains constant when the differential pressure is sealed into the upstream reservoir. If a constant differential pressure cannot be maintained, check for gas leaks or temperature gradients.

Step 13 Turn off the argon gas supply.

Step 14 Begin recording sensor readings and open the valve to the upstream platen after the first reading.

Step 15 Save a data file at the end of the test.

Step 16 Open the downstream platen valve.

Step 17 Bleed the pressure from the system.

Step 18 Readjust the confining pressure to maintain effective confining pressure.

b. 'High' Pressure Method

Use the 'high' pressure transient permeability test method when the differential pressure available with the Channel No. 2 transducer will not decay. Conduct the 'high' pressure transient permeability test by the following revisions to the 'low' pressure method steps:

Step 0 Connect the high pressure Argon gas supply to the panel board gas inlet which bypasses the panel board regulators.

Step 2 Remove the upstream back pressure transducer from the upstream reservoir and install with the positive side of the sensor to the upstream side of the sample. Cap off the upstream reservoir.

Step 4 Close both platen valves to the sample.

Step 6 Adjust the back pressure to 500 psi then open both platen valves to the sample.

Step 10 Adjust the Argon gas pressure to the capacity of the differential pressure transducer.

5. Test Completion

Dismantle the permeability test system and perform the following steps:

Step 1 Measure and record the average sample length to the nearest 0.001 inch using a caliper.

Step 2 Measure and record the average sample diameter to the nearest 0.001 inch using a Pi Tape.

Step 3 Measure and record the sample weight to the nearest 0.01 gram using a balance.

Step 4 Identify the sample by writing the sample number/numbers and project number on the sample.

Step 5 Photograph the sample.

Step 6 Store the sample in a sealed plastic container.

B.2.5 Data Reduction and Presentation

1. Constant Head Test

The computer program 'Pressure Vessel Constant' was developed to reduce the data acquired during constant head permeability testing of crushed salt in the pressure vessel. The program operation and required inputs are analagous to the 'Hoek Cell Constant' program except that the input for 'Intensifier Zero' replaces the input for 'Incremental Volume Change'. The intensifier zero input is required because the intensifier LVDT is re-zeroed when the piston travel exceeds one inch. This allows the program to account for the total piston travel used for computation of sample volume change while maintaining the voltage restriction of the data acquisition system. The program outputs are also analogous to 'Hoek Cell Constant' except that a later modification included the printout of the axial strain of the sample. Further data reduction and presentation is completed as described for the fracture healing tests. A detailed explanation of the program and typical output is presented in the 'Pressure Vessel Constant Program Verification' project file.

2. Transient Falling Head Test

The 'Hoek Cell Transient' program has been modified for the reduction of data collected during transient head testing of crushed salt samples in the pressure vessel. Several variations of the 'Pressure Vessel Transient' program have been developed due to the pressure transducer modifications performed during the test series. Program outputs have been included which indicate the total cell pressure, back pressure and effective cell pressure acting on the sample.

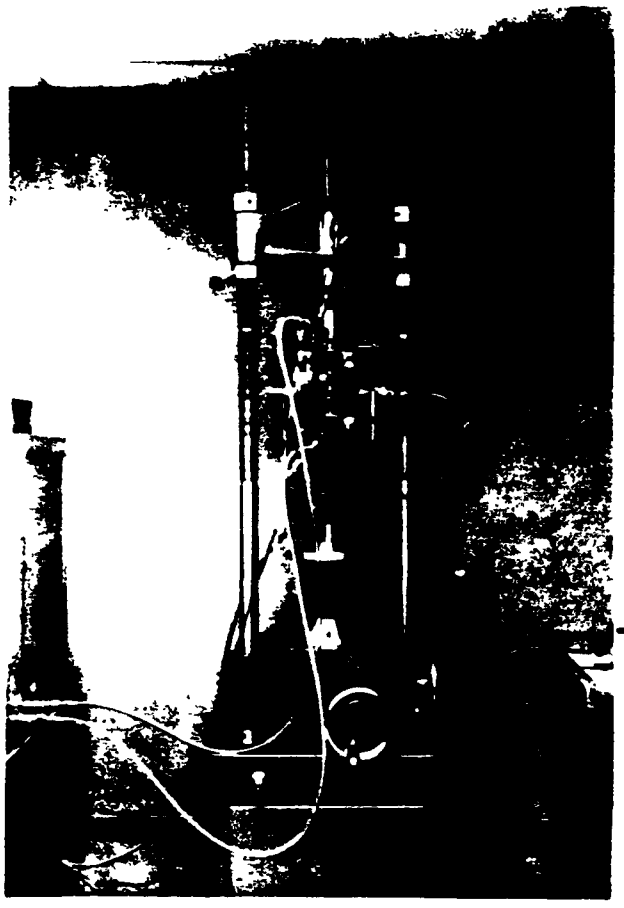

Figure B-1.

Hoek Cell Test Assembly

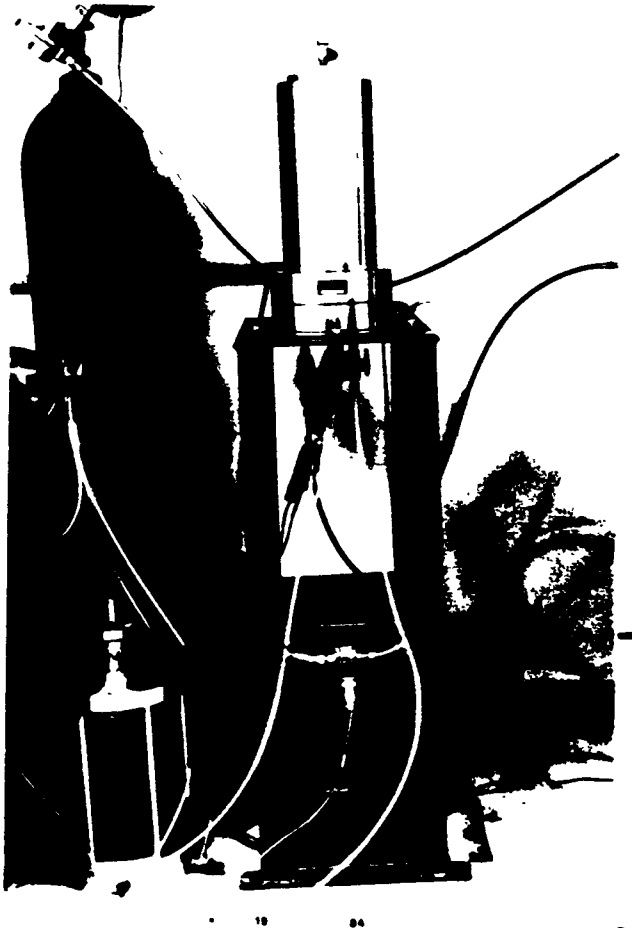

Figure B-2.

Pressure Vessel Test Assembly

APPENDIX C
ERROR ANALYSIS

APPENDIX C - ERROR ANALYSIS

An analysis was performed to estimate the systematic and random errors involved in the permeability measurements. Two techniques were used to measure permeability. For high permeability samples (10-1000 md), steady state or constant head permeability tests were performed. For low permeability samples (<1 md), a transient pressure step method similar to those presented by Sutherland and Cave (1980) was used. While the error analysis was conducted specifically for the tests conducted in the pressure vessel, the conclusions apply generally also to tests conducted in the Hoek cell. The following sections present underlying theoretical principles, systematic errors, and random errors for the two types of permeability tests.

C.1 STEADY STATE PERMEABILITY TEST

C.1.1 Systematic Errors

In the steady state permeability test, the sample (approximately 11 cm in length and 7 cm in diameter) is subjected to a differential pressure which induces steady-state flow of argon gas through the sample. Permeability is then calculated by a direct application of Darcy's Law for fluid flow through a porous medium. The permeability for the constant head permeability test for dry gas is given by ASTM STP 417 (Baptist, 1967):

$$K = \frac{2000\ q_g\ P_o\ L\ \mu_g}{(P_i^2 - P_o^2)\ A} \qquad (1)$$

where

K = gas permeability (md),

q_g = rate of gas flow through the sample (cm^3/sec),

μ_g = viscosity of gas at mean pressure and temperature (centipoises),

L = length of sample (cm),

A = cross-sectional area perpendicular to direction of flow (cm^2),

P_i = inlet pressure (atmospheres absolute), and

P_o = outlet pressure (atmospheres absolute).

The validity of test results is related to the applicability of Darcy's Law for the flow conditions. Experiments have shown that Darcy's Law applies when the Reynolds number, which expresses the ratio of inertial to viscous forces, is less than one (Todd, 1980). Reynolds number, N_R, is expressed by:

$$N_R = \frac{\rho V d_{10}}{\mu} \tag{2}$$

where

ρ = fluid density,

V = fluid velocity,

μ = absolute viscosity, and

d_{10} = the diameter corresponding to 10 percent finer by weight on the grain size distribution curve.

Considering values of gas velocity, density, and absolute viscosity for argon and grain size diameter d_{10} applicable to the current tests, the calculated maximum Reynolds number is much less than one and Darcy's Law is considered valid. Consequently, systematic errors for the constant head or steady state test are considered to be negligible in comparison to random errors.

C.1.2 Random Errors

The evaluation of random errors follows a method presented by Wilson (1950). The measured permeability, K, is related to the flow, pressure, fluid and geometric parameters by the relation:

$$K = F(X_1, X_2 \ldots X_n) \tag{3}$$

The square of the error is given as:

$$(dK)^2 = \sum_{i,\ j} \left(\frac{\partial F}{\partial X_i}\right)\left(\frac{\partial F}{\partial X_j}\right) dX_i\ dX_j \tag{4}$$

If the components are independently distributed and symmetrical with respect to positive and negative values, then:

$$(dK)^2 = \sum_{i=1}^{n} \left(\frac{\partial F}{\partial X_i}\right)^2 (dX_i)^2 \qquad (5)$$

If the error dX_i is set equal to the standard error, σ_i, for each of the independent variables X_i, then

$$\sigma_K^2 = \sum_{i=1}^{n} \left(\frac{\partial F}{\partial X_i}\right)^2 \sigma_i^2 \qquad (6)$$

Thus, the error in K is related to the square root of the sum of the products of each variable's sensitivity squared times the standard error squared for each variable.

The random error analysis is performed by applying Equation (6) to Equation (1) and accounting for gas flow rate, specimen length, specimen cross-sectional area, and pressures. It is generally found that the error is dominated by the product of sensitivity and standard error for a single parameter. However, the dominant parameter may change with respect to the magnitude of the quantity measured. In addition, it is difficult to judge a priori which source is dominant because of the complexity of the resulting sensitivity functions. Each of these potential sources of error is discussed subsequently.

The flow rate, q_g, of argon gas was measured by a Kurz flowmeter. The flow sensor operates as a constant-temperature thermal anemometer and responds to the mass flow by sensing the cooling effect of the air as it passes over the heated flow sensor. The flowmeter was calibrated by the manufacturer with an NBS traceable flowmeter. The calibration data indicate a nonlinear response of voltage with flow. This necessitated nonlinear regression analysis for estimation of the standard error. The standard error for nonlinear regression analysis was calculated as (Natrella, 1963):

$$\sigma^2 = \frac{1}{n-k} \sum_{i=1}^{n} r_i^2 \qquad (7)$$

where

σ = standard error in nonlinear regression analysis,

n = number of measurements in the calibration test,

k = number of constants in the nonlinear regression relation, and

r_i = residual value for the ith data point.

The calculated value for the error is ± 0.6 cm^3/sec when using the above relation for the whole range of flows in the test program.

The outlet pressure is assumed to be equal to 1 atmosphere, and thus would be subject to barometric pressure fluctuations during the course of the test. For a short-term test, the maximum error was estimated to be .03 atmospheres absolute.

As opposed to the measurement of inlet pressure, the differential pressure across the sample was measured. The differential pressure is measured by a Validyne differential pressure transducer, which is operational over a range of pressures of 0.08 to 3200 psi. This transducer was calibrated against a Digigage pressure transducer with a resolution of 0.02 psi. The value from the pressure transducer was corrected for system head loss for flow through the porous stones and piping.

Since pressure drop across the sample is not strictly independent of the variable flow rate, the issue arises as to the applicability of Equation (6), which treats flow rate and pressure differential as separate sources of error. A calculation was performed to compare the product of head loss sensitivity and error in flow rate to the standard error for calibration of the pressure transducer. This comparative analysis indicated that the error associated with system head loss was second order and negligible in comparison to the standard error from calibration. This provides a justification for treating flow rate and pressure differential measurements as separate sources of error. The error for the pressure differential was estimated at 0.004 atmospheres absolute.

The length of the sample was measured prior to testing using a caliper to within 0.002 cm, and then corrected for sample strain under confinement during the test. The correction for sample strain involved averaging two DCLVDT measurements which are estimated to have an error of 0.004 cm. The combined error in length measurement is, therefore, 0.006 cm.

The area was determined by calculation of the initial diameter (hence area) by a caliper, and then correcting for sample strain under confinement. The actual correction in area was determined by accounting for errors in system compliance and change in volume in the air/oil intensifier and dividing by the correct length. In a strict sense, the area measurement is not independent of the length measurement. However, the effects of the length correction are second order and ignored. The combined error from the several sources is estimated at 0.13 cm^2.

The random error analysis for the steady state permeability test was performed by applying Equation (6) to Equation (1) for errors in flow rate, specimen length, cross-sectional area, outlet pressure and inlet pressure. The calculations were performed for measured test data for permeability, ranging from several thousand millidarcies down to several millidarcies, as summarized in Table C-1.

The results indicate that there are two dominant sources of error for the steady state permeability measurements. When measured permeabilities are high (>1000 md), the measured flow rates are high under a low differential pressure, and errors are dominated by the differential pressure transducer measurements. When measured permeabilities are low (<1000 md), the flow rates are low and differential pressures are high, and errors are dominated by the flow measurements. The results indicate that the errors in permeability measurements are 10% or 3 md, whichever is greater for the range 10,000 to 3 md. This in turn indicates that the lower limit of permeability measured by this method with the current equipment is in the range 20 to 10 md.

Table C-1. Summary of Random Error Analysis for Steady-State Permeability Tests

Measured Permeability (md)	Estimated Error (md)	Percentage Error (%)	Dominant Source of Error
8700	800	9	Differential Pressure
4100	300	7	Differential Pressure
2000	100	5	Differential Pressure
780	18	2	Flowmeter/Differential Pressu
250	4.2	2	Flowmeter
95	4.4	5	Flowmeter
2.6	2.3	88	Flowmeter

C.2 TRANSIENT PERMEABILTIY TEST

Brace et al. (1968) introduced a transient permeability test method to measure the permeability of Westerly Granite. The experimental arrangement consisted of two pressure reservoirs separated by the specimen. At the start of the experiment, the fluid pressure in the upstream reservoir is suddenly increased. As this pressure decays, fluid flows from the upstream reservoir across the specimen to the downstream reservoir. If it is assumed that the sample does not exhibit compressive storage, then permeability is given by:

$$K = S \left(\frac{l}{A}\right) \frac{V_s \mu_g \beta_g}{9.87 \times 10^{-12}} \qquad (8)$$

where

K = permeability (md),
S = slope of the ln (P/P_o) vs. time curve (dimensionless),
V_s = volume of the downstream reservoir (cm^3),
l = length of the specimen (cm),
A = cross-sectional area of the specimen (cm^2),
μ_g = gas viscosity (poise),
β_g = gas compressibility ($cm/sec^2/gm$),
P = differential pressure across the specimen, and
P_o = initial differential pressure across the specimen.

The test method has been used by Sutherland and Cave (1980) to measure the permeability of low porosity WIPP rocksalt.

C.2.1 Systematic Errors

The applicability of the test method is tied closely to the assumption of negligible compressive storage in the specimen. Generally the method has been used for rocks such as granite or rocksalt which have low porosity. Hsieh et al. (1981) and Neuzil et al. (1981) present a detailed theoretical discussion of the method and develop type curves that can be used for data reduction in case of samples with non-

negligible porosity. Neuzil et al. present a solution that can be used to estimate the systematic error associated with compressive storage:

$$K' = K\left[\frac{\phi_1}{\tan\phi_1} + \frac{\beta}{1+\gamma}\right] \tag{9}$$

where

K' = hydraulic conductivity as calculated by Equation 8,

K = hydraulic conductivity as calculated by the method presented by Neuzil,

ϕ_1 = first root of the transcendental equation given below,

$$\frac{\phi_1^2}{\beta} = \frac{\beta}{\gamma} + \frac{(1+\gamma)}{\gamma}\frac{\phi_1}{\tan\phi_1}$$

$\beta = \dfrac{S_s A l}{S_u}$ = ratio of compressive storage of the specimen to compressive storage of the upstream reservoir,

$\gamma = \dfrac{S_d}{S_u}$ = ratio of compressive storage of the upstream reservoir to the downstream reservoir, and

S_s = specific storage of the specimen.

If it is assumed that the upstream and downstream reservoirs are rigid and that the specific storage of the specimen is dominated by the compressibility of the argon gas, then:

$$\beta = n \cdot A \cdot l / V_u \tag{10}$$

$$\gamma = \frac{V_d}{V_u} \tag{11}$$

where

n = porosity of the specimen,

V_u = volume of the upstream reservoir, and

V_d = volume of the downstream reservoir.

The applicability of the transient permeability test is thus seen to depend on the ratio of compressive storage of the sample to that in the upstream reservoir and the ratio of the downstream reservoir volume to the upstream reservoir volume. When the value of β is greater than .01, the method may underestimate the permeability if the porosity of the sample is not accounted for.

The above method was applied to evaluate tests conducted on specimens with porosities ranging from 5 to 15 percent. At a porosity of 15 percent the estimated ratio β is .02. At a porosity of 5 percent, the estimated ratio β is .008. The analysis indicated that the permeability at 15 percent porosity would be underestimated by about 40 percent if Equation (8) was used (i.e. ignoring porosity effects). At about 5 percent porosity, permeability would be underestimated by about 20 percent. The error is lower for lower porosities because the compressive storage of the sample is lower.

Another investigator (Trimmer, 1981) presented a different method for evaluating the systematic error attributable to compressive storage. In this analysis, the one-dimensional fluid transport equation was solved numerically to generate pressure decay vs. time curves on a logarithmic scale. Equation (8) was then used to calculate a permeability value which could be compared with the assumed permeability in the numerical analysis.

An empirical relationship developed by Trimmer was applied to test data obtained from the third consolidation test over a range of porosities from 12 percent to 5 percent. The method indicated that the permeabilities calculated using Equation (8) would underestimate the true value by from 30 percent (for 12 percent porosity) to 15 percent (for 5 percent porosity). Therefore, the analysis presented by Trimmer is in general agreement with the analysis presented by Neuzil et al.

In conclusion, the analyses presented above indicate that there is a systematic error associated with compressive storage of the sample. For high porosity samples, the permeability is underestimated by up to 40 percent. Unfortunately, the analysis does not provide a ready method for correcting each test result. This would require a numerical analyses of each test.

C.2.2 Random Errors

A. Instrumentation Errors

The evaluation of random errors follows the method presented by Wilson (1950) in which Equation (6) is applied to Equation (8) for errors in the slope of the pressure decay vs time curve, specimen length, specimen area, and volume of the downstream reservoir. Each of these sources of error is discussed below.

The slope of the pressure decay vs time curve is determined by semilogarithmic linear regression analysis. Natrella (1963) presents a method for estimating the variance of the slope from the data. The variance incorporates the errors in measurement by the downstream pressure transducers and fluctuations in temperature that would affect temperature measurement during the test. The temperature effects are thus treated as a random variable under control during the experiment.

Two sets of data were evaluated for purposes of estimating the slope variance of the pressure decay vs time curve. One set applied to a measured permeability of .02 md with data recorded over a three-minute time period. The other set applied to a measured permeability of 1.4×10^{-6} md with data recorded over several hours. The estimated slope variance for the first data set, expressed as a percentage of the reduced slope is 0.3%. The estimated slope variance for the second set is 17%, indicating that much smaller pressure changes, which are closer to instrument resolution, were measured in the second test.

The determination of specimen length is the same as the determination of length in the constant pressure head test (Section C.1.2) The same error of 0.006 cm is assumed for analysis.

The determination of specimen area was performed by measurement of an initial diameter and correcting for changes in area of the specimen under confining stress. The determination parallels the random error analysis in the steady state test. The estimated error in area is 0.13 cm^2.

The downstream reservoir volume was measured by initially weighing the downstream apparatus, saturating the reservoir with water, and weighing the filled apparatus. The volume was determined from the difference in weights and the unit weight of water. The resolution in weighing the apparatus is .02 grams. The estimated error in the volume measurement is 0.02 cm^3.

The results of the random error analysis indicated that pressure decay was the dominant source of error over a range of permeability from 10^{-2} md to 10^{-6} md. The estimated error from the analysis is 1% or 10^{-6} md, whichever is greater.

B. Interpretation Errors

An examination of the permeability vs porosity data obtained from transient tests in the third consolidation test reveals some scatter, suggesting that the actual error may be higher than the value of 10^{-6} md calculated above. For example, two tests were performed on the same sample at times of 96 hours and 168 hours after application of 2500 psi effective confining pressure (3000 psi total pressure). The porosities calculated from the axial strains measured at the times of the two tests are 5.8 and 5.4 percent respectively. The confining pressure was held constant (within 25 psi) between the two tests and the test method was the same. Any systematic error due to specimen storage (Section C.2.1) should be roughly the same since there is little difference in poro-

sity. Accordingly, the permeabilities measured from the two tests should be similar. Based on the expected trend, the permeability from the test at 168 hours should be slightly lower. In fact, the reported permeabilities are 2.4×10^{-6} md from the first test at 96 hours and 5.9×10^{-6} md from the second test at 168 hours.

The semilogarithmic pressure decay plots from the two tests discussed above are shown in Figures C-1 and C-2. The permeabilities reported above were calculated from the slopes drawn on the figures. It will be noted that the pressure decay plots are not perfectly linear and that some subjectivity is involved in curve fitting. Indeed, the difference in the two permeabilities reported above can be explained by an error in curve fitting. A lower value for the second test at 168 hours could be obtained from a linear fit to the pressure decay curve after 7000 seconds rather than from the linear fit to the data over the range 3000-10000 seconds.

Characteristically, none of the pressure decay curves obtained from all of the tests displays a truly linear segment, although many are less difficult to interpret than those shown in Figures C-1 and C-2. Figure C-3 is an example of a curve obtained from a higher porosity material in which the pressure decay was much more rapid than in Figures C-1 and C-2. In this case the curve is essentially linear over a significant part, although there is some "tailing off" towards the end of the test.

Conceptually, there are many factors which might influence the shape of the pressure decay curves obtained from transient tests. These might include:

- compressive storage effects due to high porosity
- material properties changing during the course of a test due to creep (although the maximum test duration was less than 5 hours and was only a few minutes in several cases)
- experimental factors such as sizes of reservoirs

- experimental control, e.g. rate of pressure application
- temperature or barometric pressure fluctuations (although again the test durations were relatively short).

The present error analysis does not distinguish the relative influence of these parameters on the shapes of the pressure decay curves and hence on the reported permeability values. From examination of the permeability vs porosity data from Test 3, a tentative conclusion is that the scatter (hence the error) in the permeability value is ± 50%. The significance of this apparently large error is diminished by consideration that the permeability testing program (steady state and transient methods) covers a range of values of 11 orders of magnitude.

It is recommended that interpretation of future tests should utilize dimensionless type curves similar to those presented by Neuzil et al. These curves could be developed for a specific equipment set-up and for samples of varying porosity using a numerical method. Curve matching could be performed to estimate permeability and specific storage. Additionally, specific storage could be calculated by knowledge of compressibilities and porosity. Curve matching would provide insight into flow mechanisms during the test and allow material response to be delineated.

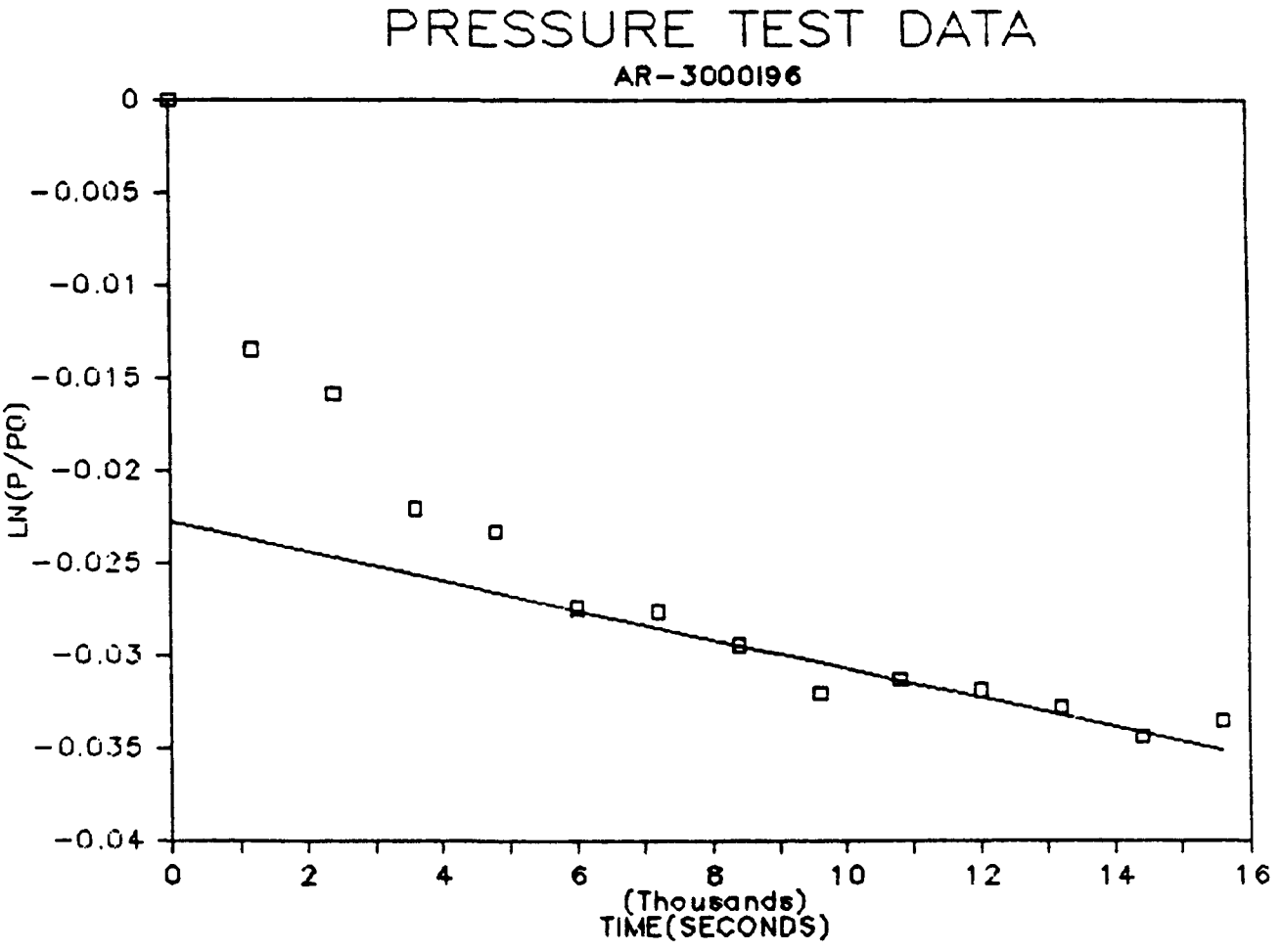

Figure C-1. Pressure Decay Curve from Test After 96 Hours at 3000 psi Total Confining Pressure

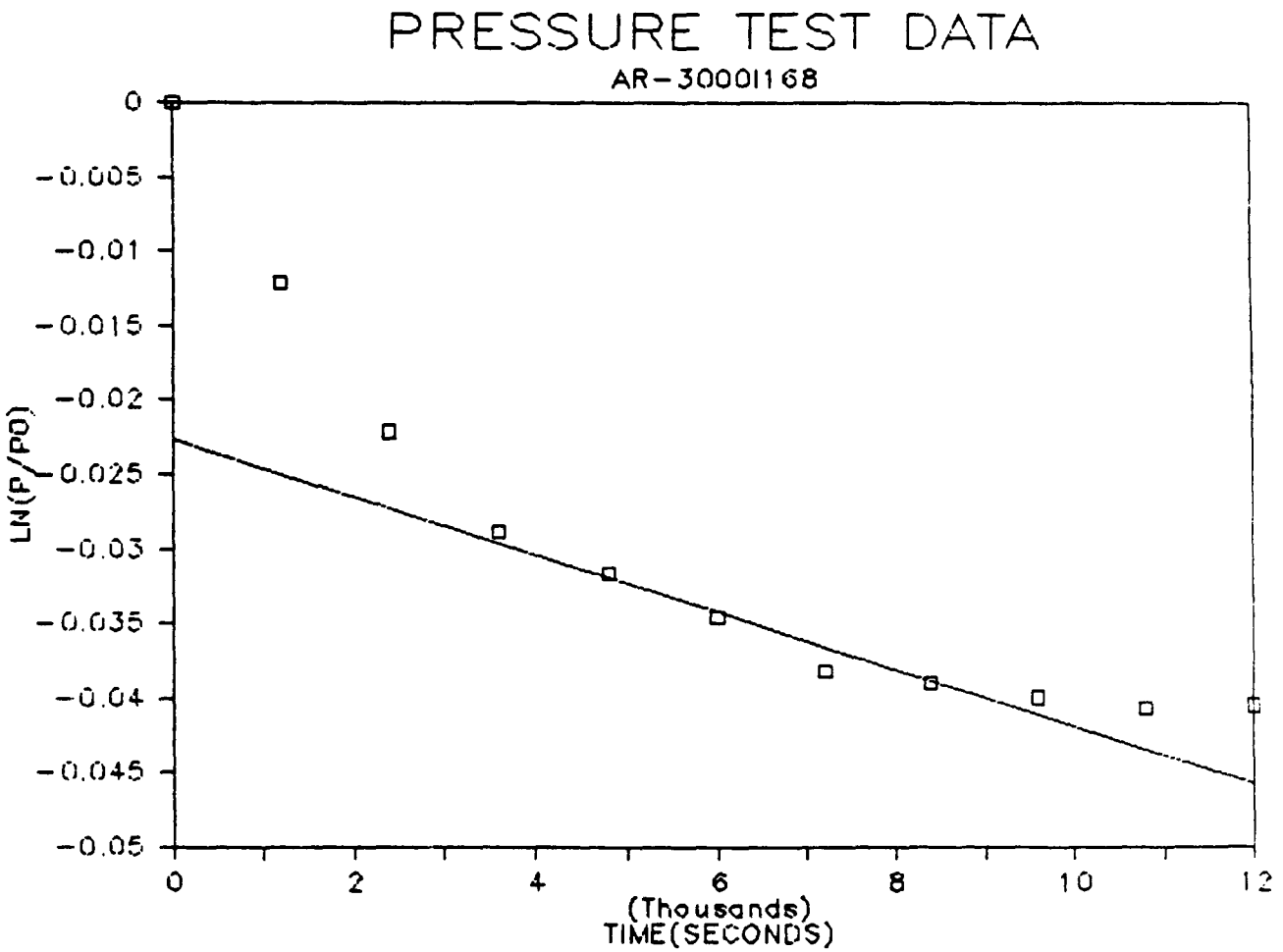

Figure C-2. Pressure Decay Curve from Test After 168 Hours at 3000 psi Total Confining Pressure

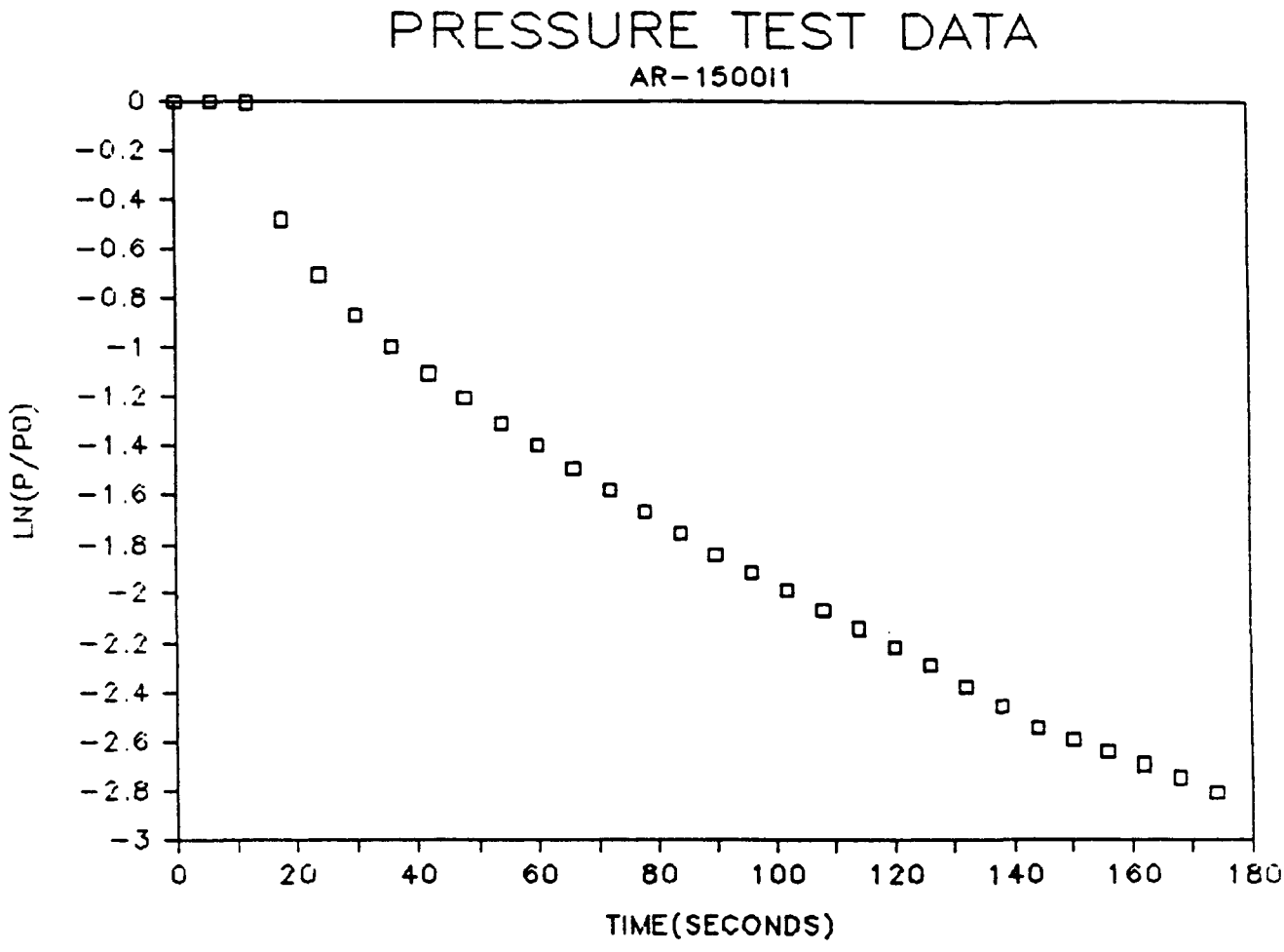

Figure C-3. Pressure Decay Curve from Test After 1 Hour at 1500 psi Total Confining Pressure

APPENDIX C REFERENCES

Baptist, O. C., 1967, "Permeability and Capillarity in Petroleum Reservoir Engineering," Permeability and Capillarity of Soils, ASTM STP 417, American Society of Testing Materials, p. 88.

Brace, W. F., J. B. Walsh and W. T. Frangos, 1968, "Permeability of Granite Under High Pressure," Journal of Geophysical Research, Vol. 73, pp. 2225-2236.

Hsieh, P. A., J. V. Tracy, C. E. Neuzil, J. B. Bredehoeft and S. E. Silliman, 1981, "A Transient Laboratory Method for Determining the Hydraulic Properties of 'Tight' Rocks; I - Theory," International Journal of Rock Mechanics, Mining Sciences and Geomechanics Abstracts, Vol. 18, pp. 245-252.

Natrella, M. G., 1963, Experimental Statistics, National Bureau of Standards Handbook 91, National Bureau of Standards, Washington, DC.

Neuzil, C. E., C. Cooley, S. E. Silliman, J. D. Bredehoeft and P. A. Hsieh, 1981, "A Transient Laboratory Method for Determining the Hydraulic Properties of 'Tight' Rocks; II - Application," International Journal of Rock Mechanics, Mining Sciences and Geomechanics Abstracts, Vol. 18, pp. 253-258.

Sutherland, H. J. and S. P. Cave, 1980, "Argon Gas Permeability of New Mexico Rock Salt Under Hydrostatic Compression," International Journal of Rock Mechanics, Mining Sciences and Geomechanics Abstracts, Vol. 17, pp. 281-288.

Todd, D. K., 1980, Groundwater Hydrology, John Wiley and Sons, New York, NY, 2nd edition.

Trimmer, D. A., 1981, "Design Criteria for Laboratory Measurements of Low Permeability Rocks," Geophysical Research Letters, Vol. 8, No. 9, pp. 973-975.

Wilson, E. B., 1950, Introduction to Scientific Research, McGraw Hill, New York.

APPENDIX D
TEST DATA

This Appendix presents test data obtained from the testing program together with computed values for porosity and bulk modulus. Complete test data are filed on floppy disks compatible with an Apple microcomputer.

D.1 CONSOLIDATION TESTS

Data are presented for four tests:

Test No.	Sample No.	Salt Type
1	M10	WIPP, max grain size 10mm, dry
2	M1	WIPP, max grain size 0.9mm, dry
3	AR	WIPP, max grain size 20mm, 2.3% moisture
4	AM10	Avery Island, max grain size 10mm, dry

The following data are presented:

Initial Porosity -	determined prior to test by direct measurement of sample volume and weight
Final Porosity -	determined after test by direct measurement of sample volume and weight
Compliance Porosity -	calculated from the initial porosity according to the volume of oil injected into the cell considering the compliance of the system
Corrected Porosity -	calculated from the initial and final porosities and the total corresponding axial strain, assuming that change in porosity is proportional to axial strain
Confining Pressure -	oil pressure in the cell
Effective Confining Pressure -	oil pressure in the cell minus the gas pressure in the sample
Time of Pressure Application -	duration since the cell pressure was raised to the value from time = zero for each confining pressure
Axial Strain -	average of 2 axial LVDTs
Bulk Modulus -	pressure change divided by volumetric strain, calculated for a

	quasi-static pressure increment, where volumetric strain is referenced to the volume at the beginning of the pressure increment
Permeability -	permeability to argon gas by steadystate or transient method; means ($\bar{x}$) and standard deviations ($\bar{\sigma}$) are presented for (typically) 3 sensor readings taken at each of several flow rates for each confining pressure

MEASURED INITIAL AND FINAL POROSITIES - ALL CONSOLIDATION TESTS

Test No.	Sample No.	Initial Measured Sample Data				Final Measured Sample Data		
		Weight (gm)	Length (in.)	Diameter (in.)	Porosity	Length (in.)	Diameter (in.)	Porosity
1	M10	730.60	4.50	2.80	0.262	4.242	2.702	0.159
2	M1	634.38	4.474	2.811	0.360	4.065	2.626	0.193
3	AR	696.72	4.529	2.813	0.307	3.989	2.554	0.045
4	AM10	730.26	4.526	2.787	0.256	4.269	2.661	0.135

CONSOLIDATION TEST 1 - TEST DATA
Sample Number: M10

MEASURED VALUES			INTRINSIC PERMEABILITY		COMPUTED VALUES	
CONFINING PRESSURE (psi)	TIME OF PRESSURE APPLICATION (hrs)	AXIAL STRAIN	$\bar{X}$ (md)	$\bar{\sigma}$ (md)	COMPLIANCE POROSITY	CORRECTED POROSITY
0	0	0				0.262
50	0	0.00447	3966	62	0.271	0.255
54	23	0.00465	3606	206	0.262	0.255
53	40	0.00473	3735	84	0.261	0.255
501	0	0.02243	1864	59	0.236	0.228
518	2	0.02393	1663	71	0.235	0.226
504	4	0.02474	1557	75	0.237	0.225
504	6	0.02545	1473	68	0.240	0.224
505	10	0.02568	1531	56	0.244	0.223
504	24	0.02571	1396	39	0.239	0.223
994	0	0.03353	954	39	0.226	0.211
1014	4	0.03640	824	43	0.223	0.207
1007	6	0.03697	781	40	0.224	0.206
1017	8	0.03725	775	39	0.225	0.206
1014	24	0.03769	749	32	0.220	0.205
986	32	0.03862	612	29	-	0.204
1000	48	0.03883	715	28	0.217	0.203
1501	0	0.04349	582	29	0.210	0.196
1505	2	0.04553	486	43	0.207	0.193
1483	4	0.04460	479	24	0.209	0.195
1478	6	0.04495	500	37	0.209	0.194
1505	8	0.04541	463	22	0.209	0.193
1505	24	0.04754	435	30	0.200	0.190
1505	28	0.04796	423	20	0.204	0.190
1502	32	0.04832	460	22	0.205	0.189
1498	48	0.04840	433	20	0.198	0.189
2003	0	0.05114	354	17	0.195	0.185

CONSOLIDATION TEST 1 - TEST DATA (continued)
Sample Number: M10

MEASURED VALUES					COMPUTED VALUES	
			INTRINSIC PERMEABILITY			
CONFINING PRESSURE (psi)	TIME OF PRESSURE APPLICATION (hrs)	AXIAL STRAIN	$\bar{X}$ (md)	$\bar{\sigma}$ (md)	COMPLIANCE POROSITY	CORRECTED POROSITY
2002	2	0.05330	308	23	0.192	0.182
1985	4	0.05410	309	14	0.193	0.180
2019	6	0.05443	313	15	0.194	0.180
2005	8	0.05450	268	16	0.195	0.180
2003	28	0.05541	302	16	0.187	0.178
2004	48	0.05617	247	14	0.183	0.177
2003	72	0.05694	266	13	0.188	0.176
2007	96	0.05765	243	12	0.182	0.175
2494	0	0.05895	196	12	0.182	0.173
2501	2	0.06041	202	12	0.180	0.171
2498	4	0.06074	189	8	0.182	0.170
2492	6	0.06108	187	9	0.180	0.170
2511	8	0.06147	187	9	0.179	0.169
2505	24	0.06258	173	8	0.172	0.168
2492	28	0.06286	167	7	0.175	0.167
2513	32	0.06297	159	8	0.175	0.167
2498	48	0.06387	145	5	0.170	0.166
2513	75	0.06446	149	6	0.170	0.165
2510	97	0.06500	135	5	0.167	0.164
2516	108	0.06518	138	6	0.170	0.164
2499	120	0.06541	138	9	0.168	0.163
2502	144	0.06579	135	5	0.170	0.163
2505	168	0.06619	109	6	0.167	0.162
2499	192	0.06652	126	6	0.168	0.162
2502	216	0.06672	111	7	0.167	0.161
2497	253	0.06725	108	9	0.164	0.160

CONSOLIDATION TEST 1 - TEST DATA (continued)
Sample Number: M10

MEASURED VALUES					COMPUTED VALUES	
			INTRINSIC PERMEABILITY			
CONFINING PRESSURE (psi)	TIME OF PRESSURE APPLICATION (hrs)	AXIAL STRAIN	$\bar{X}$ (md)	$\bar{\sigma}$ (md)	COMPLIANCE POROSITY	CORRECTED POROSITY
2499	288	0.06747	115	6	0.161	0.160
2506	312	0.06766	108	6	0.162	0.160
2512	336	0.06797	114	5	0.165	0.159
2502	360	0.06795	109	3	0.161	0.159
2502	384	0.06823	108	4	0.165	0.159
2501	412	0.06824	113	4	0.164	0.159
0						0.159

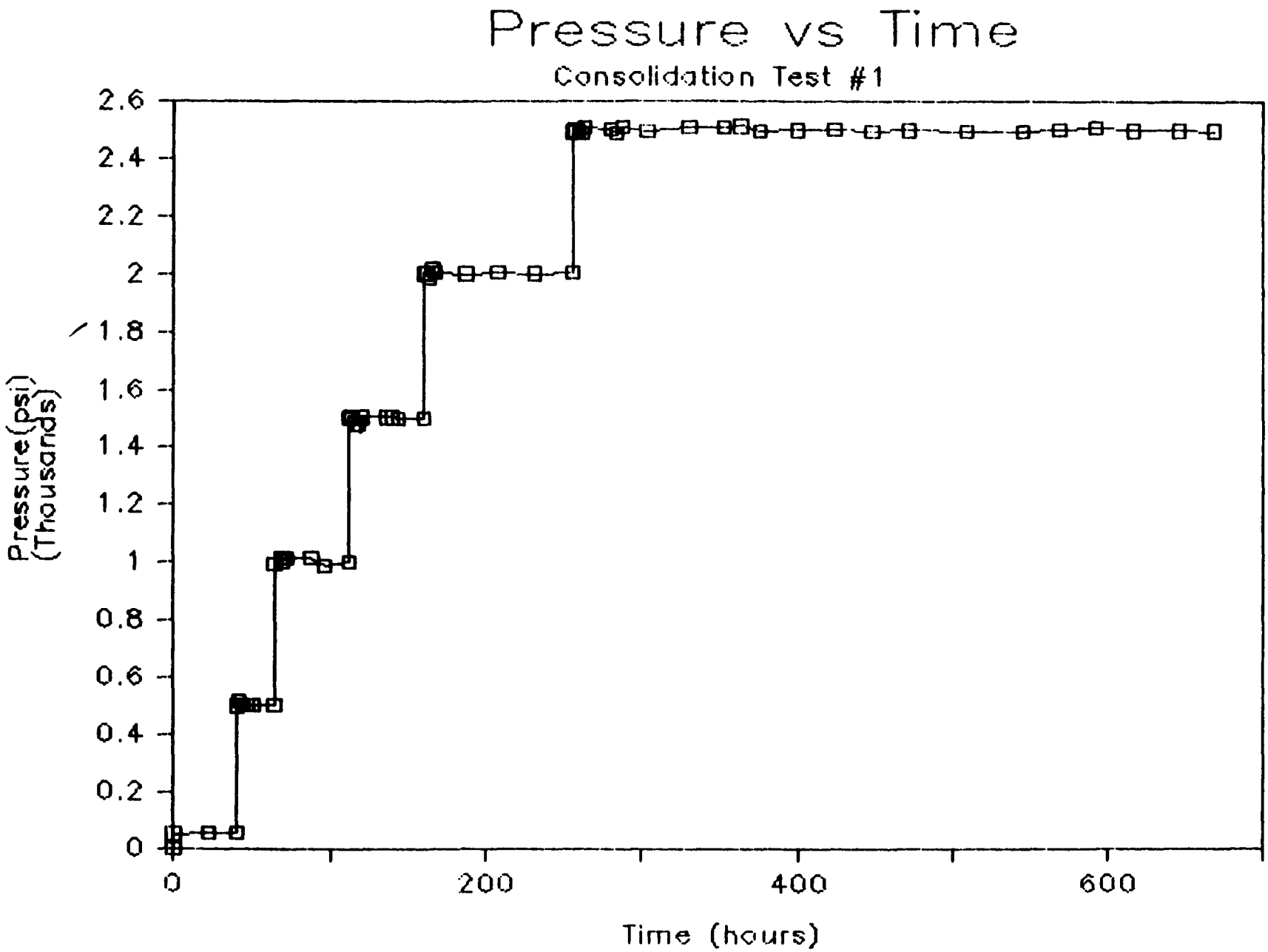
Pressure vs Time
Consolidation Test #1
Pressure(psi)
(Thousands)
2.6
2.4
2.2
2
1.8
1.6
1.4
1.2
1
0.8
0.6
0.4
0.2
0
0
200
400
600
Time (hours)

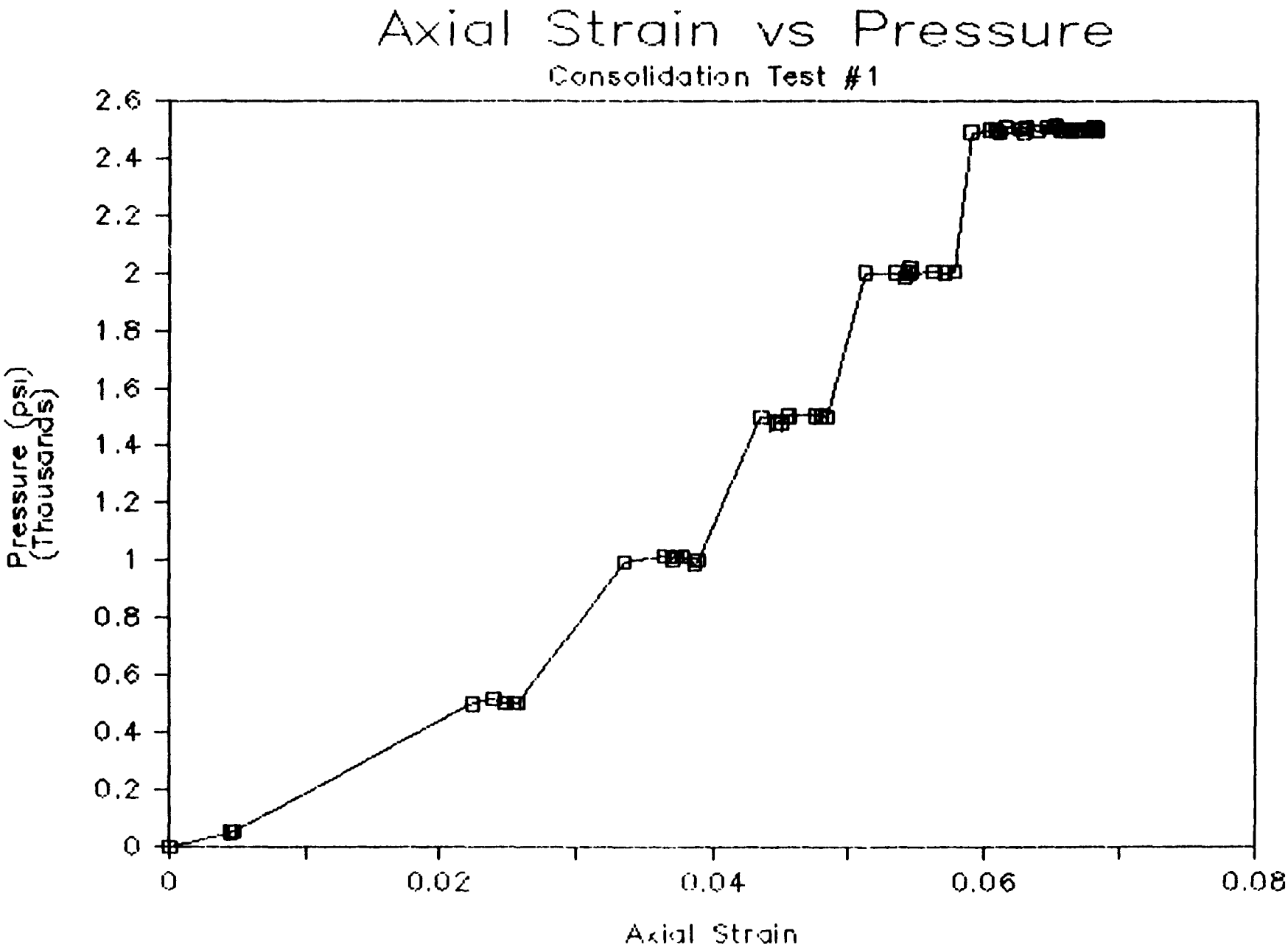
Axial Strain vs Pressure
Consolidation Test #1
Pressure (psi)
(Thousands)
2.6
2.4
2.2
2
1.8
1.6
1.4
1.2
1
0.8
0.6
0.4
0.2
0
0
0.02
0.04
0.06
0.08
Axial Strain

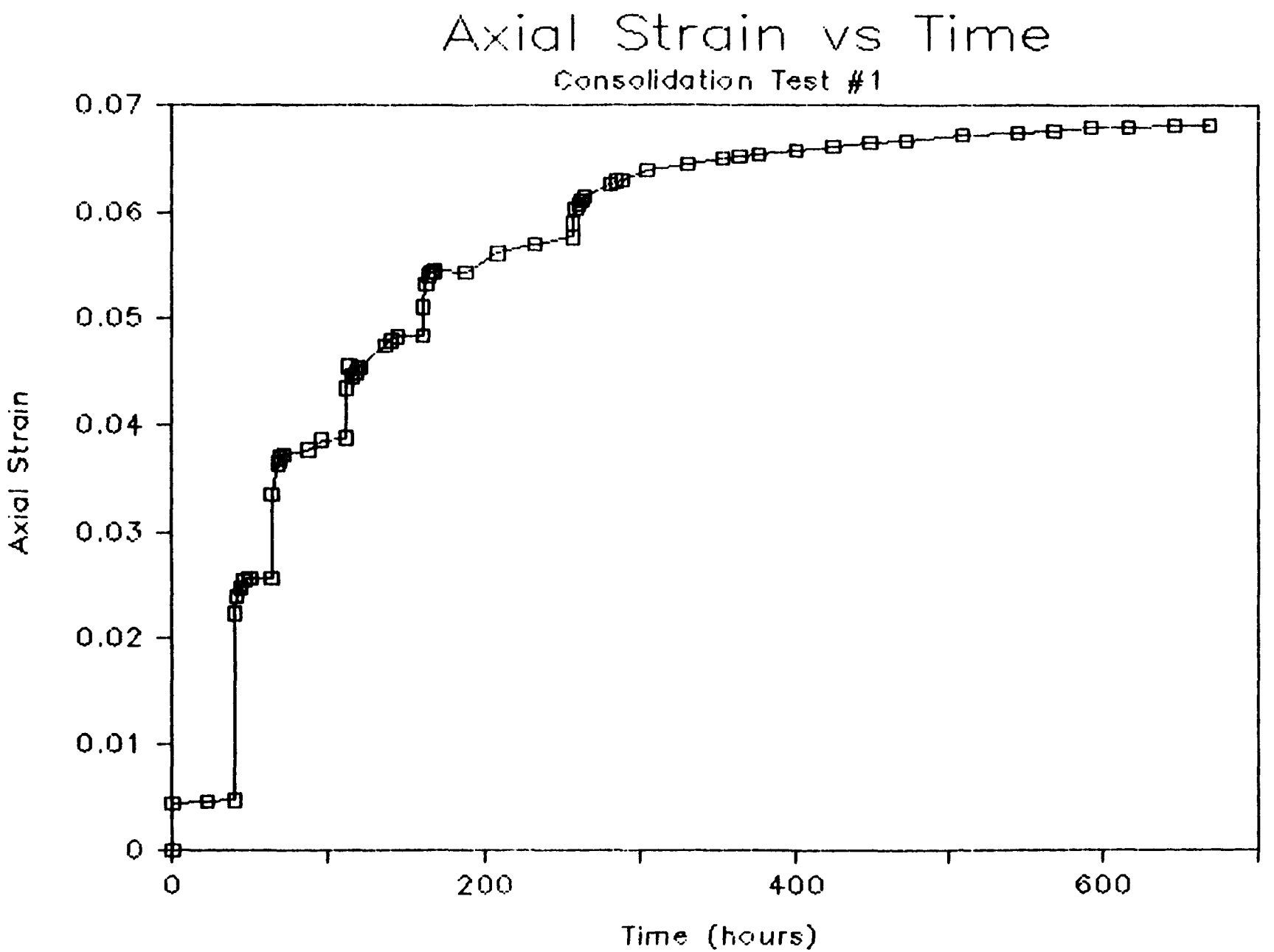
Axial Strain vs Time
Consolidation Test #1
Axial Strain
0.07
0.06
0.05
0.04
0.03
0.02
0.01
0
0
200
400
600
Time (hours)

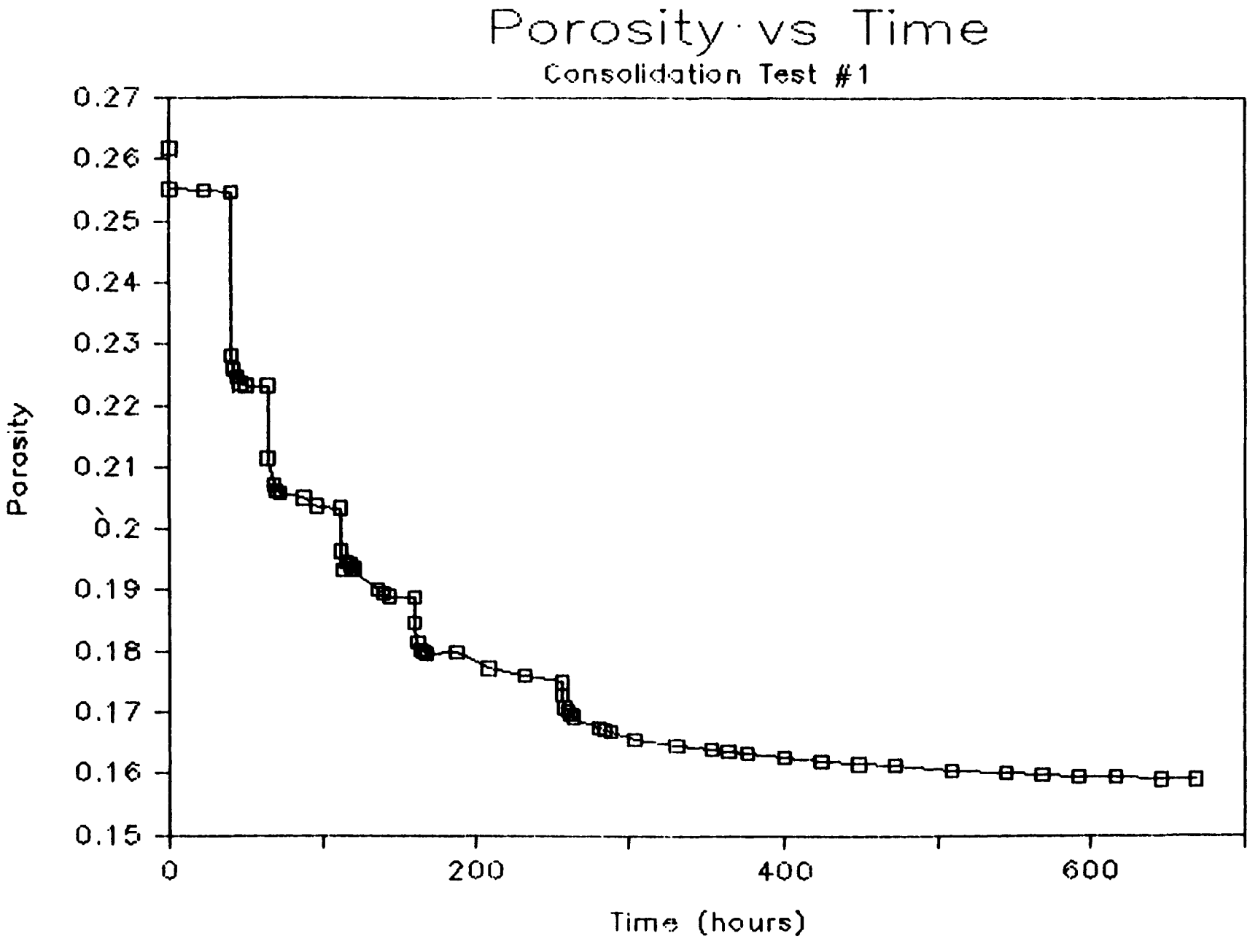
Porosity vs Time
Consolidation Test #1
Porosity
0.27
0.26
0.25
0.24
0.23
0.22
0.21
0.2
0.19
0.18
0.17
0.16
0.15
0
200
400
600
Time (hours)

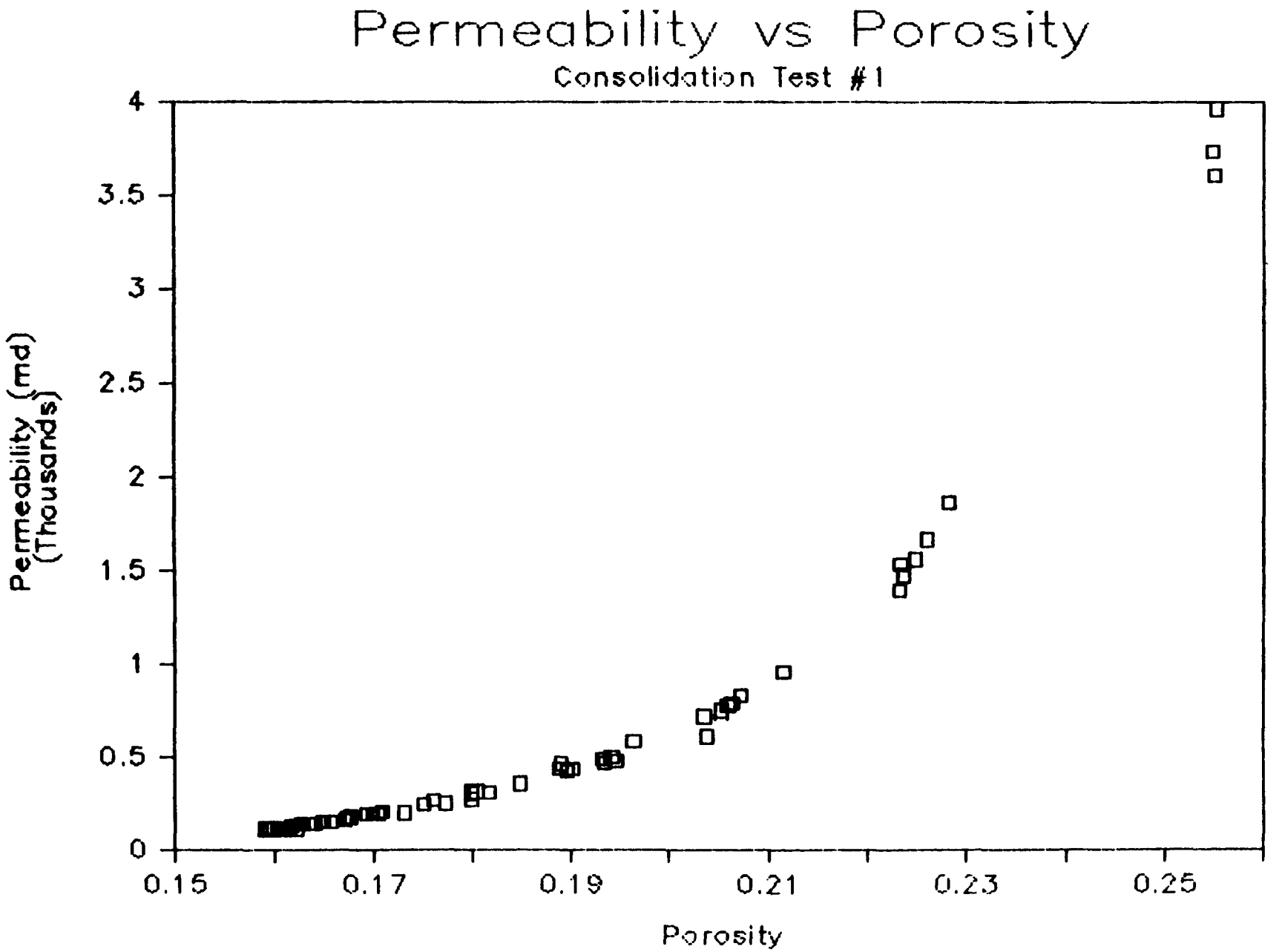
Permeability vs Porosity
Consolidation Test #1
Permeability (md)
(Thousands)
4
3.5
3
2.5
2
1.5
1
0.5
0
0.15
0.17
0.19
0.21
0.23
0.25
Porosity

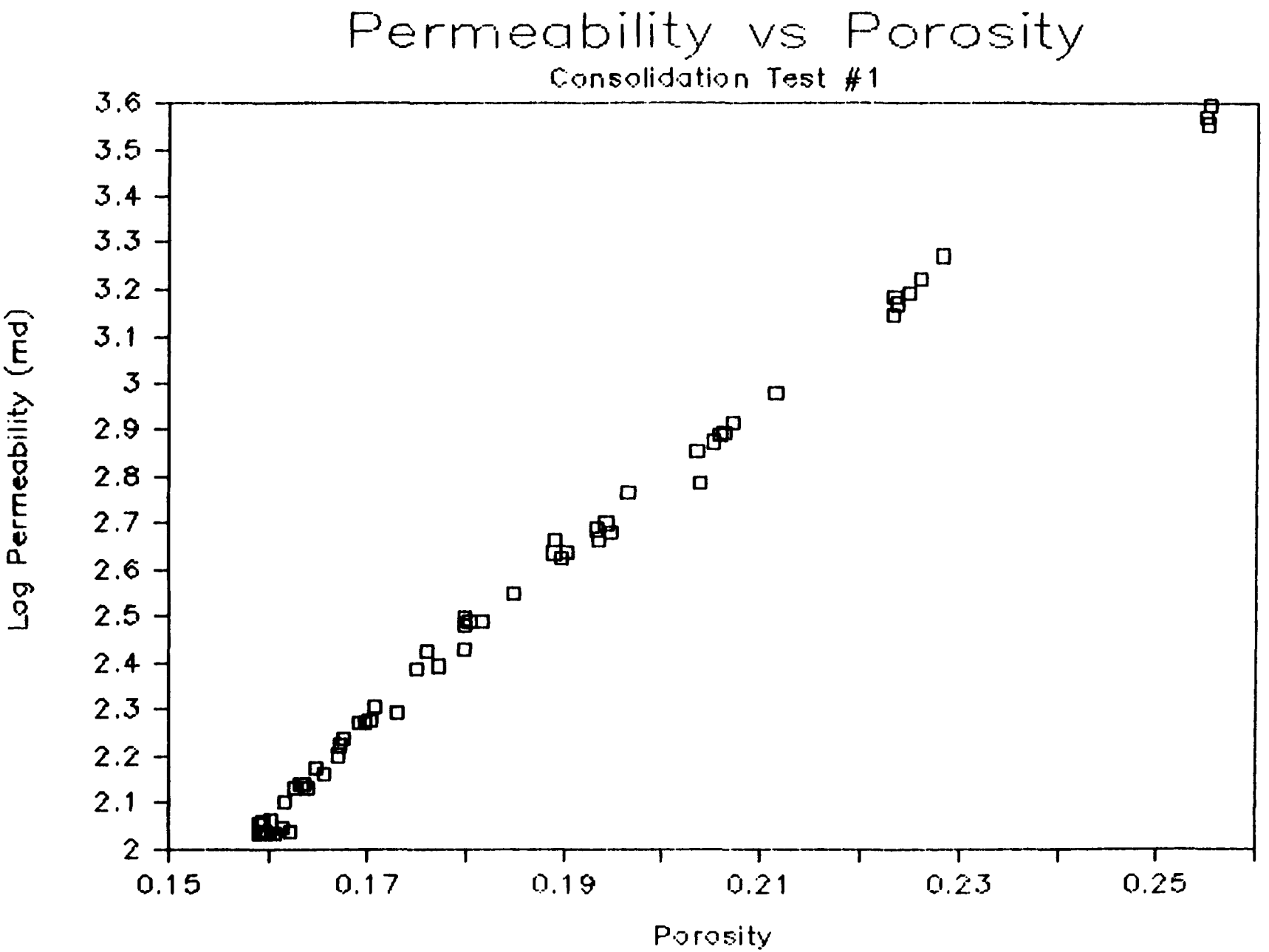
Permeability vs Porosity
Consolidation Test #1
Log Permeability (md)
3.6
3.5
3.4
3.3
3.2
3.1
3
2.9
2.8
2.7
2.6
2.5
2.4
2.3
2.2
2.1
2
0.15
0.17
0.19
0.21
0.23
0.25
Porosity

CONSOLIDATION TEST 2 - TEST DATA
Sample Number: M1

MEASURED VALUES					COMPUTED VALUES	
			INTRINSIC PERMEABILITY			
CONFINING PRESSURE (psi)	TIME OF PRESSURE APPLICATION (hrs)	AXIAL STRAIN	- X (md)	- σ (md)	COMPLIANCE POROSITY	CORRECTED POROSITY
0	0	0				0.360
49	0	0.00270	2166	87	0.373	0.355
62	3	0.00390	1777	117	0.374	0.353
45	6	0.00380	1773	177	0.371	0.354
49	9	0.00387	1829	96	0.372	0.353
53	21	0.00388	2008	79	0.371	0.353
496	0	0.02923	989	46	0.335	0.310
500	2	0.03123	964	38	0.333	0.307
501	4	0.03171	824	61	0.333	0.306
500	6	0.03227	827	53	0.334	0.305
497	24	0.03302	923	35	0.326	0.304
499	28	0.03326	915	38	0.328	0.303
501	32	0.03346	907	39	0.330	0.303
501	48	0.03373	903	39	0.325	0.302
499	81	0.03441	871	41	0.325	0.301
497	103	0.03455	845	38	0.320	0.301
498	168	0.03663	826	33	0.320	0.297
1009	0	0.04733	597	26	0.303	0.279
1007	2	0.04990	517	32	0.300	0.275
1005	4	0.05078	497	35	0.299	0.273
1001	6	0.05144	525	27	0.299	0.272
997	8	0.05171	485	31	0.298	0.272
998	23	0.05252	475	29	0.294	0.270
1001	32	0.05341	517	23	0.294	0.269
1011	48	0.05431	496	23	0.292	0.267
1506	0	0.06121	404	15	0.282	0.255

CONSOLIDATION TEST 2 - TEST DATA (Continued)
Sample Number: M1

MEASURED VALUES					COMPUTED VALUES	
			INTRINSIC PERMEABILITY			
CONFINING PRESSURE (psi)	TIME OF PRESSURE APPLICATION (hrs)	AXIAL STRAIN	$\bar{X}$ (md)	$\bar{\sigma}$ (md)	COMPLIANCE POROSITY	CORRECTED POROSITY
1485	2	0.06387	332	26	0.277	0.251
1427	4	0.06436	361	17	0.276	0.250
1502	6	0.06478	361	16	0.275	0.249
1489	9	0.06577	307	23	0.275	0.248
1497	23	0.06741	329	13	0.271	0.245
1505	33	0.06903	311	13	0.275	0.242
1504	48	0.06958	310	14	0.269	0.241
1993	0	0.07681	237	10	0.258	0.229
2002	2	0.07746	224	16	0.256	0.228
1998	4	0.07787	223	9	0.256	0.227
2003	47	0.07934	208	9	0.244	0.224
2001	72	0.08113	198	8	0.243	0.221
2002	96	0.08223	184	8	0.244	0.220
2003	120	0.08319	181	7	0.240	0.218
2505	0	0.08480	166	7	0.239	0.215
2506	2	0.08658	154	6	0.236	0.212
2498	4	0.08778	147	7	0.236	0.210
2506	6	0.08857	140	6	0.237	0.209
2506	10	0.08926	137	9	0.233	0.208
2506	24	0.09032	131	5	0.228	0.206
2509	36	0.09162	120	6	0.227	0.204
2508	49	0.09241	120	6	0.226	0.202
2500	95	0.09325	115	6	0.223	0.201
2495	124	0.09353	102	7	0.228	0.200
2495	144	0.09632	98	5	0.217	0.195
2493	168	0.09666	97	5	0.216	0.195

CONSOLIDATION TEST 2 - TEST DATA (continued)
Sample Number: M1

MEASURED VALUES					COMPUTED VALUES	
			INTRINSIC PERMEABILITY			
CONFINING PRESSURE (psi)	TIME OF PRESSURE APPLICATION (hrs)	AXIAL STRAIN	$\bar{X}$ (md)	$\bar{\sigma}$ (md)	COMPLIANCE POROSITY	CORRECTED POROSITY
2499	192	0.09678	93	5	0.218	0.195
2496	264	0.09718	85	8	0.213	0.194
2493	288	0.09722	90	4	0.217	0.194
2493	312	0.09740	93	3	0.214	0.194
2489	336	0.09771	85	5	0.215	0.193
2492	360	0.09774	87	5	0.218	0.193
1987	0	0.09777	87	5	0.217	0.193
1995	2	0.09769	85	5	0.219	0.193
1999	24	0.09762	89	4	0.218	0.193
994	0	0.09738	80	6	0.216	0.194
992	2	0.09747	73	7	0.220	0.194
992	46	0.09745	91	4	0.215	0.194
0						0.193

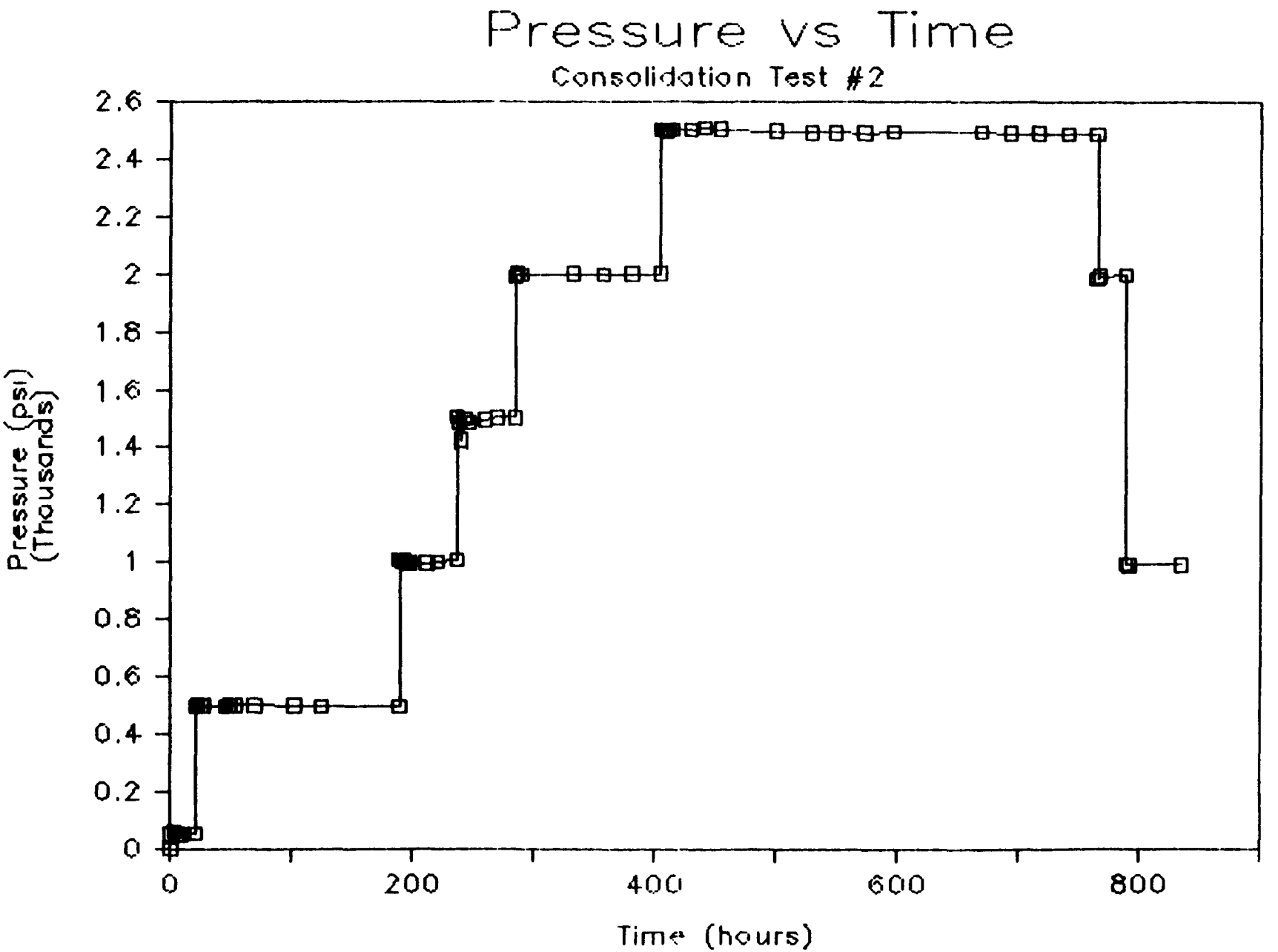
Pressure vs Time
Consolidation Test #2
Pressure (psi)
(Thousands)
2.6
2.4
2.2
2
1.8
1.6
1.4
1.2
1
0.8
0.6
0.4
0.2
0
0
200
400
600
800
Time (hours)

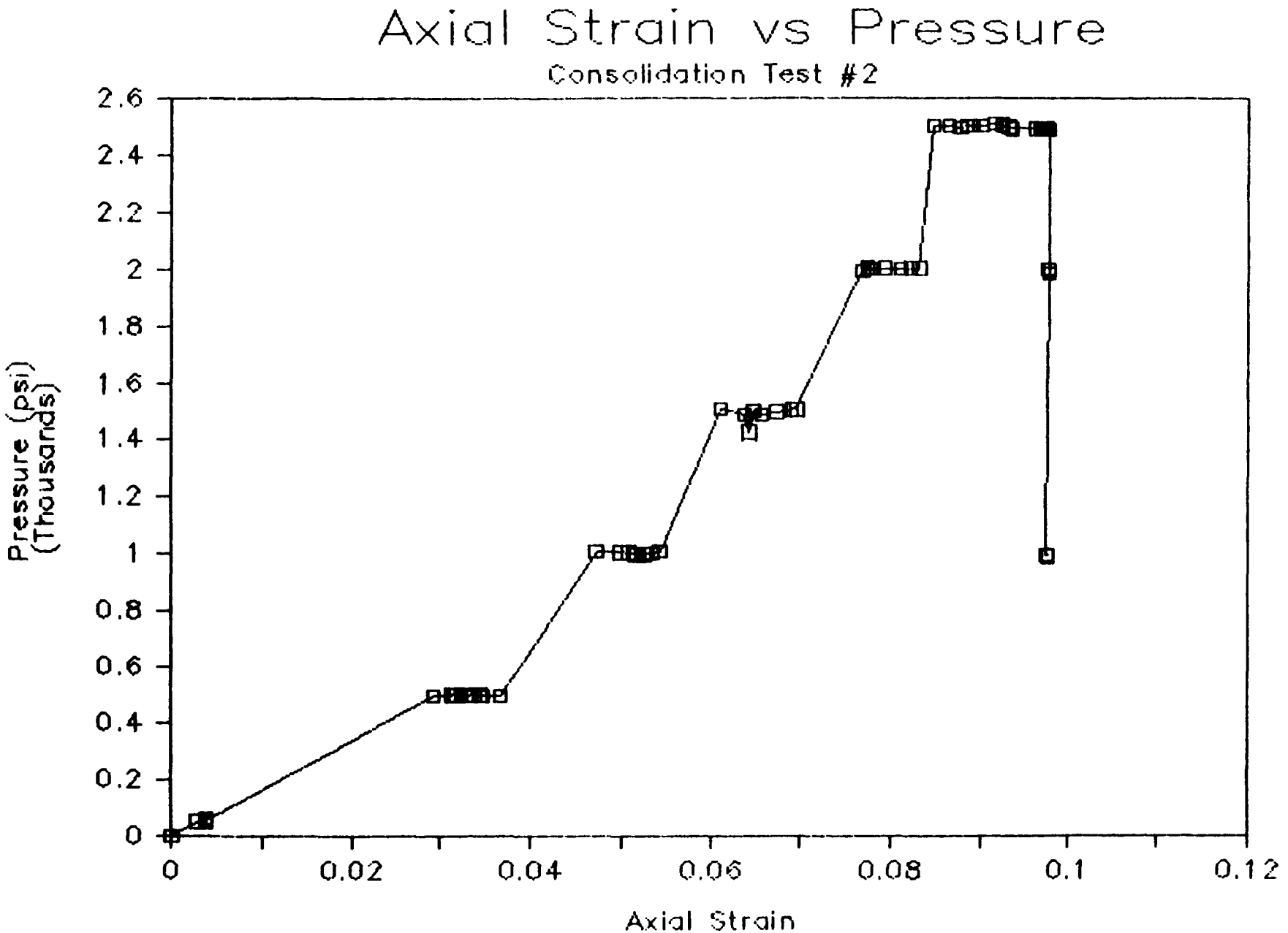
Axial Strain vs Pressure
Consolidation Test #2
Pressure (psi)
(Thousands)
2.6
2.4
2.2
2
1.8
1.6
1.4
1.2
1
0.8
0.6
0.4
0.2
0
0
0.02
0.04
0.06
0.08
0.1
0.12
Axial Strain

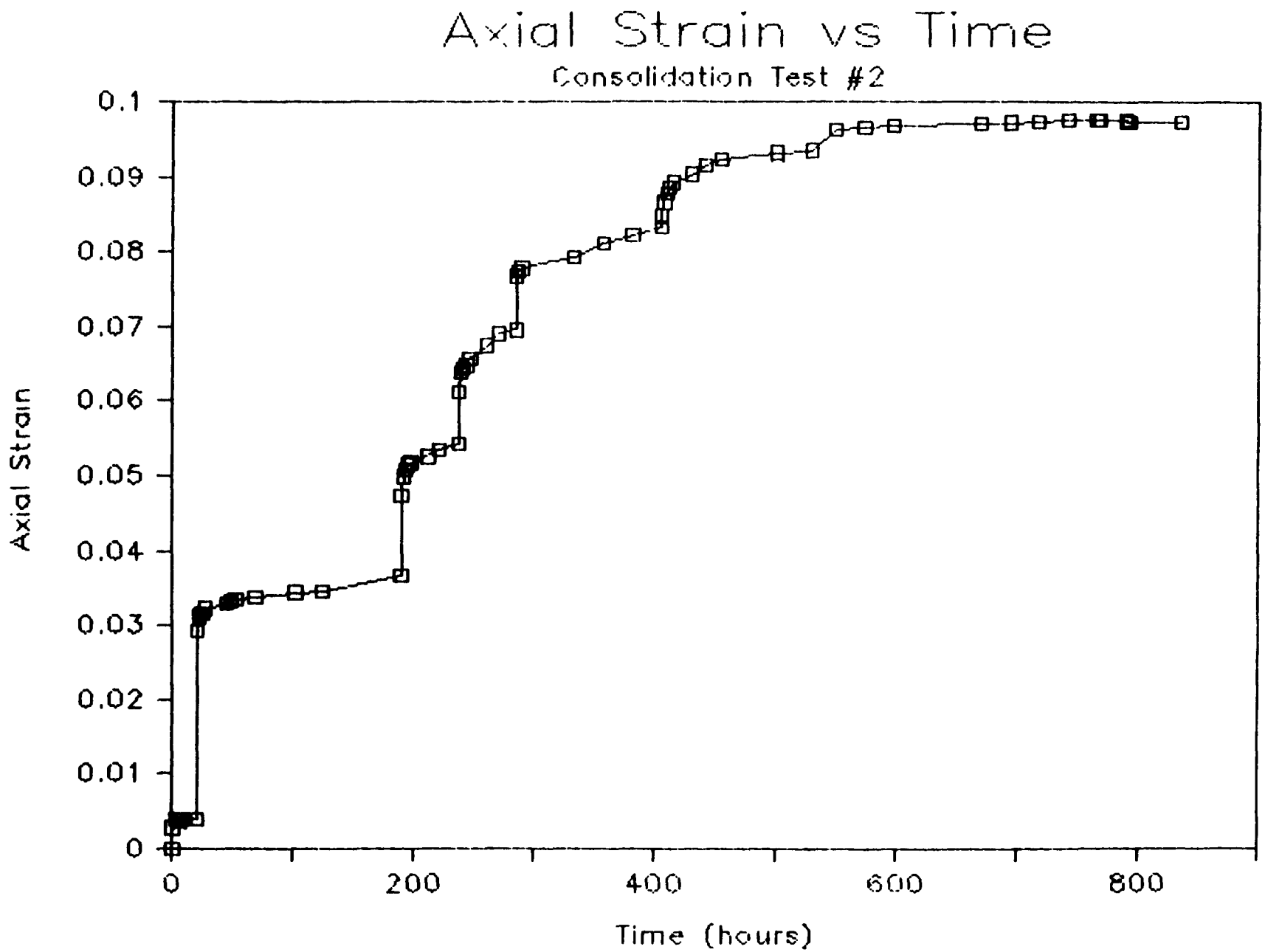
Axial Strain vs Time
Consolidation Test #2
Axial Strain
0.1
0.09
0.08
0.07
0.06
0.05
0.04
0.03
0.02
0.01
0
0
200
400
600
800
Time (hours)

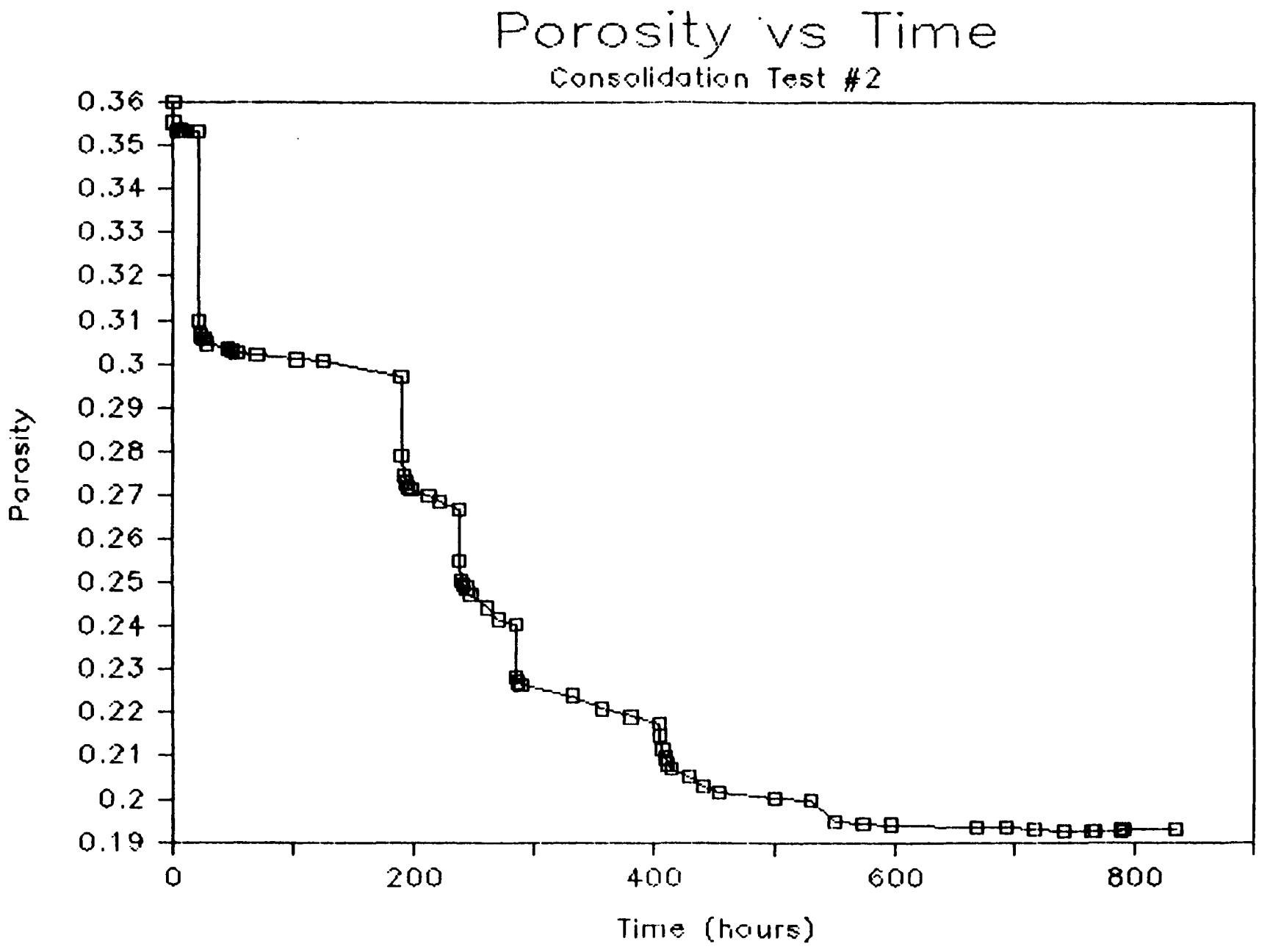
Porosity vs Time
Consolidation Test #2
Porosity
0.36
0.35
0.34
0.33
0.32
0.31
0.3
0.29
0.28
0.27
0.26
0.25
0.24
0.23
0.22
0.21
0.2
0.19
0
200
400
600
800
Time (hours)

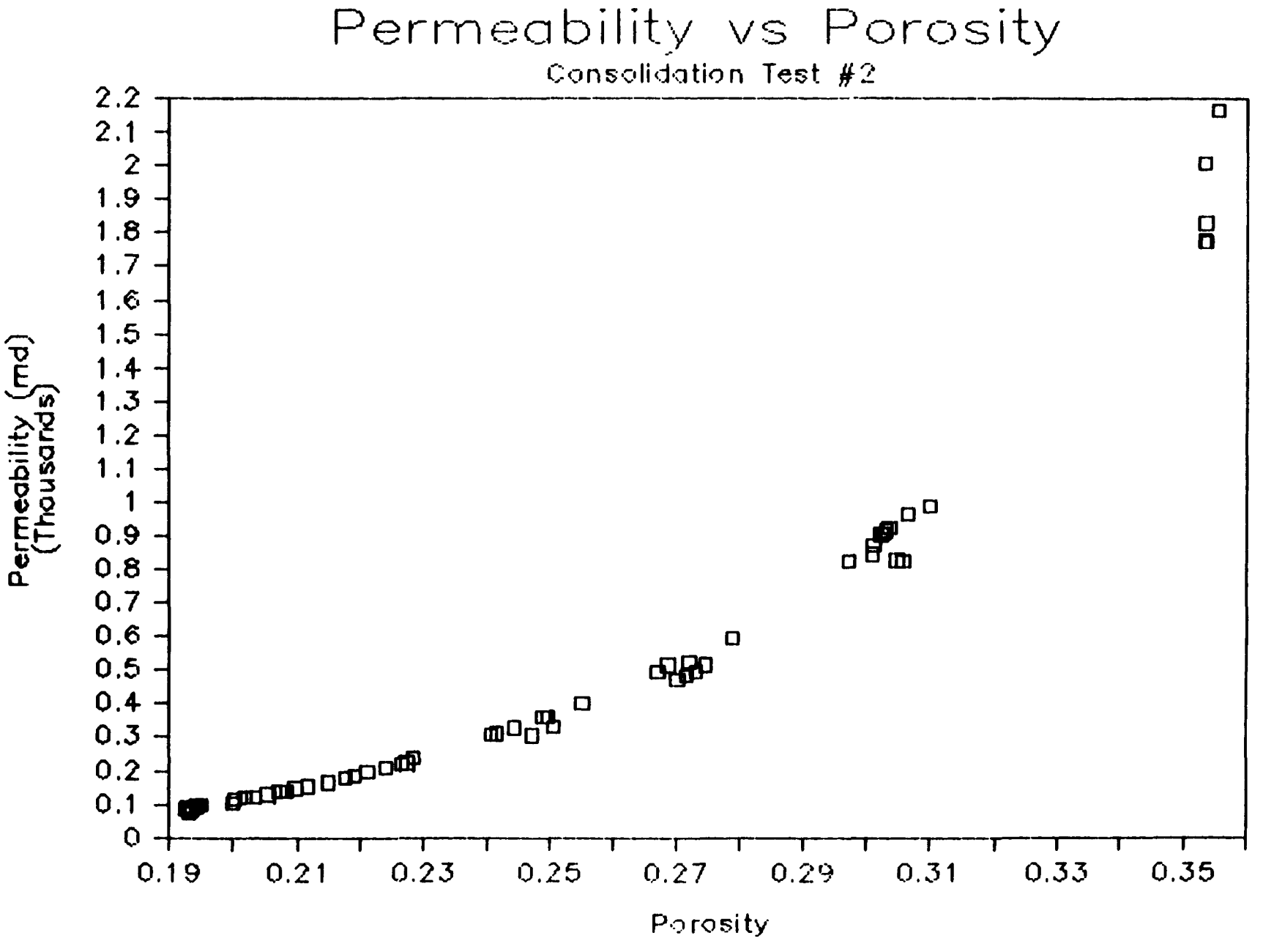
Permeability vs Porosity
Consolidation Test #2
Permeability (md)
(Thousands)
2.2
2.1
2
1.9
1.8
1.7
1.6
1.5
1.4
1.3
1.2
1.1
1
0.9
0.8
0.7
0.6
0.5
0.4
0.3
0.2
0.1
0
0.19
0.21
0.23
0.25
0.27
0.29
0.31
0.33
0.35
Porosity

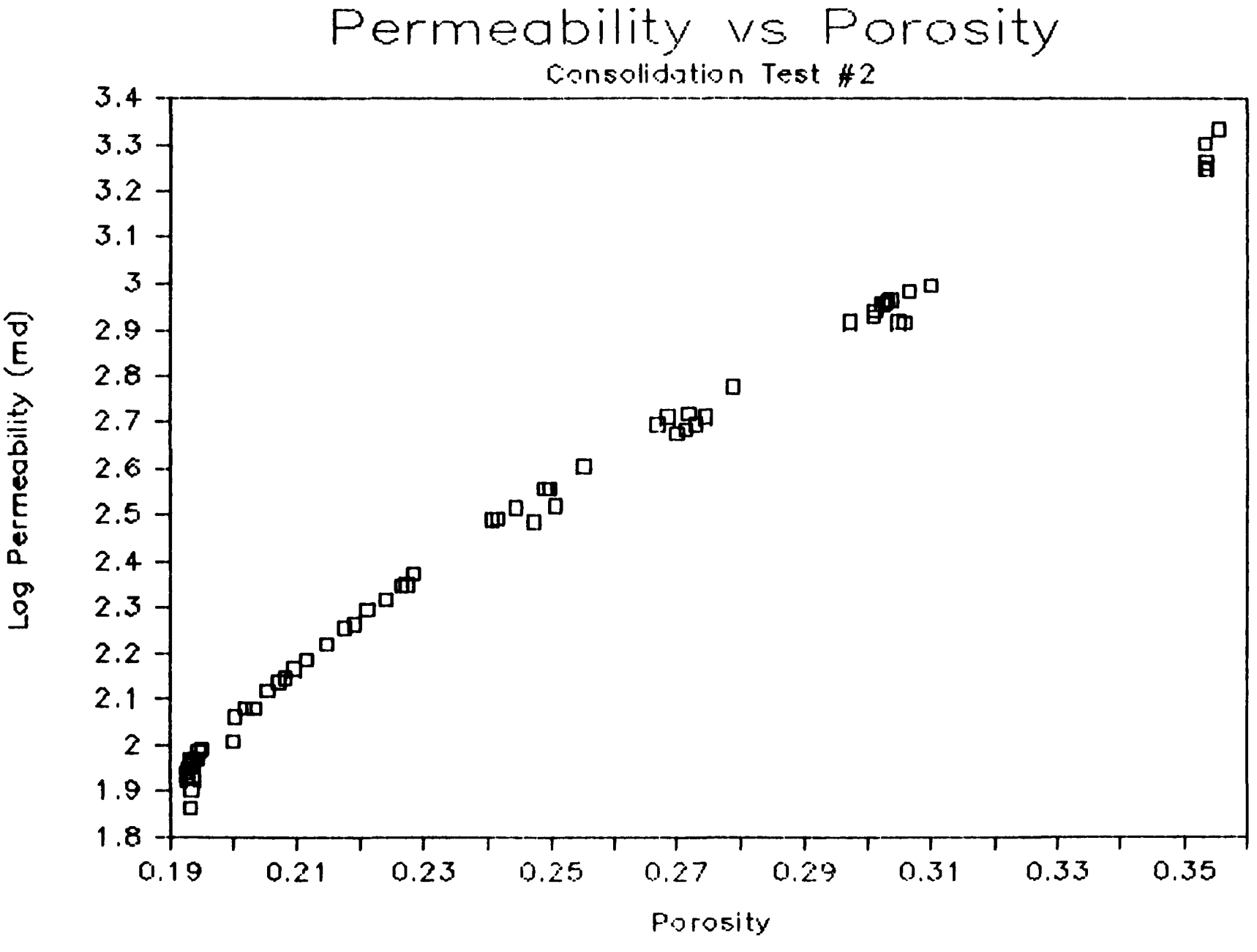
Permeability vs Porosity
Consolidation Test #2
Log Permeability (md)
3.4
3.3
3.2
3.1
3
2.9
2.8
2.7
2.6
2.5
2.4
2.3
2.2
2.1
2
1.9
1.8
0.19
0.21
0.23
0.25
0.27
0.29
0.31
0.33
0.35
Porosity

CONSOLIDATION TEST 3 - TEST DATA
Sample Number: AR

MEASURED VALUES					COMPUTED VALUES	
			INTRINSIC PERMEABILITY			
CONFINING PRESSURE (psi)	TIME OF PRESSURE APPLICATION (hrs)	AXIAL STRAIN	$\bar{X}$ (md)	$\bar{\sigma}$ (md)	COMPLIANCE POROSITY	CORRECTED POROSITY
0	0	0				0.307
36	0	.00333	50442	10237	0.309	0.300
52	1	.00716	21384	6533	0.302	0.292
53	6	.01168	18279	3416	0.295	0.283
53	20	.01572	18385	1704	0.284	0.274
499	0	.02870	9610	663	0.269	0.247
491	2	.04355	3470	159	0.242	0.216
492	4	.04757	2781	164	0.237	0.207
501	7	.05098	2425	139	0.231	0.200
500	10	.05427	1713	100	0.225	0.193
498	12	.05549	1541	95	0.218	0.191
503	24	.06094	967	75	0.202	0.179
545	31	.06333	714	59	0.202	0.174
510	36	.06430	592	58	0.201	0.172
507	48	.06706	399	49	0.195	0.166
999	0.25	.06861	292	43	0.191	0.163
988	3	.07088	186	26	0.187	0.158
1009	8	.07342	119	19	0.183	0.153
1016	30	.07728	55	10	0.172	0.145
996	56	.08060	18	5	0.166	0.138
1005	96	.08391	3.7	0.9	0.157	0.131

(end of steady state tests)

CONSOLIDATION TEST 3 - TEST DATA (continued)
Sample Number: AR

MEASURED VALUES				COMPUTED VALUES	
CONFINING PRESSURE (psi)	TIME OF PRESSURE APPLICATION (hrs)	AXIAL STRAIN	INTRINSIC PERMEABILITY $\bar{X}$ (md x 10^{-6})	COMPLIANCE POROSITY	CORRECTED POROSITY
(beginning of transient tests)					
1057	1	.08715	67800	0.153	0.124
1056	2	.08783	446000	0.153	0.123
1046	5	.08926	41600	0.155	0.120
1045	7	.08935	21100	0.156	0.120
1037	10	.08954	20600	0.159	0.119
1045	24	.09290	151000	0.146	0.112
1042	28	.09321	33000	0.150	0.112
1037	33	.09351	56700	0.150	0.111
1039	48	.09432	53200	0.143	0.109
1522	0	.09464	23600	0.144	0.109
1536	2	.09525	25400	0.144	0.107
1534	4	.09591	37200	0.146	0.106
1533	6	.09624	28800	0.147	0.105
1536	24	.09852	15200	0.138	0.100
1534	30	.09933	7020	0.137	0.099
1528	48	.10055	5250	0.132	0.096
2114	1	.10233	954	0.128	0.092
2117	3	.10296	211	0.127	0.091
2105	5	.10346	144	0.127	0.090
2113	8	.10402	167	0.127	0.089
2109	26	.10593	-	0.121	0.085
1989	51	.10889	21.78	0.119	0.079
2499	24	.11291	3.91	0.118	0.070
2487	48	.11517	2.26	0.109	0.065
2497	72	.11725	2.73	0.105	0.061
2490	96	.11859	2.39	0.101	0.058

CONSOLIDATION TEST 3 - TEST DATA (continued)
Sample Number: AR

MEASURED VALUES				COMPUTED VALUES	
CONFINING PRESSURE (psi)	TIME OF PRESSURE APPLICATION (hrs)	AXIAL STRAIN	INTRINSIC PERMEABILITY $\bar{X}$ (md x 10^{-6})	COMPLIANCE POROSITY	CORRECTED POROSITY
2501	168	.12066	5.89	0.101	0.054
2474	192	.12124	3.22	0.102	0.053
2499	216	.12164	6.88	0.097	0.052
2500	240	.12234	4.54	0.097	0.050
2492	264	.12268	-	0.086	0.050
2505	336	.12361	-	0.091	0.048
2547	360	.12369	-	0.088	0.048
2496	384	.12376	-	0.088	0.047
2490	408	.12433	-	0.087	0.046
2496	432	.12441	-	0.085	0.046
1986	0	.12470	-	0.082	0.045
1977	2	.12463	-	0.085	0.046
999	0	.12492	-	0.081	0.045
0	0				0.045
2485[1]	24	.00731	5.22	0.049	-

[1] Retest of sample after cutting off porous stones.

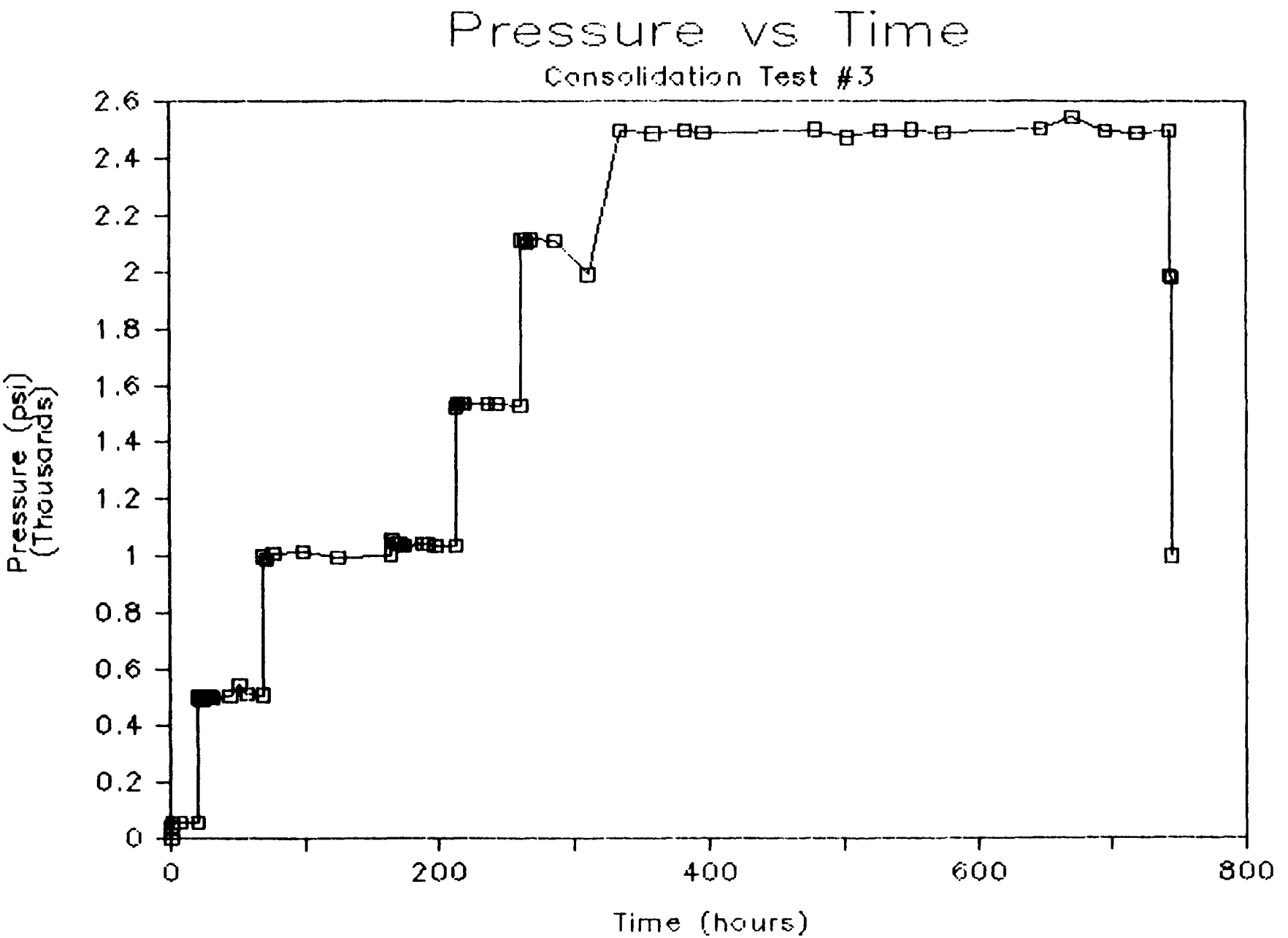
Pressure vs Time
Consolidation Test #3
Pressure (psi)
(Thousands)
2.6
2.4
2.2
2
1.8
1.6
1.4
1.2
1
0.8
0.6
0.4
0.2
0
0
200
400
600
800
Time (hours)

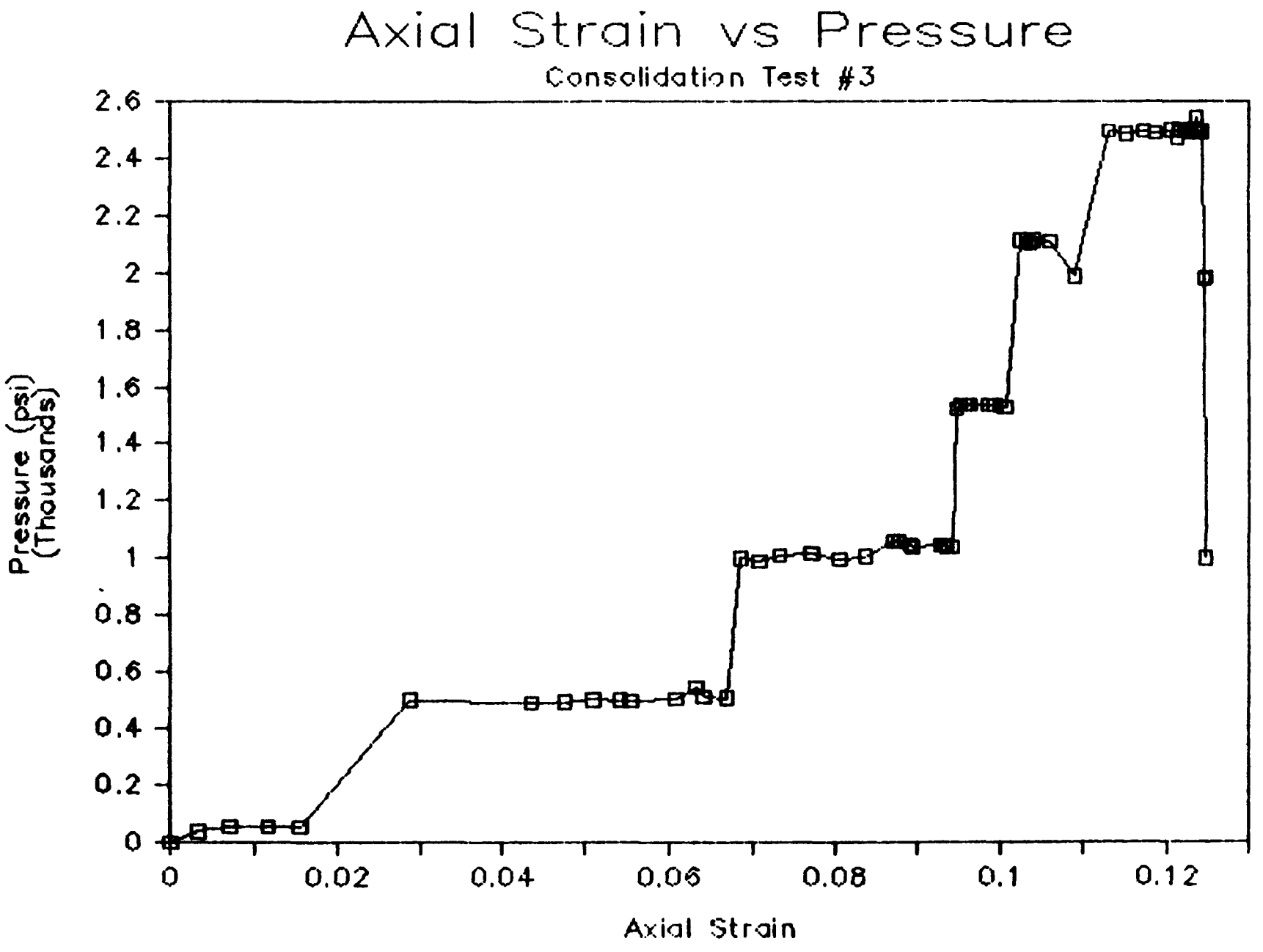
Axial Strain vs Pressure
Consolidation Test #3
Pressure (psi)
(Thousands)
2.6
2.4
2.2
2
1.8
1.6
1.4
1.2
1
0.8
0.6
0.4
0.2
0
0
0.02
0.04
0.06
0.08
0.1
0.12
Axial Strain

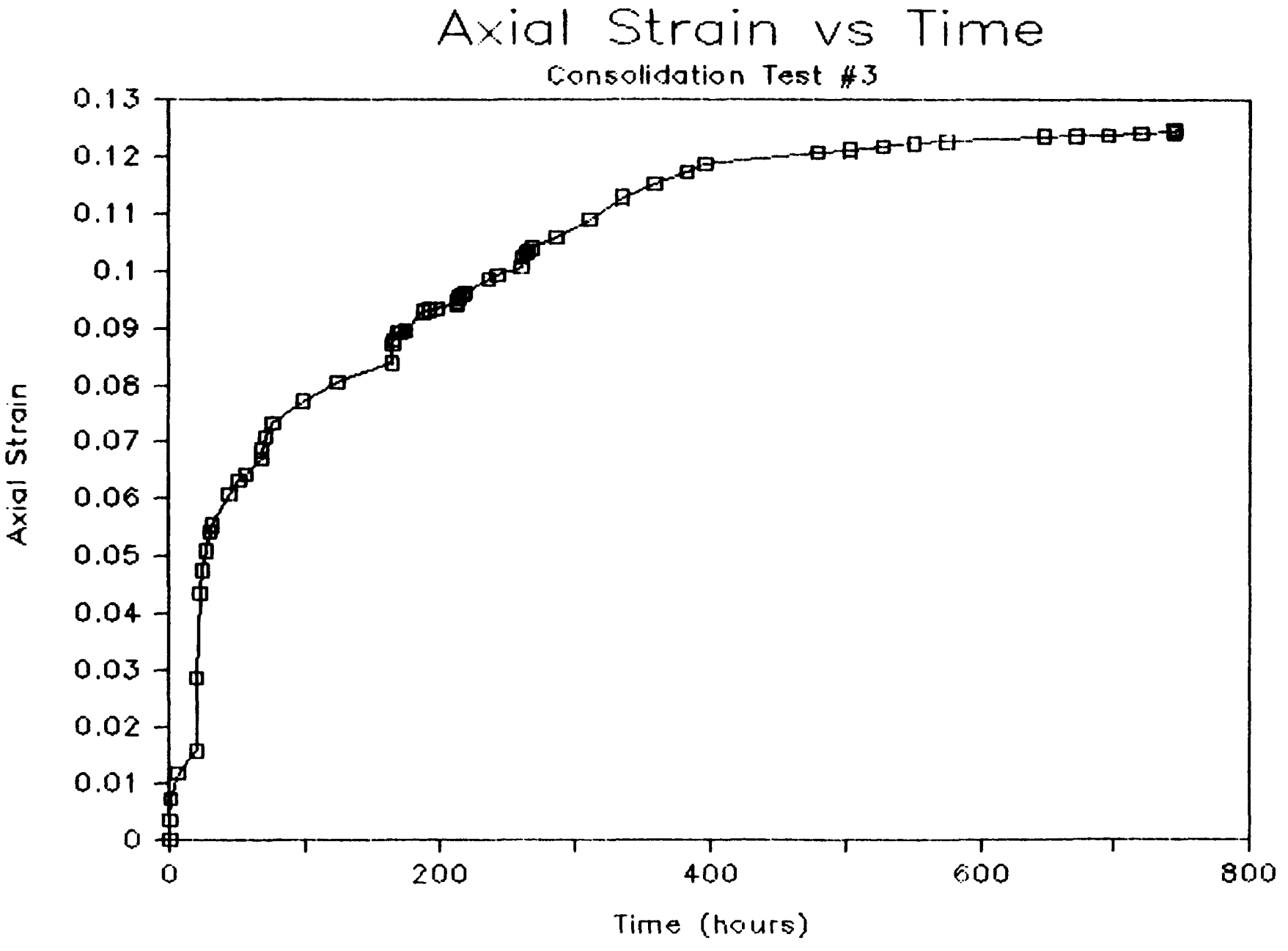
Axial Strain vs Time
Consolidation Test #3
Axial Strain
0.13
0.12
0.11
0.1
0.09
0.08
0.07
0.06
0.05
0.04
0.03
0.02
0.01
0
0
200
400
600
800
Time (hours)

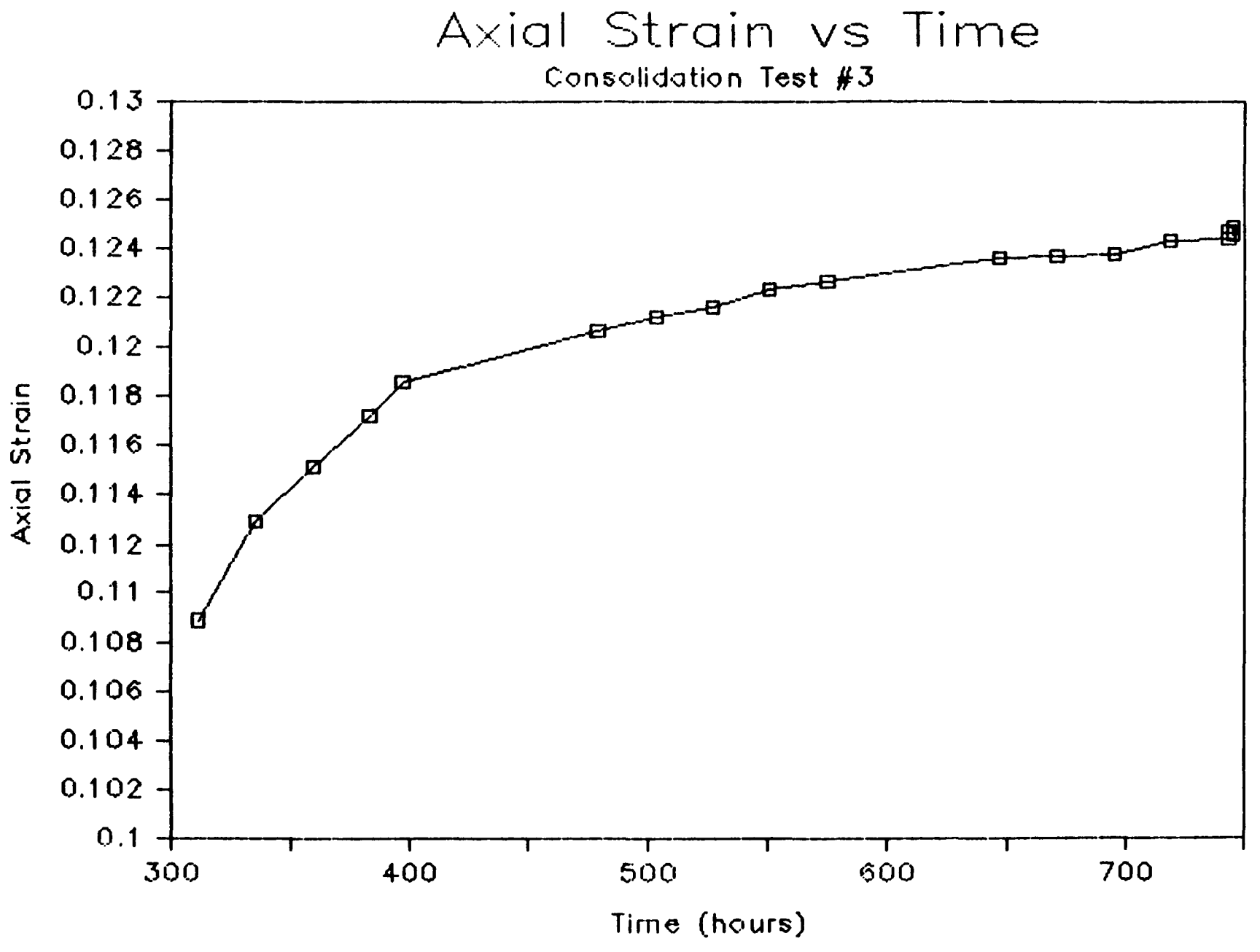
Axial Strain vs Time
Consolidation Test #3
Axial Strain
0.13
0.128
0.126
0.124
0.122
0.12
0.118
0.116
0.114
0.112
0.11
0.108
0.106
0.104
0.102
0.1
300
400
500
600
700
Time (hours)

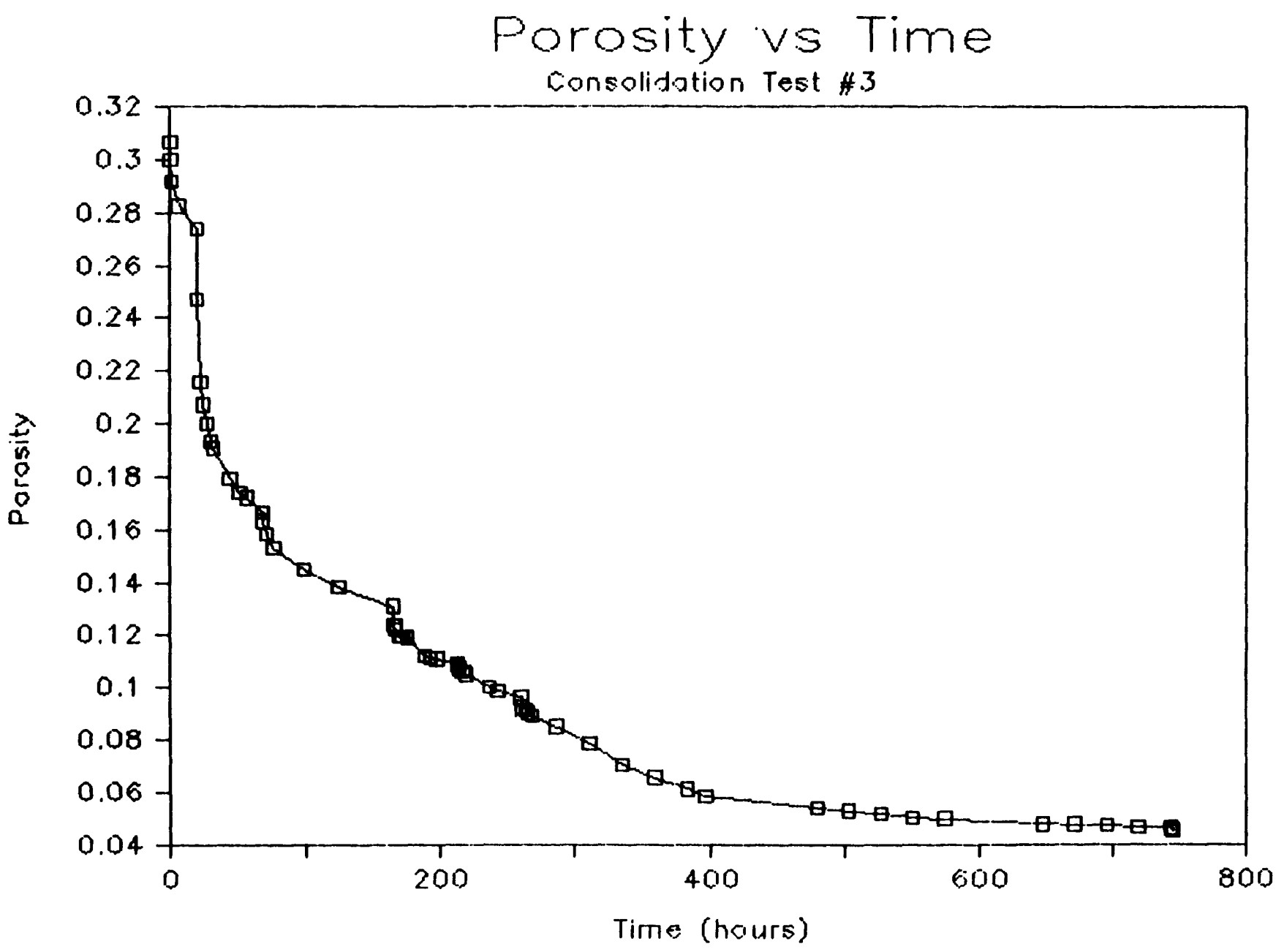
Porosity vs Time
Consolidation Test #3
Porosity
0.32
0.3
0.28
0.26
0.24
0.22
0.2
0.18
0.16
0.14
0.12
0.1
0.08
0.06
0.04
0
200
400
600
800
Time (hours)

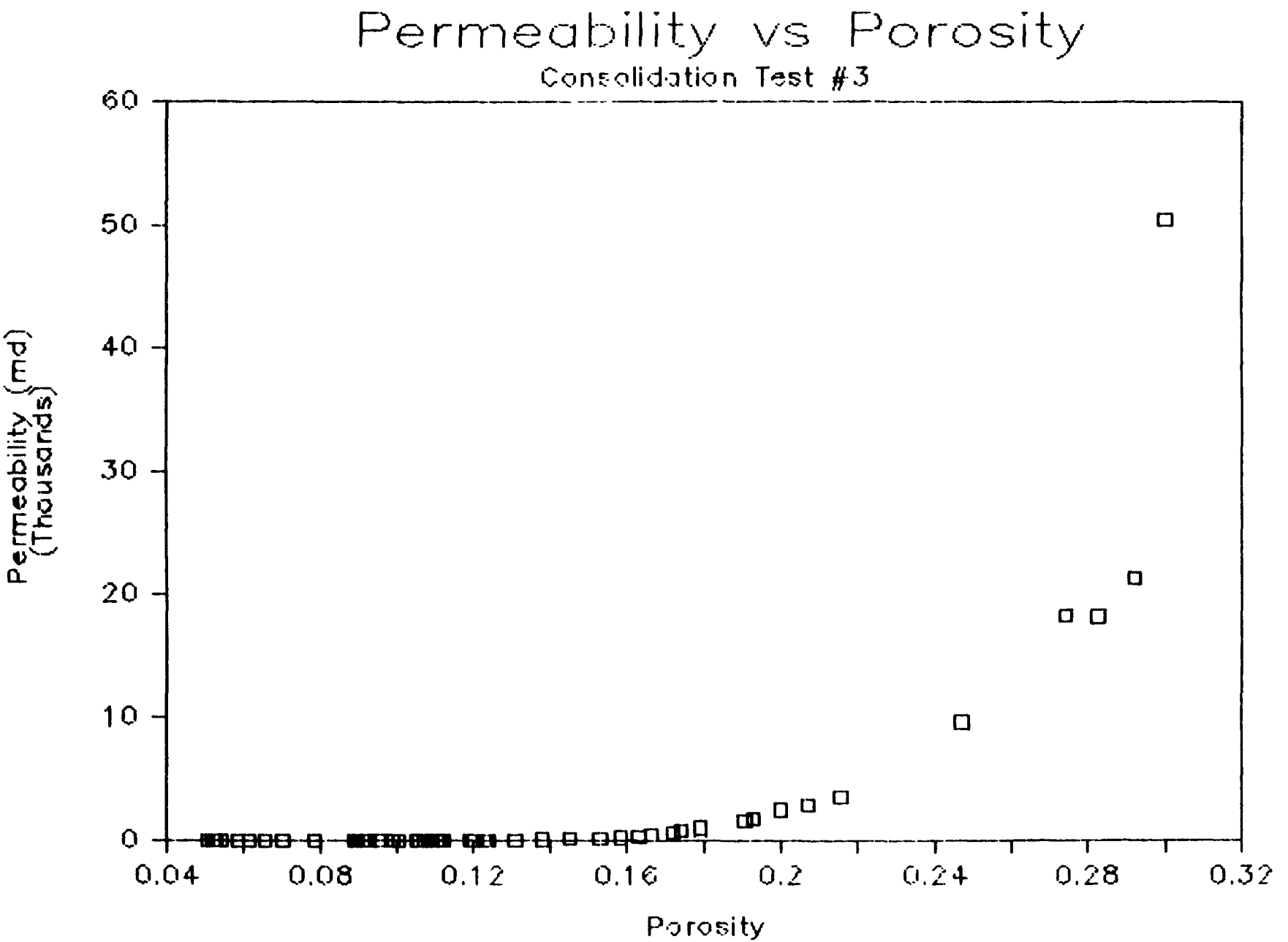
Permeability vs Porosity
Consolidation Test #3
Permeability (md)
(Thousands)
60
50
40
30
20
10
0
0.04
0.08
0.12
0.16
0.2
0.24
0.28
0.32
Porosity

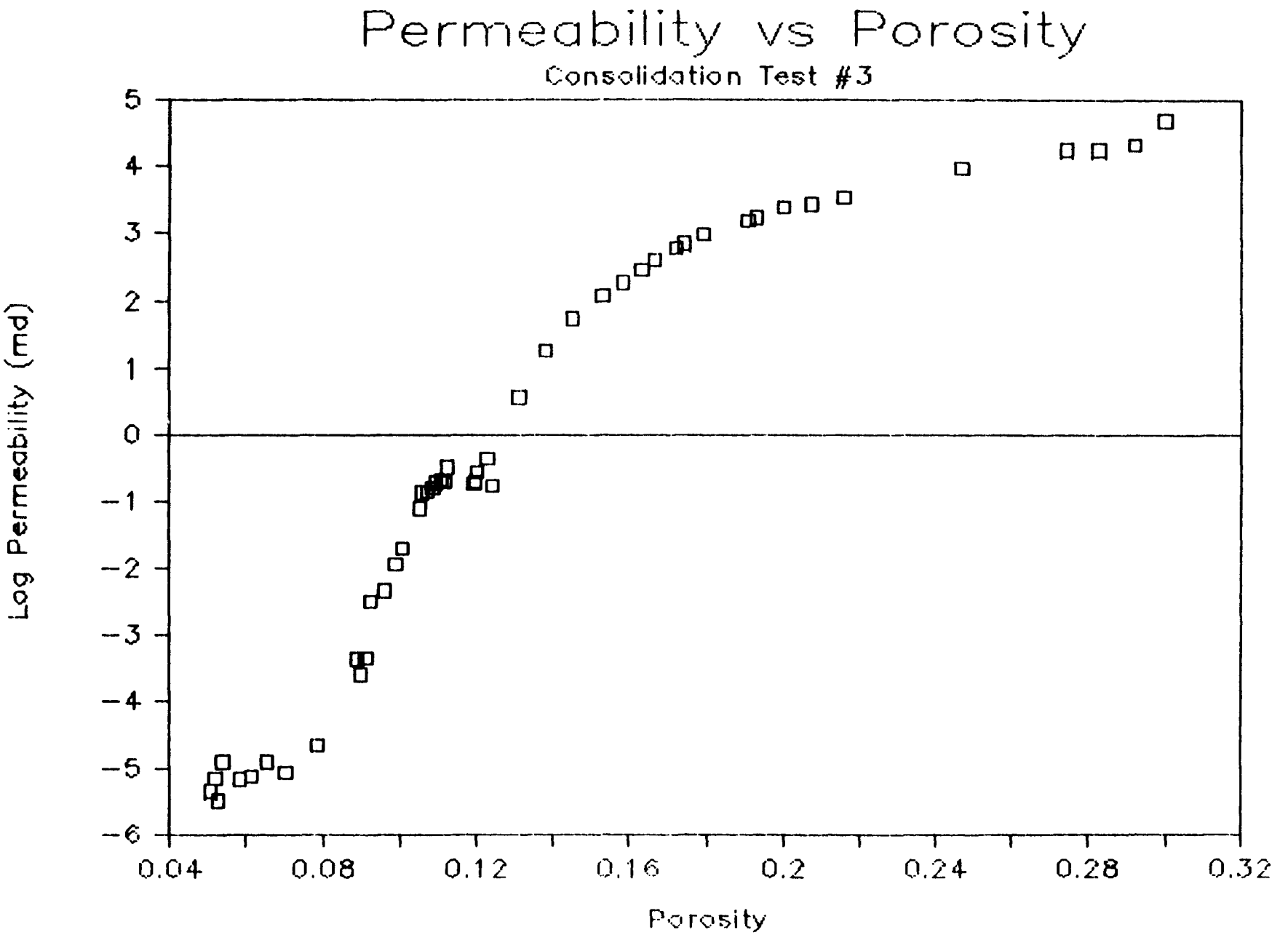
Permeability vs Porosity
Consolidation Test #3
Log Permeability (md)
5
4
3
2
1
0
−1
−2
−3
−4
−5
−6
0.04
0.08
0.12
0.16
0.2
0.24
0.28
0.32
Porosity

CONSOLIDATION TEST 4 - TEST DATA
Sample Number: AM10

MEASURED VALUES					COMPUTED VALUES	
CONFINING PRESSURE (psi)	TIME OF PRESSURE APPLICATION (hrs)	AXIAL STRAIN	INTRINSIC PERMEABILITY $\bar{X}$ (md)	INTRINSIC PERMEABILITY $\bar{\sigma}$ (md)	COMPLIANCE POROSITY	CORRECTED POROSITY
0	0	0.0				0.256
55	0	0.00197	3532	147	0.267	0.252
54	2	0.00198	2989	151	0.266	0.252
504	0	0.01828	1538	85	0.235	0.221
500	2	0.01981	1451	89	0.230	0.218
502	4	0.01999	1436	84	0.229	0.218
501	17	0.02033	1378	90	0.230	0.217
1001	0	0.02938	817	48	0.211	0.200
1007	2	0.03183	678	43	0.207	0.195
1009	4	0.03223	722	47	0.209	0.194
1006	6	0.03255	685	44	0.212	0.194
1003	8	0.03298	662	43	0.213	0.193
1005	24	0.03371	640	46	0.205	0.191
1009	30	0.03388	606	40	0.201	0.191
1004	35	0.03406	606	47	0.201	0.191
998	48	0.03444	587	39	0.205	0.190
1493	0	0.03850	422	27	0.197	0.182
1498	2	0.03995	384	26	0.191	0.179
1504	4	0.04118	349	26	0.187	0.177
1512	6	0.04151	342	23	0.186	0.176
1499	8	0.04188	335	23	0.185	0.176
1514	27	0.04287	321	23	0.189	0.174
1494	72	0.04431	283	20	0.183	0.171
1990	0	0.04638	235	18	0.179	0.167
2003	2	0.04808	207	15	0.173	0.164
2002	4	0.04876	201	14	0.171	0.162
2002	6	0.04911	196	14	0.170	0.162

CONSOLIDATION TEST 4 - TEST DATA (continued)
Sample Number: AM10

MEASURED VALUES					COMPUTED VALUES	
			INTRINSIC PERMEABILITY			
CONFINING PRESSURE (psi)	TIME OF PRESSURE APPLICATION (hrs)	AXIAL STRAIN	$\bar{x}$ (md)	$\bar{\sigma}$ (md)	COMPLIANCE POROSITY	CORRECTED POROSITY
1999	8	0.04947	190	14	0.169	0.161
2008	24	0.05078	169	11	0.167	0.159
1992	30	0.05105	169	10	0.164	0.158
2005	36	0.05124	166	11	0.161	0.158
1944	48	0.05193	158	8	0.162	0.156
2013	72	0.05246	149	8	0.163	0.155
1999	96	0.05261	148	8	0.159	0.155
2007	124	0.05305	144	8	0.162	0.154
1989	147	0.05310	144	8	0.160	0.154
2012	168	0.05345	142	6	0.159	0.153
2502	0	0.05436	129	7	0.159	0.152
2508	2	0.05556	115	7	0.156	0.149
2511	4	0.05579	111	7	0.155	0.149
2504	6	0.05621	110	6	0.155	0.148
2492	8	0.05637	106	6	0.154	0.148
2509	24	0.05708	98	5	0.149	0.146
2499	33	0.05745	96	5	0.151	0.146
2495	48	0.05756	93	4	0.147	0.146
2495	72	0.05840	87	5	0.147	0.144
2498	96	0.05871	85	4	0.145	0.143
2498	120	0.05916	78	5	0.148	0.142
2496	168	0.06025	73	4	0.151	0.140
2496	192	0.06041	65	2	0.152	0.140
2497	193	0.06040	63	5	0.150	0.140
2496	216	0.06046	68	3	0.144	0.140
2497	240	0.06079	64	4	0.145	0.139
2608	264	0.06080	61	3	0.147	0.139

CONSOLIDATION TEST 4 - TEST DATA (continued)
Sample Number: AM10

MEASURED VALUES			INTRINSIC PERMEABILITY		COMPUTED VALUES	
CONFINING PRESSURE (psi)	TIME OF PRESSURE APPLICATION (hrs)	AXIAL STRAIN	$\bar{X}$ (md)	σ (md)	COMPLIANCE POROSITY	CORRECTED POROSITY
2527	292	0.06100	61	3	0.147	0.139
2495	336	0.06131	64	3	0.147	0.138
2480	360	0.06146	59	3	0.142	0.138
2501	384	0.06139	60	4	0.142	0.138
2465	388	0.06153	58	3	0.141	0.138
2496	408	0.06157	58	3	0.141	0.138
2480	432	0.06146	58	3	0.145	0.138
2500	458	0.06174	54	3	0.142	0.138
2493	487	0.06169	54	3	0.143	0.138
2510	504	0.06176	54	3	0.141	0.137
2486	528	0.06177	53	3	0.145	0.137
2497	554	0.06176	53	3	0.136	0.137
2546	577	0.06200	53	3	0.140	0.137
2507	602	0.06211	52	3	0.137	0.137
2505	626	0.06192	51	3	0.135	0.137
2502	651	0.06198	50	3	0.136	0.137
2506	672	0.06205	51	3	0.140	0.137
2504	696	0.06220	51	3	0.140	0.137
2473	769	0.06242	50	2.8	0.138	0.136
2505	864	0.06257	49	2.6	0.133	0.136
2503	912	0.06290	48	2.6	0.133	0.135
2610	1000	0.06315	44	2.3	0.137	0.135
2642	1080	0.06353	43	2.1	0.135	0.134
2496	1176	0.06363	44	2.1	0.124	0.134
2002	0	0.06364	44	2.3	0.124	0.134
1499	0	0.06368	44	2.3	0.124	0.134
1016	0	0.06358	46	2.5	0.124	0.134
512	0	0.06346	45	2.2	0.126	0.134
93	0	0.06306	48	2.5	0.124	0.135

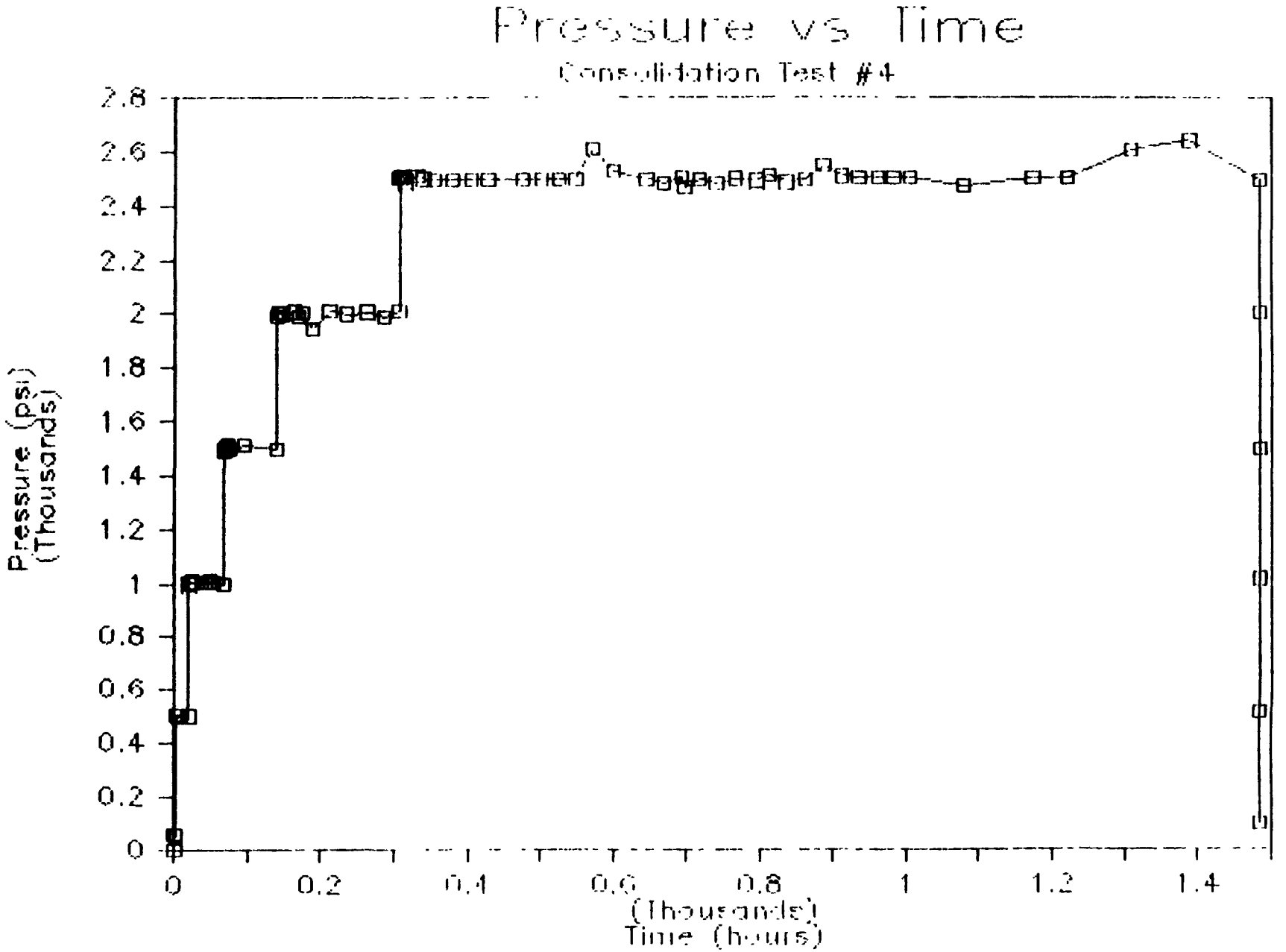
Pressure vs Time
Consolidation Test #4
Pressure (psi)
(Thousands)
2.8
2.6
2.4
2.2
2
1.8
1.6
1.4
1.2
1
0.8
0.6
0.4
0.2
0
0
0.2
0.4
0.6
0.8
1
1.2
1.4
(Thousands)
Time (hours)

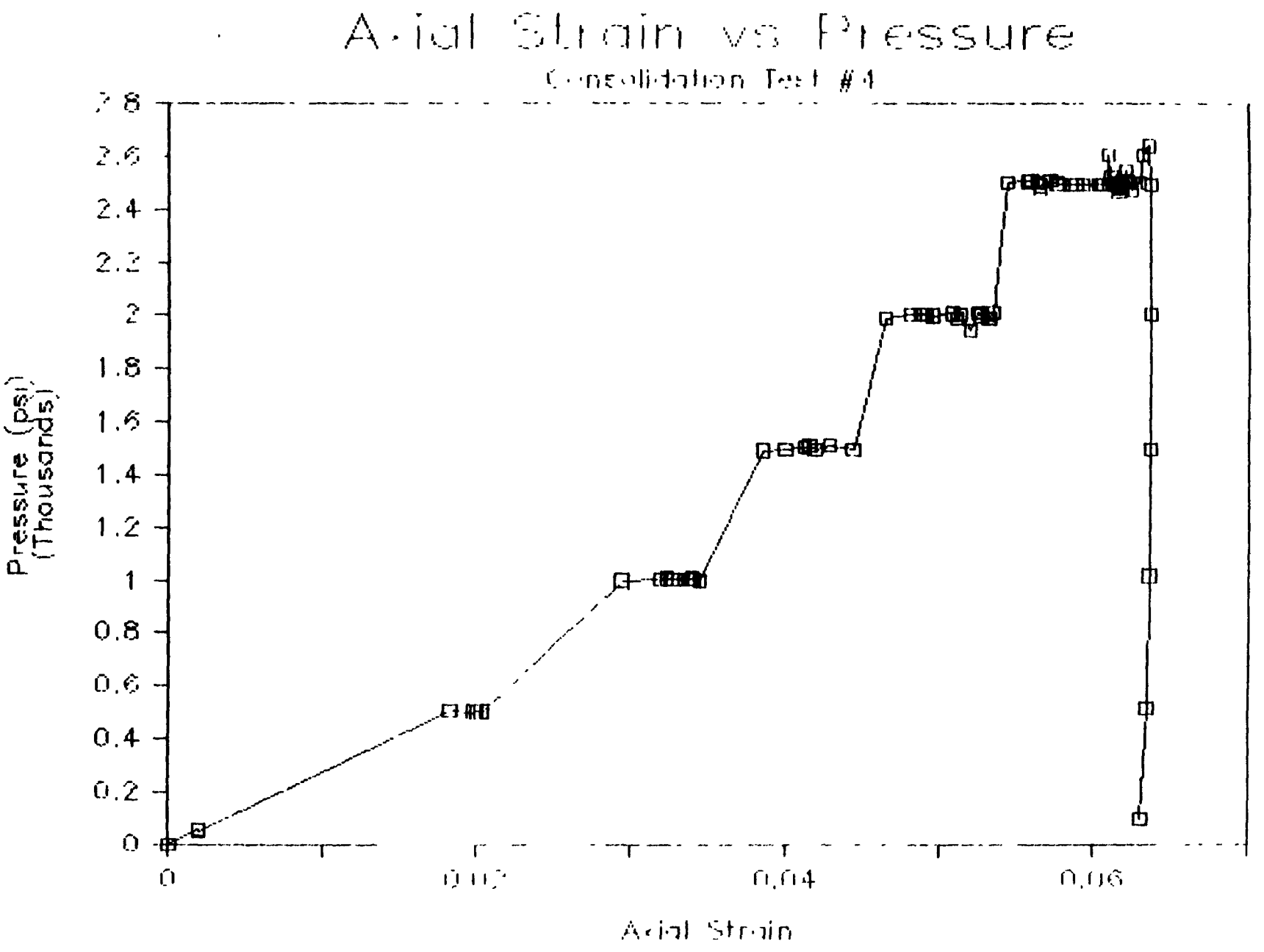
Axial Strain vs Pressure
Consolidation Test #4
Pressure (psi)
(Thousands)
2.8
2.6
2.4
2.2
2
1.8
1.6
1.4
1.2
1
0.8
0.6
0.4
0.2
0
0
0.02
0.04
0.06
Axial Strain

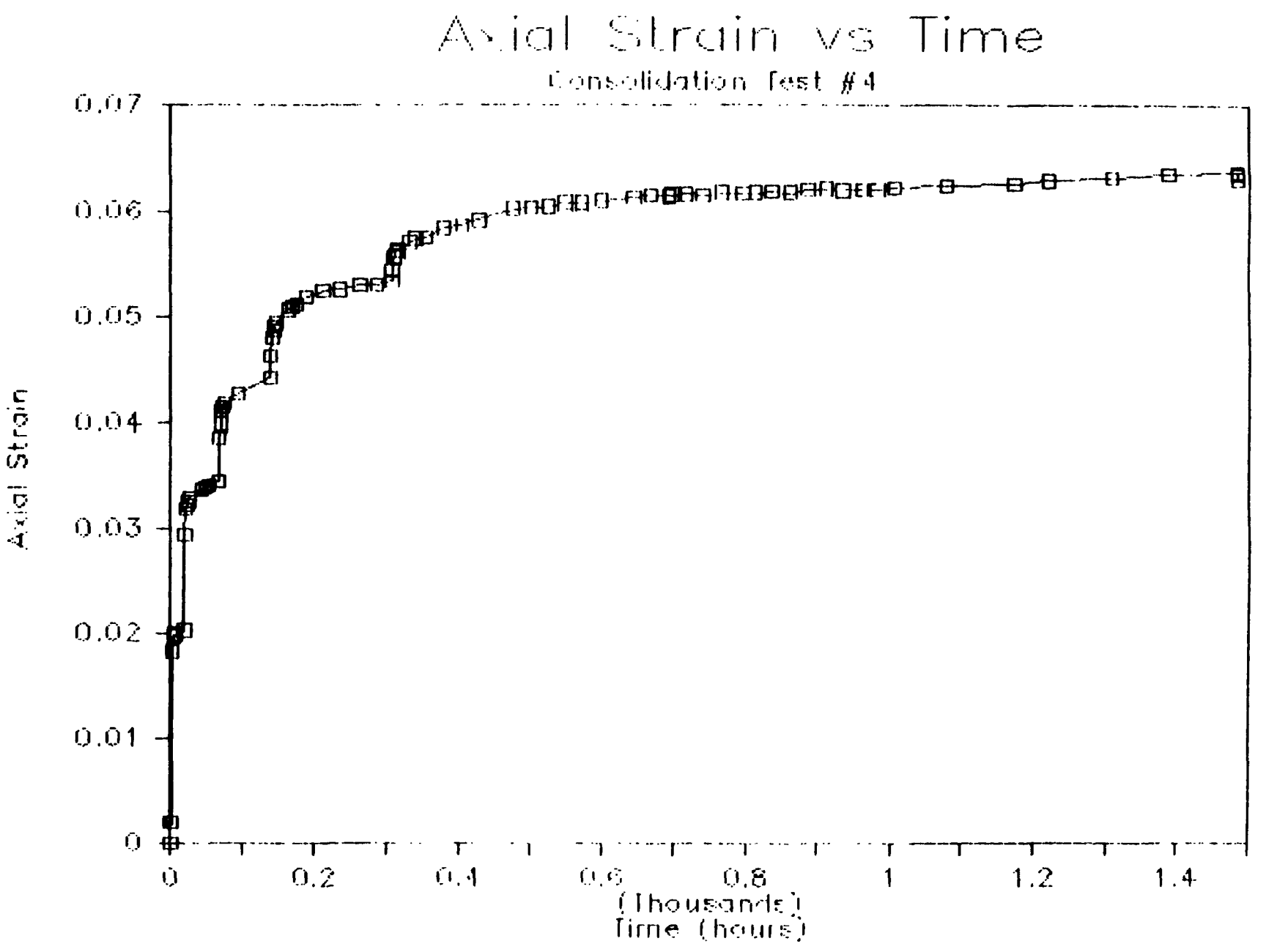
Axial Strain vs Time
Consolidation Test #4
Axial Strain
0.07
0.06
0.05
0.04
0.03
0.02
0.01
0
0
0.2
0.4
0.6
0.8
1
1.2
1.4
(Thousands)
Time (hours)

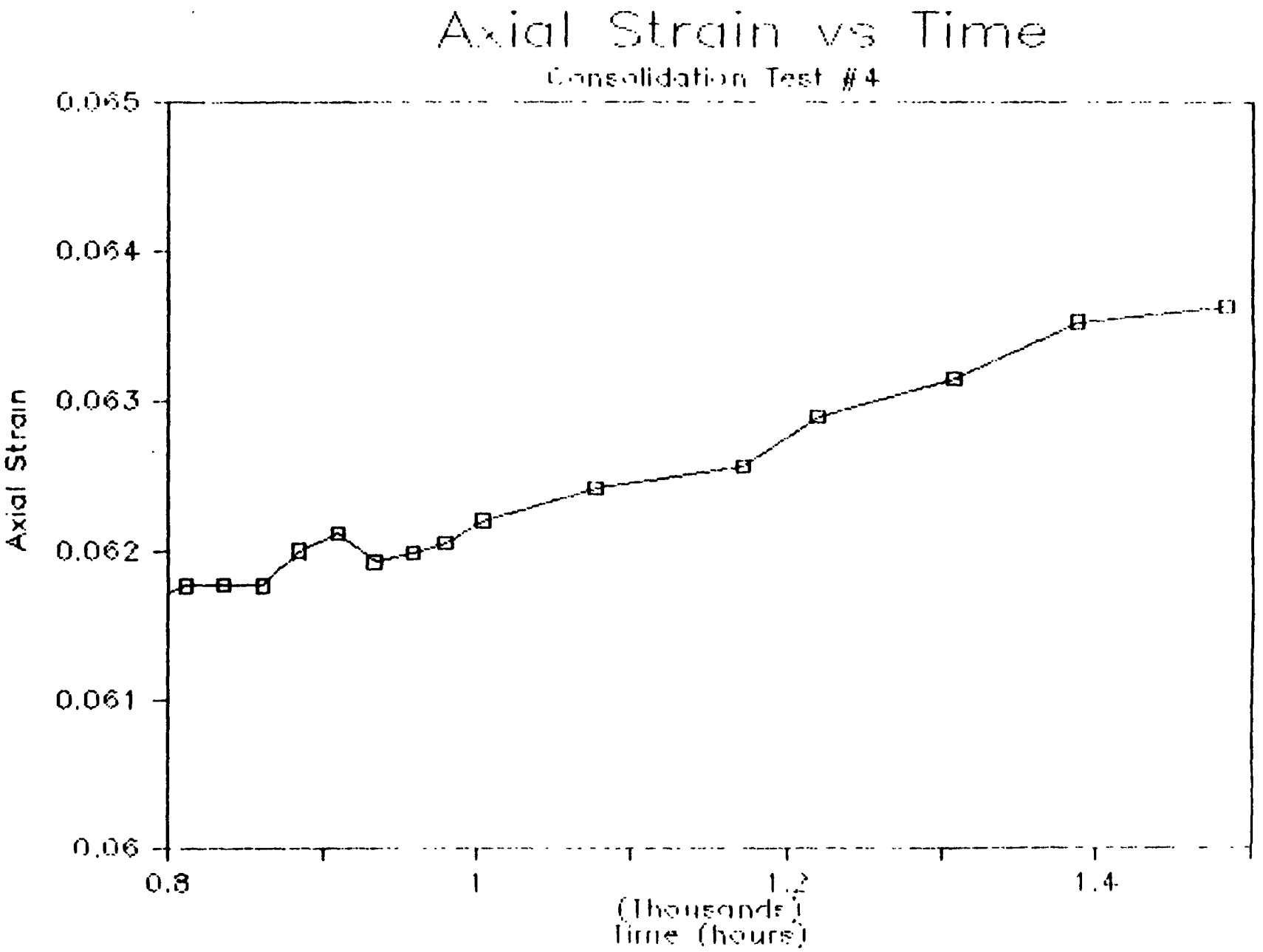
Axial Strain vs Time
Consolidation Test #4
0.065
0.064
0.063
0.062
0.061
0.06
Axial Strain
0.8
1
1.2
1.4
(Thousands)
Time (hours)

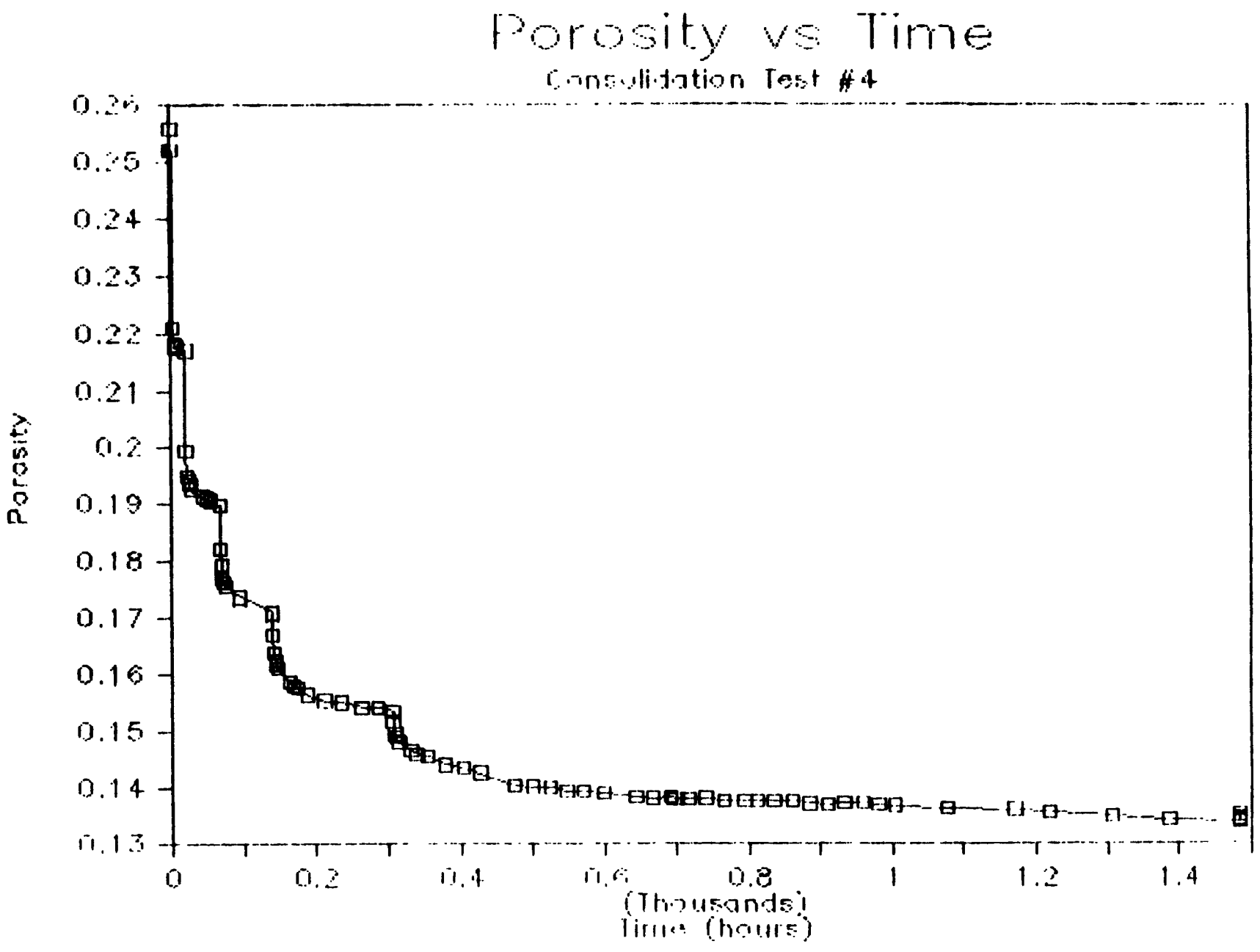
Porosity vs Time
Consolidation Test #4
Porosity
0.26
0.25
0.24
0.23
0.22
0.21
0.2
0.19
0.18
0.17
0.16
0.15
0.14
0.13
0
0.2
0.4
0.6
0.8
1
1.2
1.4
(Thousands)
Time (hours)

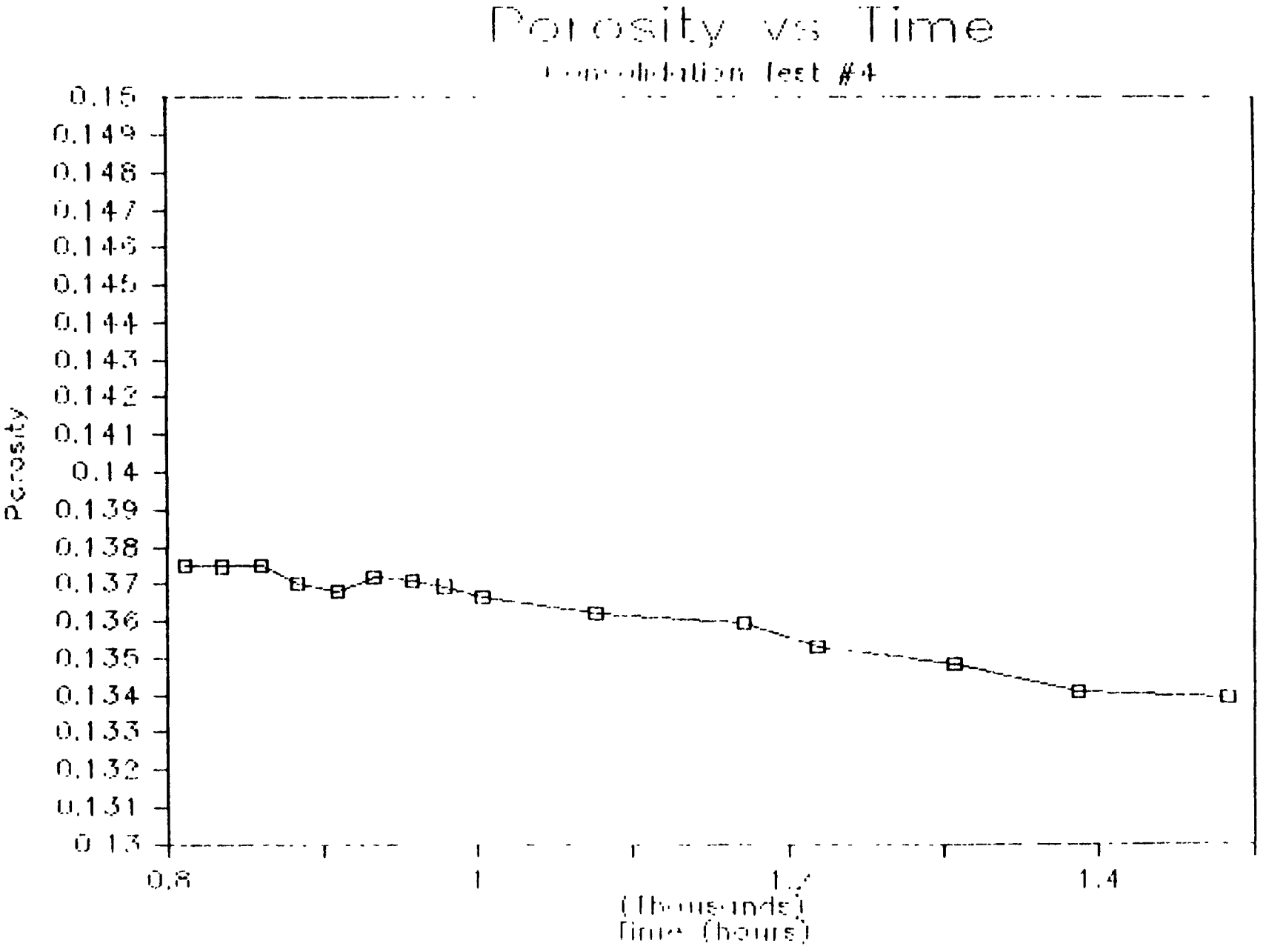
Porosity vs Time
Consolidation test #4
0.15
0.149
0.148
0.147
0.146
0.145
0.144
0.143
0.142
0.141
0.14
0.139
0.138
0.137
0.136
0.135
0.134
0.133
0.132
0.131
0.13
Porosity
0.8
1
1.4
(Thousands)
Time (hours)

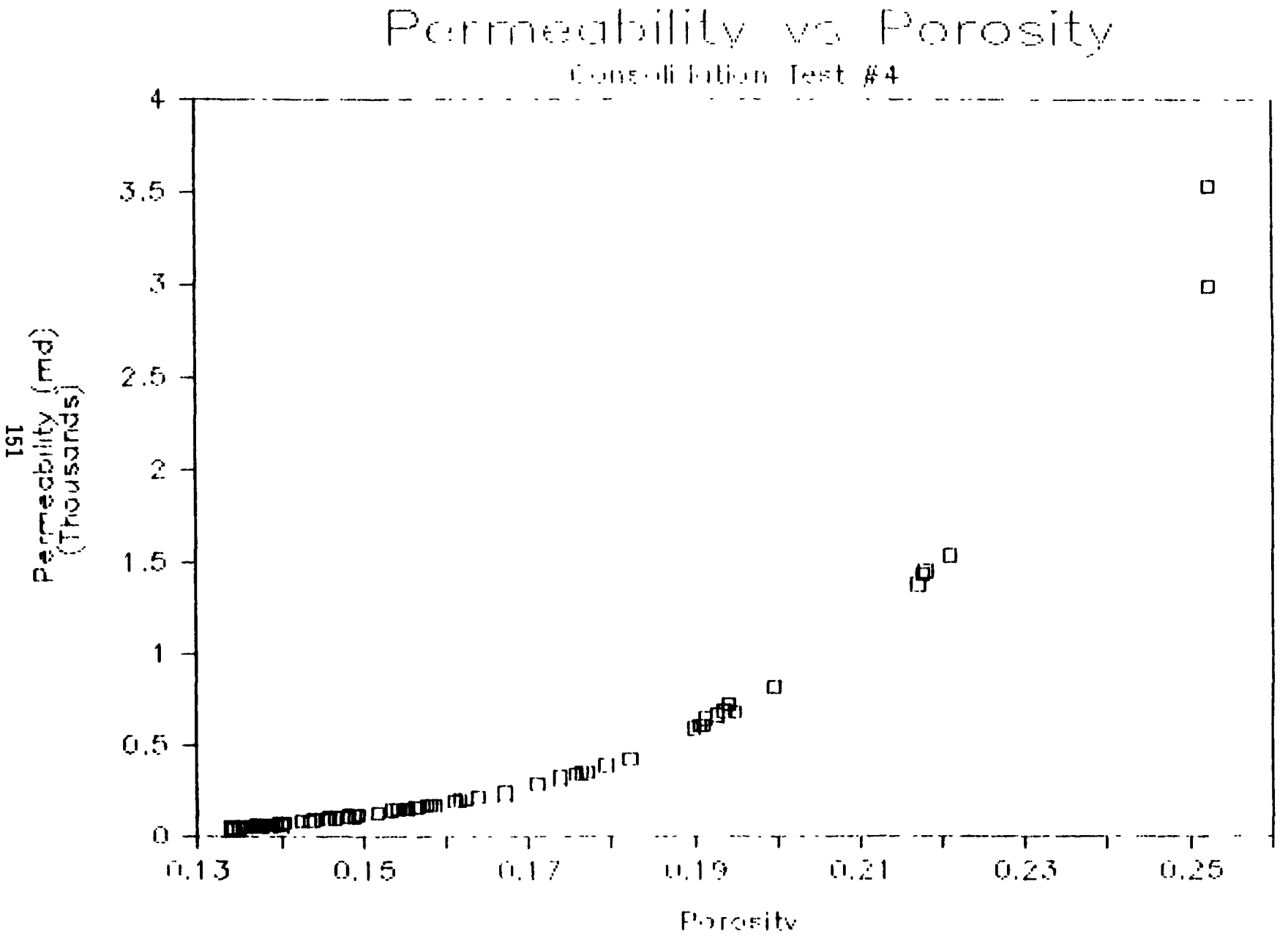
Permeability vs. Porosity
Consolidation Test #4
Permeability (md)
(Thousands)
151
4
3.5
3
2.5
2
1.5
1
0.5
0
0.13
0.15
0.17
0.19
0.21
0.23
0.25
Porosity

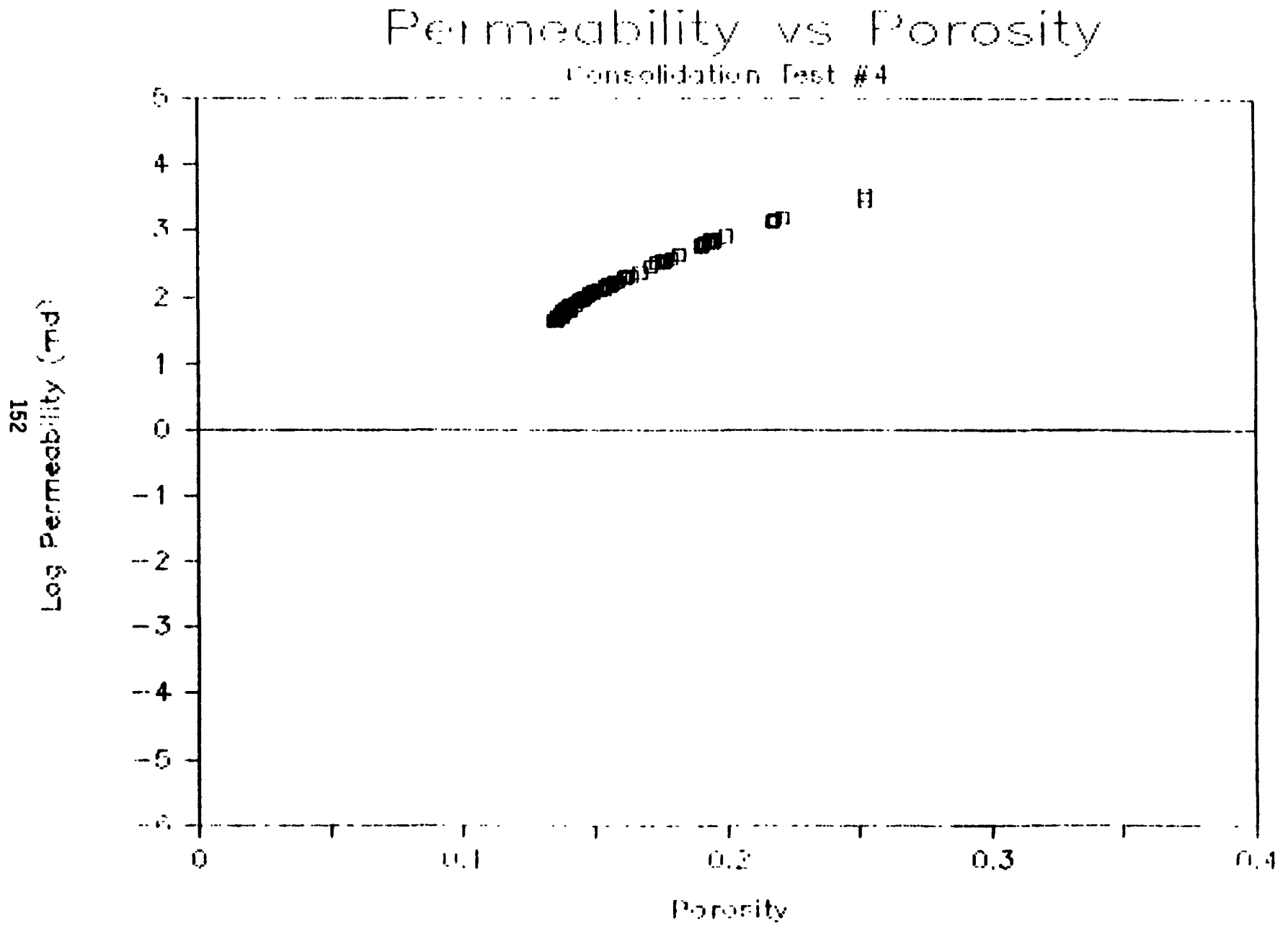
Permeability vs Porosity
Consolidation Test #4
Log Permeability (md)
152
5
4
3
2
1
0
-1
-2
-3
-4
-5
-6
0
0.1
0.2
0.3
0.4
Porosity

D.2 FRACTURE HEALING TESTS

Permeability tests have been conducted on fractured and unfractured samples as follows:

Test No.	Sample No.	File Name	Salt Type	Fracture Type	Moisture Condition	Maximum Hydrostatic Stress (psi)	Duration (days)
1	IT1-1	COHND	block	unfractured		3000	1
2	IM1-1	COIND	block	unfractured		3000	1
3	IB1-1	COLND	block	unfractured		3000	1
4	(1)	COISD	block	saw	dry	3000	3
5	(1)	COISM	block	saw	moist	3000	2
6	IM1-1	COIFM(2)	block	split	moist	2500	3
7	CR5	CRAND	WIPP	unfractured		3000	2
8	CR5	CRAFD	WIPP	split	dry	2500	2
9	CR6	CRAND2	WIPP	unfractured		2500	1
10	CR6	CRAFM	WIPP	split	moist	2500	3
11	CR7	CRAND3	WIPP	unfractured		2500	1
12	CR7	CRASM	WIPP	saw	moist	2500	2
13	AI1	AI1	Avery Is.	unfractured		2500	7
14	AI1FD	AI1FD	Avery Is.	split	dry	2500	7
15	AI3	AI3	Avery Is.	unfractured		2500	8
16	AI3FM	AI3FM	Avery Is.	split	moist	2500	8
17	I1	I1	block	unfractured		2500	7
18	I1FD	I1FD	block	saw	dry	2500	10
19	I2	I2	block	unfractured		2500	3
20	I2FM	I2FM	block	saw	moist	2500	8

(1) No sample number assigned.

(2) Same sample as COIND (Test 2)

The following data were obtained or computed:

Confining Pressure -	hydrostatic confining pressure acting on sample
Time of Pressure Application -	duration of pressure application since time = zero
Initial Porosity -	calculated from measured volume and weight prior to test
Test Porosity -	porosity at time permeability measured, calculated from initial porosity and change in sample volume indicated by axial strain
Bulk Modulus -	pressure difference for each quasi-static pressure increment divided by volumetric strain
Permeability -	argon gas permeability at indicated confining pressure; means ($\bar{x}$), standard deviation (σ) are given for (typically) 3 sensor readings at each of several flow rates at each confining pressure

Axial strain was monitored in Tests 1, 2, 3, 17 and 19.

FRACTURE HEALING TEST 1

Test Number: 1
Sample Number: IT1-1
File Name: COHND
Type of Salt: Block
Fracture Type: Unfractured
Moisture Condition: Dry
Initial Porosity: 0.151

Confining Pressure (psi)	Time of Pressure Application (hrs)	Cumulative Time (hrs)	Axial Strain	Permeability $\bar{X}$ (md)	Permeability $\bar{\sigma}$ (md)
50	1	0	1.121E-3	43.4	1.1
500	1	1	1.629E-3	40.2	0.7
1000	1	2	1.921E-3	39.8	0.7
1500	1	3	2.271E-3	39.5	0.7
2000	1	4	2.568E-3	38.3	0.6
2500	1	5	2.832E-3	38.1	0.6
3000	0	5	3.182E-3	36.6	0.7

FRACTURE HEALING TEST 2

Test Number: 2
Sample Number: IM1-1
File Name: COIND
Type of Salt: Block
Fracture Type: Unfractured
Moisture Condition: Dry
Initial Porosity: 0.124

Confining Pressure (psi)	Time of Pressure Application (hrs)	Cumulative Time (hrs)	Axial Strain	Permeability $\bar{X}$ (md)	Permeability $\bar{\sigma}$ (md)
50	1	1	1.513E-3	13.6	0.3
500	1	2	2.253E-3	13.6	0.4
1000	1	3	2.373E-3	13.6	0.3
1500	1	4	2.475E-3	13.4	0.3
2000	1	5	2.54E-3	13.1	0.5
2500	1	5	2.647E-3	14.4	0.5
3000	0	6	2.767E-3	13.2	0.3

FRACTURE HEALING TEST 3

Test Number: 3
Sample Number: IB1-1
File Name: COLND
Type of Salt: Block
Fracture Type: Unfractured
Moisture Condition: Dry
Initial Porosity: 0.096

Confining Pressure (psi)	Time of Pressure Application (hrs)	Cumulative Time (hrs)	Axial Strain	Permeability $\bar{X}$ (md)	Permeability $\bar{\sigma}$ (md)
50	1	1	8.59E-4	4.0	0.2
500	1	2	1.051E-3	3.4	0.3
1000	1	3	1.228E-3	3.1	0.3
1500	1	4	1.463E-3	3.3	0.3
2000	1	5	1.75E-3	3.4	0.3
2500	1	6	1.985E-3	3.1	0.3
3000	0	6	2.342E-3	3.2	0.2

FRACTURE HEALING TEST 4

Test Number: 4
Sample Number:
File Name: COISD
Type of Salt: Block
Fracture Type: Sawcut
Moisture Condition: Dry
Initial Porosity: 0.112

Confining Pressure (psi)	Time of Pressure Application (hrs)	Cumulative Time (hrs)	Axial* Strain	Permeability $\bar{X}$ (md)	Permeability $\bar{\sigma}$ (md)
50	1	1		20.3	2.6
500	1	1		5.6	0.1
1000	1	2		4.4	0.1
1500	1	2		4.8	0.2
2000	1	2		3.8	0.0
2500	0	3		3.6	0.1
2500	22	25		4.2	0.2
3000	0	25		3.3	0.0
3000	25	50		3.2	0.0

* Not recorded in this test.

FRACTURE HEALING TEST 5

Test Number: 5
Sample Number:
File Name: COISM
Type of Salt: Block
Fracture Type: Sawcut
Moisture Condition: Moist
Initial Porosity: 0.114

Confining Pressure (psi)	Time of Pressure Application (hrs)	Cumulative Time (hrs)	Axial* Strain	Permeability $\bar{X}$ (md)	Permeability $\bar{\sigma}$ (md)
50	0	0		16.4	1.0
500	1	1		5.4	0.2
1000	1	2		4.6	0.2
1500	1	3		4.2	0.1
2000	1	4		3.6	0.1
2500	0	4		3.4	0.1
2500	44	48		1.9	0.1
3000	0	48		1.7	0.1
3000	20	68		2.0	0.0

* Not recorded in this test.

FRACTURE HEALING TEST 6

Test Number: 6
Sample Number: IM1-1
File Name: COIFM
Type of Salt: Block
Fracture Type: Tensile
Moisture Condition: Moist
Initial Porosity: 0.124 (unfractured)

Confining Pressure (psi)	Time of Pressure Application (hrs)	Cumulative Time (hrs)	Axial* Strain	Permeability $\bar{X}$ (md)	Permeability $\bar{\sigma}$ (md)
50	0	0		15.6	1.3
500	0	0		13.5	0.9
1000	0	0		13.4	1.1
1500	0	1		13.0	1.0
2000	4	5		12.3	0.9
2500	0	5		11.3	0.9
2500	46	51		9.8	1.0

* Not recorded in this test.

FRACTURE HEALING TEST 7

Test Number: 7
Sample Number: CR5
File Name: CRAND
Type of Salt: WIPP
Fracture Type: Unfractured
Moisture Condition: Dry
Initial Porosity: 0.014

Confining Pressure (psi)	Time of Pressure Application (hrs)	Cumulative Time (hrs)	Axial* Strain	Permeability $\bar{X}$ (md)	Permeability $\bar{\sigma}$ (md)
500	20	20		$5.3E^{-2}$	$1.8E^{-3}$
1000	2	22		$2.4E^{-2}$	$8.1E^{-5}$
1500	1	23		$1.1E^{-2}$	$4.5E^{-5}$
2000	1	24		$5.4E^{-3}$	$1.5E^{-5}$
2500	17	41		$3.0E^{-3}$	$1.1E^{-5}$
3000	1	42		$5.7E^{-4}$	$1.1E^{-6}$

* Not recorded in this test.

FRACTURE HEALING TEST 8

Test Number: 8
Sample Number: CR5
File Name: CRAFD
Type of Salt: WIPP
Fracture Type: Tensile
Moisture Condition: Dry
Initial Porosity: 0.014 (unfractured)

Confining Pressure (psi)	Time of Pressure Application (hrs)	Cumulative Time (hrs)	Axial* Strain	Permeability $\bar{X}$ (md)	Permeability $\bar{\sigma}$ (md)
500	1	1		306.8	54.7
1000	2	3		92.6	18.8
1500	2	5		41.0	10.1
2000	1	6		13.4	2.4
2500	0	6		4.6	0.8
2500	24	30		1.3	0.1

* Not recorded in this test.

FRACTURE HEALING TEST 9

Test Number: 9
Sample Number: CR6
File Name: CRAND2
Type of Salt: WIPP
Fracture Type: Unfractured
Moisture Condition: Dry
Initial Porosity: 0.031

Confining Pressure (psi)	Time of Pressure Application (hrs)	Cumulative Time (hrs)	Axial* Strain	Permeability $\bar{X}$ (md)	Permeability $\bar{\sigma}$ (md)
500	0	0		15.7	1.6
1000	0	0		12.2	1.7
1500	0	1		7.6	0.9
2000	0	1		5.2	0.7
2500	0	2		3.0	0.3

* Not recorded in this test.

FRACTURE HEALING TEST 10

Test Number: 10
Sample Number: CR6
File Name: CRAFM
Type of Salt: WIPP
Fracture Type: Tensile
Moisture Condition: Moist
Initial Porosity: 0.031 (unfractured)

Confining Pressure (psi)	Time of Pressure Application (hrs)	Cumulative Time (hrs)	Axial* Strain	Permeability $\bar{X}$ (md)	Permeability $\bar{\sigma}$ (md)
500	0	0		4.4	2.2
1000	2	2		1.0	0.1
1500	0	2		0.7	0.1
1500	44	46		4.2	1.5
2000	5	51		4.0	1.3
2500	0	51		2.8	0.9
2500	19	70		1.6	0.2

* Not recorded in this test.

FRACTURE HEALING TEST 11

Test Number: 11
Sample Number: CR7
File Name: CRAND3
Type of Salt: WIPP
Fracture Type: Unfractured
Moisture Condition: Dry
Initial Porosity: 0.028

Confining Pressure (psi)	Time of Pressure Application (hrs)	Cumulative Time (hrs)	Axial* Strain	Permeability $\bar{X}$ (md)	Permeability $\bar{\sigma}$ (md)
50	0	0		35.3	5.7
500	0	0		18.7	2.9
1000	0	0		10.8	1.8
1500	0	1		6.4	1.0
2000	4	5		3.9	0.5
2500	0	5		2.2	0.1

* Not recorded in this test.

FRACTURE HEALING TEST 12

Test Number: 12
Sample Number: CR2
File Name: CRASM
Type of Salt: WIPP
Fracture Type: Sawcut
Moisture Condition: Moist
Initial Porosity: 0.031 (unfractured)

Confining Pressure (psi)	Time of Pressure Application (hrs)	Cumulative Time (hrs)	Axial* Strain	Permeability $\bar{X}$ (md)	Permeability $\bar{\sigma}$ (md)
50	0	0		927.9	74.9
500	0	0		446.2	44.5
1000	0	0		235.9	28.8
1500	1	1		128.7	19.9
2000	2	3		82.2	9.7
2500	0	3		54.7	5.9
2500	42	45		34.7	8.1

* Not recorded in this test.

FRACTURE HEALING TEST 13

Test Number: 13
Sample Number: AI1
File Name: AI1
Type of Salt: Avery Island
Fracture Type: Unfractured
Moisture Condition: Dry
Initial Porosity: 0.032

Confining Pressure (psi)	Time of Pressure Application (hrs)	Cumulative Time (hrs)	Axial* Strain	Permeability (md)
52	0	0		4.6
504	0	0		0.8
1059	0	1		$2.64E^{-1}$
1543	0	2		$1.12E^{-1}$
2021	0	3		$4.74E^{-2}$
2527	0	4		$2.64E^{-2}$
2510	3	6		$2.11E^{-3}$
2517	16	19		$1.09E^{-2}$
2530	27	30		$9.16E^{-3}$
2536	46	49		$6.08E^{-3}$
2517	89	91		$3.73E^{-3}$
2532	112	115		$3.22E^{-3}$
2529	137	140		$2.73E^{-3}$
2525	160	163		$2.18E^{-3}$
2045	0	163		$2.41E^{-3}$
1082	0	164		$3.14E^{-3}$

* Not recorded in this test.

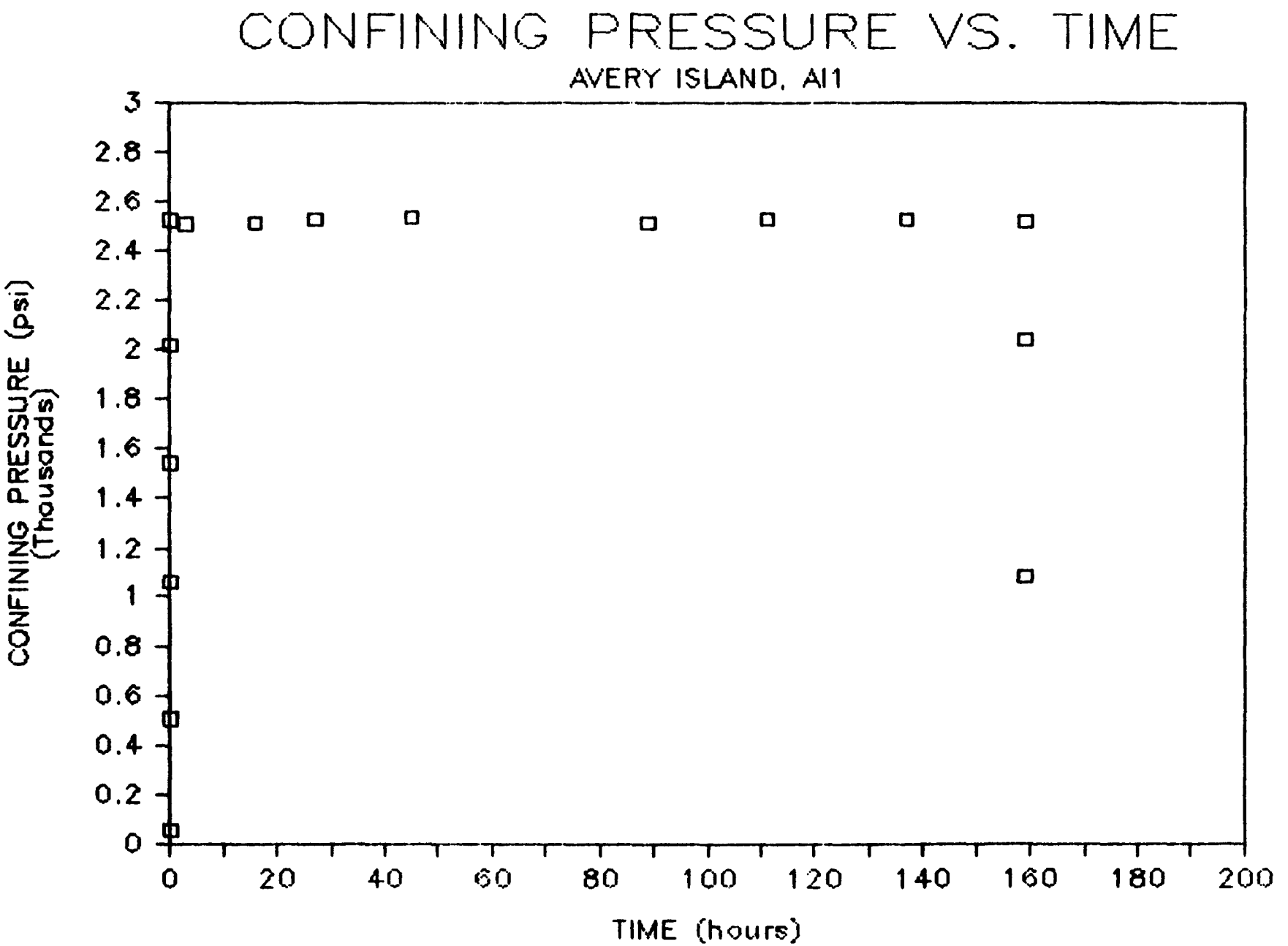
CONFINING PRESSURE VS. TIME
AVERY ISLAND, A11
CONFINING PRESSURE (psi)
(Thousands)
3
2.8
2.6
2.4
2.2
2
1.8
1.6
1.4
1.2
1
0.8
0.6
0.4
0.2
0
0
20
40
60
80
100
120
140
160
180
200
TIME (hours)

PERMEABILITY VS. CONFINING PRESSURE

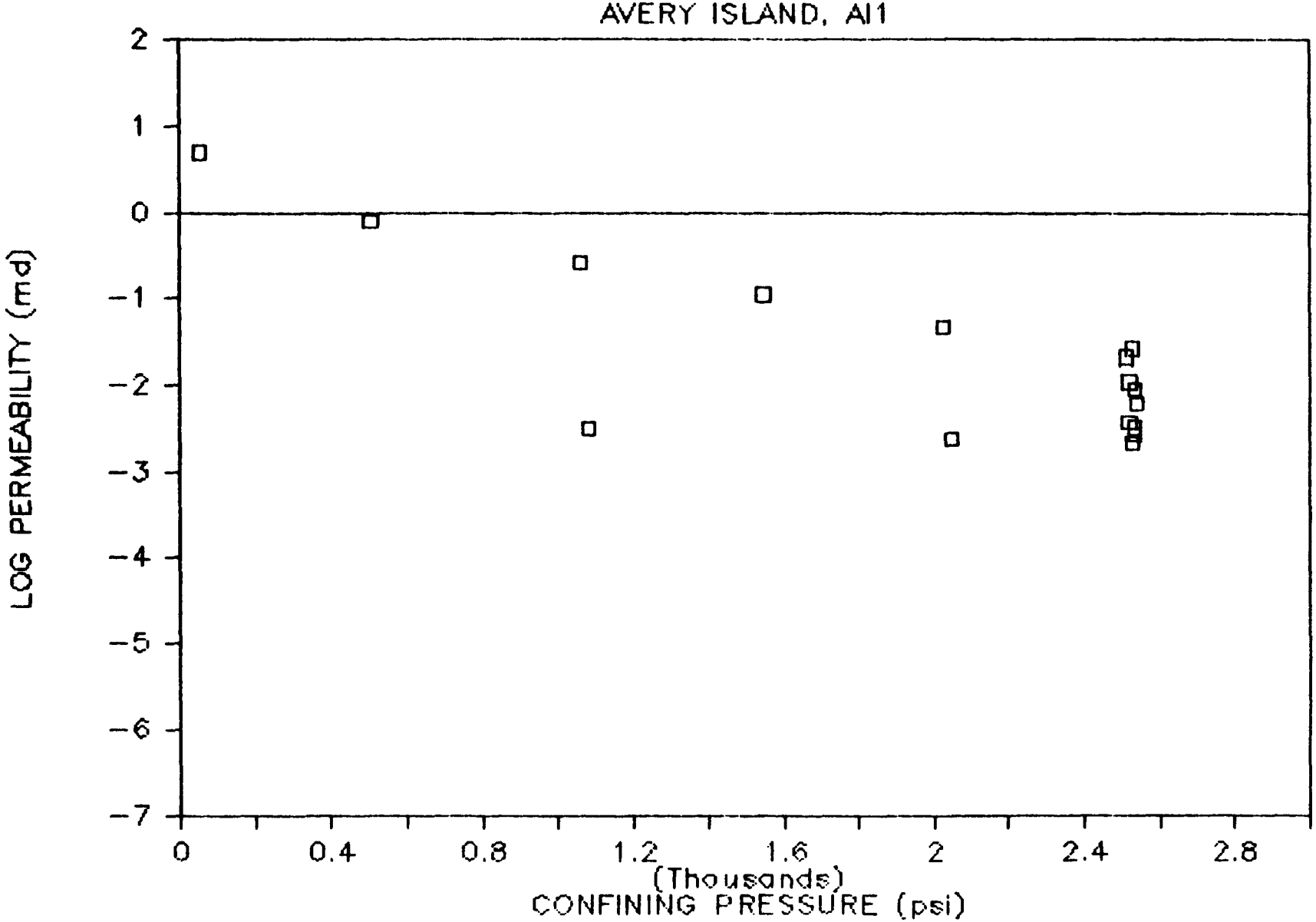

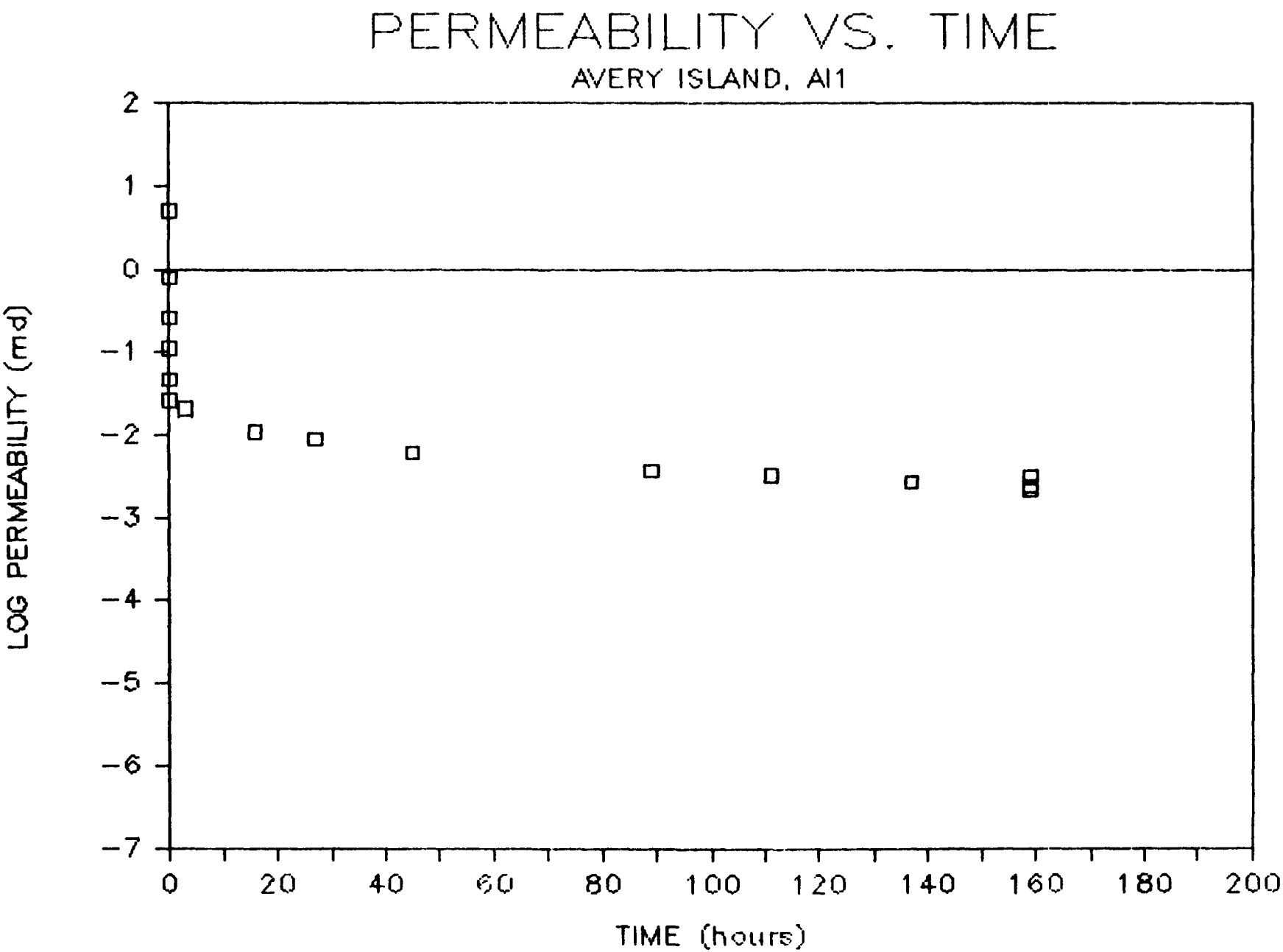
PERMEABILITY VS. TIME
AVERY ISLAND, A11
LOG PERMEABILITY (md)
2
1
0
-1
-2
-3
-4
-5
-6
-7
0
20
40
60
80
100
120
140
160
180
200
TIME (hours)

FRACTURE HEALING TEST 14

Test Number: 14
Sample Number: AI1FD
File Name: AI1FD
Type of Salt: Avery Island
Fracture Type: Tensile
Moisture Condition: Dry
Initial Porosity: 0.032 (unfractured)

Confining Pressure (psi)	Time of Pressure Application (hrs)	Cumulative Time (hrs)	Axial* Strain	Permeability (md)
56	0	0		13.2
506	0	0		6.2
1010	0	2		0.7
1547	0	3		$1.34E^{-1}$
2021	0	4		$3.37E^{-2}$
2532	0	5		$1.36E^{-2}$
2539	15	20		$2.64E^{-3}$
2534	39	44		$1.00E^{-3}$
2533	63	68		$3.28E^{-4}$
2542	136	141		$1.08E^{-4}$
2490	141	146		$6.20E^{-5}$
2531	160	165		$3.73E^{-5}$
2018	0	167		$9.29E^{-5}$
1023	0	167		$6.92E^{-4}$

* Not recorded in this test.

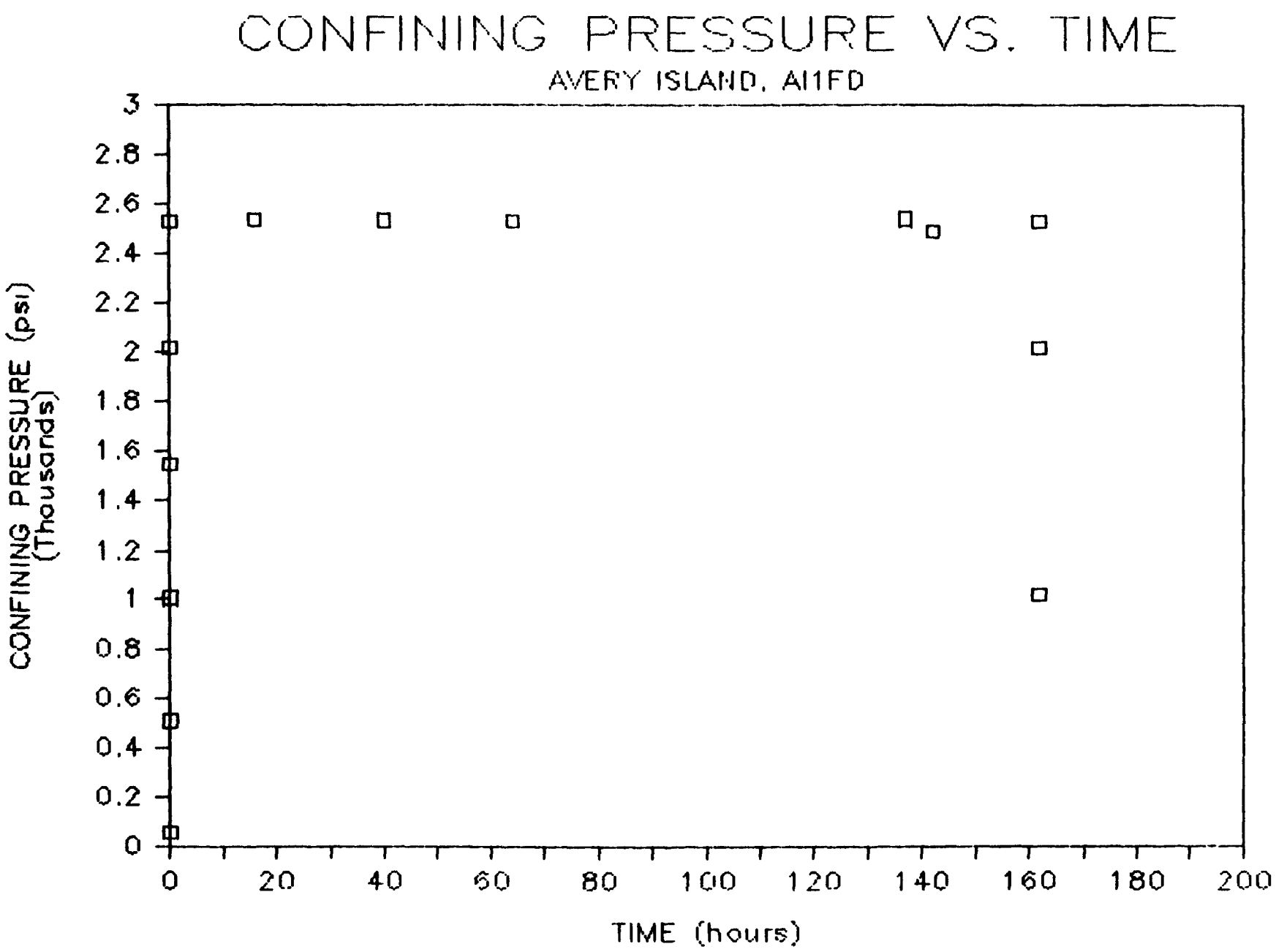
CONFINING PRESSURE VS. TIME
AVERY ISLAND, A11FD
CONFINING PRESSURE (psi)
(Thousands)
3
2.8
2.6
2.4
2.2
2
1.8
1.6
1.4
1.2
1
0.8
0.6
0.4
0.2
0
0
20
40
60
80
100
120
140
160
180
200
TIME (hours)

PERMEABILITY VS. CONFINING PRESSURE

AVERY ISLAND, A11FD

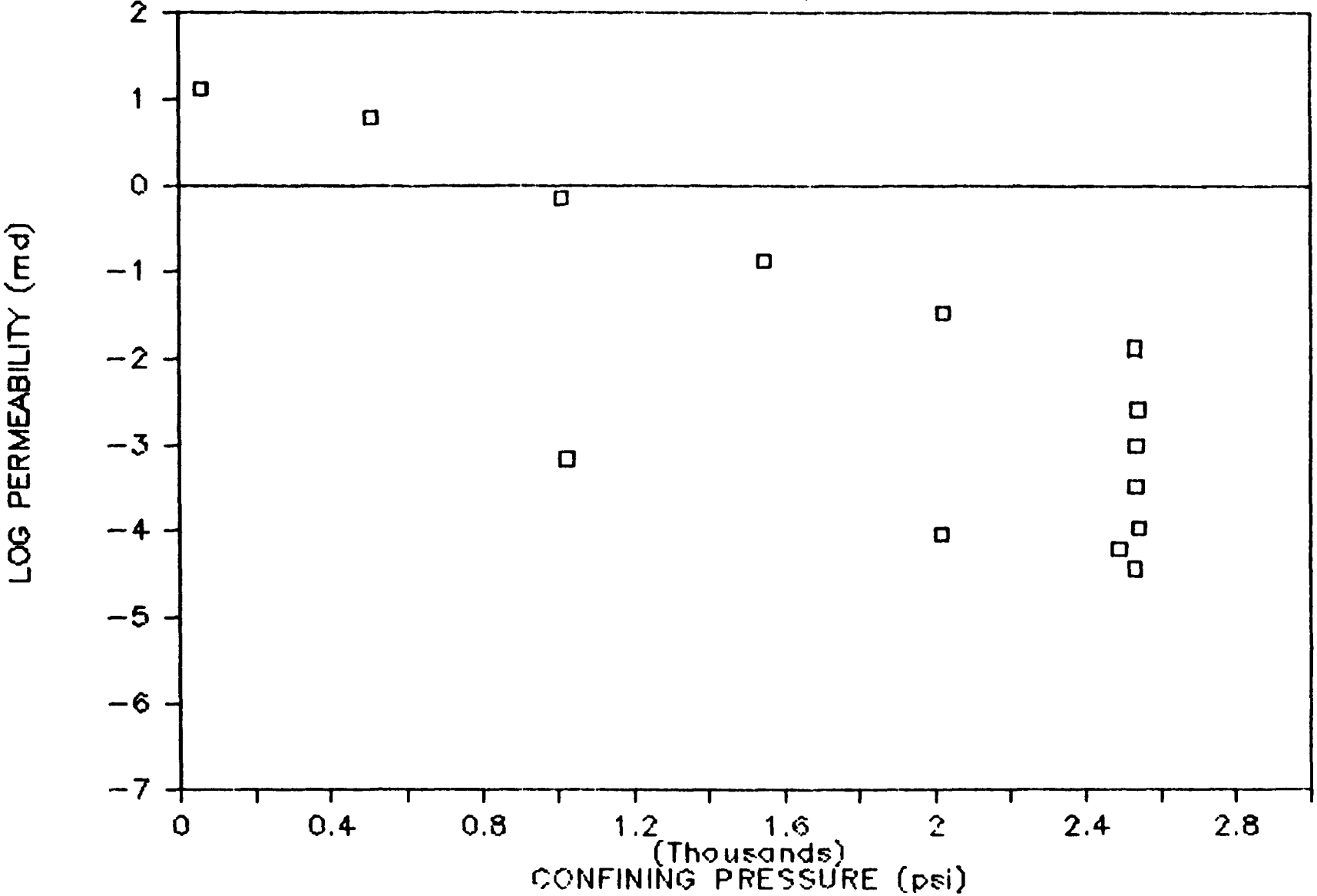

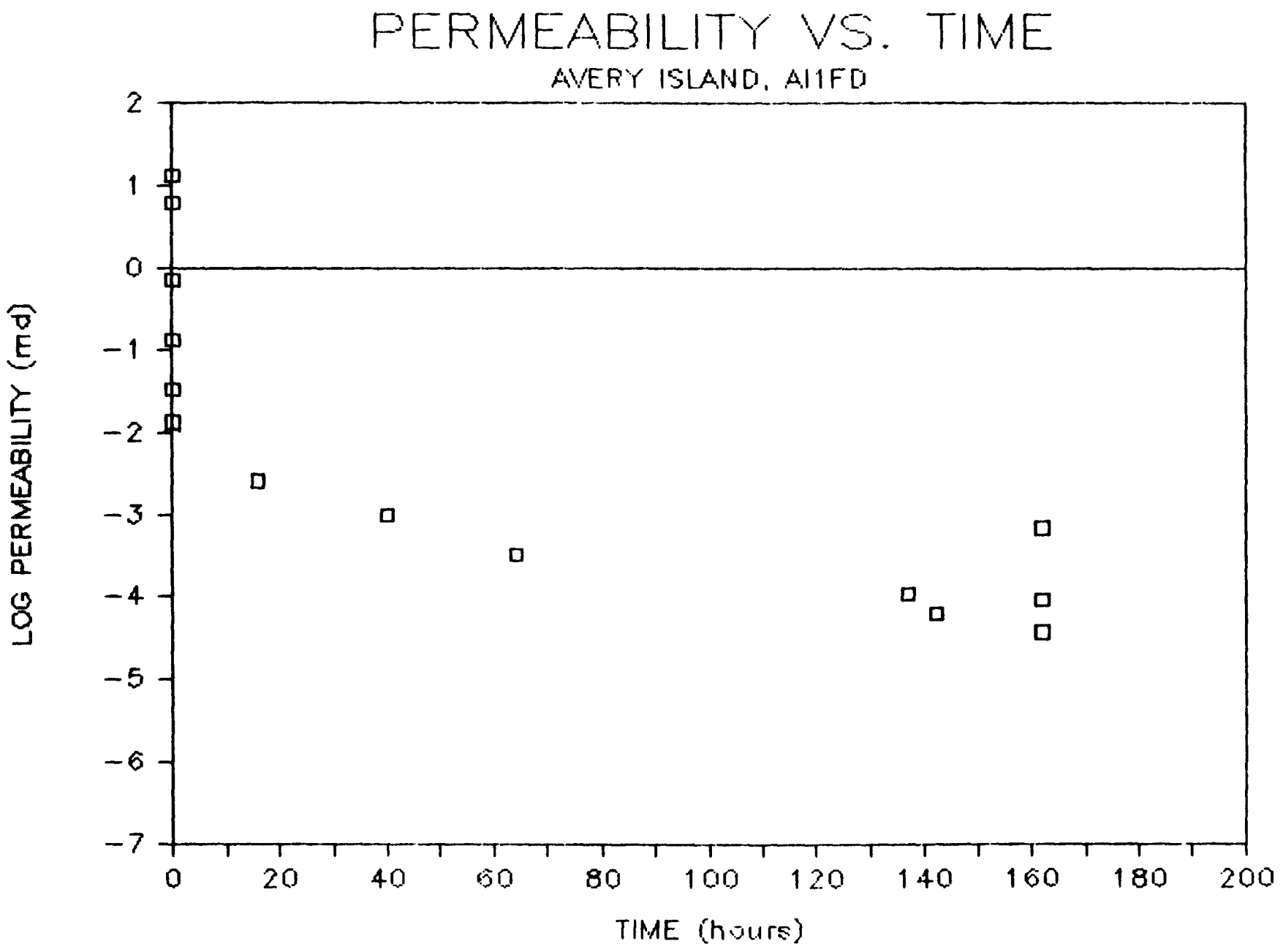
PERMEABILITY VS. TIME
AVERY ISLAND, A11FD
LOG PERMEABILITY (md)
2
1
0
-1
-2
-3
-4
-5
-6
-7
0
20
40
60
80
100
120
140
160
180
200
TIME (hours)

PERMEABILITY VS. TIME

AVERY ISLAND A11 & A11FD

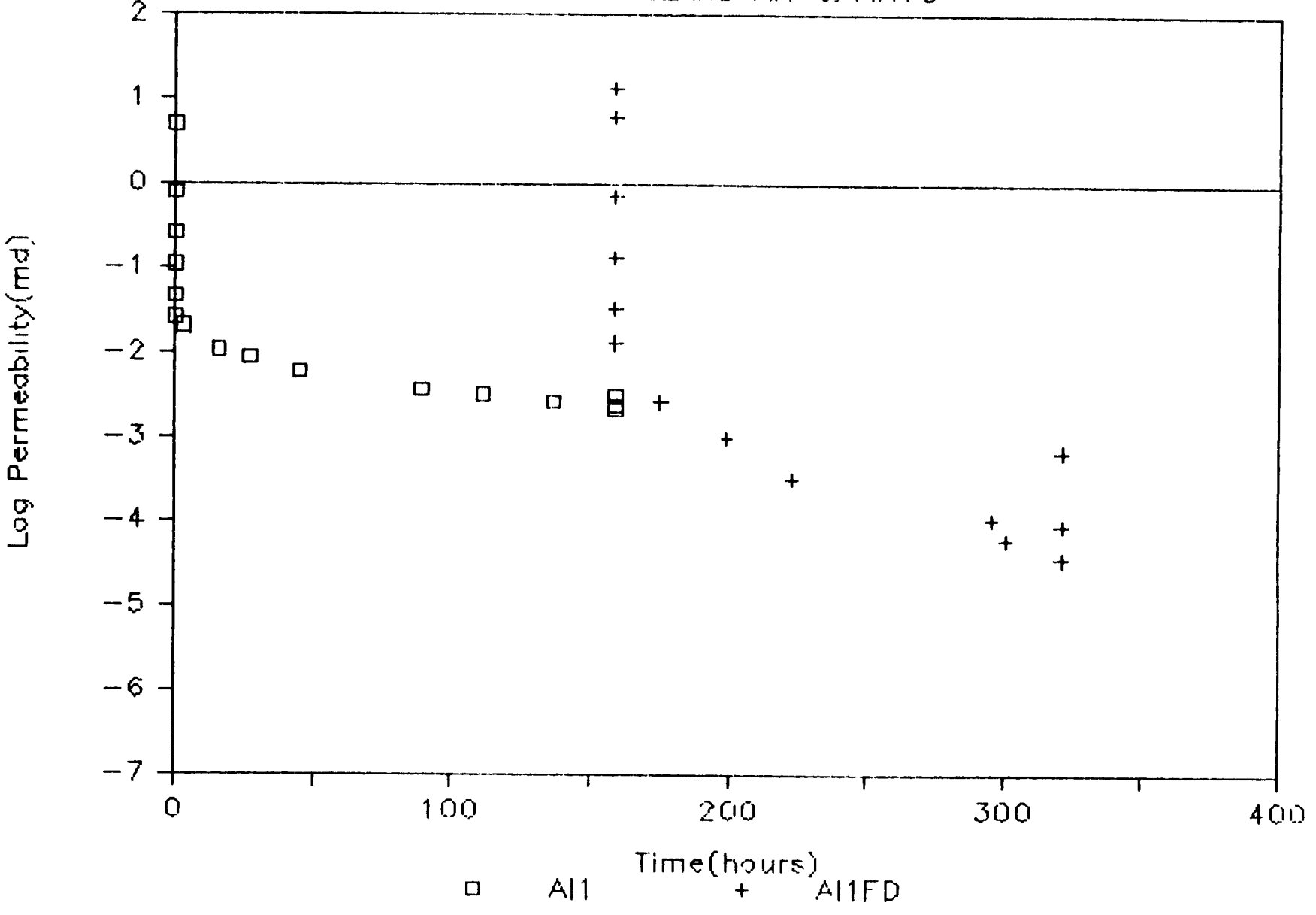

PERMEABILITY VS. CONFINING PRESSURE

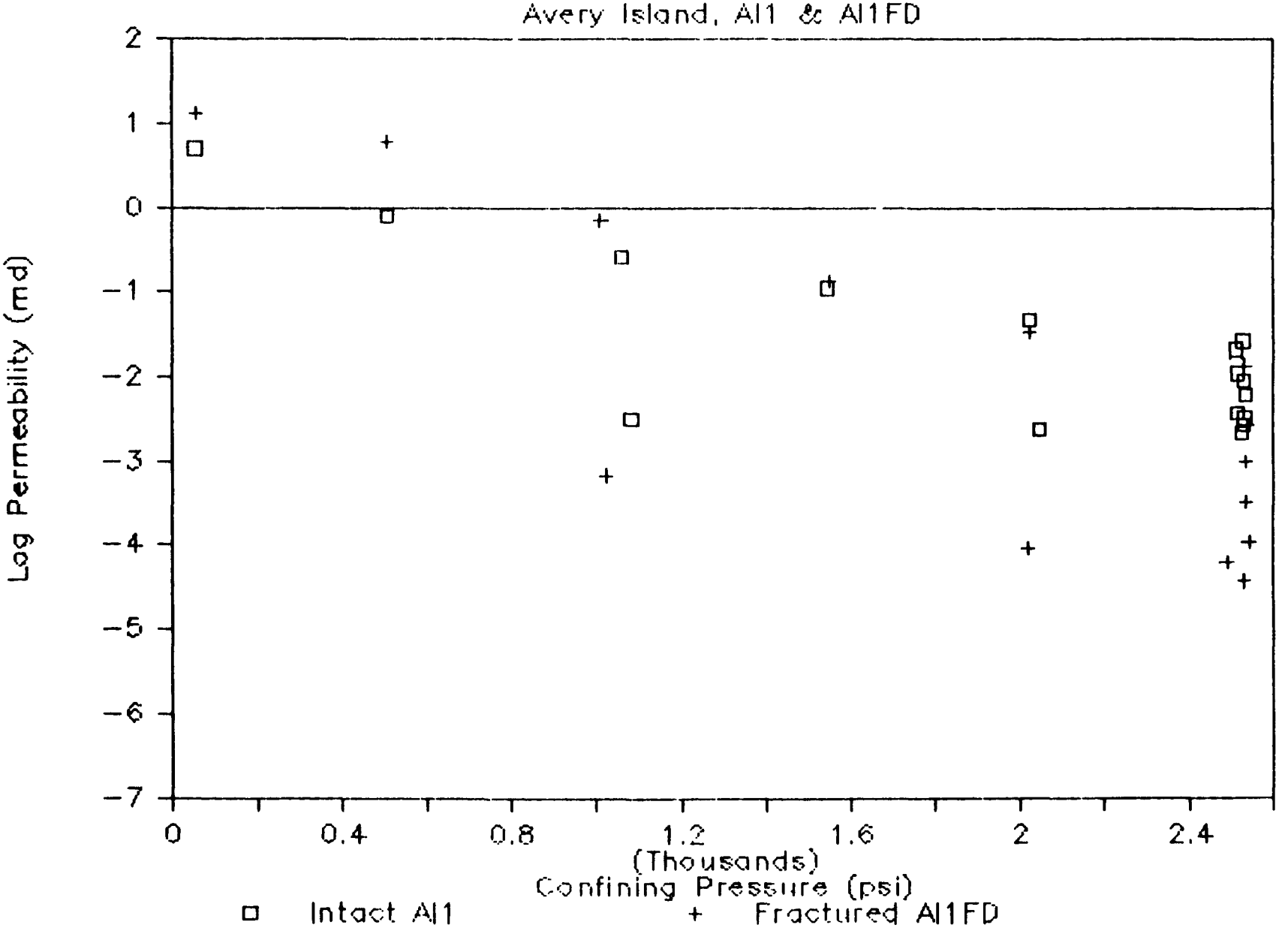

FRACTURE HEALING TEST 15

Test Number: 15
Sample Number: AI3
File Name: AI3
Type of Salt: Avery Island
Fracture Type: Unfractured
Moisture Condition: Dry
Initial Porosity: 0.017

Confining Pressure (psi)	Time of Pressure Application (hrs)	Cumulative Time (hrs)	Axial* Strain	Permeability (md)
52	0	0		1.6
628	0	0		$3.82E^{-1}$
1047	0	1		$1.17E^{-1}$
1528	0	2		$3.18E^{-2}$
2029	0	2		$1.03E^{-2}$
2527	0	3		$3.99E^{-3}$
2526	6	9		$1.62E^{-3}$
2531	24	27		$3.48E^{-4}$
2525	50	53		$1.54E^{-4}$
2518	76	79		$8.44E^{-5}$
2535	92	95		$8.98E^{-5}$
2530	142	145		$1.70E^{-4}$
2517	171	174		$1.64E^{-4}$
2016	0	189		$7.83E^{-5}$

* Not recorded in this test.

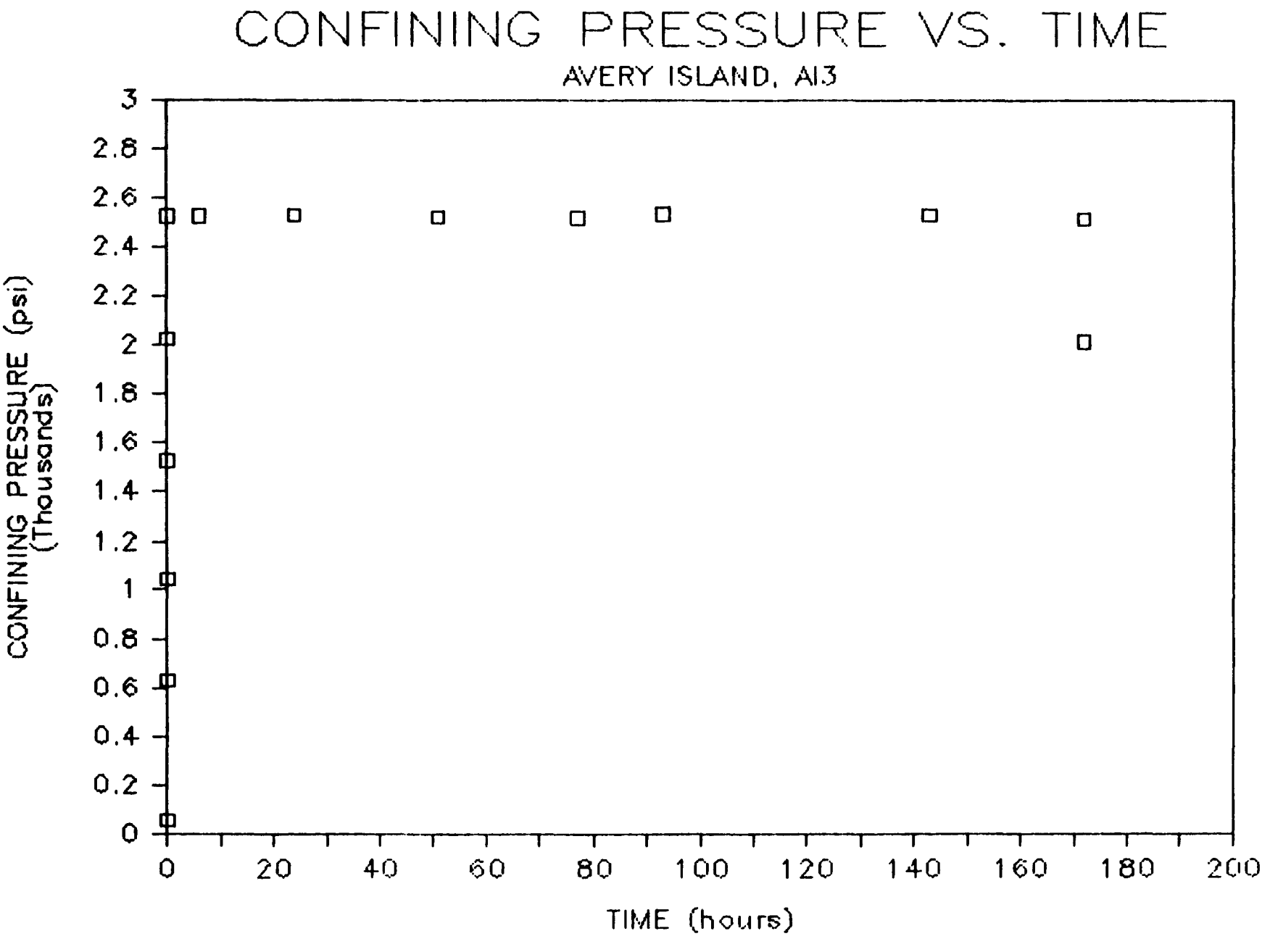
CONFINING PRESSURE VS. TIME
AVERY ISLAND, AI3
CONFINING PRESSURE (psi)
(Thousands)
3
2.8
2.6
2.4
2.2
2
1.8
1.6
1.4
1.2
1
0.8
0.6
0.4
0.2
0
0
20
40
60
80
100
120
140
160
180
200
TIME (hours)

PERMEABILITY VS. CONFINING PRESSURE

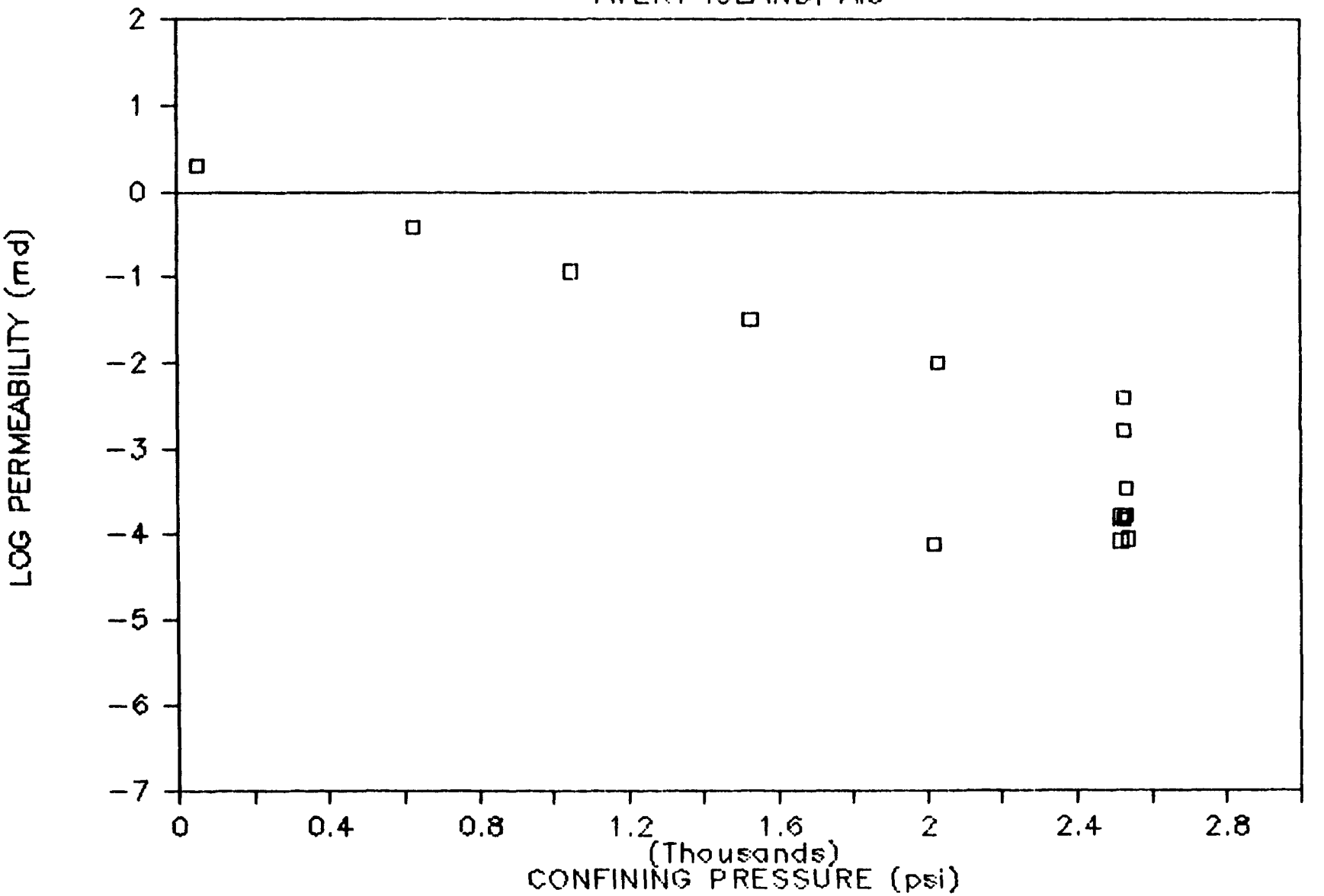

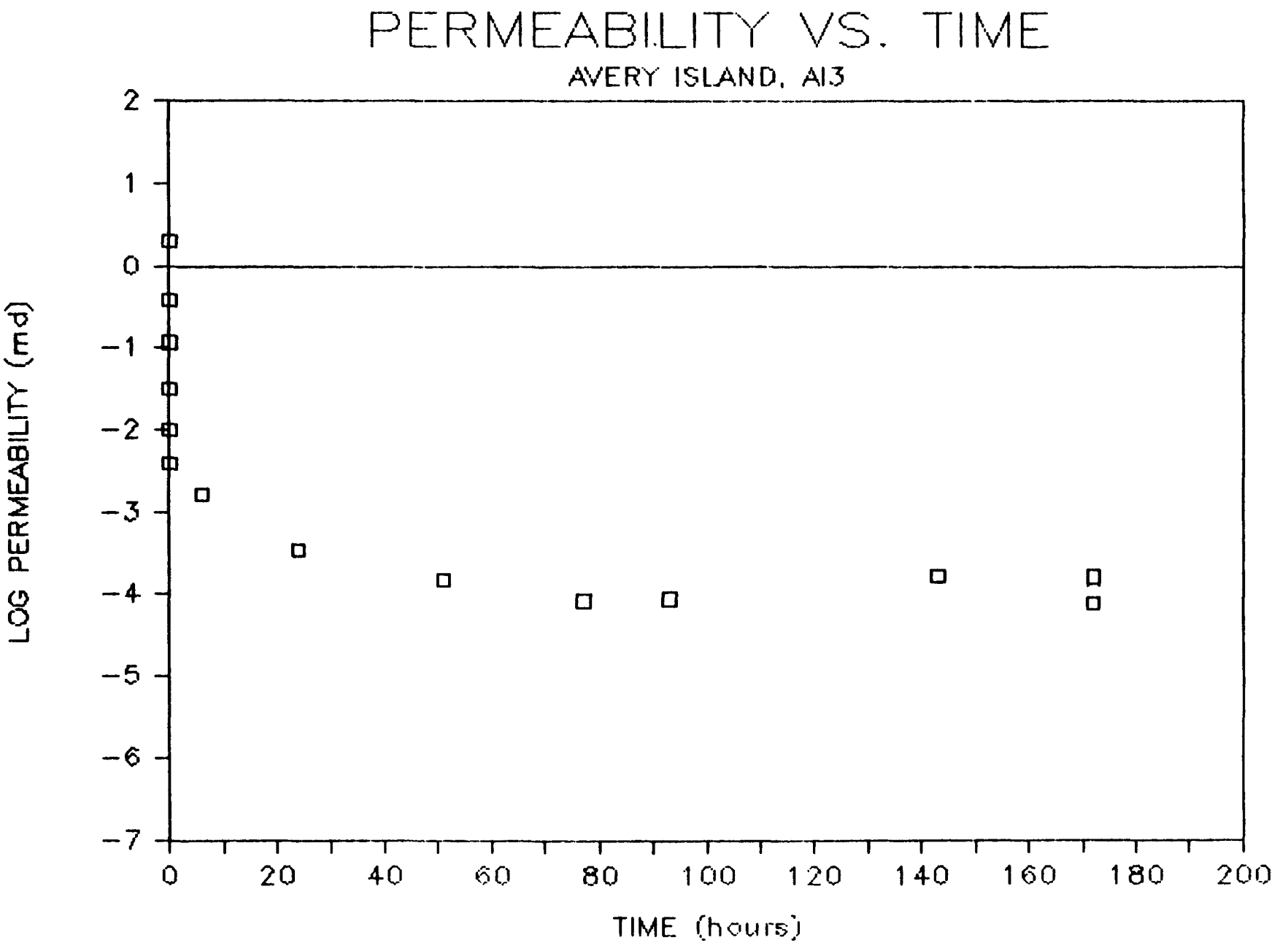
PERMEABILITY VS. TIME
AVERY ISLAND, AI3
LOG PERMEABILITY (md)
2
1
0
-1
-2
-3
-4
-5
-6
-7
0
20
40
60
80
100
120
140
160
180
200
TIME (hours)

FRACTURE HEALING TEST 16

Test Number: 16
Sample Number: AI3FM
File Name: AI3FM
Type of Salt: Avery Island
Fracture Type: Tensile
Moisture Condition: Moist
Initial Porosity: 0.017 (unfractured)

Confining Pressure (psi)	Time of Pressure Application (hrs)	Cumulative Time (hrs)	Axial* Strain	Permeability (md)
59	0	0		4.2
583	0	0		$3.67E^{-2}$
1017	0	1		$2.91E^{-2}$
1530	0	2		$1.88E^{-2}$
2020	0	3		$7.93E^{-2}$
2507	0	3		$1.99E^{-3}$
2441	7	10		$9.27E^{-4}$
2536	24	27		$2.26E^{-4}$
2537	78	81		$3.05E^{-4}$
2478	95	98		$1.68E^{-4}$
2528	120	123		$2.26E^{-4}$
2529	144	147		$2.26E^{-4}$
2515	167	170		$3.08E^{-6}$
1998	0	173		$1.79E^{-6}$
2025	5	178		$0.78E^{-6}$
1068	0	195		$12.2E^{-6}$

* Not recorded in this test.

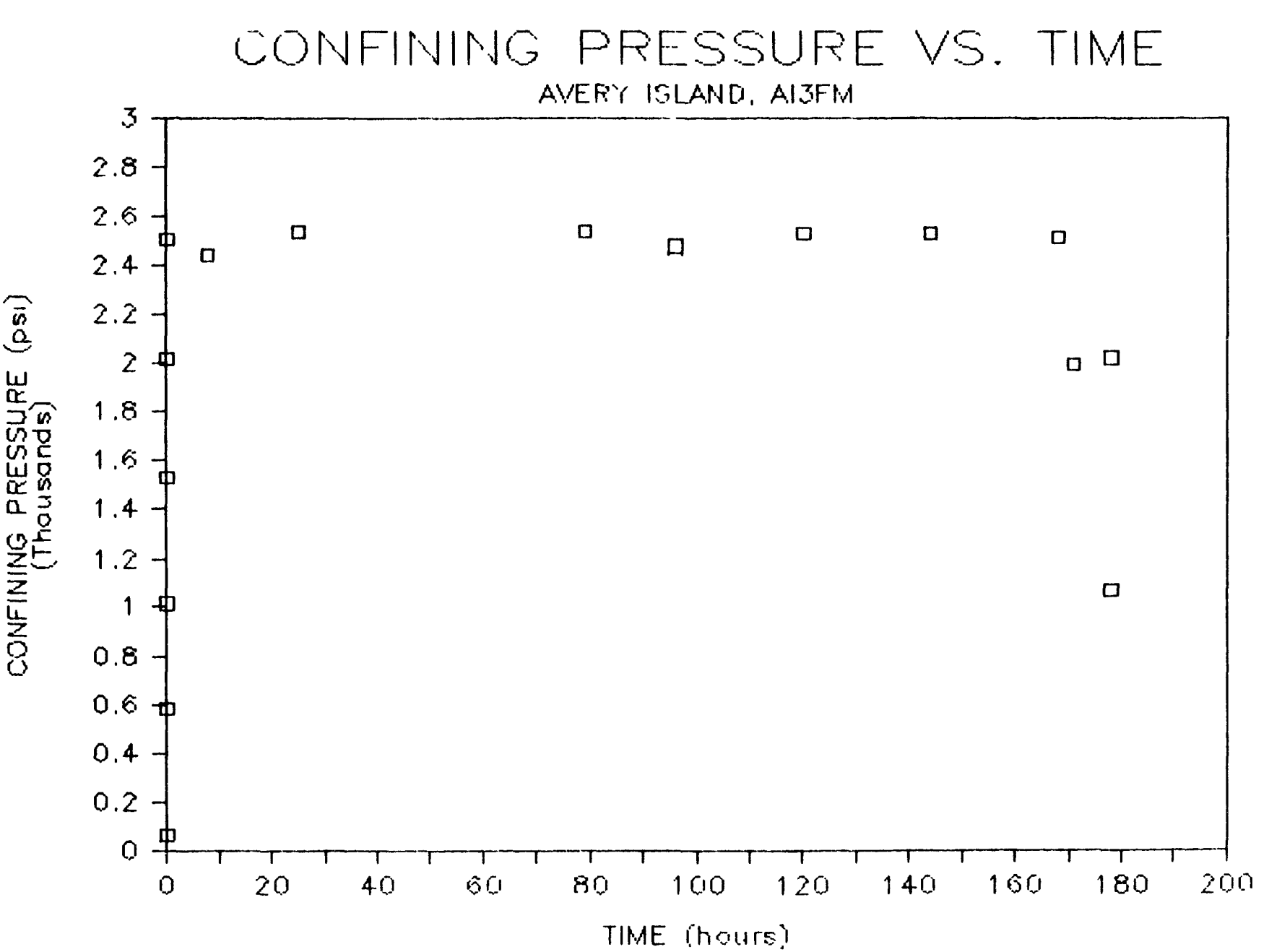
CONFINING PRESSURE VS. TIME
AVERY ISLAND, AI3FM
CONFINING PRESSURE (psi)
(Thousands)
3
2.8
2.6
2.4
2.2
2
1.8
1.6
1.4
1.2
1
0.8
0.6
0.4
0.2
0
0
20
40
60
80
100
120
140
160
180
200
TIME (hours)

PERMEABILITY VS. CONFINING PRESSURE

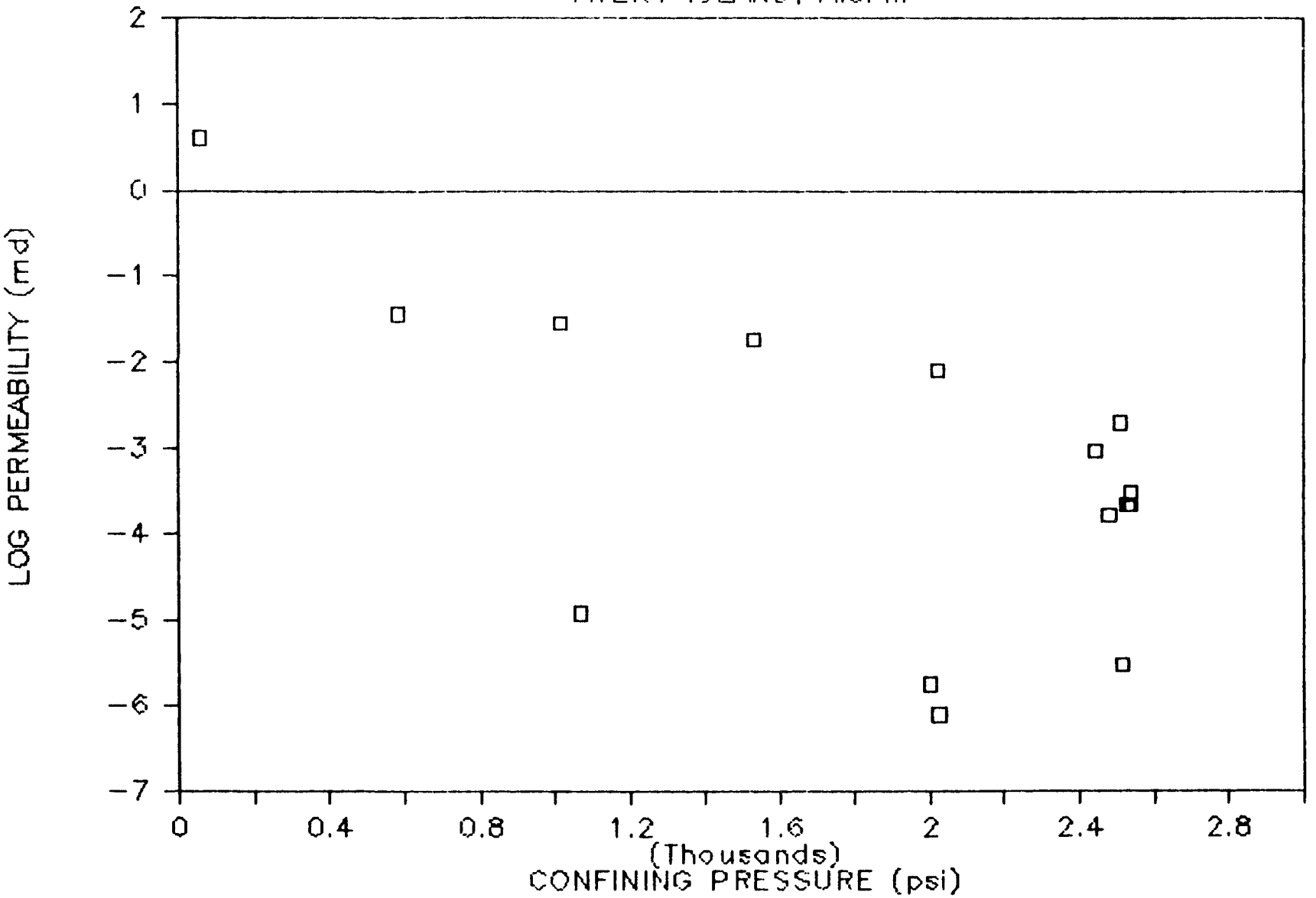

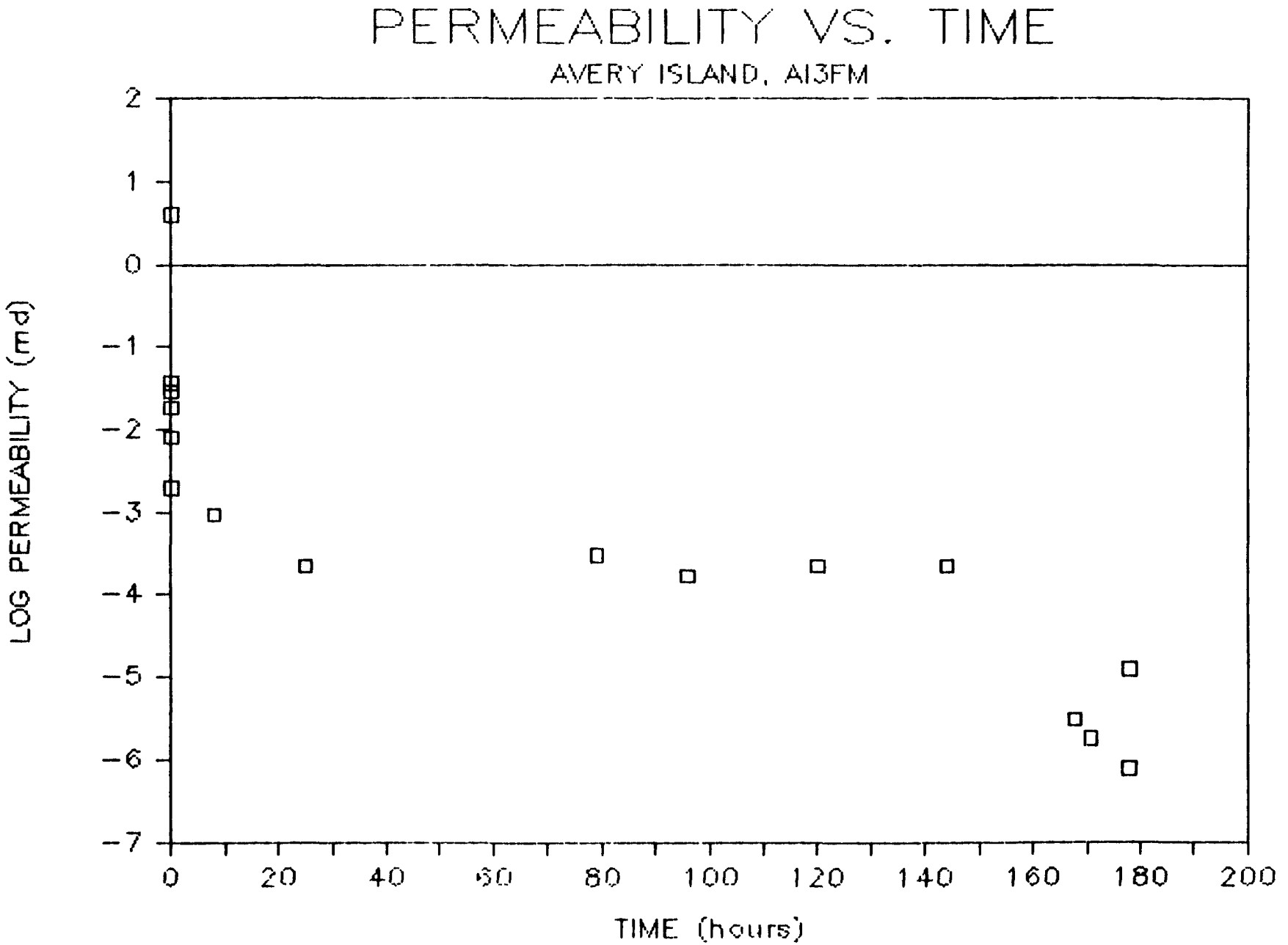
PERMEABILITY VS. TIME
AVERY ISLAND, AI3FM
LOG PERMEABILITY (md)
2
1
0
-1
-2
-3
-4
-5
-6
-7
0
20
40
60
80
100
120
140
160
180
200
TIME (hours)

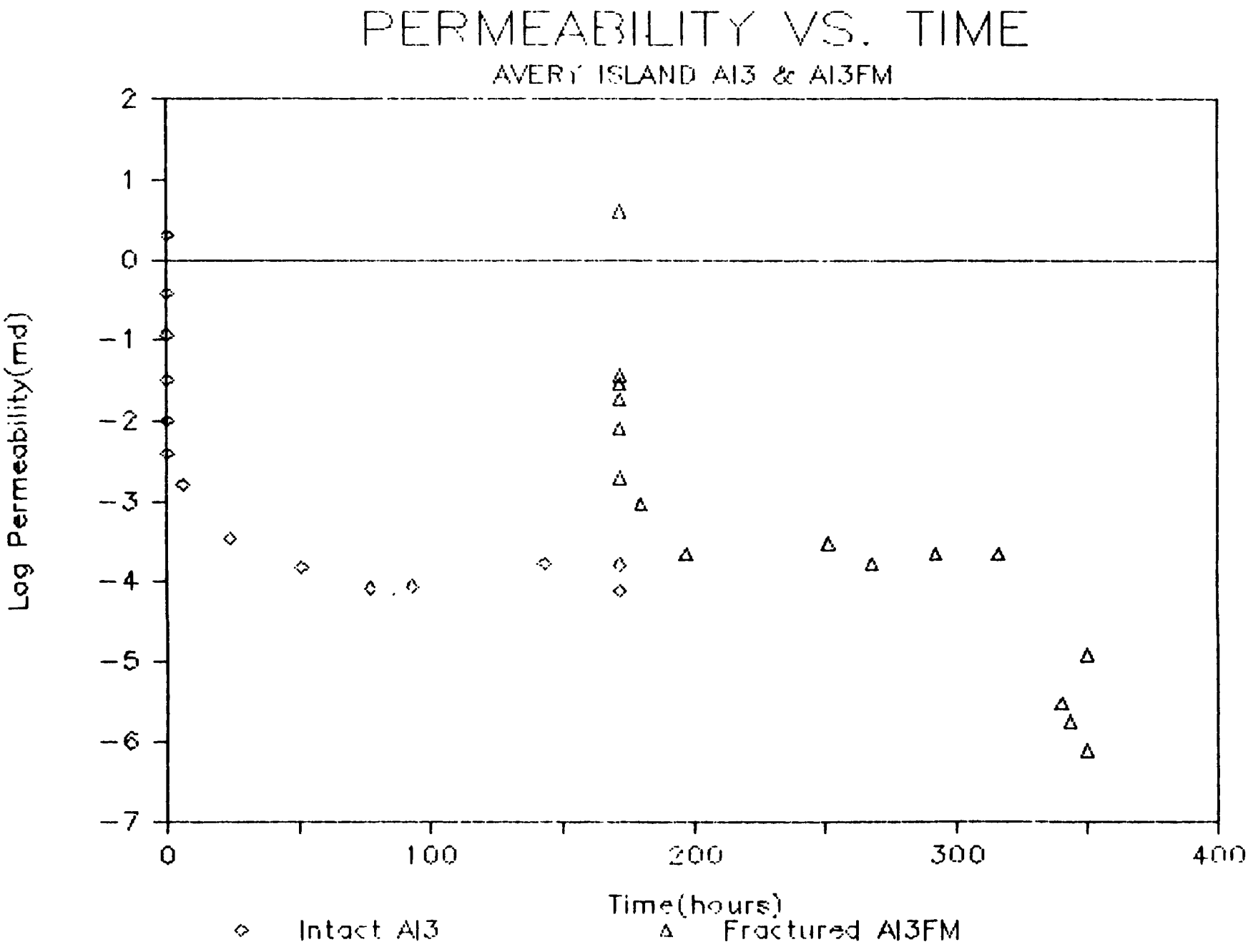
PERMEABILITY VS. TIME
AVERY ISLAND AI3 & AI3FM
Log Permeability(md)
2
1
0
-1
-2
-3
-4
-5
-6
-7
0
100
200
300
400
Time(hours)
Intact AI3
Fractured AI3FM

PERMEABILITY VS. CONFINING PRESSURE

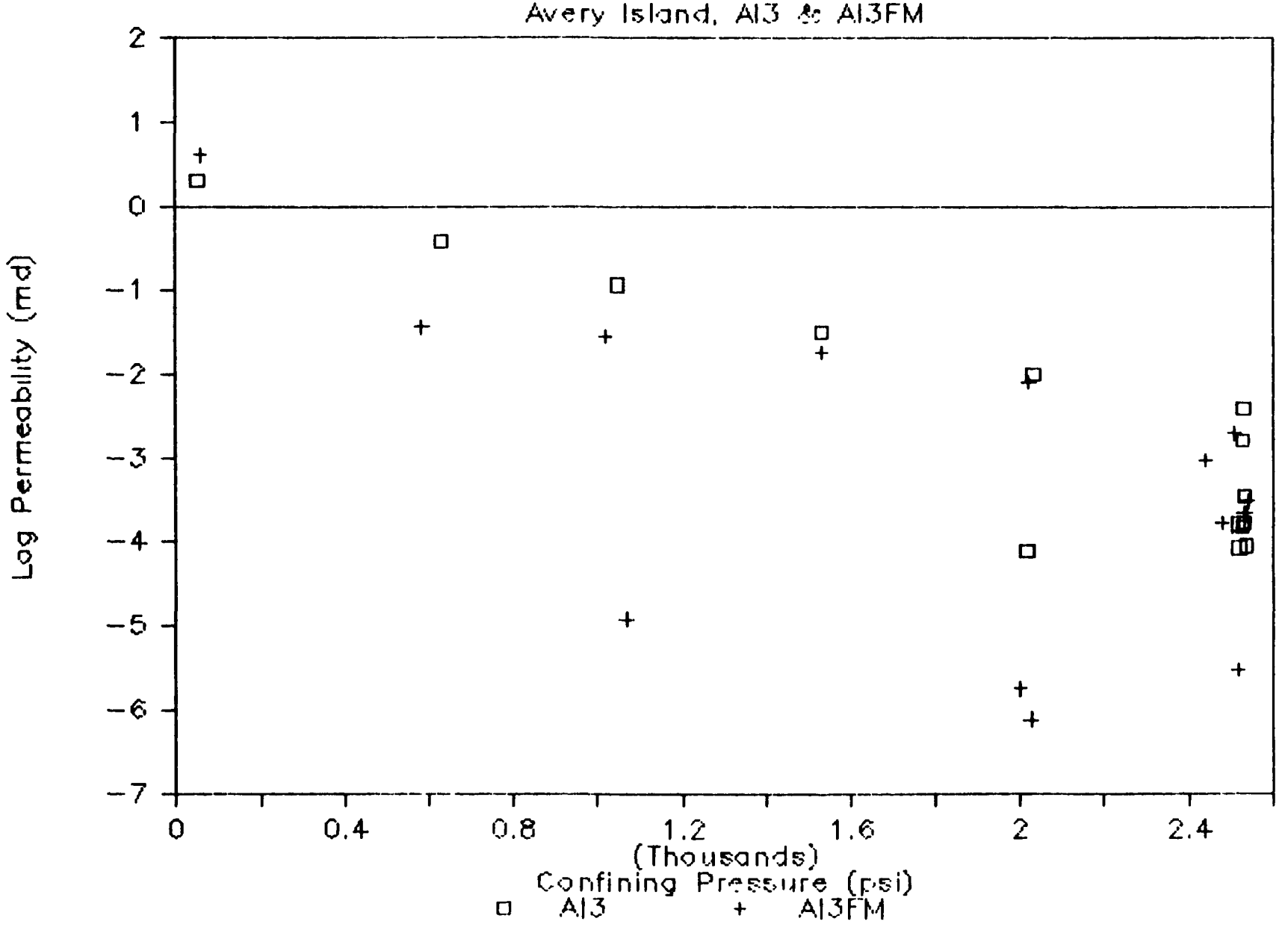

FRACTURE HEALING TEST 17

Test Number: 17
Sample Number: I1
File Name: I1
Type of Salt: Block
Fracture Type: Unfractured
Moisture Condition: Dry
Initial Porosity: 0.138

Confining Pressure (psi)	Time of Pressure Application (hrs)	Cumulative Time (hrs)	Axial Strain	Permeability (md)
52	0	0	$7.86E^{-4}$	66.1
502	0	1	$3.206E^{-3}$	33.8
1005	0	1	$4.417E^{-3}$	33.2
1510	0	2	$5.442E^{-3}$	31.9
2008	0	2	$6.101E^{-3}$	31.4
2524	0	3	$6.79E^{-3}$	30.5
2524	6	9	$7.472E^{-3}$	28.5
2525	21	23	$8.015E^{-3}$	26.4
2526	48	51	$9.227E^{-3}$	25.1
2523	70	73	$9.312E^{-3}$	24.3
2530	96	99	$9.541E^{-3}$	23.9
2519	119	122	$9.83E^{-3}$	23.5
2526	144	147	$9.779E^{-3}$	23.6
2525	165	168	$9.878E^{-3}$	23.6
2014	0	168	$9.788E^{-3}$	23.5
1017	0	169	$9.368E^{-3}$	24.1

* Not recorded in this test.

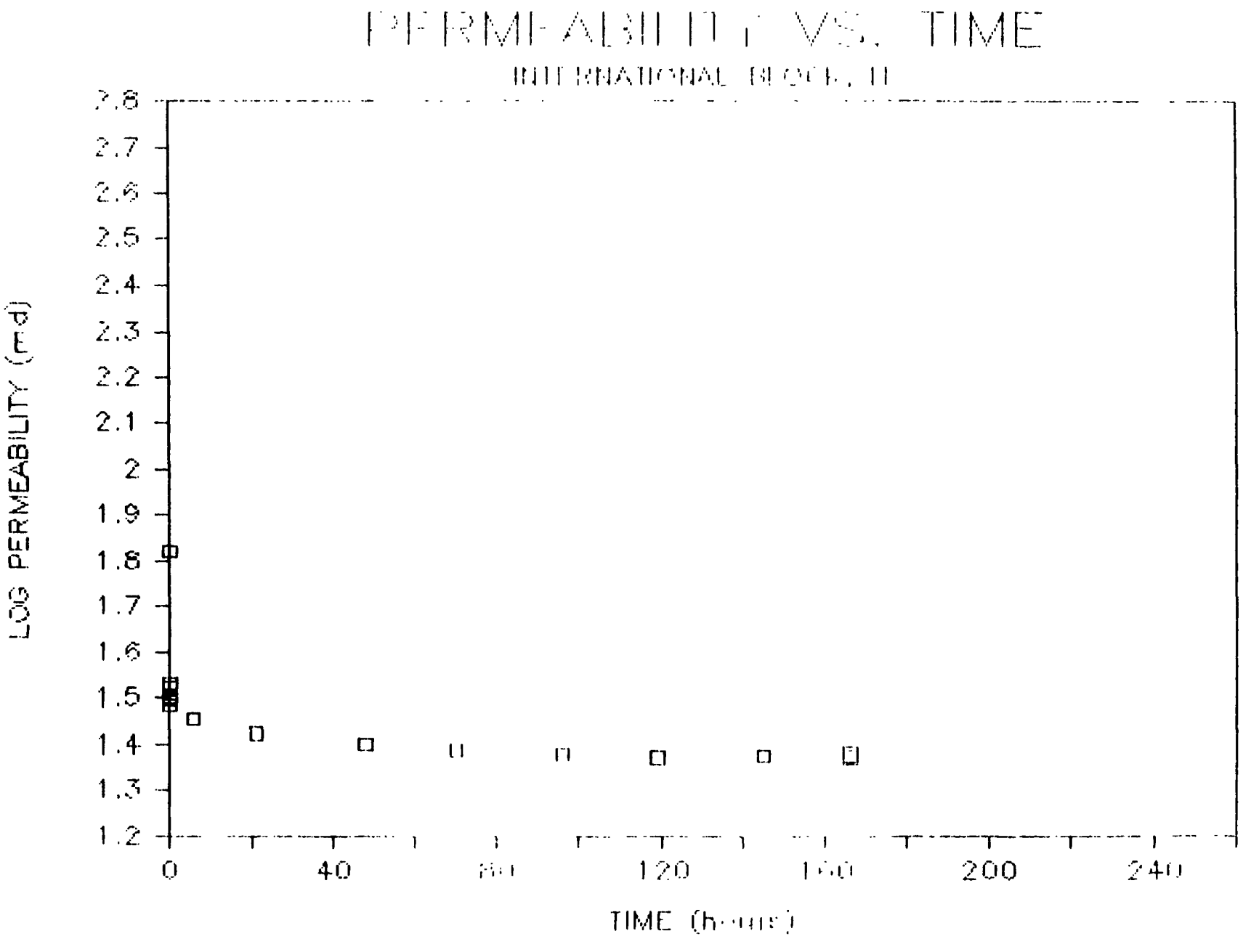
PERMEABILITY VS. TIME
INTERNATIONAL BLOCK, II
LOG PERMEABILITY (md)
2.8
2.7
2.6
2.5
2.4
2.3
2.2
2.1
2
1.9
1.8
1.7
1.6
1.5
1.4
1.3
1.2
0
40
120
200
240
TIME (hours)

FRACTURE HEALING TEST 18

Test Number: 18
Sample Number: I1FD
File Name: I1FD
Type of Salt: Block
Fracture Type: Sawcut
Moisture Condition: Dry
Initial Porosity: 0.138 (Unfractured)

Confining Pressure (psi)	Time of Pressure Application (hrs)	Cumulative Time (hrs)	Axial* Strain	Permeability (md)
55	0	0		600
515	0	0		44.7
1024	0	1		31.9
1535	0	1		27.0
2043	0	2		25.5
2557	0	2		24.1
2556	6	8		23.4
2553	50	52		22.0
2558	74	76		21.9
2556	98	100		22.0
2561	123	125		22.1
2558	145	147		21.6
2559	169	171		21.6
2558	240	240		22.2
2049	0	245		21.8
1023	0	246		22.7

* Not recorded in this test.

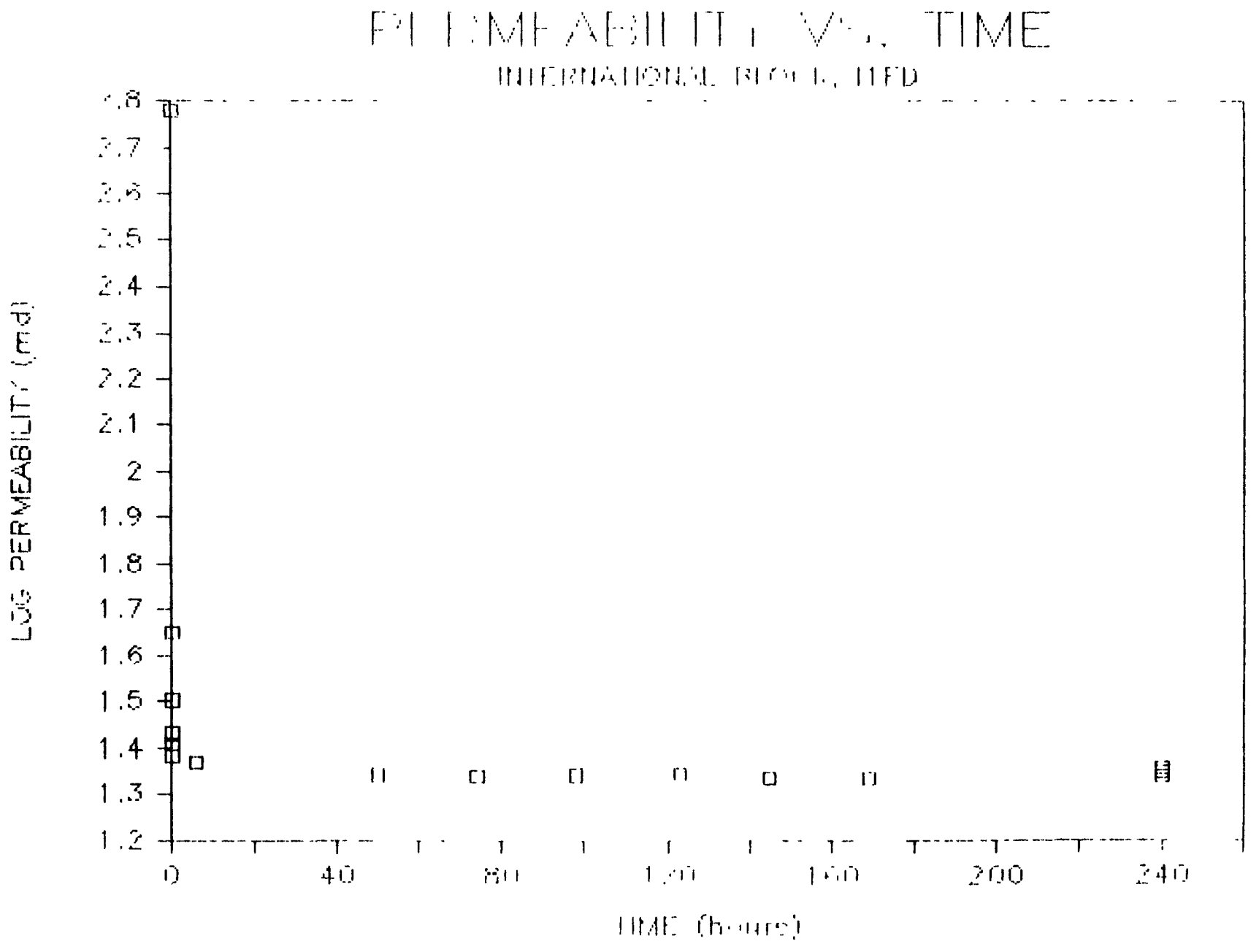
PERMEABILITY VS. TIME
INTERNATIONAL BOOK, LTD
LOG PERMEABILITY (md)
2.8
2.7
2.6
2.5
2.4
2.3
2.2
2.1
2
1.9
1.8
1.7
1.6
1.5
1.4
1.3
1.2
0
40
80
120
160
200
240
TIME (hours)

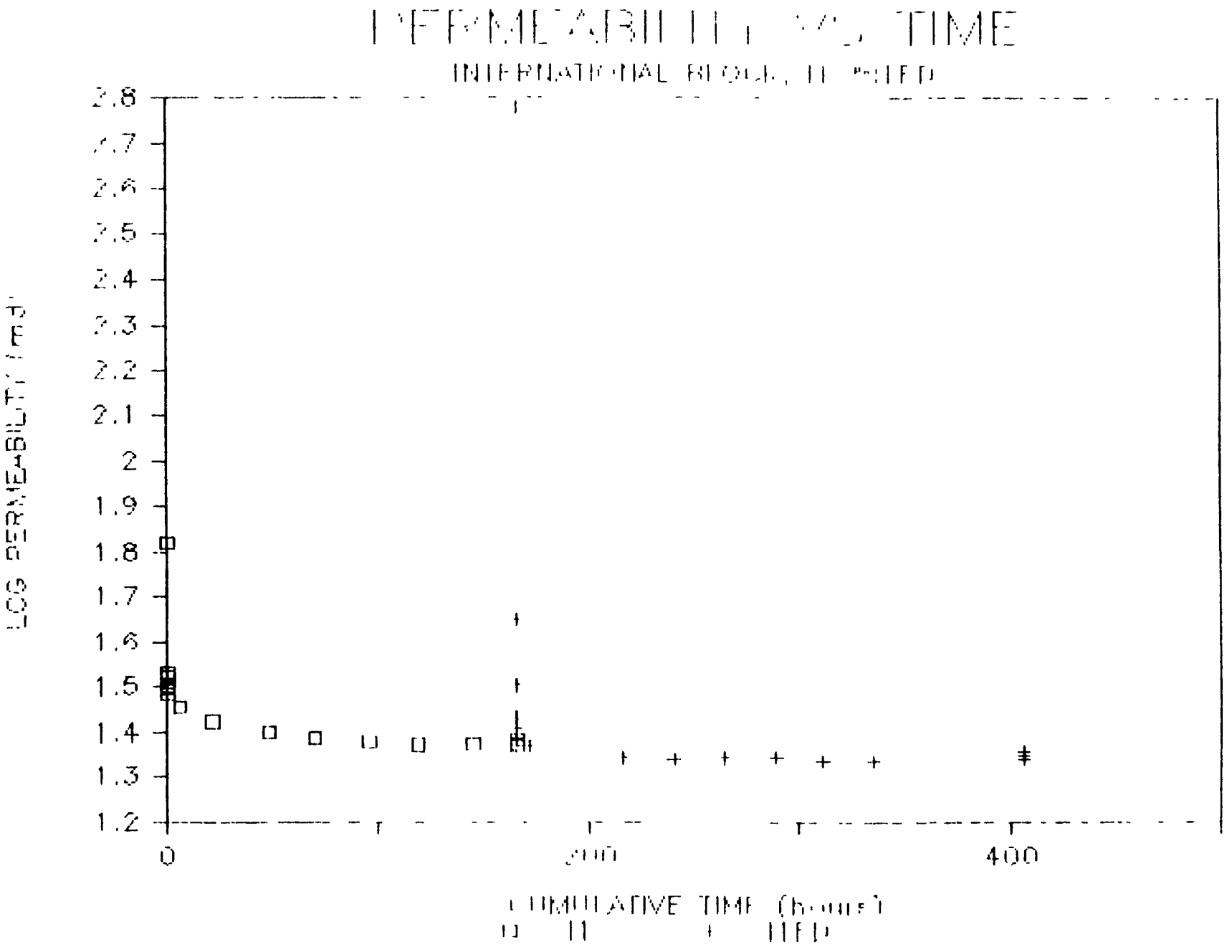
PERMEABILITY VS. TIME
INTERNATIONAL BIOLOGICAL LIMITED
LOG PERMEABILITY (cm/sec)
2.8
2.7
2.6
2.5
2.4
2.3
2.2
2.1
2
1.9
1.8
1.7
1.6
1.5
1.4
1.3
1.2
0
200
400
CUMULATIVE TIME (hours)
INTERNATIONAL BIOLOGICAL LIMITED

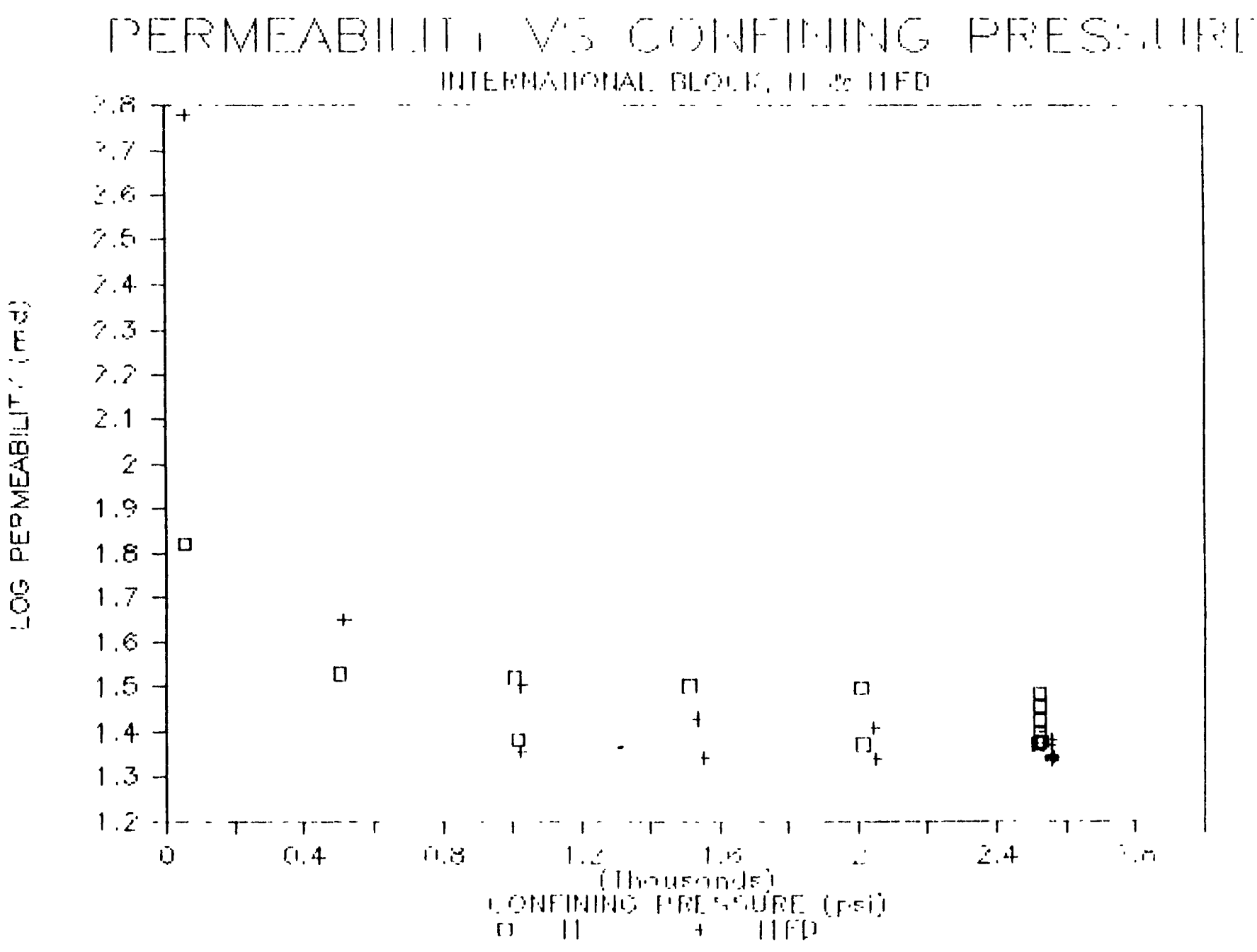
PERMEABILITY VS CONFINING PRESSURE
INTERNATIONAL BLOCK, 11.5% IIFD
LOG PERMEABILITY (md)
2.8
2.7
2.6
2.5
2.4
2.3
2.2
2.1
2
1.9
1.8
1.7
1.6
1.5
1.4
1.3
1.2
0
0.4
0.8
1.2
1.6
2
2.4
(Thousands)
CONFINING PRESSURE (psi)
11
IIFD

FRACTURE HEALING TEST 19

Test Number: 19
Sample Number: I2
File Name: I2
Type of Salt: Block
Fracture Type: Unfractured
Moisture Condition: Dry
Initial Porosity: 0.135

Confining Pressure (psi)	Time of Pressure Application (hrs)	Cumulative Time (hrs)	Axial Strain	Permeability (md)
55	0	0	$3.59E^{-4}$	53.4
504	0	0	$2.961E^{-3}$	31.6
1006	0	1	$4.159E^{-3}$	31.0
1513	0	2	$5.009E^{-3}$	30.1
2012	0	2	$5.627E^{-3}$	29.2
2518	0	2	$6.091E^{-3}$	28.6
2518	6	8	$6.458E^{-3}$	27.9
2516	24	26	$6.78E^{-3}$	26.8
2505	48	50	$7.018E^{-3}$	26.4
2521	72	74	$7.063E^{-3}$	25.8
2014	0	74	$6.934E^{-3}$	25.8
1008	0	74	$6.496E^{-3}$	26.3

* Not recorded in this test.

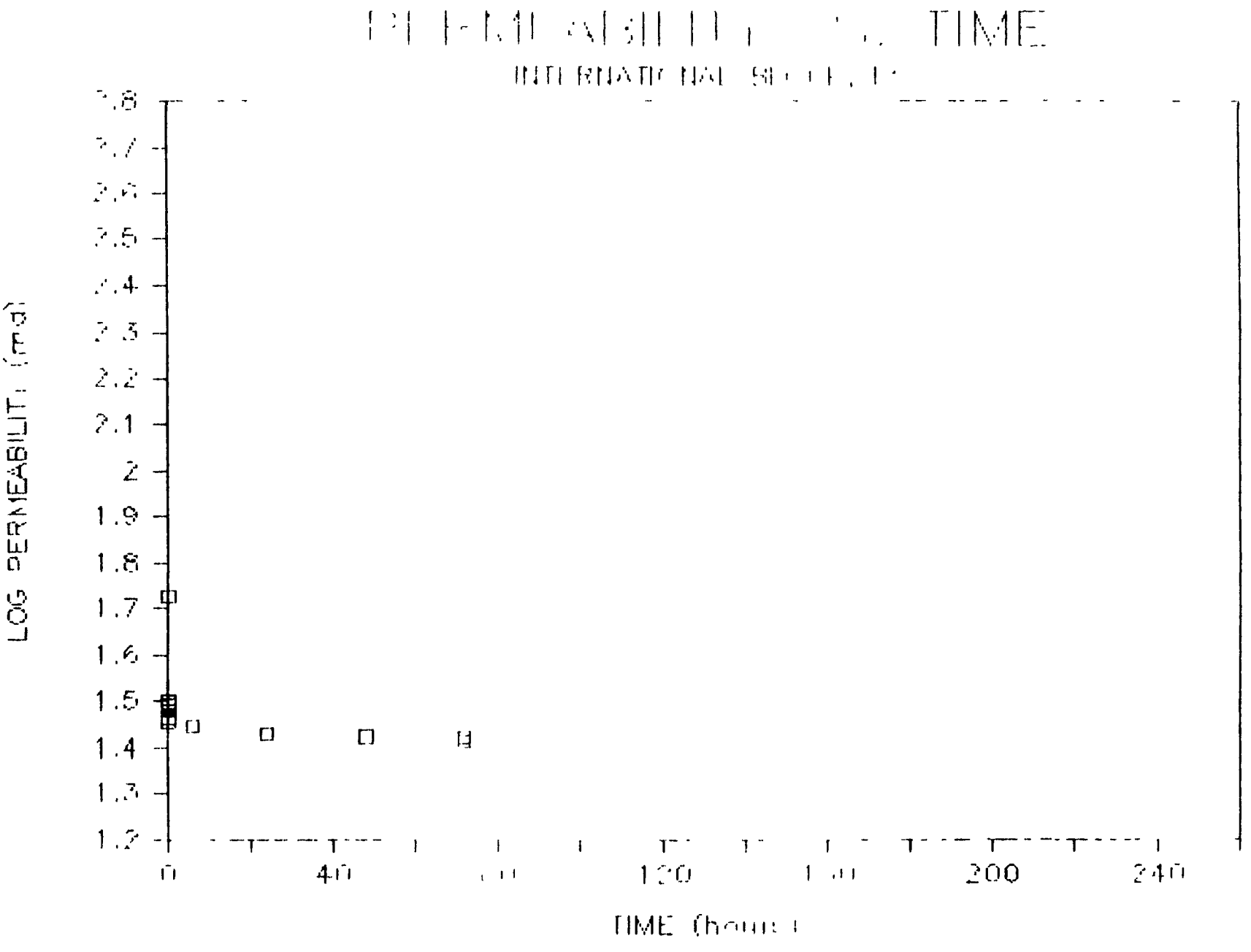
TIME
LOG PERMEABILITY (md)
2.8
2.7
2.6
2.5
2.4
2.3
2.2
2.1
2
1.9
1.8
1.7
1.6
1.5
1.4
1.3
1.2
0
40
120
200
240
TIME (hours)

FRACTURE HEALING TEST 20

Test Number: 20
Sample Number: I2FM
File Name: I2FM
Type of Salt: Block
Fracture Type: Sawcut
Moisture Condition: Moist
Initial Porosity: 0.135 (Unfractured)

Confining Pressure (psi)	Time of Pressure Application (hrs)	Cumulative Time (hrs)	Axial* Strain	Permeability (md)
54	0	0		306.1
512	0	0		71.5
1016	0	1		50.5
1516	0	2		40.6
2040	0	2		36.4
2556	0	3		31.5
2552	2	5		28.7
2561	24	27		19.6
2551	49	52		18.3
2556	92	95		17.7
2554	120	123		17.7
2561	144	147		17.6
2563	168	171		17.4
2554	184	187		17.4
2045	0	187		17.8
1021	0	188		18.1

* Not recorded in this test.

LOG PERMEABILITY (md)
TIME (hours)

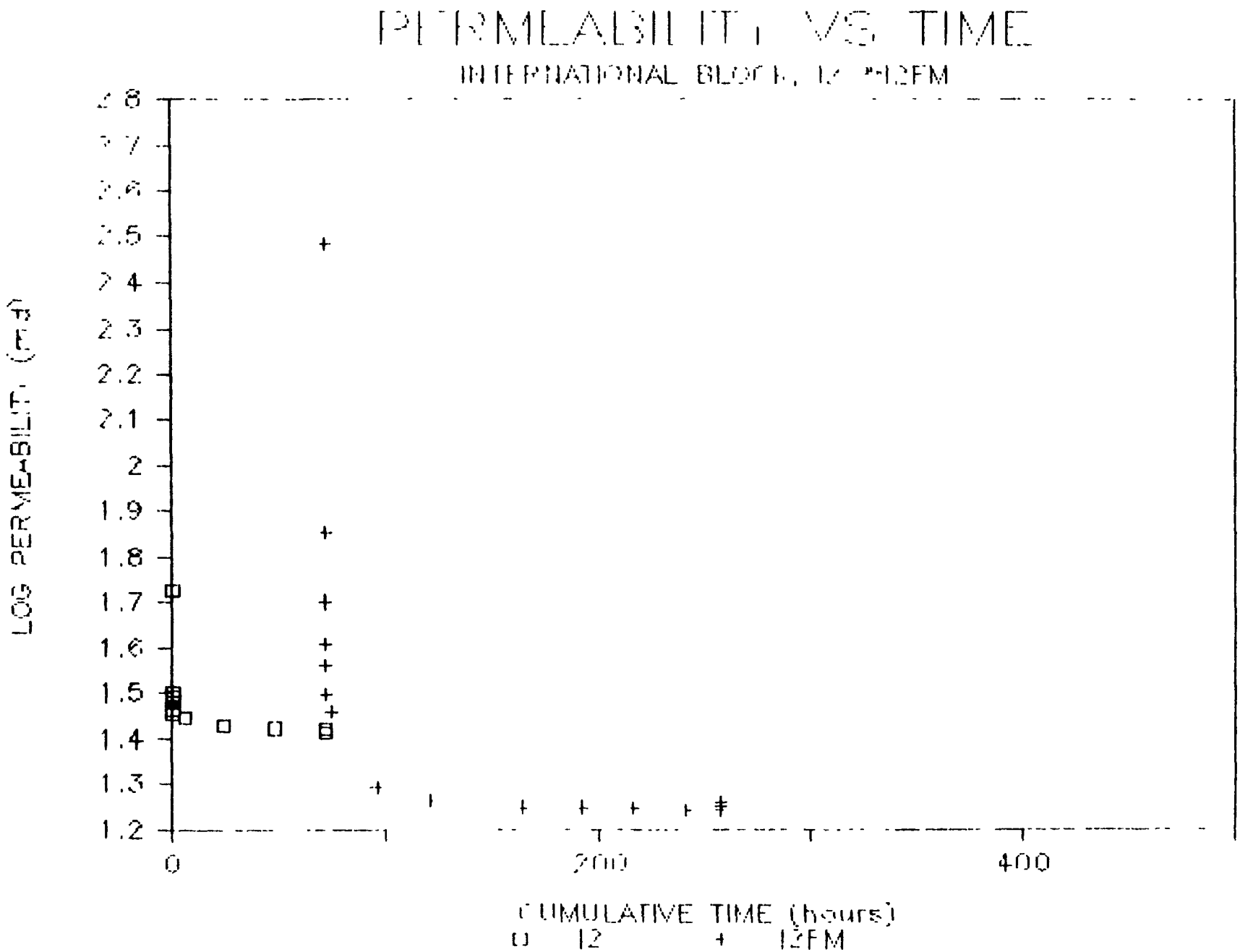
PERMEABILITY VS TIME
INTERNATIONAL BLOCK, 12 *12FM
LOG PERMEABILITY (md)
2.8
2.7
2.6
2.5
2.4
2.3
2.2
2.1
2
1.9
1.8
1.7
1.6
1.5
1.4
1.3
1.2
0
200
400
CUMULATIVE TIME (hours)
□ 12 + 12FM

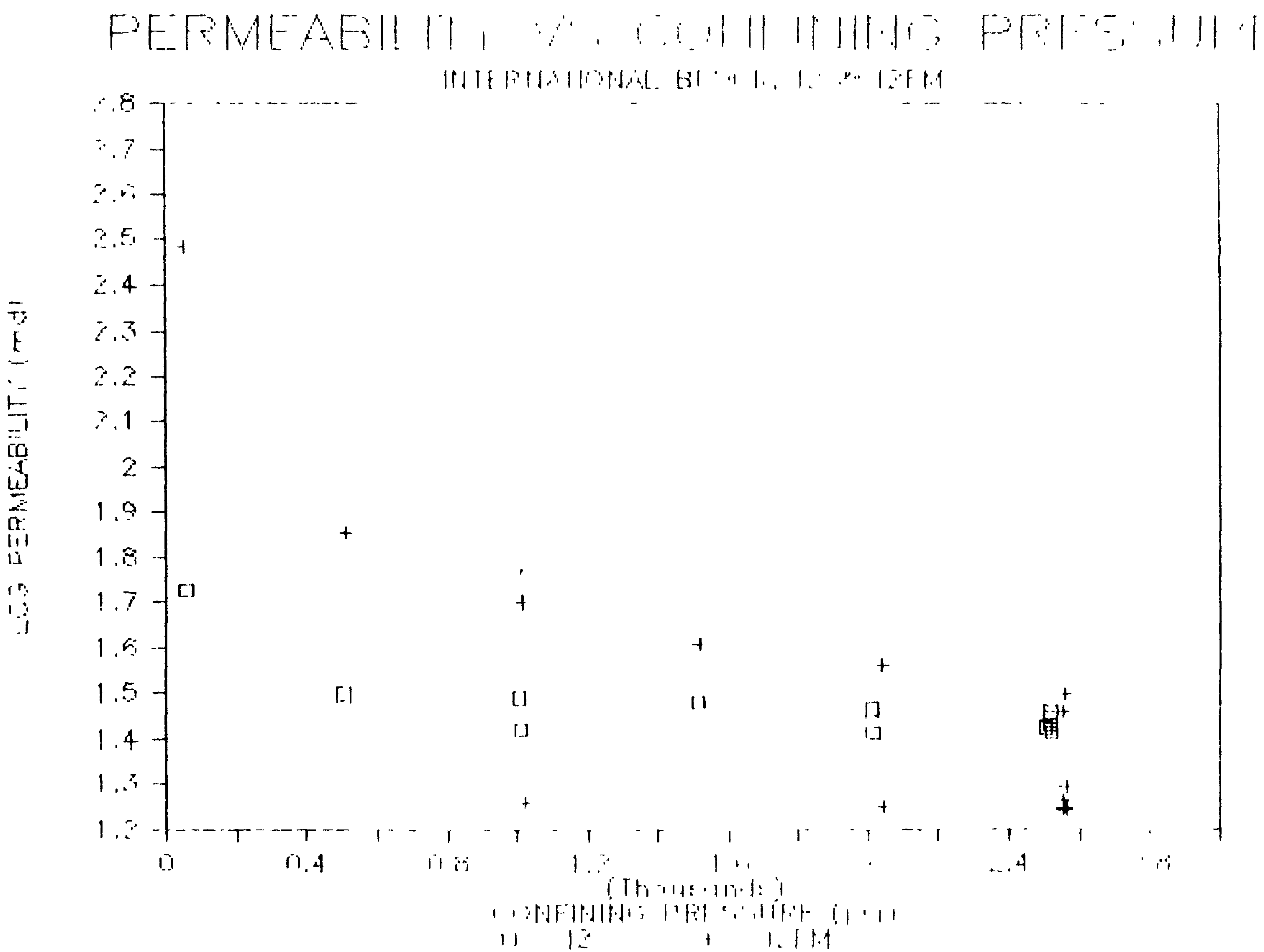
PERMEABILITY VS CONFINING PRESSURE
INTERNATIONAL
LOG PERMEABILITY (md)
2.5
2.4
2.3
2.2
2
1.9
1.8
1.7
1.6
1.5
1.4
1.3
0
0.4
(Thousands)
CONFINING PRESSURE

DISTRIBUTION LIST

ACRES INTERNATIONAL CORP
STEWART N THOMPSON
AEROSPACE CORP
R L JOHNSON
ALABAMA STATE GEOLOGICAL SURVEY
THORNTON L NEATHERY
AMARILLO PUBLIC LIBRARY
AMERICAN ROCK WRITING RESEARCH
JOHN NOXON
APPLIED RESEARCH ASSOCIATES
STEVEN WOOLFOLK
ARGONNE NATIONAL LABORATORY
DORLAND E EDGAR
DOUGLAS F HAMBLEY
WYMAN HARRISON
YU CHIEN YUAN
ARIZONA NUCLEAR POWER PROJECT
HENRY W RILEY, JR
ARTHUR D. LITTLE INC
CHARLES R HADLOCK
ATKINS RESEARCH & DEVELOPMENT—UNITED KINGDOM
T W BROYD
ATOMIC ENERGY CONSULTANTS
DONALD G ANDERSON
ATOMIC ENERGY CONTROL BOARD—CANADA
KEN SHULTZ
ATOMIC ENERGY OF CANADA LTD
T CHAN
SIEGRUN MEYER
BATTELLE MEMORIAL INSTITUTE
JEFFREY L MEANS
BCM CONVERSE INC.
ROBERT J MANUEL
BECHTEL NATIONAL INC
LESLIE J JARDINE
T R MONGAN
BERKELEY GEOSCIENCES/HYDROTECHNIQUE ASSOCIATES
BRIAN KANEHIRO
BRENK SYSTEMPLANUNG—W. GERMANY
H D BRENK
BROOKHAVEN NATIONAL LABORATORY
HELEN TODOSOW (2)
BUNDESANSTALT FUR GEOWISSENSCHAFTEN UND ROHSTOFFE—W. GERMANY
MICHAEL LANGER
HELMUT VENZLAFF
BUREAU DE RECHERCHES GEOLOGIQUES ET MINIERES—FRANCE
BERNARD FEUGA
BUTTES GAS & OIL COMPANY
ROBERT NORMAN
CALIFORNIA DEPT OF CONSERVATION
PERRY AMIMITO
CAYUGA LAKE CONSERVATION ASSOCIATION INC
D S KIEFER
CENTER FOR INTERDISCIPLINARY STUDIES
DAVID M ARMSTRONG
CITIZENS AGAINST NUCLEAR DISPOSAL INC
STANLEY D FLINT
COLORADO STATE UNIVERSITY
FRANK A KULACKI
COLUMBIA UNIVERSITY
M ASHRAF MAHTAB
CONNECTICUT DEPT OF ENVIRONMENTAL PROTECTION
KEVIN MCCARTHY
CONNECTICUT STATE SENATE
CORNELIUS OLEARY
CORSTAR RESEARCH INC
DOUGLAS K VOGT
COUNCIL OF ENERGY RESOURCE TRIBES
WYATT M ROGERS, JR
DAMES & MOORE
RON KEAR
DEAF SMITH COUNTY LIBRARY
DEPARTMENT OF THE NAVY
GENNARO MELLIS
DESERET NEWS
JOSEPH BAUMAN
DEUTSCHE GESELLSCHAFT ZUM BAU UND BETRIEB VON ENDLAGERN
GERNOT GRUBLER
E I. DU PONT DE NEMOURS & CO
A B MILLER
E.R. JOHNSON ASSOCIATES INC
E R JOHNSON
G L JOHNSON
EARTH SCIENCE AND ENGINEERING INC
LOU BLANCK
EARTH SCIENCES CONSULTANTS INC
HARRY L CROUSE
EAST TENNESSEE STATE UNIVERSITY
ALBERT F IGLAR
EBASCO SERVICES INC
KATHLEEN E L HOWE
RAYMOND H SHUM
ECOLOGY & ENVIRONMENT INC
MICHAEL BENNER
EG & G IDAHO INC
ROBERT M NEILSON, JR
BRENT F RUSSELL
ELEKTRIZITAETS-GES. LAUFENBURG - SWITZERLAND
H N PATAK
ELSAM—DENMARK
ARNE PEDERSEN
ENGINEERS INTERNATIONAL INC
ROBERT A CUMMINGS
LIBRARY
MADAN M SINGH
ENVIRONMENTAL DEFENSE FUND
JAMES B MARTIN
ENVIRONMENTAL POLICY INSTITUTE
DAVID M BERRICK
EXXON NUCLEAR IDAHO COMPANY INC
GARY WAYMIRE
F.J. SCHLUMBERGER
PETER ALEXANDER
FENIX & SCISSON INC
CHARLENE U SPARKMAN
FERRIS STATE COLLEGE
MICHAEL E ELLS
FINNISH CENTRE FOR RADIATION AND NUCLEAR SAFETY
KAI JAKOBSSON
FLORIDA INSTITUTE OF TECHNOLOGY
JOSEPH A ANGELO, JR
FLUID PROCESSES RESEARCH GROUP BRITISH GEOLOGICAL SURVEY
NEIL A CHAPMAN
FLUOR TECHNOLOGY INC
WILLIAM LEE (F2X)
THOMAS O MALLONEE, JR (F2X)
GARTNER LEE ASSOCIATES LTD—CANADA
ROBERT E J LEECH
GEOLOGICAL SURVEY OF NORWAY
SIGURD HUSEBY
GEOMIN INC
J A MACHADO
GEORGIA INSTITUTE OF TECHNOLOGY
ALFRED SCHNEIDER
GEOSTOCK—FRANCE
CATHERINE GOUGNAUD
GEOTRANS INC
JAMES MERCER
GOLDER ASSOCIATES
MELISSA MATSON
J W VOSS
GOLDER ASSOCIATES—CANADA
CLEMENT M K YUEN
GRAM INC
KRISHAN K WAHI
GRAND COUNTY HIGH SCHOOL LIBRARY
GRAND COUNTY PUBLIC LIBRARY
H & R TECHNICAL ASSOCIATES INC
WILLIAM R RHYNE
H. LAWROSKI & ASSOCIATES P.A
HARRY LAWROSKI
H-TECH LABORATORIES INC
BRUCE HARTENBAUM
HANFORD OVERSIGHT COMMITTEE
LARRY CALDWELL
HARVARD UNIVERSITY
RAYMOND SIEVER
HARZA ENGINEERING COMPANY
PETER CONROY
HEALTH & ENERGY INSTITUTE
ARJUN MAKHIJAN
HEREFORD NUCLEAR WASTE INFORMATION OFFICE
MARTHA SHIRE
HIGH LEVEL NUCLEAR WASTE OFFICE
PATRICK D SPURGIN (5)
HIGH PLAINS WATER DISTRICT
DON MCREYNOLDS
A WAYNE WYATT
HITACHI WORKS, HITACHI LTD
MAKOTO KIKUCHI
HOUGH-NORWOOD HEALTH CARE CENTER
GEORGE H BROWN M D
ILLINOIS DEPT OF NUCLEAR SAFETY
JOHN COOPER
ILLINOIS STATE GEOLOGICAL SURVEY
MORRIS W LEIGHTON
INSTITUT FUR TIEFLAGERUNG—W. GERMANY
WERNT BREWITZ
E R SOLTER
INSTITUTE OF GEOLOGICAL SCIFNCES—ENGLAND
STEPHEN THOMAS HORSEMAN
INSTITUTE OF PLASMA PHYSICS
H AMANO
INSTITUTO DE INVESTIGACIONES FISCOQUIMICAS TEORICAS Y APLICADAS
J R VILCHE
INTER/FACE ASSOCIATES INC
RON GINGERICH
INTERA TECHNOLOGIES INC
JOHN F PICKENS
MARK REEVES
INTERNATIONAL ENERGY ASSOCIATES LTD
BLYTHE J LYONS
INTERNATIONAL ENGINEERING COMPANY INC
MAX ZASLAWSKY

INTERNATIONAL RESEARCH AND EVALUATION
R. DANFORD
INTERNATIONAL SALT COMPANY
LEWIS P. BUSH
JOHN VOIGT
IOWA STATE UNIVERSITY
BERNARD I. SPINRAD
ISTITUTO SPERIMENTALE MODELLI E STRUTTURE S.P.A.—ITALY
FERRUCCIO GERA
IT CORP
PETER C. KELSALL
LIBRARY
CARL E. SCHUBERT
ITASCA CONSULTING GROUP INC
CHARLES FAIRHURST
ROGER HART
J.F.T. AGAPITO & ASSOCIATES INC
MICHAEL P. HARDY
CHRISTOPHER M. ST. JOHN
J.L. MAGRUDER & ASSOCIATES
J. L. MAGRUDER
JACOBY & COMPANY
CHARLES H. JACOBY
JGC CORPORATION—JAPAN
MASAHIKO MAKINO
JONES COUNTY JUNIOR COLLEGE LIBRARY
KANSAS DEPT OF HEALTH AND ENVIRONMENT
GERALD W. ALLEN
KANSAS STATE GEOLOGICAL SURVEY
WILLIAM W. HAMBLETON
KELLER WREATH ASSOCIATES
FRANK WREATH
KERNFORSCHUNGSZENTRUM KARLSRUHE GMBH—W. GERMANY
K. D. CLOSS
R. KOESTER
KIHN ASSOCIATES
HARRY KIHN
KLM ENGINEERING INC
B. GEORGE KNIAZEWYCZ
KUTA RADIO
KUTV-TV
ROBERT LOY
LAW ENGINEERING TESTING COMPANY
JOSEPH P. KLEIN III
LAWRENCE BERKELEY LABORATORY
JOHN A. APPS
EUGENE P. BINNALL
J. WANG
LAWRENCE LIVERMORE NATIONAL LABORATORY
WASTE PACKAGE TASK LIBRARY
LEAGUE OPPOSING SITE SELECTION
LINDA S. TAYLOR
LIBRARY OF MICHIGAN
RICHARD J. HATHAWAY
LOCKHEED ENGINEERING & MANAGEMENT COMPANY
STEVE NACHT
LOUISIANA GEOLOGICAL SURVEY
RENWICK P. DEVILLE
JAMES J. FRILOUX
SYED HAQUE
LOUISIANA TECHNICAL UNIVERSITY
LIBRARY
R. H. THOMPSON
LYLE FRANCIS MINING COMPANY
LYLE FRANCIS
MARTIN MARIETTA
CATHY S. FORE
MARYLAND DEPT OF HEALTH & MENTAL HYGIENE
MAX EISENBERG
MASSACHUSETTS INSTITUTE OF TECHNOLOGY
DANIEL METLAY
MCDERMOTT INTERNATIONAL
KAREN L. FURLOW
MELLEN GEOLOGICAL ASSOCIATES INC
FREDERIC F. MELLEN
MEMBERS OF THE GENERAL PUBLIC
DONNA AHRENS
ROGER H. BROOKS
LAWRENCE CHASE, PH.D.
TOM & SUSAN CLAWSON
ROBERT H. CURTIS
GHISLAIN DEMARSILY
ROBERT EINZIGER
WARREN EISTER
JERRY L. ELLIS
OSWALD H. GREAGER
KENNETH GUSCOTT
MICHAEL T. HARRIS
MICHAEL R. HELFERT
JOSEPH M. HENNIGAN
B. JEANINE HULL
YOZO ISOGAI
LINDA LEHMAN
GEORGE LOUDDER
STEVEN J. MAHERAS
MAX MCDOWELL
A. ALAN MOGHISSI
F. L. MOLESKI
CAROLINE PETTI
L. M. PIERSON
MARTIN RATHKE
PETER J. SABATINI, JR.
ZUBAIR SALEEM
OWEN SEVERANCE
LEWIS K. SHUMWAY
FRANK STEINBRUNN
EBIMO D. UMBU
MERRIMAN AND BARBER CONSULTING ENGINEERS INC
GENE R. BARBER
MICHIGAN DISTRICT HEALTH DEPT NO. 4
EDGAR KREFT
MICHIGAN ENVIRONMENTAL COUNCIL
ROOM 305
MICHIGAN TECHNOLOGICAL UNIVERSITY
DAE S. YOUNG
MICHIGAN UNITED CONSERVATION CLUBS
WAYNE SCHMIDT
MIDDLETON LIBRARY
M. S. BOLNER
MINDEN NUCLEAR WASTE INFORMATION OFFICE
SHIRLEY JOHNSON
MINE CRAFT INC
NORBERT PAAS
MINNESOTA DEPT OF ENERGY AND DEVELOPMENT
MINNESOTA DEPT OF HEALTH
ALICE T. DOLEZAL-HENNIGAN
MINNESOTA F.A.I.R.
DELORES SWOBODA
MINNESOTA GEOLOGICAL SURVEY
MATT S. WALTON
MISSISSIPPI BUREAU OF GEOLOGY
MICHAEL B. E. BOGRAD
MISSISSIPPI DEPT OF ENERGY AND TRANSPORTATION
DON CHRISTY
MISSISSIPPI DEPT OF NATURAL RESOURCES
ALVIN R. BICKER, JR.
CHARLES L. BLALOCK
MISSISSIPPI LIBRARY COMMISSION
SARA TUBB
MISSISSIPPI MINERAL RESOURCES INSTITUTE
MISSISSIPPI STATE DEPT OF HEALTH
EDDIE S. FUENTE
MITRE CORP
LESTER A. ETTLINGER
MONTICELLO HIGH SCHOOL LIBRARY
MEDIA CENTER
MORRISON-KNUDSEN COMPANY INC
BOB ACKARET
BILL GALE
PAUL W. MCKIE
MICHELLE L. PAURLEY
NAGRA—SWITZERLAND
CHARLES MCCOMBIE
NATIONAL ACADEMY OF SCIENCES
JOHN T. HOLLOWAY
NATIONAL BOARD FOR SPENT NUCLEAR FUEL, KARNBRANSLENAMDEN—SWEDEN
NILS RYDELL
NATIONAL GROUND WATER INFORMATION CENTER
JANET BIX
NATIONAL PARKS & CONSERVATION ASSOCIATION
TERRI MARTIN
NATIONAL SCIENCE FOUNDATION
ROYAL E. ROSTENBACH
NATIONAL WATER WELL ASSOCIATION
VALERIE ORR
NEW MEXICO ENVIRONMENTAL EVALUATION GROUP
ROBERT H. NEILL
NEW YORK DEPT OF HEALTH
DAVID AXELROD, M.D.
NEW YORK ENERGY RESEARCH & DEVELOPMENT AUTHORITY
JOHN P. SPATH (8)
NEW YORK STATE ASSEMBLY
WILLIAM B. HOYT
NEW YORK STATE DEPT OF ENVIRONMENTAL CONSERVATION
PAUL MERGES
NEW YORK STATE HEALTH DEPT
JOHN MATUSZEK
NEW YORK STATE PUBLIC SERVICE COMMISSION
FRED HAAG
NEYER, TISEO, & HINDO LTD
KAL R. HINDO
NIAGARA MOHAWK POWER CORPORATION
GERALD K. RHODE
NORTHEAST UTILITIES SERVICE COMPANY
PATRICIA ANN OCONNELL
NORTHWESTERN UNIVERSITY
BERNARD J. WOOD
NUCLEAR ASSURANCE CORP
JOHN V. HOUSTON
NUCLEAR SAFETY RESEARCH ASSOCIATION
HIDETAKA ISHIKAWA
NUCLEAR WASTE CONSULTANTS
ADRIAN BROWN
NUCLEAR WASTE INFORMATION CENTER MISSISSIPPI STATE LAW LIBRARY
JUDITH HUTSON
NUS CORP
W. G. BELTER
RODNEY J. DAVIS
DOUGLAS D. ORVIS
YONG M. PARK
NWT CORP
W. L. PEARL
OAK RIDGE NATIONAL LABORATORY
J. O. BLOMEKE
H. C. CLAIBORNE

ALLEN G. CROFF
T. F. LOMENICK
FRANCOIS G. PIN
ELLEN D. SMITH

ONR DETACHMENT
DAVID EPP

ONTARIO DEPT OF CIVIL ENGINEERING
F. SYKES

ONTARIO HYDRO—CANADA
K. A. CORNELL
C. F. LEE

ONTARIO RESEARCH FOUNDATION—CANADA
LYDIA M. LUCKEVICH

OREGON DEPT OF ENERGY
DAVID A. STEWART-SMITH

ORGANIZATION FOR ECONOMIC COOPERATION AND DEVELOPMENT—FRANCE
STEFAN G. CARLYLE

PACIFIC NORTHWEST LABORATORY
W. F. BONNER
DON J. BRADLEY
CHARLES R. COLE
FLOYD N. HODGES
J. H. JARRETT
CHARLES T. KINCAID
J. E. MENDEL

PARSONS BRINCKERHOFF QUADE & DOUGLAS INC
T. R. KUESEL
ROBERT PRIETO

PARSONS BRINCKERHOFF/PB-KBB
KAROLYN KENNEDY

PARSONS-REDPATH
KRISHNA SHRIYASTAVA
GLEN A. STAFFORD

PB-KBB INC
JUDITH G. HACKNEY

PENNSYLVANIA STATE UNIVERSITY
MICHAEL GRUTZECK
DELLA M. ROY

PERRY COUNTY CITIZENS AGAINST NUCLEAR WASTE DISPOSAL
DOROTHY G. COLE
DURLEY HANSEN

PHYSIKALISCH-TECHNISCHE BUNDESANSTALT—W. GERMANY
PETER BRENNECKE

POTASH CORPORATION OF SASKATCHEWAN - CANADA
GRAEME G. STRATHDEE

POTASH CORPORATION OF SASKATCHEWAN MINING LIMITED
PARVIZ MOTTAHED

POWER REACTOR AND NUCLEAR FUEL DEVELOPMENT CORP—JAPAN

PUBLIC SERVICE ELECTRIC & GAS
JOHN J. MOLNER

RANDALL COUNTY LIBRARY

RAYMOND KAISER ENGINEERS
W. J. DODSON

RE/SPEC INC
GARY D. CALLAHAN
PAUL F. GNIRK

RENEWABLE ENERGY COUNCIL OF NORTH CAROLINA
JANE SHARP

RHODE ISLAND OFFICE OF STATE PLANNING
BRUCE VILD

RICHTON NUCLEAR WASTE INFORMATION OFFICE
BOB FREEMAN

ROCKWELL HANFORD OPERATIONS
JAMES L. ASH
HARRY BABAD
KUNSOO KIM
KARL M. LA RUE

ROCKWELL INTERNATIONAL ENERGY SYSTEMS GROUP
HARRY PEARLMAN

ROGERS & ASSOCIATES ENGINEERING CORP
ROBERT E. WILEMS

ROY F. WESTON INC
JAMES L. ASH
MICHAEL CONROY
DAVID F. FENSTER
MARTIN HANSON
WILLIAM IVES
VIC MONTENYOHL
JILL RUSPI
KAREN ST. JOHN
LAWRENCE A. WHITE

ROYAL INSTITUTE OF TECHNOLOGY—SWEDEN
IVARS NERETNIEKS

ROYCES ELECTRONICS INC
ROYCE HENNINGSON

SAN DIEGO GAS & ELECTRIC COMPANY
STEPHEN B. ALLMAN

SAN JOSE STATE UNIVERSITY SCHOOL OF ENGINEERING
R. N. ANDERSON

SAN JUAN RECORD
JOYCE MARTIN

SANDIA NATIONAL LABORATORIES
JOY BEMESDERFER
ROBERT M. CRANWELL
JOE A. FERNANDEZ
ROBERT GUZOWSKI
THOMAS O. HUNTER
A. R. LAPPIN
R. W. LYNCH
RUDOLPH V. MATALUCCI
MARTIN A. MOLECKE
E. J. NOWAK
LYNN D. TYLER
WOLFGANG WAWERSIK
WENDELL WEART

SAVANNAH RIVER LABORATORY
CAROL JANTZEN
WILLIAM R. MCDONELL

SCIENCE APPLICATIONS INTERNATIONAL CORP
BARRY DIAL
JAMES E. HAMMELMAN
ROBERT R. JACKSON
DAVID H. LESTER
JOHN E. MOSIER
HOWARD PRATT
MICHAEL E. SPAETH
ROBERT T. STULA
M. D. VOEGELE

SENECA COUNTY DEPT OF PLANNING & DEVELOPMENT

SHAFER EXPLORATION COMPANY
WILLIAM E. SHAFER

SHANNON & WILSON INC
HARVEY W. PARKER
FRANK S. SHURI

SHIMIZU CONSTRUCTION COMPANY LTD—JAPAN
TAKASHI ISHII

SIERRA CLUB
MARVIN RESNIKOFF

SIERRA CLUB—MISSISSIPPI CHAPTER

SIERRA CLUB LEGAL DEFENSE FUND
H. ANTHONY RUCKEL

SIMECSOL CONSULTING ENGINEERS—FRANCE
MATTHEW LEONARD

SKBF/KBS—SWEDEN
C. THEGERSTROM

SOGO TECHNOLOGY INC
TIO C. CHEN

SOKAOGON CHIPPEWA COMMUNITY
ARLYN ACKLEY

SOUTH DAKOTA OFFICE OF ENERGY POLICY
STEVEN M. WEGMAN

SOUTHERN CALIFORNIA EDISON CO
JOHN LADESICH

SOUTHWEST RESEARCH AND INFORMATION CENTER
DON HANCOCK

SPRING CREEK RANCH
DALTON RED BRANGUS

SPRINGVILLE CITY LIBRARY

STANFORD UNIVERSITY
KONRAD B. KRAUSKOPF
IRWIN REMSON

STATE PLANNING AGENCY
BILL CLAUSEN

STATE UNIVERSITY OF NEW YORK AT STONY BROOK
S. REAVEN

STEARNS CATALYTIC CORP
VERYL ESCHEN

STONE & WEBSTER ENGINEERING CORP
JOHN PECK
ARLENE C. PORT
EVERETT M. WASHER

STUDSVIK ENERGITEKNIK AB—SWEDEN
ROLF SJOBLOM

SWISHER COUNTY LIBRARY

SYRACUSE UNIVERSITY
WALTER MEYER

SYSTEMS SCIENCE AND SOFTWARE
PETER LAGUS

TECHNICAL INFORMATION PROJECT
DONALD PAY

TERRAFORM ENGINEERS INC
FRANCIS S. KENDORSKI

TEXAS A & M UNIVERSITY
JAMES E. RUSSELL

TEXAS BUREAU OF ECONOMIC GEOLOGY
WILLIAM L. FISHER

TEXAS DEPT OF HEALTH
DAVID K. LACKER

TEXAS DEPT OF WATER RESOURCES
T. KNOWLES

TEXAS GOVERNORS OFFICE
STEVE FRISHMAN

THE DAILY SENTINEL
JIM SULLIVAN

THE EARTH TECHNOLOGY CORP
DANIEL D. BUSH
FRED A. DONATH (2)
JOSEPH G. GIBSON
MATT WERNER
KENNETH L. WILSON

THE SEATTLE TIMES
ELOUISE SCHUMACHER

THOMSEN ASSOCIATES
C. T. GAYNOR, II

TIMES-PICAYUNE
MARK SCHLEIFSTEIN

TRINITY EPISCOPAL CHURCH
BENJAMIN F. BELL

TULIA NUCLEAR WASTE INFORMATION OFFICE
NADINE COX
U.S. ARMY CORPS OF ENGINEERS
ALAN BUCK
U.S. BUREAU OF MINES
ANTHONY IANNACCHIONE
U.S. BUREAU OF RECLAMATION
REGE LEACH
UC-150 & UC-760
U.S. DEPT OF ENERGY
RICHARD BLANEY
CHED BRADLEY
C. R. COOLEY (2)
R. COOPERSTEIN
NEAL DUNCAN
JIM FIORE
MARK W. FREI
MICHAELENE PENDLETON (2)
PUBLIC READING ROOM
U.S. DEPT OF ENERGY—ALBUQUERQUE OPERATIONS OFFICE
LORETTA HELLING
U.S. DEPT OF ENERGY—CHICAGO OPERATIONS OFFICE
NURI BULUT
BARRETT R. FRITZ
PUBLIC READING ROOM
R. SELBY
U.S. DEPT OF ENERGY—ENGINEERING AND LICENSING DIVISION
RALPH STEIN
U.S. DEPT OF ENERGY - IDAHO OPERATIONS OFFICE
PUBLIC READING ROOM
U.S. DEPT OF ENERGY - OAK RIDGE OPERATIONS OFFICE
PUBLIC READING ROOM
U.S. DEPT OF ENERGY—OSTI (317)
U.S. DEPT OF ENERGY—SALT REPOSITORY PROJECT OFFICE
J. O. NEFF
U.S. DEPT OF ENERGY - SAN FRANCISCO OPERATIONS OFFICE
PUBLIC READING ROOM
U.S. DEPT OF ENERGY—WIPP
ARLEN HUNT
U.S. DEPT OF THE INTERIOR
MATTHEW JAMES DEMARCO
F. L. DOYLE
U.S. GEOLOGICAL SURVEY—DENVER
JESS M. CLEVELAND
ROBERT J. HITE
U.S. GEOLOGICAL SURVEY—RESTON
DAVID B. STEWART
U.S. NUCLEAR REGULATORY COMMISSION
R. BOYLE
EILEEN CHEN
F. ROBERT COOK
DOCKET CONTROL CENTER
PAUL F. GOLDBERG
BANAD N. JAGANNATH
CLYDE JUPITER
JOHN C. MCKINLEY
NRC LIBRARY
JEROME R. PEARRING
JACOB PHILIP
R. JOHN STARMER
NAIEM S. TANIOUS
JOHN TRAPP
TILAK R. VERMA
U.S. SENATE
CARL LEVIN
BILL SARPALIUS
UNION CARBIDE CORP
JOHN D. SHERMAN
UNION OF CONCERNED SCIENTISTS
MICHAEL FADEN
UNITED KINGDOM DEPT OF THE ENVIRONMENT
F. S. FEATES
UNIVERSITY COLLEGE LONDON
B. K. ATKINSON
UNIVERSITY OF ARIZONA
JAAK DAEMEN
I. W. FARMER
KITTITEP FUENKAJORN
AMITAVA GHOSH
JAMES G. MCCRAY
UNIVERSITY OF BRITISH COLUMBIA - CANADA
R. ALLAN FREEZE
UNIVERSITY OF CALIFORNIA AT RIVERSIDE
LEWIS COHEN
UNIVERSITY OF ILLINOIS AT URBANA—CHAMPAIGN
ALBERT J. MACHIELS
UNIVERSITY OF LOWELL
JAMES R. SHEFF
UNIVERSITY OF MARYLAND
AMERICAN NUCLEAR SOCIETY
MARVIN ROUSH
UNIVERSITY OF MISSOURI AT KANSAS CITY
EDWIN D. GOEBEL
SYED E. HASAN
UNIVERSITY OF MISSOURI AT ROLLA
ALLEN W. HATHEWAY
UNIVERSITY OF NEW MEXICO
DOUGLAS G. BROOKINS
UNIVERSITY OF PITTSBURGH
B. L. COHEN
UNIVERSITY OF SOUTHERN MISSISSIPPI
DANIEL A. SUNDEEN
UNIVERSITY OF TEXAS AT AUSTIN
BUREAU OF ECONOMIC GEOLOGY
CAROLYN E. CONDON
UNIVERSITY OF TEXAS AT SAN ANTONIO
DONALD R. LEWIS
UNIVERSITY OF TOLEDO
DON STIERMAN
UNIVERSITY OF UTAH
STEVEN J. MANNING
MARRIOTT LIBRARY
JAMES A. PROCARIONE
UNIVERSITY OF UTAH RESEARCH INSTITUTE
LIBRARY
UNIVERSITY OF WASHINGTON
WASH PIRG
UNIVERSITY OF WATERLOO
CHRIS FORDHAM
UNIVERSITY OF WISCONSIN—MILWAUKEE
HOWARD PINCUS
USGS NATIONAL CENTER
JIM ROLLO
UTAH DEPT OF HEALTH
LARRY F. ANDERSON
UTAH DEPT OF NATURAL RESOURCES & ENERGY
MARK P. PAGE
UTAH DEPT OF TRANSPORTATION
DAVID LLOYD
UTAH DIVISION OF PARKS & RECREATION
DENNIS BURNS
GORDON W. TOPHAM
UTAH ENERGY OFFICE
ROD MILLAR
UTAH MULTIPLE USE ADVISORY COUNCIL
JOHN M. GARR
UTAH SOUTHEASTERN DISTRICT HEALTH DEPT
ROBERT L. FURLOW
UTAH STATE GEOLOGIC TASK FORCE
DAVID D. TILLSON
UTAH STATE UNIVERSITY
JACK T. SPENCE
V. RAJARAM, P.E.
V. RAJARAM
VANDERBILT UNIVERSITY
FRANK L. PARKER
VEGA NUCLEAR WASTE INFORMATION OFFICE
EFFIE HARLE
VERMONT STATE NUCLEAR ADVISORY PANEL
VIRGINIA CALLAN
VIRGINIA DEPT OF HEALTH
ROBERT G. WICKLINE
VIRGINIA MILITARY INSTITUTE
HENRY D. SCHREIBER
WASHINGTON HOUSE OF REPRESENTATIVES
RAY ISAACSON
WATER INDUSTRIES
STEVE CONEWAY
WATTLAB
BOB E. WATT
WESTERN MICHIGAN UNIVERSITY
W. THOMAS STRAW
WESTERN STATE COLLEGE
FRED R. PECK
WESTINGHOUSE ELECTRIC CORP
WIPP PROJECT
WESTINGHOUSE HANFORD COMPANY
C. R. ALLEN
WESTINGHOUSE IDAHO NUCLEAR COMPANY INC
NATHAN A. CHIPMAN
ROGER N. HENRY
WILLIAMS AND ASSOCIATES INC
GERRY WINTER
WISCONSIN DEPT OF NATURAL RESOURCES
DUWAYNE F. GEBKEN
WISCONSIN ELECTRIC POWER CO.
DAVID K. ZABRANSKY
WISCONSIN STATE SENATE
JOSEPH STROHL
WITHERSPOON, AIKEN AND LANGLEY
RICHARD FORREST
WOODWARD-CLYDE CONSULTANTS
RANDALL L. LENTELL
ASHOK PATWARDHAN
WESTERN REGION LIBRARY
YALE UNIVERSITY
G. R. HOLEMAN

U.S. GOVERNMENT PRINTING OFFICE:1987-748-075/40086